THE UNIVERSITY OF TULSA

THE GRADUATE SCHOOL

WELL TEST ANALYSIS FOR HETEROGENEOUS RESERVOIRS

by
Gilvan Soares Feitosa

A dissertation submitted in partial fulfillment of
the requirements for the degree of Doctor of Philosophy
in the Discipline of Petroleum Engineering
The Graduate School
The University of Tulsa
1993

Reproduced with permission of the copyright owner. Further reproduction prohibited without permission.

THE UNIVERSITY OF TULSA

THE GRADUATE SCHOOL

WELL TEST ANALYSIS FOR HETEROGENEOUS RESERVOIRS

by

Gilvan Soares Feitosa

A DISSERTATION

APPROVED FOR THE DISCIPLINE OF

PETROLEUM ENGINEERING

By Dissertation Committee

_____, Co-Chairperson

_____, Co-Chairperson

_____

_____

_____

Reproduced with permission of the copyright owner. Further reproduction prohibited without permission.

ABSTRACT

Feitosa, G. S. (Doctor of Philosophy in Petroleum Engineering)

Well Test Analysis for Heterogeneous Reservoirs (213 pp. - Chapter V)

Co-Directed by Dr. Albert C. Reynolds, Jr. and Dr. Leslie G. Thompson

(342 words)

This work presents procedures for analyzing well-test pressure data obtained from a well located in a heterogeneous reservoir where the permeability is an arbitrary function of the distance from the well.

Two procedures to solve the inverse problem of generating permeability distribution directly from well-test pressure data are presented. In the first method, the permeability function is obtained by using a simple, recursive algorithm derived to numerically solve an integral equation of the first kind that represents the wellbore pressure derivative solution. The other procedure is based on considering the "instantaneous permeability", obtained from well-test data, as a volumetrically-weighted harmonic average of the permeability distribution between the wellbore and a radius of investigation. Both procedures can be applied to either transient drawdown data or buildup data corrected for producing-time effects.

A method to obtain the reservoir pressure profile at the instant of shut-in directly from buildup data is presented. It is shown that, under certain conditions, the pressure profile, which is initially computed up to the last radius of investigation, can be reasonably extended up to the reservoir external radius and then used to estimate the average reservoir pressure. In addition, if the pressure profile is established under either a steady-

Reproduced with permission of the copyright owner. Further reproduction prohibited without permission.

state or pseudosteady state flow condition, one can estimate the productivity index and the equivalent homogeneous permeability.

We present exact solutions for the reservoir pressure response during either steady-state or pseudosteady state flow. Using these solutions, we derived analytical equations for the average reservoir pressure, the stabilized inflow performance and the equivalent homogeneous permeability which characterizes the long-time (boundary-dominated flow) performance. The exact equation for the flow rate during boundary-dominated flow for constant pressure production is also presented.

It is shown that, when our inversion procedures are applied to well-test data obtained from a heterogeneous reservoir, where permeability and/or porosity vary with position, we obtain an equivalent radial permeability distribution with porosity constant. Both reservoir descriptions, when used as input to our simulator, yield essentially identical pressure and pressure derivative responses. This illustrates the nonuniqueness of the inverse problem.

Reproduced with permission of the copyright owner. Further reproduction prohibited without permission.

ACKNOWLEDGMENTS

I wish to express my gratitude to Prof. Albert Reynolds and Prof. Leslie Thompson for the time dedicated and the assistance as co-directors of this research project. I want to thank the dissertation committee members, Dr. Lifu Chu, Prof. Dale Doty and Prof. Peyton Cook, for their comments and suggestions.

I am specially grateful to Dr. Lifu Chu for many invaluable, brainstorming discussions which brought some light at the "end of the narrow, dark tunnel" at a time when the only light seemed to come apparently from "a train coming in the opposite direction".

I wish to acknowledge my company Petrobrás, Petróleo Brasileiro S. A., for fully supporting my studies at The University of Tulsa.

This work is dedicated to my parents Assis (in memoriam) and Gisélia, to my brother Gilson and to my sister Maria das Graças. I specially dedicate this work to my beloved wife Heliana, and my sons Tales, Tito and Tomás. With them I learned that "as important as knowledge is caring and seeing with the heart."

Reproduced with permission of the copyright owner. Further reproduction prohibited without permission.

TABLE OF CONTENTS

Page

TITLE PAGE i

APPROVAL PAGE ii

ABSTRACT iii

ACKNOWLEDGMENTS v

TABLE OF CONTENTS vi

LIST OF TABLES xi

LIST OF FIGURES xiii

CHAPTER I INTRODUCTION 1

CHAPTER II FORWARD PROBLEM: FORMULATION AND SOLUTIONS 7

2.1 Introduction 7

2.2 Areally Heterogeneous Reservoir 8

2.2.1 Problem Formulation 8

2.2.2 Approximate Analytical Solution 11

2.2.3 Numerical Solution 20

2.3 Radially Heterogeneous Reservoir 21

2.3.1 Problem Formulation 21

2.3.2 Transient Analytical Solutions 23

2.3.2.1 Approximate Solution Based on Perturbation Technique and Laplace Transform 23

Reproduced with permission of the copyright owner. Further reproduction prohibited without permission.

TABLE OF CONTENTS (Continued)

Page

2.3.3.2 Approximate Solutions Based on Flow Rate Profile Assumptions 25

2.3.3 Generalized Pressure Derivative Solution (GPDS) 31

2.3.3.1 Drawdown 31

2.3.3.2 Buildup 36

2.3.4 Numerical Solution 41

2.3.5 Comparison of Solutions 54

2.3.6 Long-time Solutions 58

2.3.6.1 Steady State Solution 58

2.3.6.2 Pseudosteady State Solution 60

2.3.6.3 Stabilized Inflow Performance Equation 64

2.3.6.4 Rate-Decline Equation for Constant Pressure Production 65

CHAPTER III INVERSE PROBLEM 69

3.1 Introduction 69

3.2 Inverse Solution Algorithm (ISA) 70

3.2.1 Drawdown 70

3.2.2 Buildup 77

3.2.2.1 Buildup after Steady-State Flow 78

3.2.2.2 Buildup after Transient Flow 79

3.2.2.3 Buildup after Pseudosteady-State Flow 80

3.2.3 Analysis Procedure 82

Reproduced with permission of the copyright owner. Further reproduction prohibited without permission.

TABLE OF CONTENTS (Continued)

Page

3.2.4 Region of Investigation 83

3.3 Inverse Solutions Based on Volumetric Average 84

3.3.1 KID as Arithmetic Average Permeability 84

3.3.2 KID as Harmonic Average Permeability 85

3.3.3 Analysis Procedure 87

3.4 Applications to Drawdown Data 88

3.4.1 Drawdown, Case 1 88

3.4.2 Drawdown, Case 2 94

3.4.3 Drawdown, Case 3 98

3.4.4 Drawdown, Case 4 98

3.5 Applications to Buildup Data 107

3.5.1 Buildup after Steady-State Flow, Case 1 107

3.5.2 Buildup after Transient Flow, Case 2 109

3.5.3 Buildup after Pseudosteady State Flow, Case 3a and 3b 111

3.6 Reservoir Pressure Profile (RPP) 115

3.6.1 RPP from Buildup Data 115

3.6.1.1 Reservoir Pressure Profile, Case 1 119

3.6.1.2 Reservoir Pressure Profile, Case 2 119

3.6.1.3 Reservoir Pressure Profile, Case 3 121

3.6.2 RPP from Computed Permeability Distribution 124

3.6.2.1 Reservoir Pressure Profile, Case 4 125

3.6.3 Average Reservoir Pressure 126

3.6.3.1 Average Reservoir Pressure, Case 1 129

Reproduced with permission of the copyright owner. Further reproduction prohibited without permission.

TABLE OF CONTENTS (Continued)

Page

3.6.3.2 Average Reservoir Pressure, Case 2 129

3.6.3.3 Average Reservoir Pressure, Case 3 130

3.6.3.4 Average Reservoir Pressure, Case 4a, 4b and 4c 130

3.6.4. Permeability Distribution 132

3.6.4.1 Permeability Distribution, Case 1a and 1b 134

3.6.4.2 Permeability Distribution, Case 2a and 2b 134

3.6.4.3 Permeability Distribution, Case 3 136

3.6.4.4 Permeability Distribution, Case 4 136

3.7 Boundary-Dominated Flow Parameters 141

3.7.1 Productivity Index 141

3.7.2 Homogeneous-Equivalent Pseudosteady State Permeability 143

3.7.3 Exponential-Decline Flow Rate for Constant Pressure Production 145

3.8 Influence of Porosity Variation 148

CHAPTER IV APPLICATION OF THE INVERSE PROBLEM SOLUTIONS TO AREALLY HETEROGENEOUS RESERVOIRS 155

4.1 Introduction 155

4.2 Equivalent Radially Heterogeneous Reservoir 156

4.2.1 Example 1 156

4.2.2 Example2 162

4.2.3 Example 3 165

4.2.4 Example 4 175

Reproduced with permission of the copyright owner. Further reproduction prohibited without permission.

TABLE OF CONTENTS (Continued)

Page

CHAPTER V CONCLUSIONS 183

NOMENCLATURE 190

REFERENCES 194

APPENDIX A FINITE-DIFFERENCE NUMERICAL SOLUTION TO THE AREALLY HETEROGENEOUS RESERVOIR INITIAL-BOUNDARY-VALUE PROBLEM 198

APPENDIX B APPROXIMATE SOLUTION TO THE RADIALLY HETEROGENEOUS RESERVOIR INITIAL-BOUNDARY-VALUE PROBLEM BASED ON RATE ASSUMPTION (i)

$$q_D = r_D k_D(r_D)\frac{\partial p_D}{\partial r_D} = -exp\left(-\frac{\alpha(t_D)r_D^2}{k_D}\right) \text{ ..... } 203$$

APPENDIX C APPROXIMATE SOLUTION TO THE RADIALLY HETEROGENEOUS RESERVOIR INITIAL-BOUNDARY-VALUE PROBLEM BASED ON RATE ASSUMPTION (ii)

$$q_D = r_D k_D(r_D)\frac{\partial p_D}{\partial r_D} = -exp\left(-\frac{r_D^2}{4t_D k_D}\right) \text{ ..... } 212$$

Reproduced with permission of the copyright owner. Further reproduction prohibited without permission.

LIST OF TABLES

Table Page

2.3.1 5-Zone Multicomposite Reservoir; Large-Size Reservoir; Drawdown Reservoir/Well System Parameters 26

2.3.2 Homogeneous Reservoir; Drawdown Reservoir/Well System Parameters 42

2.3.3 5-Zone Multicomposite Reservoir; Drawdown Reservoir/Well System Parameters 46

2.3.4 100-Zone Multicomposite, Constant Interblock Permeability Reservoir, Drawdown Reservoir/Well System Parameters 50

3.4.1a Reservoir with Smooth Permeability Distribution; Drawdown Case 4 Reservoir/Well System Parameters: (a) Permeability Distribution 102

3.4.1b Reservoir with Smooth Permeability Distribution; Drawdown Case 4 Reservoir/Well System Parameters: (b) Other Parameters 103

3.7.1 Productivity Index (STB/D/psi) 143

3.7.2 Equivalent Pseudosteady State Permeability (md) 145

3.8.1 5-Zone Multicomposite Reservoir; Variable Permeability and Porosity Reservoir/Well System Parameters 149

4.2.1 Areally Heterogeneous Reservoir; Example 1 Reservoir/Well System Parameters 157

4.2.2 Boundary-Dominated Flow Parameters; Example 1 162

4.2.3 Areally Heterogeneous Reservoir; Example 2

Reproduced with permission of the copyright owner. Further reproduction prohibited without permission.

LIST OF TABLES (Continued)

Table		Page
	Reservoir/Well System Parameters	163
4.2.4	Boundary-Dominated Flow Parameters; Example 2	168
4.2.5	Areally Heterogeneous Reservoir; Example 3 Reservoir/Well System Parameters	168
4.2.6	Boundary-Dominated Flow Parameters; Example 3	173
4.2.7	Areally Heterogeneous Reservoir; Example 4 Reservoir/Well System Parameters	177
4.2.8	Boundary-Dominated Flow Parameters; Example 4	180

Reproduced with permission of the copyright owner. Further reproduction prohibited without permission.

LIST OF FIGURES

Figure Page

2.2.1 Kernel function for pressure versus dimensionless radial distance. 15

2.2.2 Modified kernel function for pressure versus Boltzmann variable. 16

2.2.3 Modified pressure-derivative kernel function versus dimensionless radial distance. 18

2.2.4 Modified pressure-derivative kernel function versus Boltzmann variable. 19

2.3.1 Simulated dimensionless flow rate profiles; homogeneous versus multicomposite reservoir case. 27

2.3.2 Comparison of pressure derivatives; simulated versus computed with the GPDS and with Oliver's solution. 35

2.3.3 Comparison of pressure drop; simulated versus analytical drawdown results; homogeneous reservoir. 43

2.3.4 Comparison of pressure derivatives; simulated versus analytical drawdown results; homogeneous reservoir. 44

2.3.5 Comparison of dimensionless pressure derivatives; simulated versus analytical drawdown results; homogeneous reservoir. 45

2.3.6 Comparison of pressure drop; simulated versus analytical drawdown results; 5-zone multicomposite reservoir. 47

2.3.7 Comparison of pressure derivative; simulated versus analytical

Reproduced with permission of the copyright owner. Further reproduction prohibited without permission.

LIST OF FIGURES (Continued)

Figure Page

drawdown results; 5-zone multicomposite reservoir.....48

2.3.8 Variable permeability profile with a constant harmonic average permeability at gridblock interfaces.....51

2.3.9 Pressure behavior; simulated versus analytical multicomposite drawdown results. 52

2.3.10 Pressure derivative behavior; simulated versus analytical multicomposite drawdown results. 53

2.3.11 Comparison of pressure drop; simulated versus those computed with the rate-assumed solutions; forward problem. 55

2.3.12 Comparison of pressure derivatives; simulated versus those computed with the rate-assumed solutions; forward problem. 56

2.3.13 Comparison of pressure derivatives; simulated versus those from the approximate solution by Oliver and this work. 57

3.4.1 Permeability profile, actual versus KID and calculated via ISA; Drawdown Case 1.....89

3.4.2 Permeability profile, actual versus calculated via YA and MYA; Drawdown Case 1.....91

3.4.3 Permeability profile, actual versus calculated via ISA and MYA; Drawdown Case 1.....92

3.4.4 Comparison of pressure derivatives; actual versus computed from estimated permeability distributions; Drawdown Case 1.. 93

3.4.5 Comparison of pressure drop; actual versus those generated

Reproduced with permission of the copyright owner. Further reproduction prohibited without permission.

LIST OF FIGURES (Continued)

Figure Page

with estimated permeability distributions; Drawdown Case 1. 95

3.4.6 Permeability profile, actual versus calculated;

Drawdown Case 2. 96

3.4.7 Comparison of pressure derivatives; actual versus computed

from estimated permeability distributions; Drawdown Case 2... 97

3.4.8 Permeability profile, actual versus calculated;

Drawdown Case 3. 99

3.4.9 Comparison of pressure derivatives; actual versus computed

from estimated permeability distributions; Drawdown Case 3... 100

3.4.10 Permeability profile, actual versus calculated;

Drawdown Case 4. 104

3.4.11 Comparison of pressure derivatives; actual versus computed

from estimated permeability distributions; Drawdown Case 4... 105

3.4.12 Comparison of pressure drop; actual versus those generated

with estimated permeability distributions; Drawdown Case 4. 106

3.5.1 Permeability profile, actual versus calculated;

Buildup Case 1. 108

3.5.2 Permeability profile, actual versus calculated;

Buildup Case 2. 110

3.5.3 Permeability profile, actual versus calculated;

Buildup Case 3a. 112

3.5.4 Permeability profile, actual versus calculated;

Reproduced with permission of the copyright owner. Further reproduction prohibited without permission.

LIST OF FIGURES (Continued)

Figure		Page
	Buildup Case 3b.	114
3.6.1	Reservoir pressure profiles during buildup after transient flow.	117
3.6.2	Reservoir pressure profile; actual versus computed with buildup data; Reservoir Pressure Profile, Case 1.	120
3.6.3	Reservoir pressure profile; actual versus computed with buildup data; Reservoir Pressure Profile, Case 2.	122
3.6.4	Reservoir pressure profile; actual versus computed with buildup data; Reservoir Pressure Profile, Case 3.	123
3.6.5	Reservoir pressure profile; actual versus computed with drawdown and buildup data; Reservoir Pressure Profile, Cases 3a and 3b..	127
3.6.6	Permeability profile, actual versus calculated; Permeability Distribution, Cases 1a and 1b.	135
3.6.7	Permeability profile, actual versus calculated; Permeability Distribution, Cases 2a and 2b.	137
3.6.8	Permeability profile, actual versus calculated; Permeability Distribution, Case 3.	139
3.6.9	Permeability profile, actual versus calculated; Permeability Distribution, Case 4.	140
3.7.1	Flow rate for constant pressure production	147
3.8.1	Comparison of pressure drop; variation of permeability	

Reproduced with permission of the copyright owner. Further reproduction prohibited without permission.

LIST OF FIGURES (Continued)

Figure Page

and porosity; Cases (i), (ii) and (iii). 150

3.8.2 Comparison of pressure derivative; variation of permeability and porosity; Cases (i), (ii) and (iii) 151

3.8.3 Permeability profile, actual versus calculated; Cases (ii) and (iii). 153

3.8.4 Comparison of pressure derivative; simulator versus ISA, Case (iii). 154

4.2.1 Comparison of pressure derivatives computed using the actual $k(r,\theta)$ and the harmonic, geometric and arithmetic average of $k(r,\theta)$ over θ; Example 1. 159

4.2.2 Comparison of permeability profiles computed via ISA and via the harmonic and arithmetic average of $k(r,\theta)$ over θ; Example 1 160

4.2.3 Comparison of pressure derivatives: actual versus computed from ISA's results; Example 1. 161

4.2.4 Comparison of pressure derivatives computed using the actual $k(r,\theta)$ and the harmonic, geometric and arithmetic average of $k(r,\theta)$ over θ; Example 1. 164

4.2.5 Comparison of permeability profiles computed via ISA and via the harmonic and arithmetic average of $k(r,\theta)$ over θ; Example 2 166

4.2.6 Comparison of pressure derivatives: actual versus

Reproduced with permission of the copyright owner. Further reproduction prohibited without permission.

LIST OF FIGURES (Continued)

Figure Page

computed from ISA's results; Example 2. 167

4.2.7 Comparison of pressure derivatives computed using the actual $k(r,\theta)$ and the harmonic, geometric and arithmetic average of $k(r,\theta)$ over θ; Example 3. 170

4.2.8 Comparison of permeability profiles computed via ISA and via the harmonic, geometric and arithmetic average of $k(r,\theta)$ over θ; Example 3 171

4.2.9 Comparison of pressure derivatives: actual versus computed from ISA's results; Example 3. 172

4.2.10 Flow rate for constant pressure production: simulated versus computed; Example 3 174

4.2.11 Reservoir permeability distribution, $k(x,y)$, md. Example 4. 176

4.2.12 Permeability profile computed with ISA and MYA. Example 4. 178

4.2.13 Comparison of pressure derivatives: actual versus computed. Example 4. 179

4.2.14 Flow rate for constant pressure production: simulated versus computed; Example 4 181

Reproduced with permission of the copyright owner. Further reproduction prohibited without permission.

CHAPTER I

INTRODUCTION

Transient well-test have long been used to investigate the features of reservoir/well systems. The main goals, in general, are characterization of the reservoir and the well performance. Considerable work has been done to determine pressure distribution in reservoirs with homogeneous permeability. Early work by Hurst[1,2] and Muskat[3,4] established theoretical foundations of single-phase flow through homogeneous reservoirs. A variety of studies on relevant problems and fundamental solutions followed[5,6]. The subject of reservoirs with variable permeability was introduced by Muskat[4]. Since then, significant work has been done in deriving methods for analyzing well-test pressure data from reservoirs characterized by a stepwise change in permeability. Classic studies involve the following: linear discontinuities[6,7], radial discontinuities[9-12], naturally fractured reservoirs[13], and layered reservoirs[14]. However, little work has been done to solve the problem of flow in the case where reservoir properties vary continuously in an arbitrary manner as pointed out by recent works[15,16].

The objective of this work is to develop techniques for analyzing well-test pressure data obtained from a well located in a heterogeneous reservoir in which the permeability is a continuous, arbitrary function of the distance from the well. Although we have focused primarily on pure radial flow problems with permeability as a function of only radial distance from the well (with porosity constant), we also briefly investigated reservoirs with permeability as a function of r and θ (or x and y), and additionally, considered the effect of porosity variations.

Reproduced with permission of the copyright owner. Further reproduction prohibited without permission.

We considered the single-phase flow of a slightly compressible fluid of constant compressibility and constant viscosity to a fully-penetrating well in the center of a cylindrical reservoir of uniform thickness, constant porosity and rock compressibility, with closed top and bottom boundaries. We neglected gravity, wellbore storage, skin and capillary effects, and assumed a uniform initial pressure.

The direct problem of determining the pressure response to a constant rate production well in a heterogeneous reservoir characterized by a continuously variable permeability in one dimension (radial) and two dimensions (areal) is treated in Chapter II. Carslaw and Jaeger[17] considered the problem of heat conduction in a solid where thermal properties (thermal conductivity and/or specific heat) vary with the power of the distance in a linear system. They used Laplace transformation and presented analytical solutions in terms of modified Bessel functions. Loucks[18] presented steady-state and transient pressure solutions for the case of a radial heterogeneous reservoir where permeability varies with the power of the radial distance from the wellbore, $k = k\left(r^p\right)$, for the values of $p = 0, \pm\frac{1}{3}, \pm 1$, and ± 2. He considered constant rate and constant pressure production coupled with either a no-flow or a constant pressure outer boundary and derived solutions for a finite wellbore radius and "line-source" well. The solutions were derived using the Laplace transformation and are in the form of a linear combination of Bessel functions of the first kind of fractional order. Hantush[19] presented solutions for the problem of groundwater flow to a well located in an aquifer with the thickness changing exponentially in the x-direction while remaining uniform in the y-direction, $h = h\left[c\exp(\alpha x)\right]$, in an (x, y) flow geometry, for several flow conditions. The solutions, which are obtained by Laplace transformation and then inverted to real time, are presented in the form of exponential functions and modified Bessel functions. All of the above analytical solutions were developed for systems where one or more flow parameters vary with one spatial dimension according to a known function. To the best of our knowledge, no exact

Reproduced with permission of the copyright owner. Further reproduction prohibited without permission.

analytical solution has been developed for the case of a continuous, arbitrary permeability distribution function.

Only very recently, an approximate analytical solution to the problem of a well producing at a constant rate from an areally heterogeneous reservoir where the permeability is an arbitrary function of position, $k = k(r, \theta)$, has been presented by Oliver[16]. Besides the standard assumptions, he assumed a small variation of permeability about a mean value $\bar{k}$, which is supposed to be obtained from semilog analysis of pressure drawdown data. Using perturbation theory and the Laplace transform, Oliver[16] derived the transient wellbore pressure and pressure derivative approximate solutions. As a result of the assumptions and definitions used in their derivation, Oliver's wellbore pressure and pressure derivative solutions for a two-dimensional permeability distribution, $k = k(r, \theta)$, are identical to the solutions for an equivalent radial permeability, $k = k(r)$, where $k(r)$ is the harmonic average of $k(r, \theta)$ over θ. We show later that this is valid only for small variation of permeability in $\theta-$direction. The major limitations in Oliver's solution are the assumption of small variation in permeability and its dependence on a fixed reference permeability.

In Chapter II, we present a generalized pressure derivative solution (GPDS). This solution was obtained via an intuitive modification of Oliver's[16] solution. The accuracy of the GPDS is demonstrated through extensive numerical experiments, although it has not been rigorously derived. The GPDS simplifies and extends the applicability of Oliver's solution by alleviating the requirement of a small variation in permeability and eliminating the dependence on a fixed reference permeability value. The solution, which was originally developed for transient drawdown, is extended for buildup by using superposition. In addition, we derive analytical expressions for long-time solutions, for both constant rate and constant pressure production with a no-flow outer boundary. In particular, we present the flow rate equation for constant pressure production, whereas for constant rate

Reproduced with permission of the copyright owner. Further reproduction prohibited without permission.

production, we derive the exact equations for (i) the pseudosteady state pressure solution valid everywhere in the reservoir; (ii) the average reservoir pressure; (iii) the inflow performance relationship in the form of a productivity index; and (iv) the homogeneous-equivalent pseudosteady-state permeability. Also presented are two approximate semianalytical wellbore pressure and pressure derivative solutions based on an assumed flow rate profile for the infinite acting period. A comparison of all four approximate transient analytical solutions mentioned above is shown. Finally, we present a finite-difference numerical simulator which was developed to solve the problem of flow in an areally heterogeneous reservoir. Utilizing this simulator, we generated the wellbore pressure and reservoir pressure profile investigated in this work.

Chapter III considers the inverse problem of determining reservoir/well system parameters from the wellbore pressure response to a constant rate production well producing a heterogeneous reservoir characterized by a continuously variable radial permeability. As pointed out in Ref. 16, the problem of estimating an arbitrary permeability distribution from well-test pressure data has received little attention in the well-testing literature. However, a considerable amount of work has been done in the context of reservoir simulation, in general, involving production and pressure data collected from a large number of wells over a long period of time. Kamal[20] presents a review of these reservoir simulation works and also discusses the use of single-well and multiple-well tests for reservoir characterization. He points out that a single-well test is an important detection tool when a sharp discontinuity exists (e.g., sealing fault), but multiple-well test is more sensitive to heterogeneities. His work focuses on the analysis of interference and pulse test, and emphasizes the use of parameter estimation techniques, basically nonlinear regression analysis, for characterization of heterogeneous reservoirs. Based on his approximate wellbore pressure drawdown solution[16], Oliver[22] presented a method to approximate the radial permeability distribution using the Backus-Gilbert

Reproduced with permission of the copyright owner. Further reproduction prohibited without permission.

method[23]. He applied the method to a 3-zone, multicomposite reservoir, where the permeability value in the first and last zones is 1500 md and is 2000 md in the middle zone. He shows that the computed permeability distribution is only a smooth version of the true distribution, and illustrates the nonuniqueness of the inverse problem by obtaining different permeability distributions using different values of a smoothing parameter which is part of his inversion solution. Rosa and Horne[24] considered the same problem as Oliver[16], but used a pulse test. They concluded that the pressure response at the observation well for a multirate test is more sensitive to reservoir heterogeneities. They presented a solution to the inverse problem for the actual two-dimensional permeability distribution reservoir by considering an equivalent multicomposite reservoir, with a limited number of zones with arbitrarily assigned values for the radii, where the permeability in each zone is computed by nonlinear regression analysis technique. The arbitrariness in choosing the sizes of the zones and the requirement of limited number of zones to apply the regression, clearly place a considerable limitation on the applicability of their solution for the purpose of reservoir characterization. Yeh and Agarwal[25] presented a procedure to estimate the mobility profile from falloff data obtained after water injection into an oil reservoir under radial flow conditions. The mobility profile at the instant of shut-in is estimated based on the assumption that the mobility value computed from the instantaneous wellbore pressure derivative represents the volumetric average of all mobility values from the well up to a radius of investigation. They also presented a method to construct the reservoir pressure profile at the shut-in time.

In Chapter III, we present two procedures for generating an approximation to the permeability distribution directly from well-test pressure derivative data. The first method is based on our GPDS presented in Chapter II, and as such can be applied for large variations in permeability and in cases where no semilog straight line appears in the pressure data. This method involves a recursive algorithm that is applied to estimate the

Reproduced with permission of the copyright owner. Further reproduction prohibited without permission.

permeability values. The second method is obtained from a modification of the Yeh-Agarwal procedure adapted to single-phase flow. Both procedures yield good estimates of the permeability distribution with the results of the first procedure being slightly more accurate. Originally, these procedures were derived for transient drawdown data. We present a method to correct the buildup data for producing-time effects such that both methods applied to corrected buildup data yield identical results to those obtained with drawdown data. Applications to drawdown and buildup data are presented. We show that a procedure presented by Yeh-Agarwal[25] for falloff tests can be applied to our single-phase flow problem to compute the reservoir pressure profile at the instant of shut in from buildup data. We show that one can determine the pseudosteady state reservoir pressure profile from drawdown data. We also present a technique to determine the average reservoir pressure and boundary-dominated flow parameters. A number of examples are presented to illustrate the accuracy and reliability of these techniques. Although we have focused primarily on pure radial flow problems with permeability as a function of only radial distance of the well and porosity constant, we also briefly consider the effect of porosity variations and two-dimensional permeability distributions.

Chapter IV considers the application of the techniques developed in Chapter III to well test data obtained from areally heterogeneous reservoirs where the permeability is a function of r and θ or x and y. It is shown that the methods yield an "equivalent" radial permeability distribution with which the original well-test pressure and pressure derivatives are regenerated, and yield the estimation of the average reservoir pressure and boundary-dominated flow parameters.

Chapter V summarizes the results and conclusions of this work and points out possible extensions.

Reproduced with permission of the copyright owner. Further reproduction prohibited without permission.

CHAPTER II

FORWARD PROBLEM: FORMULATION AND SOLUTIONS

2.1 Introduction

Consider a system composed of a liquid-filled reservoir penetrated by a single well, with known parameters, at equilibrium. Suppose a perturbation is imposed on the system, for instance, the reservoir starts producing fluid through the well under specified conditions. We wish to determine the system pressure (or rate) response to the perturbation. This physical problem is mathematically posed as the *direct* or *forward problem*, the solution of which is *unique*. On the other hand, the problem of finding the system parameters using the system pressure (or rate) response to a known perturbation, e.g., a fluid production schedule, is called the *inverse problem*. The solution of the inverse problem is usually *not unique*. It may be possible to find several combinations of parameters that yield the identical response to a given perturbation.

In this chapter we formulate and present a number of analytical and semianalytical solutions to the forward problem of a heterogeneous reservoir producing at a constant flow rate from a single well. We consider both areally and radially heterogeneous reservoirs. Unless otherwise stated, the oilfield system of units is used throughout.

Reproduced with permission of the copyright owner. Further reproduction prohibited without permission.

2.2 Areally Heterogeneous Reservoir

An areally heterogeneous reservoir is defined as a porous-medium whose properties, namely permeability, porosity and thickness, are arbitrary functions of position, r and θ, in a (r, θ)-coordinate system. In this section, we focus primarily on areally heterogeneous reservoirs in which permeability is isotropic but varies arbitrarily with location, and porosity and thickness are constant. In Chapter III, we briefly consider the effect of porosity variation. Formulation and solutions to the constant rate production problem are presented in this section.

2.2.1 Problem Formulation

Our fundamental forward problem is to calculate the pressure response with time in an areally heterogeneous reservoir producing a slightly compressible fluid through a single well. Initially we consider the following basic assumptions:

- constant rate production
- closed upper and lower boundaries
- laterally infinite reservoir
- negligible wellbore storage and skin effect
- constant porosity, thickness and rock compressibility
- single-phase fluid with constant viscosity and compressibility
- uniform initial pressure throughout the reservoir
- negligible gravity and capillary effects
- fully-penetrating well
- rock and fluid properties independent of pressure.

Reproduced with permission of the copyright owner. Further reproduction prohibited without permission.

Under these assumptions the mathematical model that represents this physical model is given by the following Initial-Boundary-Value Problem (IBVP) :

- Governing partial-differential equation (PDE):

$$\frac{C_1}{r}\frac{\partial}{\partial r}\left[r\frac{k(r,\theta)}{\mu}\frac{\partial p}{\partial r}\right]+\frac{C_1}{r^2}\frac{\partial}{\partial \theta}\left[\frac{k(r,\theta)}{\mu}\frac{\partial p}{\partial \theta}\right]=\phi c_t\frac{\partial p}{\partial t}, \tag{2.2.1}$$

where $C_1 = 0.006328$ for t in days.

- Initial condition

$$p(r,\theta,t)=p_i \ \ for \ \ t=0. \tag{2.2.2}$$

- Inner boundary condition in r

$$[q]_{r_w}=\left(1.127\times 10^{-3}\right)\int_0^{2\pi}\left[hr\frac{k(r,\theta)}{\mu}\frac{\partial p}{\partial r}\right]_{r_w} d\theta, \tag{2.2.3a}$$

subject to an infinite conductivity wellbore assumption, i.e.,

$$\left[\frac{\partial p}{\partial \theta}\right]_{r_w}=0. \tag{2.2.3b}$$

- Outer boundary condition in r

$$\lim_{r\to\infty} p(r,\theta,t)=p_i. \tag{2.2.4}$$

The two other conditions required to complete the IBVP are taken from the continuity of pressure and θ-direction flux at $\theta=0$ and $\theta=2\pi$ as follows :

- Inner and outer boundary conditions in θ

$$p(r,\theta=0,t)=p(r,\theta=2\pi,t) \tag{2.2.5}$$

$$\left[\frac{\partial p}{\partial \theta}\right]_{\theta=0}=\left[\frac{\partial p}{\partial \theta}\right]_{\theta=2\pi} \tag{2.2.6}$$

Reproduced with permission of the copyright owner. Further reproduction prohibited without permission.

$$\text{with} \begin{cases} r & : \ [r_w, \infty) \\ \theta & : \ [0, 2\pi] \\ t & : \ [0, \infty) \\ p & : \ [p_i, 0]. \end{cases}$$

In the interest of generality, the IBVP above is usually represented in terms of dimensionless variables, which we define as follows:

- Dimensionless radius, r_D,

$$r_D = \frac{r}{r_w}, \tag{2.2.7}$$

- Dimensionless time, t_D,

$$t_D = \frac{C_1 \, k_{ref} \, t}{\phi \, \mu \, c_t \, r_w^2}, \tag{2.2.8}$$

- Dimensionless pressure drop, p_D,

$$p_D = \frac{k_{ref} \, h}{141.2 \, q \, \mu} \left[p_i - p(r, \theta, t) \right], \tag{2.2.9}$$

- Dimensionless permeability, k_D,

$$k_D = \frac{k(r, \theta)}{k_{ref}}, \tag{2.2.10}$$

where $C_1 = 0.006328$ for t in days and k_{ref} is an arbitrary value of permeability.

Using these definitions in the IBVP represented by Eq. 2.2.1 through Eq. 2.2.6 we then can write the problem in terms of dimensionless variables as follows:

$$\frac{1}{r_D} \frac{\partial}{\partial r_D} \left[r_D k_D(r_D, \theta) \frac{\partial p_D}{\partial r_D} \right] + \frac{1}{r_D^2} \frac{\partial}{\partial \theta} \left[k_D(r_D, \theta) \frac{\partial p_D}{\partial \theta} \right] = \frac{\partial p_D}{\partial t_D}, \tag{2.2.11}$$

$$\left[p_D(r_D, \theta, t_D) \right]_{t_D = 0} = 0, \tag{2.2.12}$$

Reproduced with permission of the copyright owner. Further reproduction prohibited without permission.

$$\frac{1}{2\pi}\left[\int_0^{2\pi} k_D(r_D,\theta)\, r_D \frac{\partial p_D}{\partial r_D} d\theta\right]_{r_D=1} = -1 \ , \tag{2.2.13a}$$

$$\left[\frac{\partial p_D}{\partial \theta}\right]_{r_D=1} = 0, \tag{2.2.13b}$$

$$\lim_{r_D\to\infty} p_D(r_D,\theta,t_D) = 0, \tag{2.2.14}$$

$$p_D(r_D,\theta=0,t_D) = p_D(r_D,\theta=2\pi,t_D), \tag{2.2.15}$$

$$\left[\frac{\partial p_D}{\partial \theta}\right]_{\theta=0} = \left[\frac{\partial p_D}{\partial \theta}\right]_{\theta=2\pi}. \tag{2.2.16}$$

2.2.2 Approximate Analytical Solution

To the best of our knowledge, no exact analytical solution to the IBVP of Eqs. 2.2.11 through 2.2.16 has been presented. Recently, Oliver[16] presented an approximate analytical solution in terms of pressure and pressure derivative, based on the application of perturbation theory and Laplace transforms. In essence, he assumed a small variation in permeability about a mean value and defined

$$k_D(r_D,\theta) = \frac{1}{\left[1-\varepsilon f(r_D,\theta)\right]}, \tag{2.2.17}$$

where ε is a small number and $f(r_D,\theta)$ is of order of magnitude 1, i.e., O(1).

Using a perturbation series approach coupled with Laplace transforms, he derived the following approximate wellbore pressure drawdown solution in Laplace space

$$\bar{p}_D(r_D=1,\theta,u) = \bar{p}_{D0}(r_D=1,u) + \varepsilon\, \bar{p}_{D1}(r_D=1,\theta,u), \tag{2.2.18}$$

Reproduced with permission of the copyright owner. Further reproduction prohibited without permission.

where u is the Laplace variable, the bar over dimensionless pressure denotes the Laplace transform,

$\bar{p}_{D0}$ is the Laplace transform of the constant-permeability solution and

$\bar{p}_{D1}$ is the first order perturbation to the constant-permeability solution,

given, respectively, by :

$$\bar{p}_{D0}(r_D = 1, u) = \frac{K_0(\sqrt{u})}{u\sqrt{u}K_1(\sqrt{u})}, \tag{2.2.19}$$

and

$$\varepsilon\,\bar{p}_{D1}(r_D = 1, \theta, u) = -\frac{1}{uK_1^2(\sqrt{u})}\int_1^{\infty}\xi\left\{K_1^2(\xi\sqrt{u})\left[\frac{1}{2\pi}\int_{-\pi}^{\pi}\left[1-\frac{1}{k_D(r,\theta)}\right]d\theta\right]\right\}d\xi. \tag{2.2.20}$$

In Eqs. 2.2.18 through 2.2.20, as well as throughout this work, unless otherwise defined, u denotes the time-correspondent Laplace variable, a bar symbol above a variable denotes it is in Laplace space and, K_0 and K_1 represent the modified Bessel functions of the second kind of order zero and one, respectively.

Eqs. 2.2.19 and 2.2.20 can be inverted numerically by the Stehfest[26] algorithm to obtain $p(r_D = 1, t) = p_{D0} + \varepsilon p_{D1}$. A long-time approximation to the solution may be derived in the standard manner by letting the Laplace variable u approach zero. In this case

$$\sqrt{u}K_1(\sqrt{u}) \cong 1, \tag{2.2.21}$$

and we can simplify the components of the solution to

$$\bar{p}_{D0}(r_D = 1, u) = \frac{K_0(\sqrt{u})}{u}, \tag{2.2.22}$$

and

Reproduced with permission of the copyright owner. Further reproduction prohibited without permission.

$$\varepsilon \bar{p}_{D1}(r_D = 1, \theta, u) = -\int_1^{\infty} \xi \left\{ K_1^2\left(\xi\sqrt{u}\right) \left[\frac{1}{2\pi} \int_{-\pi}^{\pi} \left[1 - \frac{1}{k_D(r,\theta)} \right] d\theta \right] \right\} d\xi. \qquad (2.2.23)$$

Oliver[16] obtained a long-time approximate pressure solution in real space by analytical inversion of the above Laplace space solutions.

For the homogeneous part of the solution, i.e., constant-permeability solution, we have

$$p_{D0}(r_D = 1, t_D) = -\frac{1}{2} E_i \left[-\frac{1}{4t_D} \right], \qquad (2.2.24a)$$

or, using the logarithmic approximation ($t_D \geq 25$), we obtain

$$p_{D0}(r_D = 1, t_D) \cong \frac{1}{2} \ln \left(\frac{4\, t_D}{e^{\gamma}} \right), \qquad (2.2.24b)$$

where $\gamma = 0.57721566$ is Euler's constant.

For the first order perturbation to the constant-permeability solution, we have

$$\varepsilon p_{D1}(r_D = 1, \theta, t_D) = -\int_1^{\infty} \left\{ G(\xi, t_D) \left[\frac{1}{2\pi} \int_{-\pi}^{\pi} \left[1 - \frac{1}{k_D(\xi,\theta)} \right] d\theta \right] \right\} d\xi, \qquad (2.2.25)$$

where the kernel function G is given by the following equation:

$$G(r_D, t_D) = \frac{\sqrt{\pi}}{2} \int_0^{t_D} \frac{r_D}{t^2} exp\left(-\frac{r_D^2}{2t} \right) W_{\frac{1}{2},\frac{1}{2}}\left(\frac{r_D^2}{t} \right) dt. \qquad (2.2.26)$$

Reproduced with permission of the copyright owner. Further reproduction prohibited without permission.

In Eq. 2.2.26 $W_{\frac{1}{2},\frac{1}{2}}(z)$ is the Whittaker's function defined in Refs. 27 and 28. Oliver[16] presents approximations to this function. In Eq. C-1 of Ref. 16, $-2\sqrt{\pi}/z$ should be replaced by $+2\sqrt{\pi}/z$, i.e., there should be a plus sign instead of a minus one.

In Fig. 2.2.1, we plot the kernel function G versus dimensionless radial distance, r_D, for five values of dimensionless time, t_D. It is clear that the larger the time, the larger the region that influences the wellbore pressure. This region extends from the wellbore radius up to a certain distance inside the reservoir where the G nearly vanishes. This distance, which could be called a radius of investigation, is treated in more detail when we consider pressure derivatives.

Although not explicit in Oliver's[16] paper, it can be easily shown that by multiplying G by $\sqrt{t_D}$, we obtain a *unique* function of the dimensionless Boltzmann variable $r_D/\sqrt{t_D}$. This is illustrated in Fig. 2.2.2, a plot of $\sqrt{t_D}\,G(r_D,t_D)$ versus $r_D/\sqrt{t_D}$, where we used the same data as in Fig. 2.2.1.

The solution in terms of dimensionless pressure derivative in real space is readily derived from the pressure solution above and is given by:

$$\frac{\partial p_D}{\partial \ln t_D} = t_D \frac{\partial p_D}{\partial t_D} = \frac{1}{2} - \int_1^{\infty} \left\{ K(\xi,t_D) \left[\frac{1}{2\pi} \int_{-\pi}^{\pi} \left[1 - \frac{1}{k_D(\xi,\theta)} \right] d\theta \right] \right\} d\xi, \qquad (2.2.27)$$

where the kernel or weighting function K is obtained from Eq. 2.2.28 which follows

$$K(r_D,t_D) = \frac{\partial G(r_D,t_D)}{\partial \ln t_D} = t_D \frac{\partial G(r_D,t_D)}{\partial t_D}, \qquad (2.2.28)$$

and consequently,

Reproduced with permission of the copyright owner. Further reproduction prohibited without permission.

Reproduced with permission of the copyright owner. Further reproduction prohibited without permission.

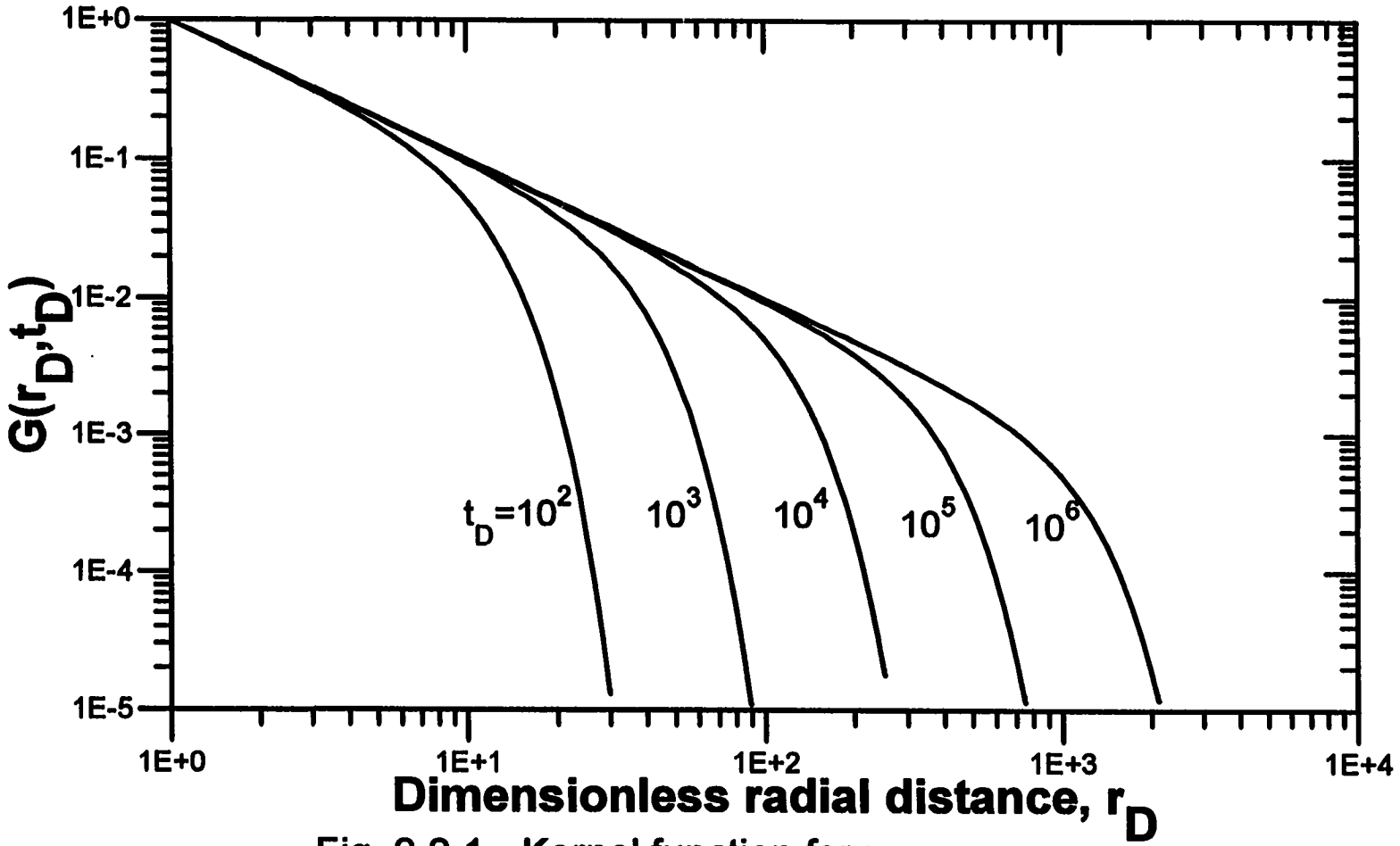

Fig. 2.2.1 - Kernel function for pressure versus dimensionless radial distance.

Reproduced with permission of the copyright owner. Further reproduction prohibited without permission.

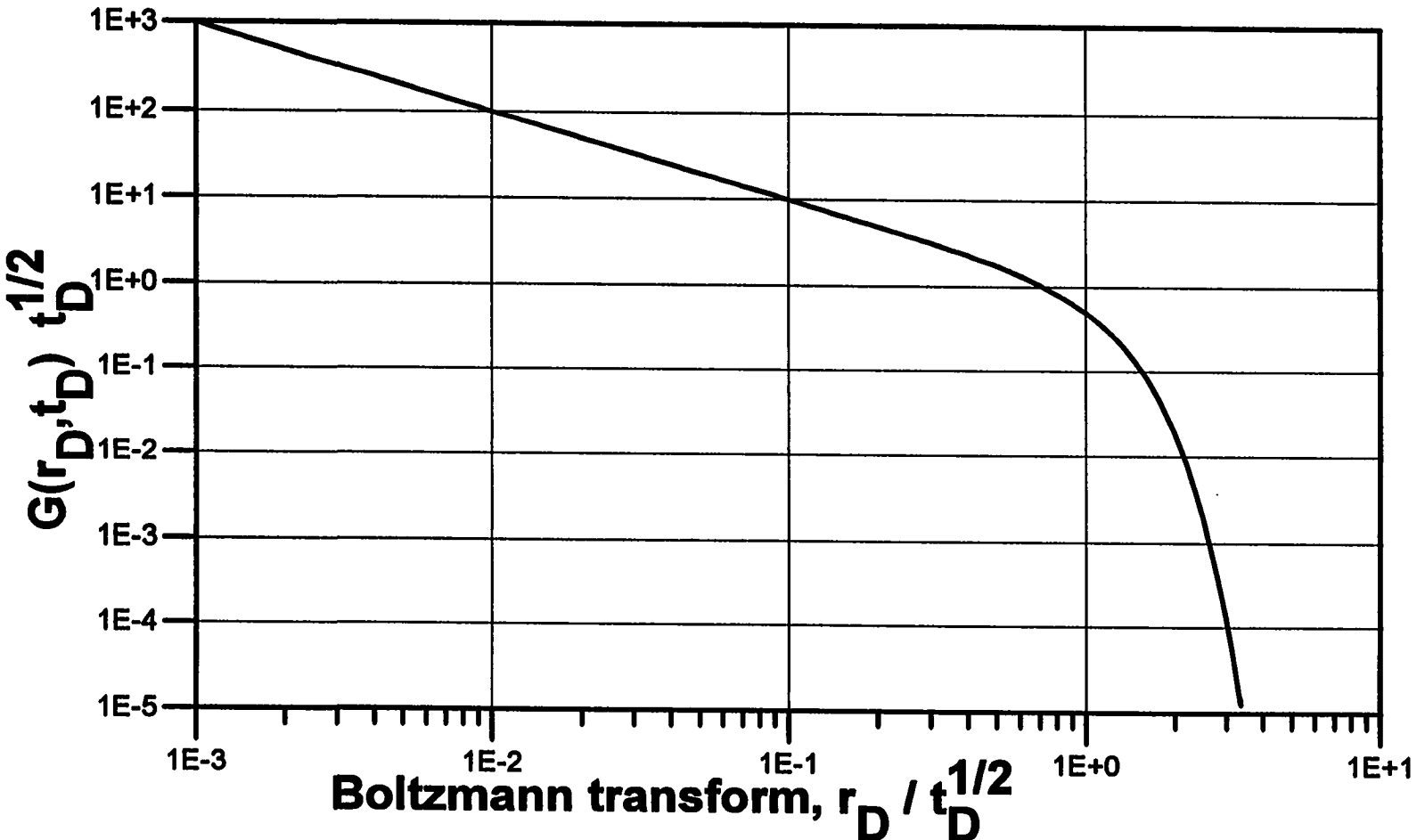

Fig. 2.2.2 - Modified kernel function for pressure versus Boltzmann variable.

$$K(r_D,t_D)=\frac{\sqrt{\pi}}{2}\frac{r_D}{t_D}exp\left(-\frac{r_D^2}{2t_D}\right)W_{\frac{1}{2},\frac{1}{2}}\left(\frac{r_D^2}{t_D}\right). \tag{2.2.29}$$

It is obvious that multiplying K by $\sqrt{t_D}$ yields a function that depends only on the dimensionless Boltzmann variable, $z_D = {r_D}/{\sqrt{t_D}}$, as Oliver[16] had observed. Fig. 2.2.3 shows the features of the modified kernel function, $\sqrt{t_D}K$, versus r_D, for three values of t_D. It is clear that a plot of $\sqrt{t_D}K$ versus ${r_D}/{\sqrt{t_D}}$, shown in Fig. 2.2.4, yields a single curve into which all curves in Fig. 2.2.3 collapse. A complete description of the features in Figs. 2.2.3 and 2.2.4 is presented in Ref. 16.

Oliver's work[16] is of paramount importance to the understanding of the averaging process that takes place when estimating permeability from well test data. Perhaps the most important contribution is the derivation of a kernel or weighting function, $K(r_D,t_D)$, for the pressure derivative. The shape of this function (see Figs. 2.2.3 and 2.2.4) indicates that the permeability obtained from the *wellbore pressure derivative is a weighted harmonic average of all permeability values within an annular region located between an inner and outer radius of investigation, respectively,* $(r_D)_{inner} = 0.12\sqrt{t_D}$ and $(r_D)_{outer} = 2.34\sqrt{t_D}$. The apparent drawback of his work, however, is that the applicability of his solution is restricted by the assumption of small variations of permeability and by the dependence of his approximate solution on the chosen value of the reference permeability, denoted in his work as $\bar{k}$. Oliver states that the reference permeability $\bar{k}$ might be obtained from the slope of a conventional semilog plot of pressure drawdown versus time. Since a small permeability variation about a mean value is assumed, a reasonable semilog straight line should be observed, from which $\bar{k}$ is calculated. Obviously, for significant variations in permeability there may not be any semilog straight line data, or several semilog straight lines might be apparent.

Reproduced with permission of the copyright owner. Further reproduction prohibited without permission.

Reproduced with permission of the copyright owner. Further reproduction prohibited without permission.

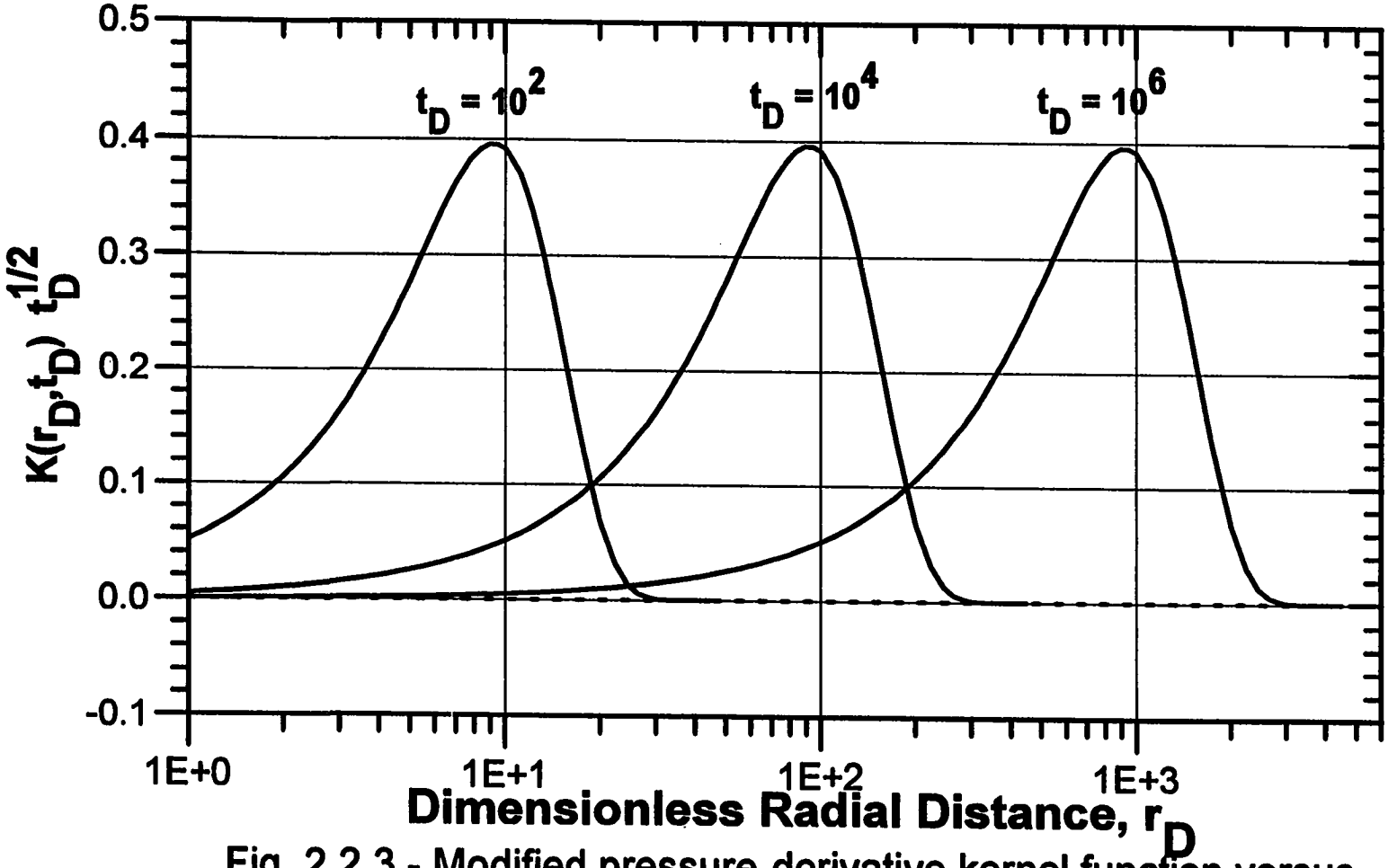

Fig. 2.2.3 - Modified pressure-derivative kernel function versus dimensionless radial distance.

Reproduced with permission of the copyright owner. Further reproduction prohibited without permission.

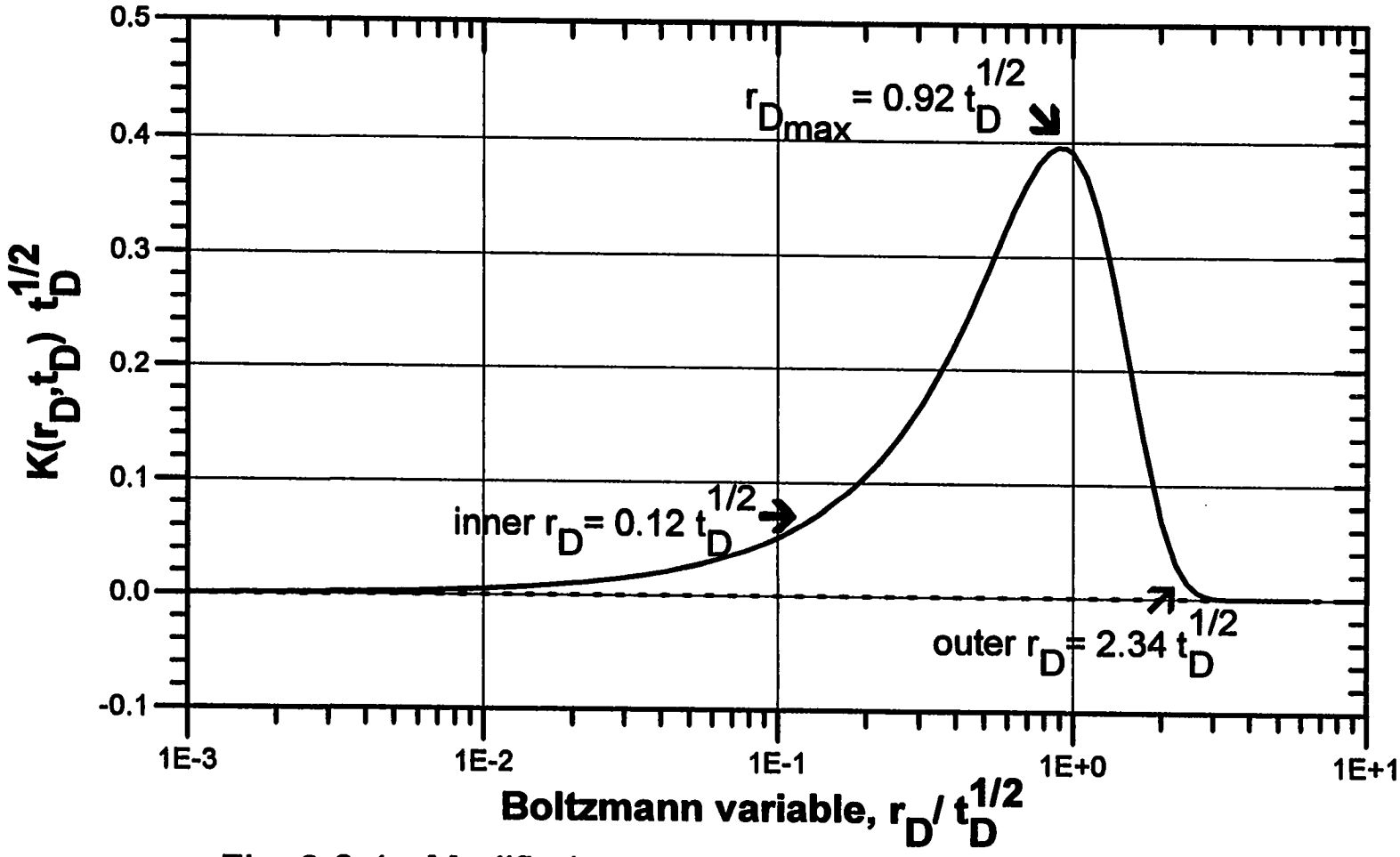

Fig. 2.2.4 - Modified pressure-derivative kernel function versus Boltzmann variable.

2.2.3 Numerical Solution

We developed a numerical solution to the IBVP represented by Eqs. 2.2.1 through 2.2.6 based on a implicit, finite-difference approximation. This solution is formulated as an areal (r,θ) numerical simulator which solves the areally heterogeneous reservoir problem of Eqs. 2.2.1 through 2.2.6 for pressure and pressure derivatives versus time. It handles all commonly encountered inner and outer boundary conditions, (i.e., constant rate or constant pressure) and any initial pressure distribution. This simulator was validated by comparison with exact analytical solutions for multicomposite reservoirs, available in the literature[32], as will be shown later on. Fundamentals on the design of this simulator are provided in Appendix A.

Reproduced with permission of the copyright owner. Further reproduction prohibited without permission.

2.3 Radially Heterogeneous Reservoirs

A radially heterogeneous reservoir refers to a reservoir in which one or more of the basic porous medium parameters, permeability, porosity and thickness, varies only with the radial distance, r, from a well taken as the origin of a (r,θ)-coordinate system. For the purpose of this work we refer here to a radially heterogeneous reservoir as one that is characterized by an arbitrary radial permeability distribution, i.e., $k = k(r)$. We present in this section the problem formulation and the transient and long-time solutions to the forward problem of a radially heterogeneous permeability reservoir producing at constant rate.

2.3.1 Problem Formulation

The forward problem requires the determination of the pressure response in a radially heterogeneous reservoir with known permeability distribution producing from a single well. We consider the same standard assumptions as in the previous section. Under these assumptions, the relevant IBVP can be written as:

- Governing PDE :

$$\frac{C_1}{r}\frac{\partial}{\partial r}\left[r\frac{k(r)}{\mu}\frac{\partial p}{\partial r}\right] = \phi c_t \frac{\partial p}{\partial t}, \tag{2.3.1}$$

where $C_1 = 0.006328$ for t in days.

- Initial condition :

$$p(r,t) = p_i \text{ for } t = 0, \tag{2.3.2}$$

- Inner boundary condition (at r_w) :

Reproduced with permission of the copyright owner. Further reproduction prohibited without permission.

$$[q]_{r_w} = \left[\frac{hr}{141.2}\frac{k(r)}{\mu}\frac{\partial p(r,t)}{\partial r}\right]_{r_w}, \tag{2.3.3}$$

- Outer boundary condition :

$$\lim_{r\to\infty} p(r,t) = p_i. \tag{2.3.4}$$

The boundary condition of Eq. 2.3.4 pertains to an infinite-acting reservoir. To obtain long-time solutions during boundary dominated flow, we assume the well is at the center of a cylindrical reservoir of radius r_e and impose either a no-flow or constant pressure boundary condition at r_e.

We define the dimensionless variables for this IBVP in the same way as we did in section 2.2 as follows:

$$r_D = \frac{r}{r_w}, \tag{2.3.5}$$

$$t_D = \frac{C_1 k_{ref} t}{\phi \mu c_t r_w^2}, \tag{2.3.6}$$

$$p_D = \frac{k_{ref} h}{141.2 q \mu}[p_i - p(r,t)], \tag{2.3.7}$$

$$k_D = \frac{k(r)}{k_{ref}}. \tag{2.3.8}$$

Applying the definitons of Eq. 2.3.5 through Eq. 2.3.8, we can write our IBVP in dimensionless variables as follows :

$$\frac{1}{r_D}\frac{\partial}{\partial r_D}\left[r_D k_D(r_D)\frac{\partial p_D}{\partial r_D}\right] = \frac{\partial p_D}{\partial t_D}, \tag{2.3.9}$$

$$p_D(r_D, t_D = 0) = 0, \tag{2.3.10}$$

Reproduced with permission of the copyright owner. Further reproduction prohibited without permission.

$$\left[r_D k_D(r_D)\frac{\partial p_D}{\partial r_D}\right]_{r_D=1} = -1, \tag{2.3.11}$$

$$\lim_{r_D\to\infty} p_D(r_D,t_D) = 0. \tag{2.3.12}$$

2.3.2 Transient Analytical Solutions

Here we consider only the infinite-acting reservoir behavior. The solutions to the above IBVP, available in the literature, in general, are based on a known, well-defined function of permeability with the radial distance, $k = k(r)$ (see Ref. 18). We will present in this section approximate solutions for *arbitrary permeability distribution.*

2.3.2.1 Approximate Solution Based on Perturbation Technique and Laplace Transform

To the best of our knowledge, the first approximate solution to the IBVP represented by Eqs. 2.3.9 through 2.3.12, in which the permeability is an *arbitrary function of distance,* was presented only recently by Oliver[16]. Defining a perturbation to the permeability parameter as

$$k_D(r_D) = \frac{1}{\left[1-\varepsilon f(r_D)\right]}, \tag{2.3.13}$$

developing $k_D(r_D)$ in Eq. 2.3.13 in Taylor series about the unit value

$$k_D = 1+\varepsilon f+\varepsilon^2 f^2+\cdots . \tag{2.3.14}$$

and then applying perturbation technique and the Laplace transform, we can express the pressure solution in Laplace space in terms of a perturbation series, as:

$$\overline{p}_D(r_D,u) = \overline{p}_{D0}(r_D,u)+\varepsilon\overline{p}_{D1}(r_D,u)+\varepsilon^2\overline{p}_{D2}(r_D,u)+\cdots . \tag{2.3.15}$$

Reproduced with permission of the copyright owner. Further reproduction prohibited without permission.

Considering only up to the first order perturbation term in this series, the general approximate pressure solution can be written as:

$$\bar{p}_D(r_D,u)=\bar{p}_{D0}(r_D,u)+\varepsilon\bar{p}_{D1}(r_D,u), \tag{2.3.16}$$

where

$$\bar{p}_{D0}(r_D,u)=\frac{K_0(r_D\sqrt{u})}{u\sqrt{u}K_1(\sqrt{u})}, \tag{2.3.17}$$

and

$$\varepsilon\bar{p}_{D1}(r_D,u)=\frac{K_0(r_D\sqrt{u})}{\sqrt{u}K_1(\sqrt{u})}\int_1^{r_D}\left\{\xi\left[\varepsilon f(\xi)\right]K_1(\xi\sqrt{u})I_1(\xi\sqrt{u})\right\}d\xi$$
$$-\frac{I_0(r_D\sqrt{u})}{\sqrt{u}K_1(\sqrt{u})}\int_{r_D}^{\infty}\left\{\xi\left[\varepsilon f(\xi)\right]K_1^2(\xi\sqrt{u})\right\}d\xi-\frac{I_1(\sqrt{u})K_0(r_D\sqrt{u})}{\sqrt{u}K_1^2(\sqrt{u})}\int_1^{\infty}\left\{\xi\left[\varepsilon f(\xi)\right]K_1^2(\xi\sqrt{u})\right\}d\xi. \tag{2.3.18}$$

At the wellbore, $r_D = 1$, the pressure solution components above reduce to

$$\bar{p}_{D0}(r_D=1,u)=\frac{K_0(\sqrt{u})}{u\sqrt{u}K_1(\sqrt{u})}, \tag{2.3.19a}$$

and

$$\varepsilon\bar{p}_{D1}(r_D=1,u)=-\frac{1}{uK_1^2(\sqrt{u})}\int_1^{\infty}\left\{\xi\left[\varepsilon f(\xi)\right]K_1^2(\xi\sqrt{u})\right\}d\xi. \tag{2.3.19b}$$

It is worthwhile to observe that the evaluation of Eq. 2.3.18 at the wellbore to obtain Eq. 2.3.19b leads to the wronskian of $K_0(\sqrt{u})$ and $I_o(\sqrt{u})$ which is equal to $1/\sqrt{u}$ (see Ref. 29), i.e.,

$$K_0(\sqrt{u})I_1(\sqrt{u})+K_1(\sqrt{u})I_0(\sqrt{u})=W\left[K_0(\sqrt{u}),I_0(\sqrt{u})\right]=\frac{1}{\sqrt{u}}. \tag{2.3.20}$$

Reproduced with permission of the copyright owner. Further reproduction prohibited without permission.

Equation 2.3.18 can be derived based on the same approach used by Oliver[16]. The result was first presented by Rosa[30] for the case of a variable flow rate. In particular, Rosa considered the case where the flow rate is a sinusoidal function of time.

Pressure and pressure derivative solutions at the wellbore in real space are obtained directly from Eqs. 2.3.19a and 2.3.19b. Hence, considering time long enough such that the inverse Laplace transform of the homogeneous solution of Eq. 2.3.19a can be replaced by the semilog approximation, we can write the wellbore pressure and pressure derivative solutions, respectively, as:

$$p_{wD}(t_D) = p_D(r_D = 1, t_D) = \frac{1}{2}\ln\left(\frac{4t_D}{e^{\gamma}}\right) - \int_1^{\infty} G(\xi, t_D)\left[1 - \frac{1}{k_D(\xi)}\right]d\xi, \qquad (2.3.21)$$

and

$$p'_{wD}(t_D) = \frac{\partial p_D(r_D = 1, t_D)}{\partial \ln t_D} = t_D \frac{\partial p_D}{\partial t_D} = \frac{1}{2} - \int_1^{\infty} K(\xi, t_D)\left[1 - \frac{1}{k_D(\xi)}\right]d\xi. \qquad (2.3.22)$$

Definitions of G and K are given by Eqs. 2.2.26 and 2.2.29, respectively.

2.3.2.2 Approximate Solutions Based on Flow Rate Profile Assumptions

We consider a multicomposite reservoir, with five concentric annular regions of constant permeability, and an associated homogeneous reservoir with permeability of the multicomposite-reservoir first zone, producing at a constant sandface flow rate through a single well located at the center. The pertinent reservoir/well system parameters are presented in Table 2.3.1. We discretized both reservoirs using 100 radial grid blockcs

Reproduced with permission of the copyright owner. Further reproduction prohibited without permission.

Table 2.3.1

5-Zone, Multicomposite, Large-Size Reservoir; Drawdown

Reservoir/Well System Parameters

$k_1 = 20$ md	$r_1 = 60$ ft	$h = 20$ ft	$\mu = 1.0$ cp	$r_w = 0.3$ ft
$k_2 = 30$ md	$r_2 = 294$ ft	$\phi = 0.20$	$c_t = 10\times10^{-6}$ psi^{-1}	$q = 20.0$ rb/d
$k_3 = 10$ md	$r_3 = 2147$ ft	$p_i = 6000$ psi		
$k_4 = 18$ md	$r_4 = 10{,}525$ ft	$r_e = 170{,}000$ ft		
$k_5 = 40$ md	$r_5 = 170{,}000$ ft			

according to Coats' grid formulation[31]. We then simulated a drawdown of 1000 days and computed flow rate profiles, shown in Fig. 2.3.1. Comparing the rate profiles in both reservoirs we observe they are nearly "parallel" to each other. However, at a given time, the rate profile in the multicomposite reservoir is shifted either to the left or to right of the homogeneous reservoir rate profile, depending on the permeability distribution. Since the homogeneous (line source) reservoir rate profile is given by $q_D(r_D,t_D) = -\exp\left(-\frac{r_D^2}{4t_D}\right)$, this suggested that we might be able to obtain approximate analytical solution to the constant sandface rate heterogeneous reservoir problem by adjusting the homogeneous reservoir rate profile to account for permeability variation. We attempted two such approaches, which are outlined in following.

(i) We first assumed the flow rate profile to be:

$$q_D(r_D,t_D) = r_D k_D(r_D)\frac{\partial p_D}{\partial r_D} = -\exp\left[-\frac{\alpha(t_D)r_D^2}{k_D}\right], \qquad (2.3.23)$$

where $\alpha(t_D)$ is a function only of t_D.

. Based on the assumption that the permeability distribution can be approximated by a piecewise constant function of the form $k_D(r_D) = k_{Di}$ for

Reproduced with permission of the copyright owner. Further reproduction prohibited without permission.

Reproduced with permission of the copyright owner. Further reproduction prohibited without permission.

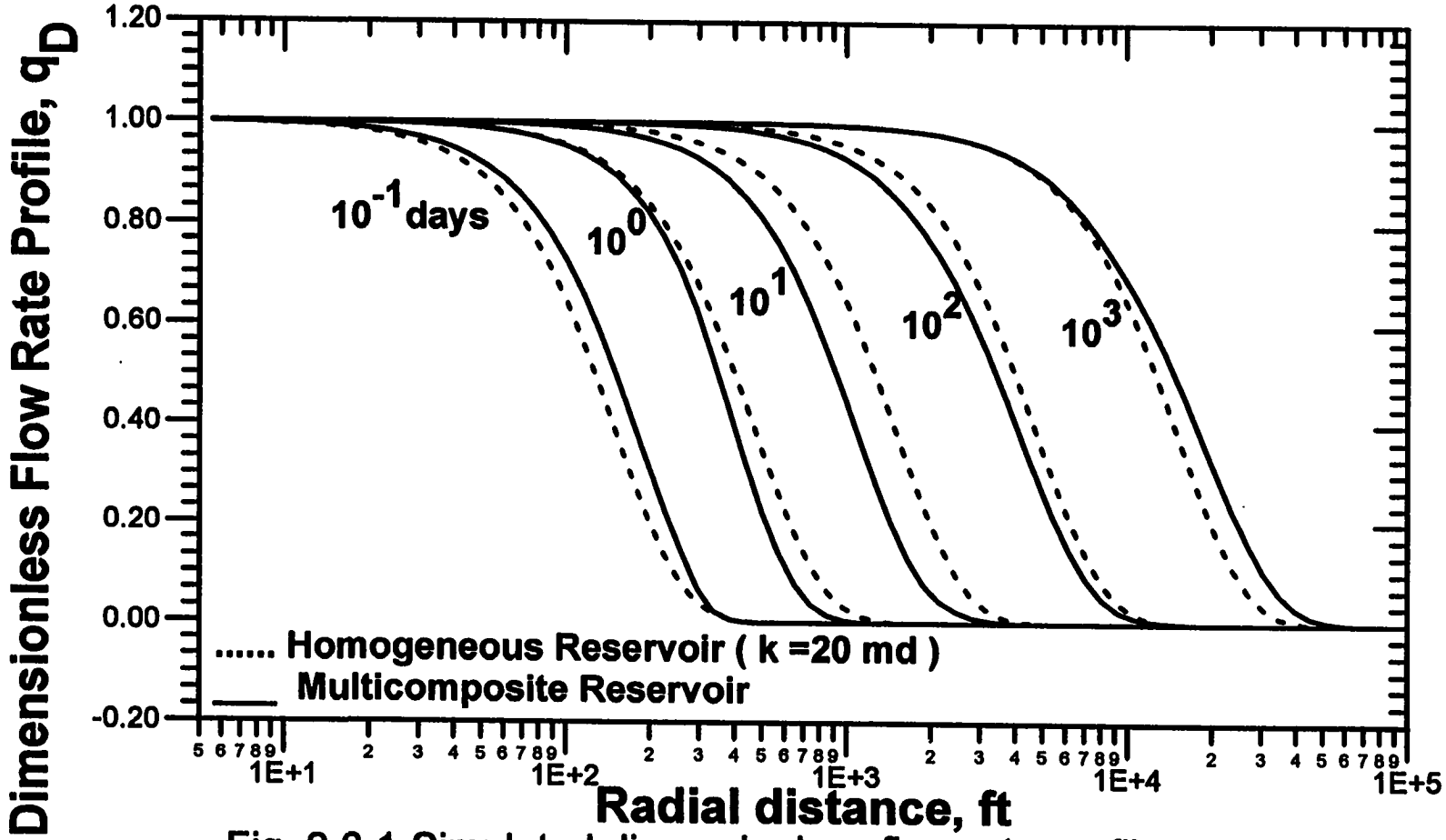

Fig. 2.3.1 Simulated dimensionless flow rate profiles; homogeneous versus multicomposite reservoir case.

$r_{Di-1/2} < r_D \le r_{Di+1/2}$, with $i = 1, 2, \cdots, \infty$, where $r_{Di+1/2}$ is the outer boundary radius of region i, and $r_{D1/2} = 1$, and under the assumption of Eq. 2.3.23, we derived in Appendix B an approximate semianalytical solution, given by

$$p_D(r_D, \alpha(t_D)) = \frac{1}{2k_{D_j}}\left[\mathrm{E}_1\left(\frac{\alpha(t_D)r_D^2}{k_{D_j}}\right) - \mathrm{E}_1\left(\frac{\alpha(t_D)r_{D_{j+1/2}}^2}{k_{D_j}}\right)\right] + \sum_{i=j+1}^{\infty}\frac{1}{2k_{D_i}}\left[\mathrm{E}_1\left(\frac{\alpha(t_D)r_{D_{i-1/2}}^2}{k_{D_i}}\right) - \mathrm{E}_1\left(\frac{\alpha(t_D)r_{D_{i+1/2}}^2}{k_{D_i}}\right)\right]. \tag{2.3.24}$$

In Eq. 2.3.24, we have assumed that the dimensionless radial distance, r_D, at which dimensionless pressure is computed, is located at a region j, i.e., $r_{Dj-1/2} < r_D < r_{Dj+1/2}$. In the summation term in the right-hand side, we perform the calculation using n terms such that, the integral involving the term $n+1$ does not contribute to the results; 10^{-6} can be used as a cut-off number.

The function $\alpha(t_D)$, in Eq. 2.3.24 must be determined by solving the following ordinary differential equation (ODE):

$$\begin{aligned}\frac{d\alpha(t_D)}{dt_D} = \exp\left(-\frac{\alpha(t_D)}{k_D(r_D=1)}\right)\Bigg\{\sum_{j=1}^{\infty}\Bigg[&\frac{1}{4\alpha^2}\left(\exp\left(-\frac{\alpha(t_D)r_{D_{j+1/2}}^2}{k_{Dj}}\right) - \exp\left(-\frac{\alpha(t_D)r_{D_{j-1/2}}^2}{k_{Dj}}\right)\right)\\ &-\frac{1}{4\alpha k_{Dj}}\left(r_{D_{j+1/2}}^2 - r_{D_{j-1/2}}^2\right)\exp\left(-\frac{\alpha(t_D)r_{D_{j+1/2}}^2}{k_{Dj}}\right)\\ &+\sum_{i=j+1}^{\infty}\frac{1}{4\alpha k_{Dj}}\left(r_{D_{j+1/2}}^2 - r_{D_{j-1/2}}^2\right)\left(\exp\left(-\frac{\alpha r_{D_{i+1/2}}^2}{k_{Di}}\right) - \exp\left(-\frac{\alpha r_{D_{i-1/2}}^2}{k_{Di}}\right)\right)\Bigg]\Bigg\},\end{aligned} \tag{2.3.25}$$

where

Reproduced with permission of the copyright owner. Further reproduction prohibited without permission.

$$\mathrm{E}_1(x) = -\mathrm{E}_i(-x) = \int_x^{\infty} \frac{\exp(-u)}{u} du. \tag{2.3.26}$$

At the wellbore $(r_D = 1)$, the pressure solution is given by

$$p_D(r_D = 1, \alpha(t_D)) = \sum_{i=1}^{\infty} \frac{1}{2k_{D_i}} \left[\mathrm{E}_1\left(\frac{\alpha(t_D) r_{D_{i-1/2}}^2}{k_{D_i}} \right) - \mathrm{E}_1\left(\frac{\alpha(t_D) r_{D_{i+1/2}}^2}{k_{D_i}} \right) \right], \tag{2.3.27}$$

and the pressure derivative is then obtained directly from the above equation as

$$\begin{aligned} \frac{\partial p_D(r_D = 1, t_D)}{\partial \ln t_D} &= t_D \frac{\partial p_{wD}}{\partial t_D} \\ &= t_D \left\{ \frac{1}{2} \sum_{j=1}^{\infty} \frac{1}{k_{D_j}} \left[-\exp\left(-\frac{\alpha(t_D) r_{D_{j-1/2}}^2}{k_{D_j}} \right) \frac{1}{\alpha(t_D)} \frac{d\alpha(t_D)}{dt_D} \right.\right. \\ &\quad \left.\left. + \exp\left(-\frac{\alpha(t_D) r_{D_{j+1/2}}^2}{k_{D_j}} \right) \frac{1}{\alpha(t_D)} \frac{d\alpha(t_D)}{dt_D} \right] \right\}. \end{aligned} \tag{2.3.28}$$

(ii) The second approach is to assume

$$\alpha(t_D) = \frac{1}{4t_D} \tag{2.3.29}$$

and then

$$q_D(r_D, t_D) = r_D k_D(r_D) \frac{\partial p_D}{\partial r_D} = -\exp\left[-\frac{r_D^2}{4t_D k_D} \right]. \tag{2.3.30}$$

Applying this assumption to our IBVP we obtain the following pressure solution:

Reproduced with permission of the copyright owner. Further reproduction prohibited without permission.

$$p_D(r_D,t_D)=\int_{r_D}^{\infty}\frac{1}{r_D^{'}k_D(r_D^{'})}\exp\left(-\frac{r_D^{'2}}{4t_Dk_D(r_D^{'})}\right)dr_D^{'} \tag{2.3.31}$$

The computation of Eq. 2.3.31 to obtain the approximate dimensionless pressure solution is accomplished by setting $\alpha(t_D)=1/4t_D$ in Eq. 2.3.24 which yields

$$\begin{aligned}p_D(r_D,t_D)=&\frac{1}{2k_{D_j}}\left[\mathrm{E_1}\left(\frac{r_D^2}{4t_Dk_{D_j}}\right)-\mathrm{E_1}\left(\frac{r_{D_{j+1/2}}^2}{4t_Dk_{D_j}}\right)\right]\\&+\frac{1}{2}\sum_{i=j+1}^{\infty}\frac{1}{k_{D_i}}\left[\mathrm{E_1}\left(\frac{r_{D_{i-1/2}}^2}{4t_Dk_{D_i}}\right)-\mathrm{E_1}\left(\frac{r_{D_{i+1/2}}^2}{4t_Dk_{D_i}}\right)\right]\end{aligned} \tag{2.3.32}$$

At the wellbore $(r_D=1)$ the approximate dimensionless pressure and pressure derivative solution are obtained by setting $\alpha(t_D)=1/4t_D$, respectively, in Eqs. 2.3.27 and 2.3.28, which yields

$$p_D(r_D=1,t_D)=\frac{1}{2}\sum_{j=1}^{\infty}\frac{1}{k_{Dj}}\left[E_1\left(\frac{r_{Dj-1/2}^2}{k_{Dj}4t_D}\right)-E_1\left(\frac{r_{Dj+1/2}^2}{k_{Dj}4t_D}\right)\right], \tag{2.3.33}$$

and

$$\frac{\partial p_D(r_D=1,t_D)}{\partial \ln t_D}=\frac{1}{2}\sum_{j=1}^{\infty}\frac{1}{k_{Dj}}\left[\exp\left(-\frac{r_{Dj-\frac{1}{2}}^2}{k_{Dj}4t_D}\right)-\exp\left(-\frac{r_{Dj+\frac{1}{2}}^2}{k_{Dj}4t_D}\right)\right]. \tag{2.3.34}$$

An approximate dimensionless wellbore pressure solution identical to Eq. 2.3.33 was also derived by Abbaszadeh and Kamal[32], based on a different approach. They developed a single-phase drawdown solution of a N-zone multicomposite reservoir, based

Reproduced with permission of the copyright owner. Further reproduction prohibited without permission.

on the classical ideas, developed by Ramey[12], of continuity of pressure and volumetric flux at the N-1 interfaces. The solution is developed in Laplace space, for either a no-flow or a constant pressure outer boundary. A long-time approximate solution is then derived for the constant pressure outer boundary case, which is inverted into real time to yield an equation (see Ref. 32, Eq. C-16) identical to Eq. 2.3.33. See Appendix C.

2.3.3 Generalized Pressure Derivative Solution (GPDS)

Our purpose here is to develop a pressure derivative solution that is valid for arbitrary variation in permeability, either small or large. Our GPDS proceeds directly from Oliver's[16] approximate solution. We develop solutions for drawdown and for buildup.

2.3.3.1 Drawdown

We start with Eq. 2.3.22 which we record again as

$$p'_{wD}(t_D) = \frac{\partial p_D(r_D = 1, t_D)}{\partial \ln t_D} = \frac{1}{2} - \int_1^{\infty} K(\xi, t_D)\left[1 - \frac{1}{k_D(\xi)}\right] d\xi. \qquad (2.3.35)$$

This equation should be able to reproduce any homogeneous reservoir problem. We recall that the dimensionless variables in this equation are based on a reference permeability $k_{ref} = \bar{k}$. Obviously, if we have a homogeneous reservoir with $k(r) = \bar{k}$, then

$$p'_{wD}(t_D) = \frac{1}{2}. \qquad (2.3.36)$$

Suppose we have now a homogeneous reservoir with permeability $k(r) = \bar{k}_1$ but we still use $\bar{k}$ as the reference permeability in Eq. 2.3.35. We must then have

Reproduced with permission of the copyright owner. Further reproduction prohibited without permission.

$$p'_{wD}(t_D) = \frac{\bar{k}h\Delta p'_w}{141.2q\mu} = \frac{1}{2}\frac{\bar{k}}{\bar{k}_1} \tag{2.3.37}$$

where $\Delta p'_w = {d\Delta p'_w}/{d\ln t}$ and $\Delta p'_w = p_i - p_{wf}$. Substituting the constant permeability value $k(r) = \bar{k}_1$ and Eq. 2.3.37 into Eq. 2.3.35, and rearranging the resulting equation yields

$$\frac{1}{2}\left(1-\frac{\bar{k}}{\bar{k}_1}\right) = \left(1-\frac{\bar{k}}{\bar{k}_1}\right)\int_1^\infty K(\xi,t_D)d\xi, \tag{2.3.38}$$

from which it becomes evident that we <u>*must*</u> have

$$\int_1^\infty K(\xi,t_D)d\xi = \frac{1}{2}. \tag{2.3.39}$$

We also verified Eq. 2.3.39 by numerical integration.

Eq. 2.3.39 was not established in Oliver's work[16]. However, it is of crucial importance to the development of our generalized pressure derivative solution (GPDS). Substituting Eq. 2.3.39 into Eq. 2.3.35, we then have

$$p'_{wD}(t_D) = \int_1^\infty K(\xi,t_D)\left(\frac{1}{k_D(\xi)}\right)d\xi. \tag{2.3.40a}$$

where t_D is given by Eq. 2.3.6, $t_D = \dfrac{C_1 k_{ref} t}{\phi\mu c_t r_w^2}$. For a small variation in permeability, one should expect an approximately constant pressure derivative from which a value of permeability can be obtained and used as k_{ref} in this equation. However, for large variation in permeability we no longer have a "nearly-constant" pressure derivative. So, if we want to apply Eq. 2.3.40a in general, we do not know how to define k_{ref} and in fact might expect that the approximate value of k_{ref} used in the definition of t_D might change with time. Note Eq. 2.3.40a is equivalent to

Reproduced with permission of the copyright owner. Further reproduction prohibited without permission.

$$\frac{h\Delta p_w^{'}}{141.2q\mu} = \int_1^{\infty} K(\xi, t_D)\left(\frac{1}{k(\xi)}\right)d\xi. \tag{2.3.40b}$$

So, k_{ref} appears only in the definition of t_D.

Numerical experiments led us to a value of the reference permeability $k_{ref} = \hat{k}$ that we defined as

$$\hat{k} = \frac{1}{2}\left(\frac{141.2\, q\, \mu}{h\, \Delta p_w^{'}}\right) \tag{2.3.41}$$

where,

$$\Delta p_w^{'} = \frac{\partial \Delta p_w}{\partial \ln t} \tag{2.3.42}$$

is the instantaneous derivative. Consequently, $\hat{k}$ is an "instantaneous permeability" value ; we refer to $\hat{k}$ as KID (permeability, k, from instantaneous derivative) in some parts this work.

We then define a dimensionless pseudotime as

$$\hat{t}_D = \frac{C_1\, \hat{k}\, t}{\phi\, \mu\, c_t\, r_w^2}. \tag{2.3.43}$$

Using this definition in the kernel function in Eq. 2.3.40a, we then obtain the ***generalized pressure derivative solution (GPDS)***

$$p_{wD}^{'}(t_D) = \int_1^{\infty} K(\xi, \hat{t}_D)\left[\frac{1}{k_D(\xi)}\right]d\xi, \tag{2.3.44a}$$

which is equivalent to

Reproduced with permission of the copyright owner. Further reproduction prohibited without permission.

$$\frac{1}{2\hat{k}} = \frac{h\Delta p_w'}{141.2q\mu} = \int_1^{\infty} K(\xi, \hat{t}_D)\left[\frac{1}{k(\xi)}\right] d\xi. \tag{2.3.44b}$$

While the derivation of Eqs. 2.3.44a and 2.3.44b is not rigorous, numerical results discussed later indicate that the equation gives a good approximation to the correct solution even when the variation in permeability is large. Thus, in effect, by rearranging Oliver's solution and using intuition, we have improved the accuracy of the approximate solution and, more importantly, we have removed the requirement of small variation in permeability, as well as the dependence on a reference permeability which could be difficult to estimate. Eq. 2.3.44b forms the basis for the inverse problem solution which will be described in Chapter III.

To validate our solution, we applied Eq. 2.3.44b to the problem of a radially heterogeneous reservoir producing at a constant rate from a single well. The reservoir is a multicomposite reservoir with five concentric zones, each one with a constant permeability value. Other pertinent data are presented in Table 2.3.1. We then compared the pressure derivatives, $\Delta p_w'$, resulting from the pressures generated by our simulator, with the pressure derivatives computed with the GPDS (Eq. 2.3.44b) and with Oliver's solution (Eq. 2.3.22). The results presented in Fig. 2.3.2 show excellent agreement between the simulated (solid curve) and the GPDS-computed $\Delta p_w'$'s (circular data points), whereas Oliver's results (cross data points) do not show as nearly as good agreement. This example illustrates the applicability of the GPDS to a case of a large variation in the permeability distribution.

Reproduced with permission of the copyright owner. Further reproduction prohibited without permission.

Reproduced with permission of the copyright owner. Further reproduction prohibited without permission.

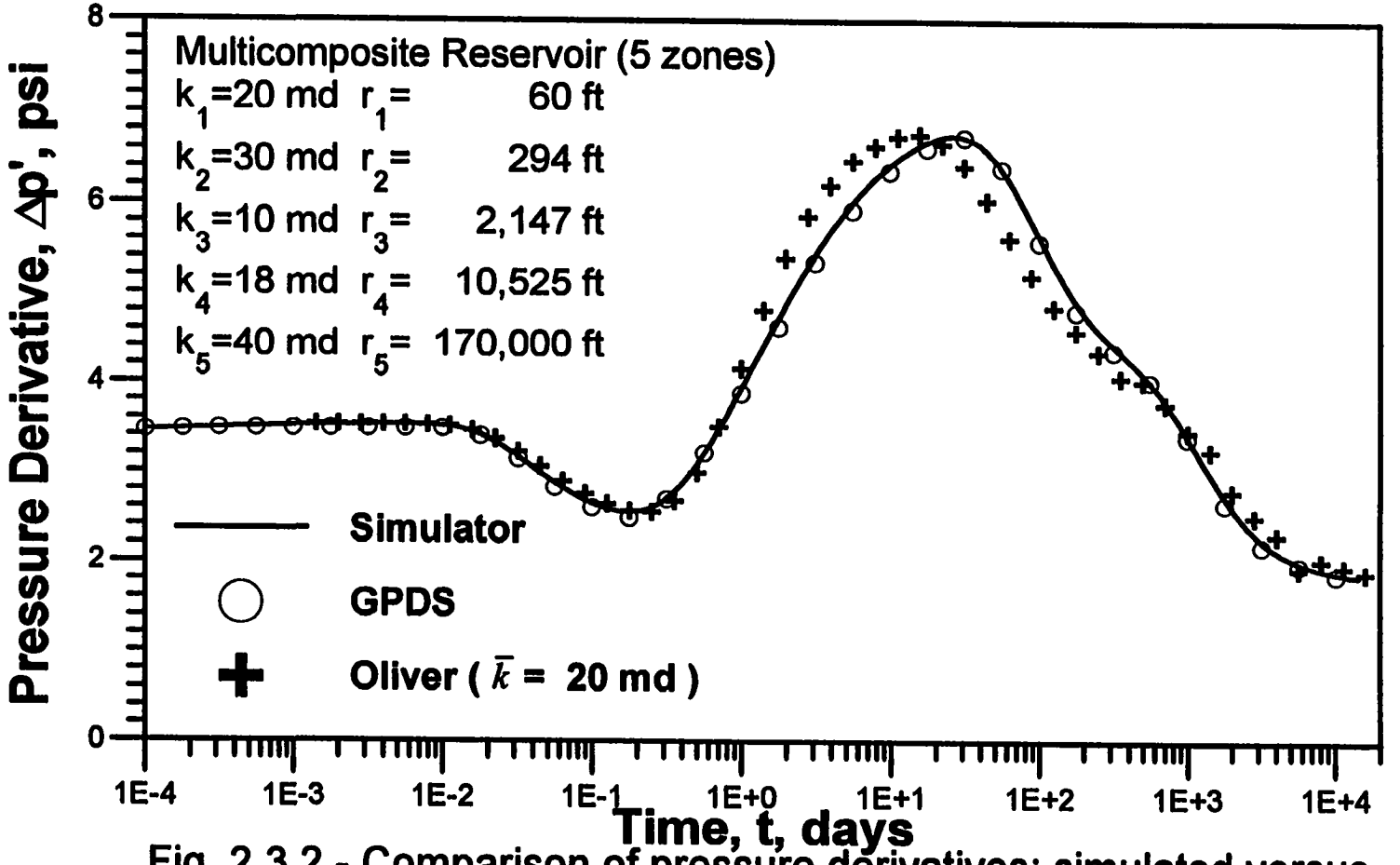

Fig. 2.3.2 - Comparison of pressure derivatives; simulated versus computed with the GPDS and with Oliver's solution.

2.3.3.2 Buildup

We examine the buildup solutions after constant rate production under steady-state, transient and pseudosteady state flow regimes.

We recognize that the IBVP's that arise from the application of the perturbation technique and Laplace transform to the original IBVP represented by Eqs. 2.3.9 through 2.3.12 are still linear problems. Therefore, ***the superposition of solutions is valid.*** The well-known general superposition buildup solution is expressed as

$$\bar{p}_{sD}(\Delta t_D) = p_{wD}(t_{pD}) - p_{wD}\left[(t_p + \Delta t)_D\right] + p_{wD}(\Delta t_D) \qquad (2.3.45)$$

where

$$\bar{p}_{sD}(\Delta t_D) = \frac{k_{ref}h}{141.2q\mu}\left[p_{ws}(\Delta t) - p_{wf,s}\right], \qquad (2.3.46)$$

t_p is the production time before the well is shut in; $p_{wf,s}$ is the bottomhole-flowing pressure at the instant of shut-in; and Δt is the current shut-in time. We consider three basic cases : buildup after (i) steady-state flow; (ii) transient flow; and (iii) pseudosteady state flow.

(i) Buildup after Steady-State Flow

In this case the first two terms in Eq. 2.3.45 exactly cancel each other. Hence, the buildup solution becomes exactly the same as the drawdown solution. So, we can write the buildup pressure solution as follows :

$$\bar{p}_{sD}(\Delta t_D) = p_{wD}(\Delta t_D), \qquad (2.3.47)$$

Reproduced with permission of the copyright owner. Further reproduction prohibited without permission.

or, in terms of pressure derivative as

$$\tilde{p}'_{sD}(\Delta t_D) = \frac{d\tilde{p}_{sD}}{d\ln(\Delta t_D)} = \frac{dp_{wD}(\Delta t_D)}{d\ln(\Delta t_D)}. \tag{2.3.48}$$

Thus, whenever Eq. 2.3.44a gives a good approximation of the drawdown solution, $\tilde{p}'_{sD}$ is well approximated by the following equation:

$$\tilde{p}'_{sD}(\Delta t_D) = \int_1^\infty K(\xi, \Delta\hat{t}_D)\left[\frac{1}{k_D(\xi)}\right]d\xi. \tag{2.3.49}$$

We develop in the following the pressure derivative solution for a buildup after either a transient or pseudosteady state flow, based on the Oliver's approximate drawdown solutions. Later, in Chapter III, we will present the correction to these solutions to obtain the generalized pressure buildup solutions which do not require the assumption of small variation in permeability as in Oliver's work[16].

(ii) <u>Buildup after Transient Flow</u>

We develop here an approximation to the pressure derivative solution for buildup following a transient flow period. We initially consider each term in the right-hand side of the general superposition buildup Eq. 2.3.45. We can write

$$p_{wD}(t_{pD}) = constant, \tag{2.3.50}$$

$$p_{wD}\left[(t_p + \Delta t)_D\right] = \frac{1}{2}\ln(t_p + \Delta t)_D + \frac{1}{2}\ln\left(\frac{4}{e^\gamma}\right) - \int_1^\infty G\left(\xi, (t_p + \Delta t)_D\right)\left[1 - \frac{1}{k_D(\xi)}\right]d\xi, \tag{2.3.51}$$

and

Reproduced with permission of the copyright owner. Further reproduction prohibited without permission.

$$p_{wD}(\Delta t_D)=\frac{1}{2}\ln\left(\frac{4\Delta t_D}{e^{\gamma}}\right)-\int_1^{\infty}G(\xi,\Delta t_D)\left[1-\frac{1}{k_D(\xi)}\right]d\xi. \qquad (2.3.52)$$

The general pressure buildup derivative equation comes directly from the buildup equation, Eq. 2.3.45, as follows

$$\tilde{p}'_{sD}(\Delta t_D)=p'_{wD}(t_{pD})-p'_{wD}\left[(t_p+\Delta t)_D\right]+p'_{wD}(\Delta t_D). \qquad (2.3.53)$$

Now recalling that

$$p'(\Delta t)=\frac{dp(\Delta t)}{d\ln\Delta t}=\Delta t\frac{dp(\Delta t)}{d\Delta t}, \qquad (2.3.54)$$

we can express the derivatives of the pressure solutions, Eqs. 2.3.50 through 2.3.52, as

$$p'_{wD}(t_{pD})=0, \qquad (2.3.55)$$

$$p'_{wD}\left[(t_p+\Delta t)_D\right]=\frac{dp_{wD}(t_p+\Delta t)_D}{d\ln\Delta t_D}=\Delta t_D\frac{dp_{wD}(t_p+\Delta t)_D}{d(t_p+\Delta t)_D}, \qquad (2.3.56)$$

$$p'_{wD}\left[(t_p+\Delta t)_D\right]=\frac{1}{2}\left(\frac{\Delta t}{t_p+\Delta t}\right)-\Delta t_D\frac{\partial}{\partial(t_p+\Delta t)_D}\left\{\int_1^{\infty}G\left(\xi,(t_p+\Delta t)_D\right)\left[1-\frac{1}{k_D(\xi)}\right]d\xi\right\}, \qquad (2.3.57)$$

Consider the second term in the right-hand side of Eq. 2.3.57. We have:

$$\Delta t_D\frac{\partial}{\partial(t_p+\Delta t)_D}\left\{\int_1^{\infty}G\left(\xi,(t_p+\Delta t)_D\right)\left[1-\frac{1}{k_D(\xi)}\right]d\xi\right\}=\Delta t_D\int_1^{\infty}\frac{\partial G\left(\xi,(t_p+\Delta t)_D\right)}{\partial(t_p+\Delta t)_D}\left[1-\frac{1}{k_D(\xi)}\right]d\xi\cdot \qquad (2.3.58)$$

Reproduced with permission of the copyright owner. Further reproduction prohibited without permission.

Using the formula for the kernel function G (Eq. 2.2.26), in Eq. 2.3.58, differentiating, and noticing that the resulting equation is now a function of the pressure derivative kernel function, K, (see Eq. 2.2.29) we then obtain:

$$\Delta t_D \int_1^\infty \frac{\partial G\left(\xi,\left(t_p+\Delta t\right)_D\right)}{\partial\left(t_p+\Delta t\right)_D}\left[1-\frac{1}{k_D(\xi)}\right]d\xi$$

$$=\Delta t_D \int_1^\infty \frac{\sqrt{\pi}}{2}\frac{\xi}{\left(t_p+\Delta t\right)_D^2}\exp\left(-\frac{\xi^2}{2\left(t_p+\Delta t\right)_D}\right)W_{\frac{1}{2},\frac{1}{2}}\left(\frac{\xi^2}{\left(t_p+\Delta t\right)_D}\right)\left[1-\frac{1}{k_D(\xi)}\right]d\xi$$

$$=\frac{\Delta t_D}{\left(t_p+\Delta t\right)_D}\int_1^\infty \left\{\frac{\sqrt{\pi}}{2}\frac{\xi}{\left(t_p+\Delta t\right)_D}\exp\left(-\frac{\xi^2}{2\left(t_p+\Delta t\right)_D}\right)W_{\frac{1}{2},\frac{1}{2}}\left(\frac{\xi^2}{\left(t_p+\Delta t\right)_D}\right)\right\}\left[1-\frac{1}{k_D(\xi)}\right]d\xi$$

$$=\frac{\Delta t_D}{\left(t_p+\Delta t\right)_D}\int_1^\infty \left\{K\left(\xi,\left(t_p+\Delta t\right)_D\right)\right\}\left[1-\frac{1}{k_D(\xi)}\right]d\xi \tag{2.3.59}$$

Using the result above in the Eq. 2.3.57, we obtain:

$$p'_{wD}\left(t_p+\Delta t\right)_D=\frac{1}{2}\frac{\Delta t_D}{\left(t_p+\Delta t\right)_D}-\frac{\Delta t_D}{\left(t_p+\Delta t\right)_D}\int_1^\infty \left\{K\left(\xi,\left(t_p+\Delta t\right)_D\right)\right\}\left[1-\frac{1}{k_D(\xi)}\right]d\xi$$

$$=\frac{\Delta t_D}{\left(t_p+\Delta t\right)_D}\int_1^\infty \left\{K\left(\xi,\left(t_p+\Delta t\right)_D\right)\right\}\frac{1}{k_D(\xi)}d\xi. \tag{2.3.60}$$

The third term in the right-hand side of Eq. 2.3.53 is given by

Reproduced with permission of the copyright owner. Further reproduction prohibited without permission.

$$p'_{wD}(\Delta t_D) = \int_1^\infty K(\xi, \Delta t_D) \frac{1}{k_D(\xi)} d\xi. \tag{2.3.61}$$

Using the derivatives given by Eqs . 2.3.55, 2.3.60 and 2.3.61 in the Eq. 2.3.53, we obtain finally :

$$\tilde{p}'_{sD}(\Delta t_D) = \int_1^\infty K(\xi, \Delta t_D) \frac{1}{k_D(\xi)} d\xi - \frac{\Delta t_D}{(t_p + \Delta t)_D} \int_1^\infty K\left(\xi, (t_p + \Delta t)_D\right) \frac{1}{k_D(\xi)} d\xi \tag{2.3.62}$$

(iii) <u>Buildup after Pseudosteady State Flow</u>

Here, we derive the buildup solution for cases where we assume that the flow period is long enough such that pseudosteady state flow exists at the time of shut in. We use the general buildup superposition Eq. 2.3.45. Consider the second term in the right-hand side of Eq. 2.3.45. It is the pseudosteady state solution which is derived in subsection 2.3.6.2 and can be written as follows :

$$p_{wD}\left[(t_p + \Delta t)_D\right] = 2\pi (t_p + \Delta t)_{AD} + C_{kD}, \tag{2.3.63}$$

where

$$C_{kD} = \frac{2k_{ref}}{(r_e^2 - r_w^2)} \int_{r_w}^{r_e} r \left[\int_{r_w}^{r} \frac{1}{k(r')} \left(\frac{1}{r'} - \frac{r'}{r_e^2} \right) dr' \right] dr. \tag{2.3.64}$$

Eq. 2.3.64 is derived in subsection 2.3.6.2.

The derivative of Eq. 2.3.63 with respect to the natural log of Δt_D yields,

Reproduced with permission of the copyright owner. Further reproduction prohibited without permission.

$$p'_{wD}\left[\left(t_p+\Delta t\right)_D\right]=\frac{dp_{wD}\left[\left(t_p+\Delta t\right)_D\right]}{d\ln\Delta t_D}=2\pi\frac{r_w^2}{A}\Delta t_D, \tag{2.3.65}$$

where $A=\pi r_e^2$.

Using Eqs. 2.3.61 and 2.3.65 in the general pressure buildup derivative, Eq. 2.3.53, we finally obtain:

$$\bar{p}'_{sD}(\Delta t_D)=\int_1^\infty K(\xi,\Delta t_D)\left[\frac{1}{k_D(\xi)}\right]d\xi \;-\; \frac{2r_w^2}{r_e^2}\Delta t_D. \tag{2.3.66}$$

- **Remarks**

Eqs. 2.3.62 and 2.3.66, for buildup after a transient and pseudosteady state flow, respectively, represent the approximation of $\bar{p}'_{sD}=dp'_{sD}/d\ln\Delta t_D$ obtained by using Oliver's approximate solution for all transient drawdown dimensionless pressure terms in Eq. 2.3.53. Later, in Chapter III, we will consider a method to modify Eqs. 2.3.62 and 2.3.66 by using an appropriate expression for the reference permeability in the dimensionless time terms used in the kernel function.

2.3.4 Numerical Solution

A numerical solution to the IBVP given by Eqs. 2.3.1 through 2.3.4 is a particular solution to the IBVP for an areally heterogeneous reservoir $k=k(r,\theta)$ with no permeability variation in θ direction. In fact, our areal (r,θ) simulator becomes a pure radial simulator by considering only one gridblock in θ direction.

Here, the numerical solution is validated using the exact analytical drawdown solutions for homogeneous, and multicomposite reservoirs available in the literature. For all runs we use a equally logarithmic-spaced time interval and forty points per log cycle.

Reproduced with permission of the copyright owner. Further reproduction prohibited without permission.

The simulator reproduces pressure and pressure derivatives for the above reservoir models with high accuracy; thus, substantiating the reliability of our numerical model.

Case (a) Homogeneous Reservoir

We consider a homogeneous reservoir producing at constant sandface rate. The basic parameters are given in Table 2.3.2.

Table 2.3.2 Homogeneous Reservoir; Drawdown Reservoir/Well System Parameters			
$k = 40$ md	$h = 20$ ft	$\mu = 1.0$ cp	$r_w = 0.3$ ft
	$\phi = 0.20$	$c_t = 10\times10^{-6}$ psi^{-1}	$q = 300.0$ rb/d
	$p_i = 6000$ psi	$r_e = 5{,}000$ ft	

Using these data, we ran our simulator for the time period from 10^{-6} up to 30 days and compared wellbore pressures and pressure derivatives with those obtained from two analytical solutions: the rigorous finite-wellbore radius solution, which is obtained by inversion of Eq. 2.2.19 from Laplace space using the Stehfest[26] algorithm, and the approximate line-source solution given by Eq. 2.2.24a. There is an excellent agreement in terms of pressure and pressure derivative over almost the full range of time between the simulator and the rigorous finite-wellbore radius analytical solution results, shown, respectively, in Figs. 2.3.3 and 2.3.4. The close agreement starts at about 10^{-5} days (0.9 seconds) and extends over the rest of the simulated time period. At very early times (about one to a few seconds in this example), it is well known that pressure is not a linear function of natural logarithm of time, even without wellbore storage and skin effects. This is clearly seen in Fig. 2.3.4. We present in Fig. 2.3.5 the dimensionless pressure

Reproduced with permission of the copyright owner. Further reproduction prohibited without permission.

Reproduced with permission of the copyright owner. Further reproduction prohibited without permission.

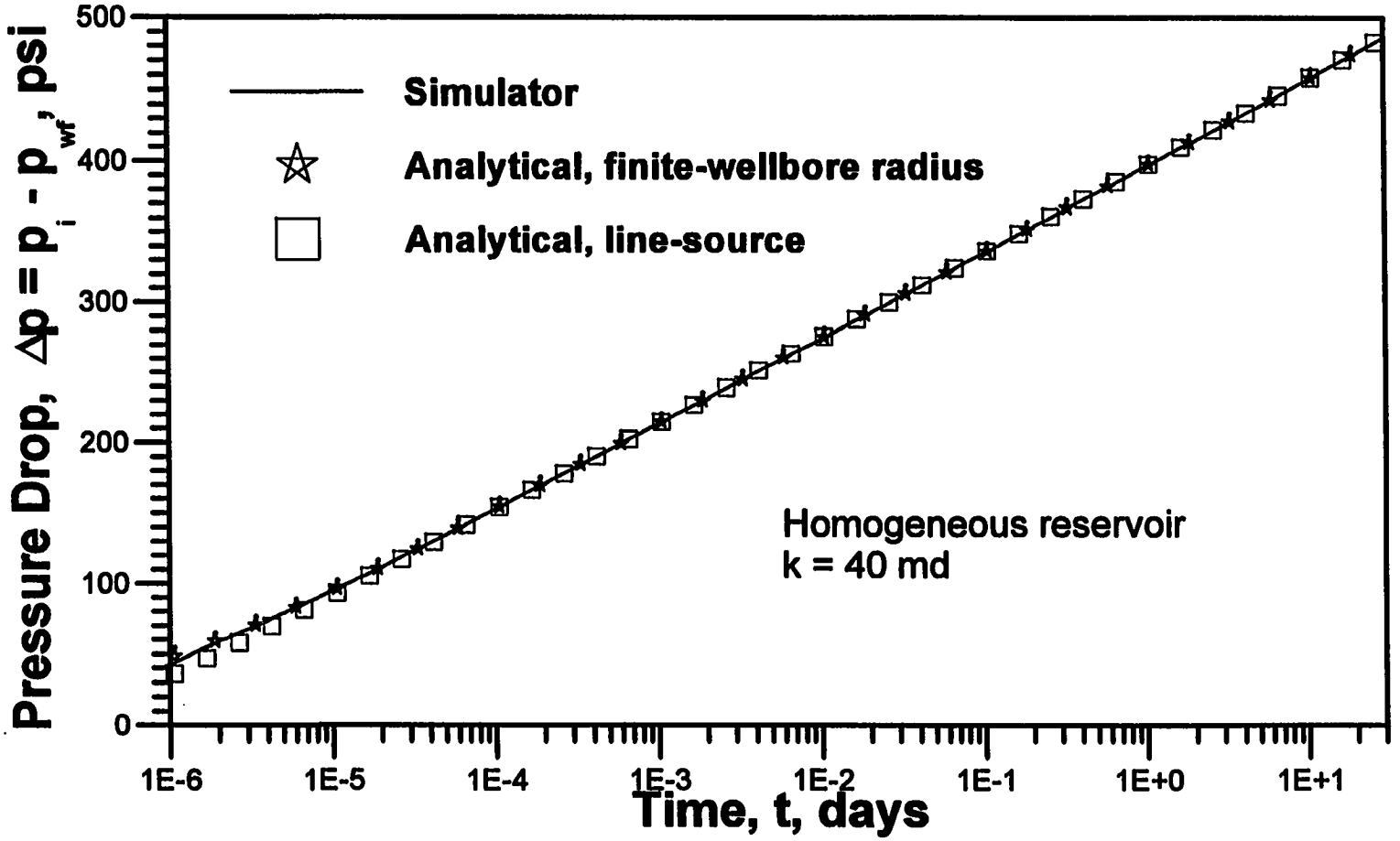

Fig. 2.3.3 - Comparison of pressure drop: simulated versus analytical drawdown results; homogeneous reservoir.

Reproduced with permission of the copyright owner. Further reproduction prohibited without permission.

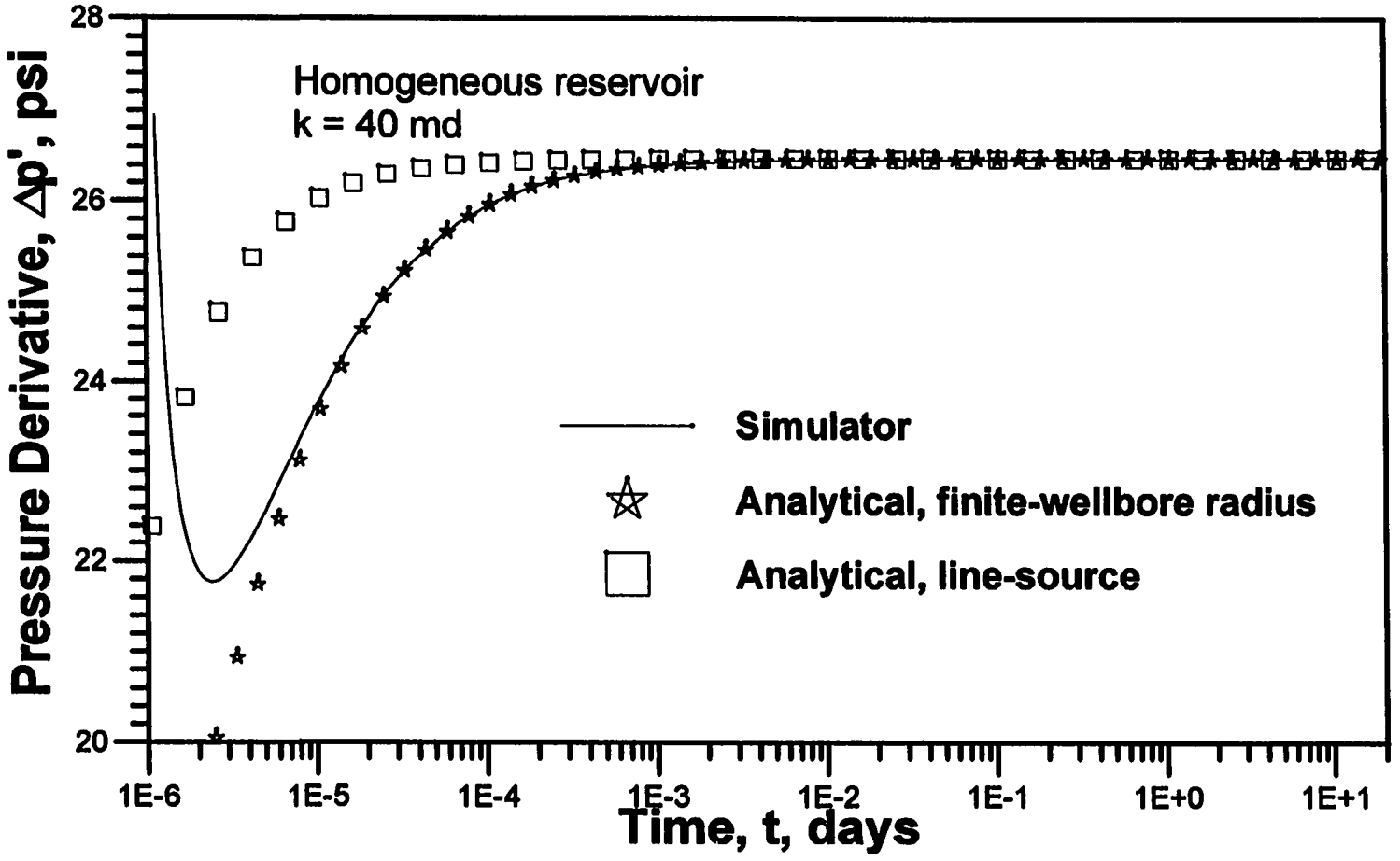

Fig. 2.3.4 - Comparison of pressure derivatives: simulated versus analytical drawdown results; homogeneous reservoir.

Reproduced with permission of the copyright owner. Further reproduction prohibited without permission.

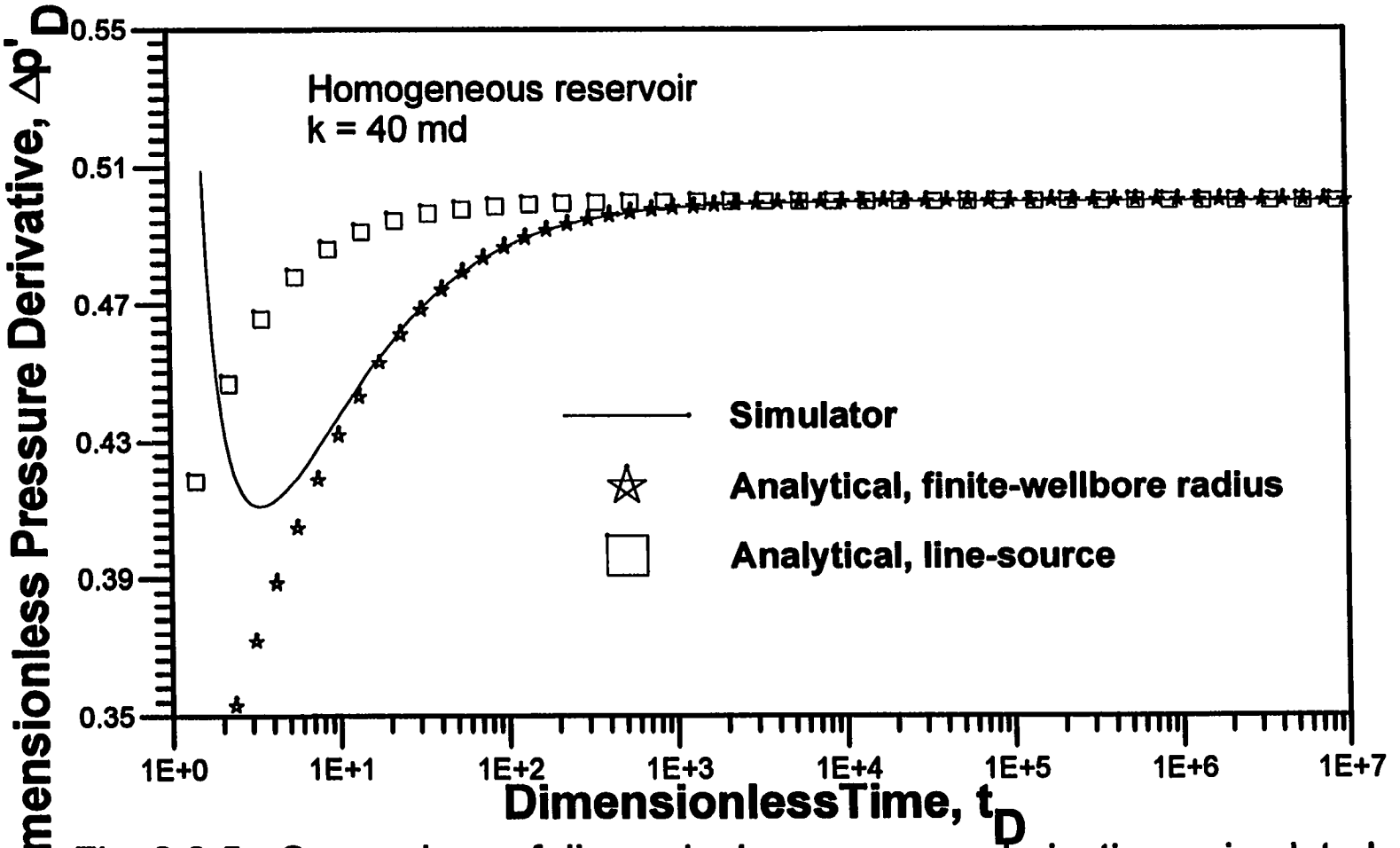

Fig. 2.3.5 - Comparison of dimensionless pressure derivatives: simulated versus analytical drawdown results; homogeneous reservoir.

derivatives. Notice that for $t_D > 100$ the finite-well-radius analytical solution and the simulator results are in good agreement. Typically, $t_D = 100$ corresponds to a few seconds (6 seconds in this case).

Case (b) Multicomposite, 5-Zone Reservoir

In this case, we compare the results of our simulator with the multicomposite analytical solution presented by Abbaszadeh and Kamal[32] for a 5-zone multicomposite reservoir. The principal parameters are summarized in Table 2.3.3. Here, r_j and k_j denote, respectively, the outer radius and the permeability of zone j.

Table 2.3.3

5-Zone Multicomposite Reservoir; Drawdown

Reservoir/Well System Parameters

$k_1 = 20$ md	$r_1 = 32$ ft	$h = 20$ ft	$\mu = 1.0$ cp	$r_w = 0.3$ ft
$k_2 = 30$ md	$r_2 = 151$ ft	$\phi = 0.20$	$c_t = 10\times10^{-6}$ psi^{-1}	$q = 300$ rb/d
$k_3 = 10$ md	$r_3 = 534$ ft	$p_i = 6000$ psi		
$k_4 = 18$ md	$r_4 = 1{,}055$ ft			
$k_5 = 40$ md	$r_e = 5{,}000$ ft			

In Figs. 2.3.6 and 2.3.7, respectively, the pressure and pressure derivative are shown for a transient flow period of duration 27 days. We observe very good agreement between simulated and analytical results. These results again confirm the reliability and accuracy of our simulator.

Reproduced with permission of the copyright owner. Further reproduction prohibited without permission.

Reproduced with permission of the copyright owner. Further reproduction prohibited without permission.

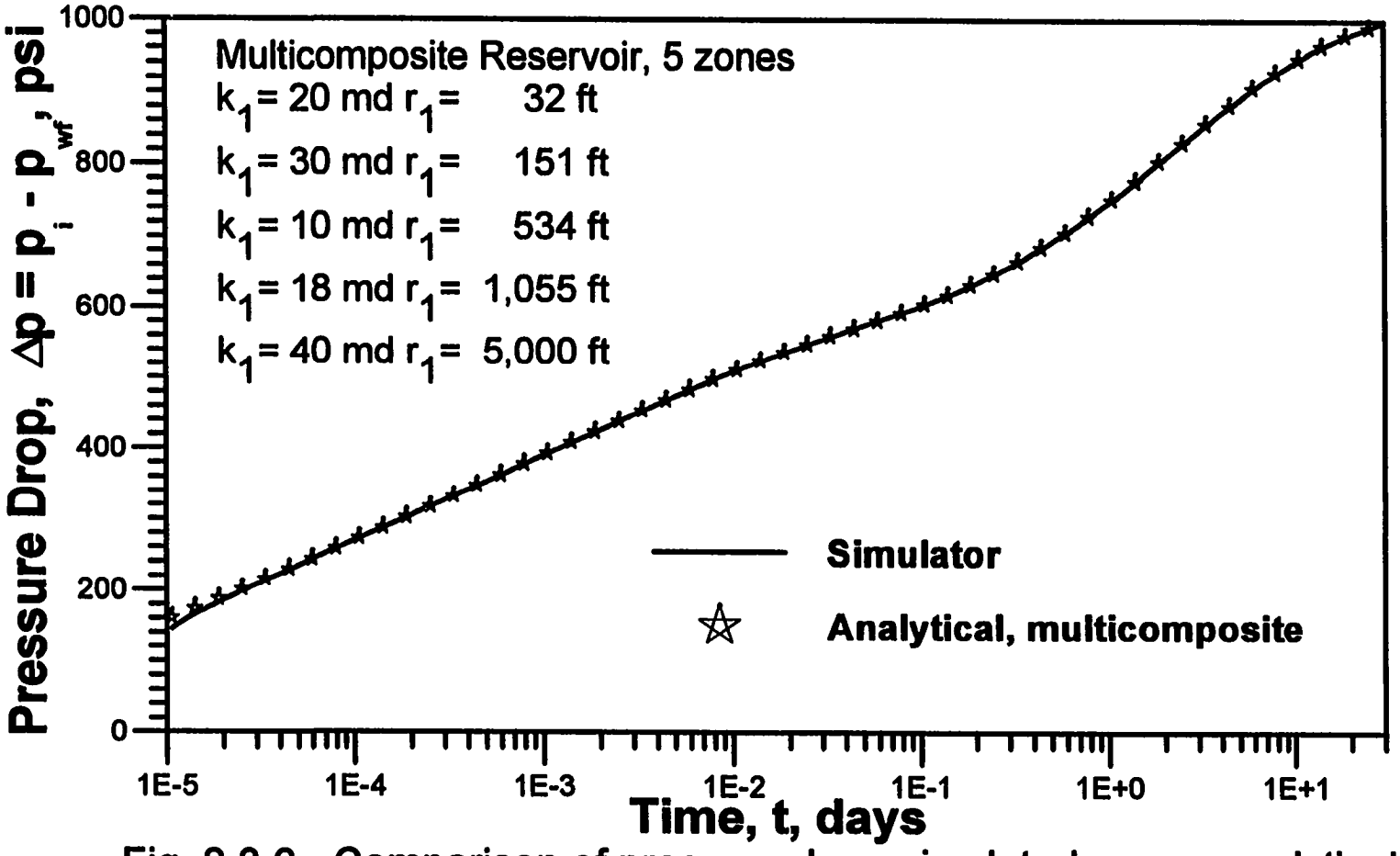

Fig. 2.3.6 - Comparison of pressure drop: simulated versus analytical drawdown results; 5-zone multicomposite reservoir.

Reproduced with permission of the copyright owner. Further reproduction prohibited without permission.

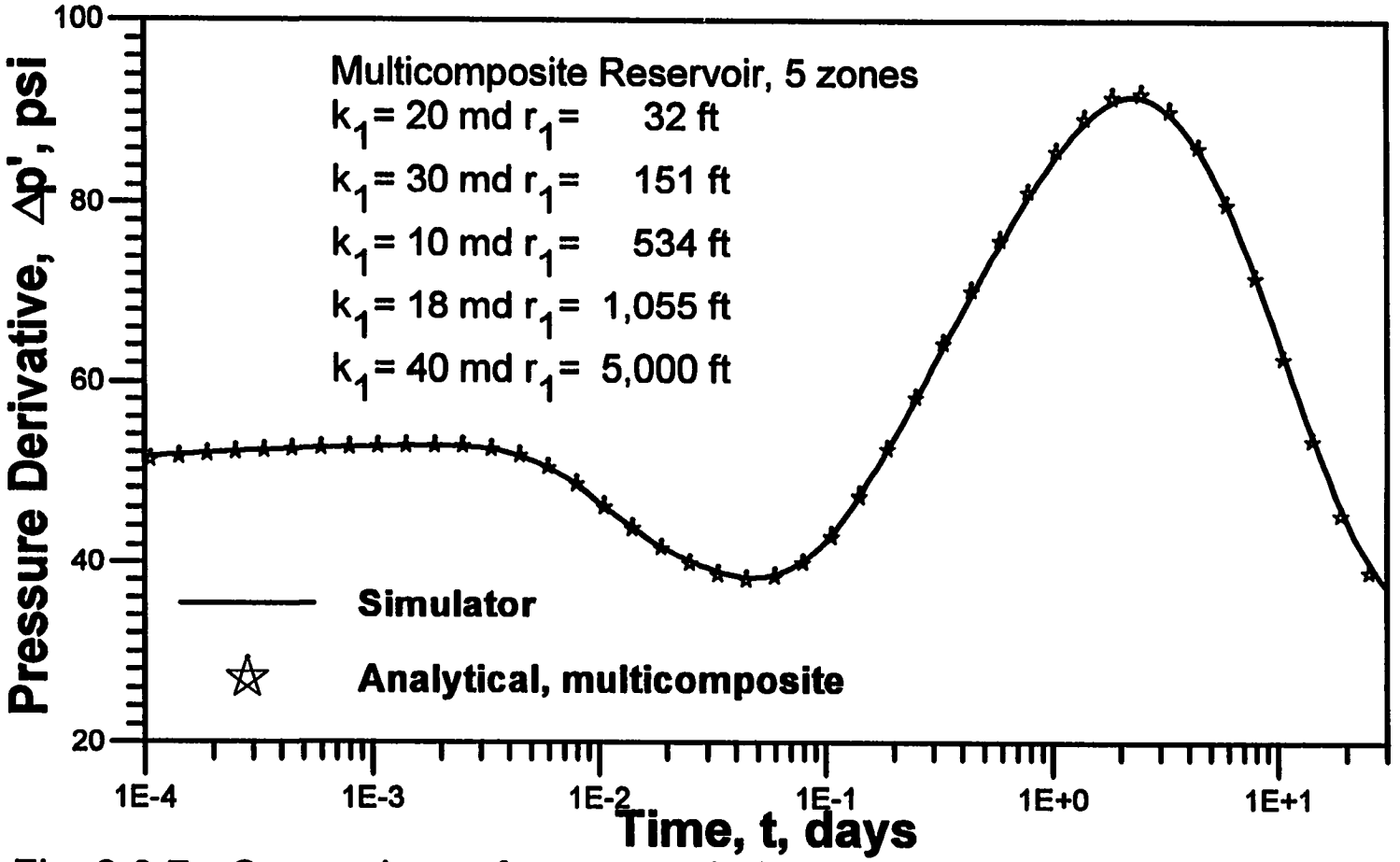

Fig. 2.3.7 - Comparison of pressure derivative: simulated versus analytical drawdown results; 5-zone multicomposite reservoir.

Case (c) Multicomposite, 100-Zones Reservoir

Our simulator is based on a finite-difference approach. The basic finite-difference equation (see Appendix A) involves interblock transmissibilities that are obtained using a weighted harmonic average of the transmissibilities of radially adjacent gridblocks. Since we consider constant reservoir thickness and fluid viscosity, we can say that at the interface between two blocks, we have a weighted harmonic average permeability given by

$$k_{i+1/2} = \frac{k_i k_{i+1} \ln(r_{i+1}/r_i)}{k_i \ln(r_{i+1}/r_{i+1/2}) + k_{i+1} \ln(r_{i+1/2}/r_i)}. \tag{2.3.67}$$

This harmonic weighted average interblock permeability is derived based on steady state flow between contiguous gridblocks i and $i+1$ (see Ref. 33). For a heterogeneous reservoir, with permeability changing from gridblock to gridblock, it is unclear whether our finite-difference simulator, which uses Eq. 2.3.67, is sufficiently accurate to handle transient flow. Another question of high interest is whether the pressure response of a heterogeneous reservoir with a permeability distribution such that the interblock permeabilities are all equal will be identical to the analogous homogeneous reservoir pressure response.

We now address these questions. We generate a piecewise constant permeability distribution, shown in Fig. 2.3.8, with constant interblock permeability of 109 md. We use a fixed 100-gridblock system, assign the value 100 md to the first gridblock, and use Eq. 2.3.67 to calculate the permeability of each gridblock keeping $k_{i+1/2}$ fixed at 109 md. Other pertinent data are shown in Table 2.3.4.

We run this case for 1000 days. The pressures and pressure derivatives obtained with our simulator are then compared with those calculated with the *multicomposite*

Reproduced with permission of the copyright owner. Further reproduction prohibited without permission.

analytical solution by Abbaszadeh and Kamal[32]. While the analytical solution uses the permeability values in each radial zone, the simulator uses the interblock permeability values. The excellent agreement between simulated and analytical results, shown in Figs. 2.3.9 and 2.3.10, illustrates again the accuracy and reliability of our finite-difference simulator. Also, we observe that indeed the wellbore pressure follows the behavior obtained for a homogeneous reservoir. The permeability calculated from the slope of the semilog plot of pressure, which is directly obtained from Fig. 2.3.10 as 16.2 psi, gives exactly the value of 109 md for the "homogeneous" permeability which is the value of $k_{i+1/2}$ for all $i \geq 1$.

These results show that the ***averaging process of permeability estimation from well test data under radial flow condition is harmonic in nature***. They also demonstrate that more than one permeability distribution can yield the same wellbore response to a given flow rate history, clearly showing the nonuniqueness of the inverse problem, which is to obtain the permeability distribution from pressure data.

Table 2.3.4

100-Zone Multicomposite, Constant Interblock Permeability Reservoir; Drawdown

Reservoir/Well System Parameters

$k_{i+1/2} = 109$ md	$h = 20$ ft	$\mu = 1.0$ cp	$r_w = 0.3$ ft
	$\phi = 0.20$	$c_t = 10\times10^{-6}$ psi^{-1}	$q = 500.$ RB/D
	$p_i = 6000$ psi	$r_e = 170{,}000$ ft	

Reproduced with permission of the copyright owner. Further reproduction prohibited without permission.

Reproduced with permission of the copyright owner. Further reproduction prohibited without permission.

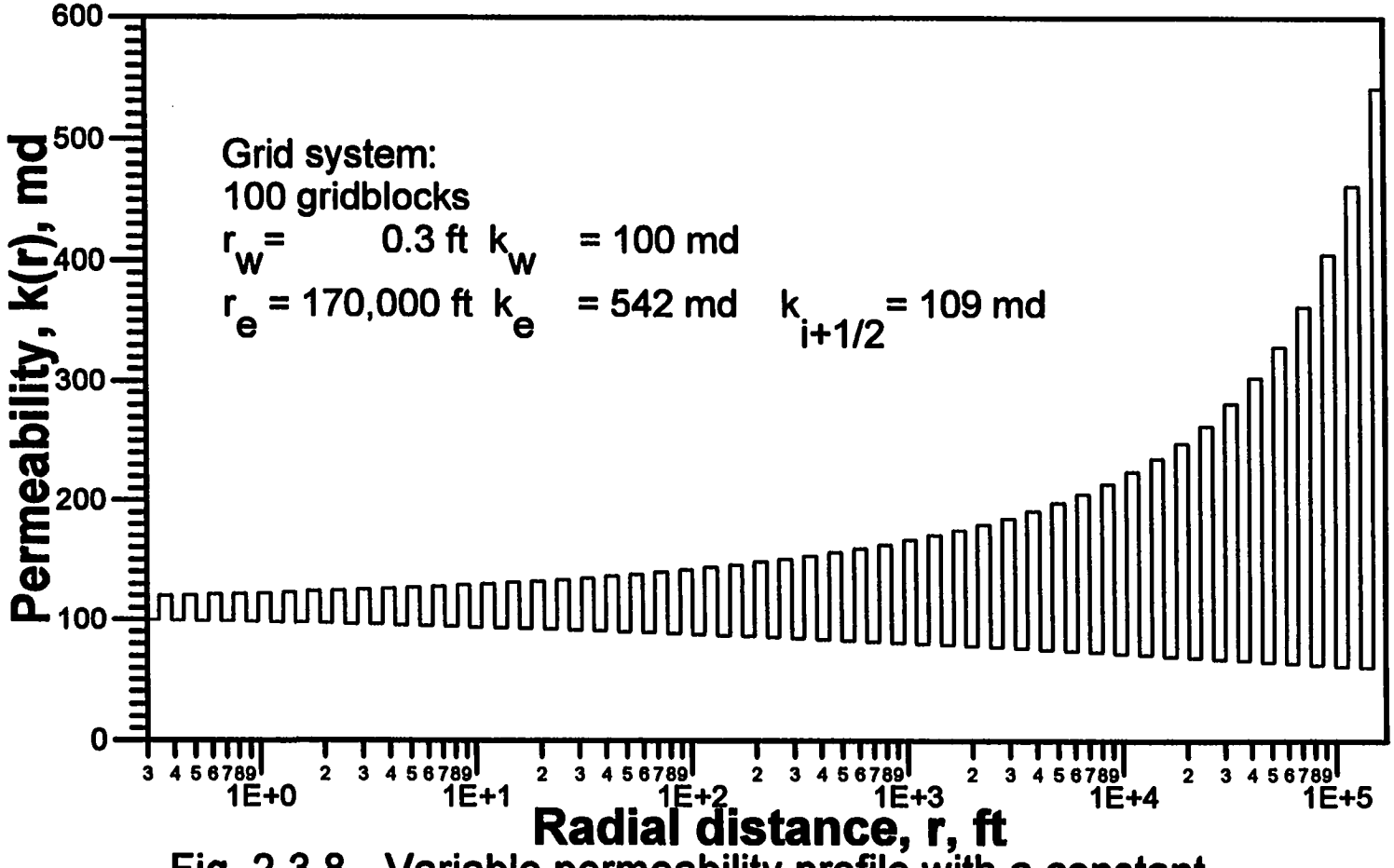

Fig. 2.3.8 - Variable permeability profile with a constant harmonic average permeability at gridblock interfaces.

Reproduced with permission of the copyright owner. Further reproduction prohibited without permission.

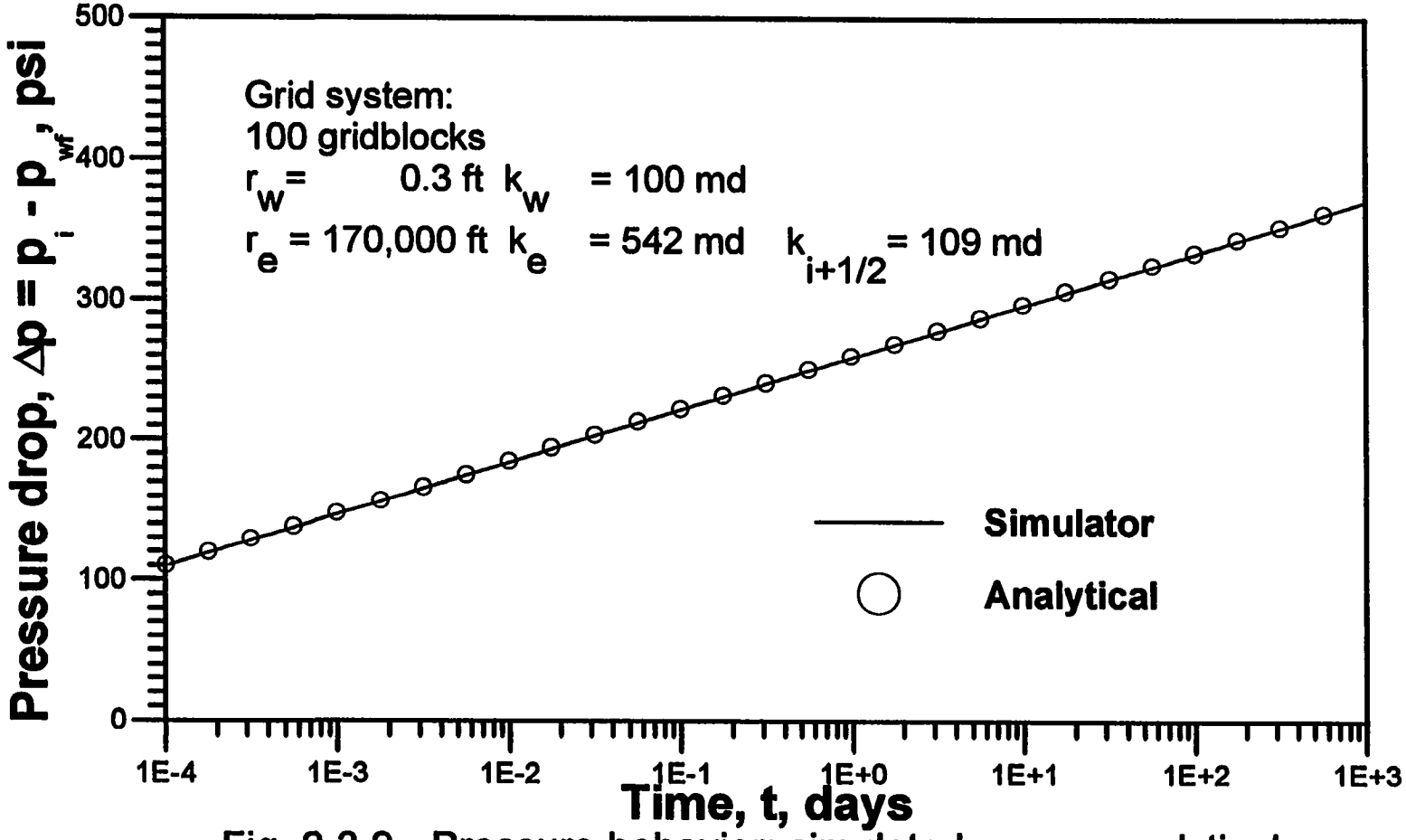

Fig. 2.3.9 - Pressure behavior; simulated versus analytical multicomposite drawdown results.

Reproduced with permission of the copyright owner. Further reproduction prohibited without permission.

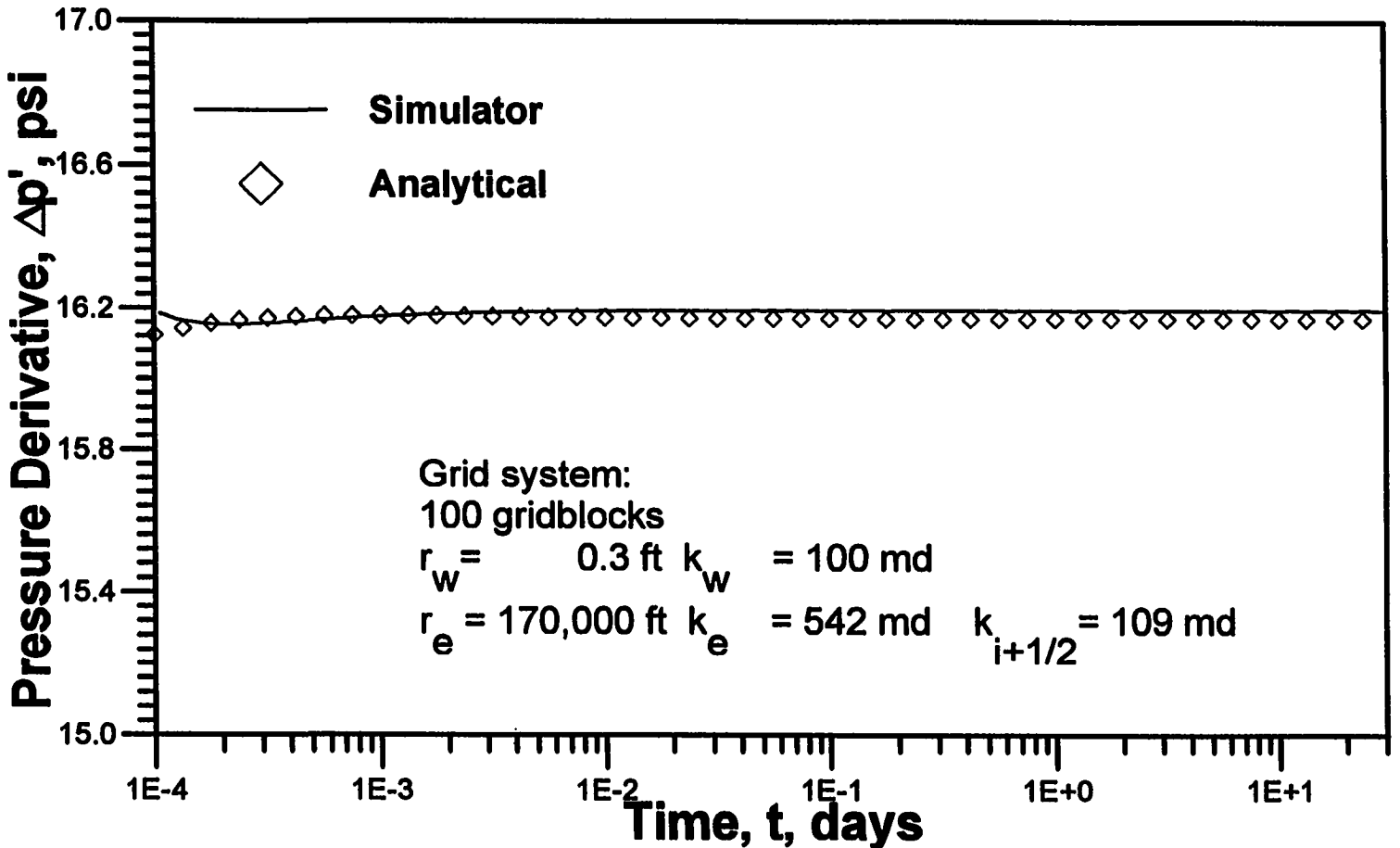

Fig. 2.3.10 - Pressure derivative behavior; simulated versus analytical multicomposite drawdown results.

2.3.5 Comparison of Solutions

In this section we compare the four analytical solutions presented before with the simulator results. We use the reservoir/well system parameters presented in Table 2.3.3. First we compare pressures obtained with the solutions based on the flow rate profile assumptions, Eqs. 2.3.27 and 2.3.33, respectively, curves labeled QD2 and QD1 in Fig. 2.3.11. The agreement with the simulator results is reasonable. However, when we compared pressure derivatives computed, respectively, using Eqs. 2.3.28 and 2.3.34, shown in Fig. 2.3.12, the agreement is not nearly as reasonable as for pressure. These two solutions based on rate profile, although interesting in the sense that they indicate the region of the reservoir that is contributing to the wellbore pressure and pressure derivative, were not used in our work due to the lack of accuracy in terms of pressure derivatives.

In Fig. 2.3.13, we compare the pressure derivative solution from Oliver[16] and our generalized pressure derivative solution, GPDS, given by Eqs. 2.3.22 and 2.3.44b, respectively. We clearly see that the GPDS shows a nearly perfect match with simulator results, whereas, Oliver's results do not agree as well. This suggests that the solution developed in this work represents an improvement over Oliver's solution when considering large variations in permeability.

Reproduced with permission of the copyright owner. Further reproduction prohibited without permission.

Reproduced with permission of the copyright owner. Further reproduction prohibited without permission.

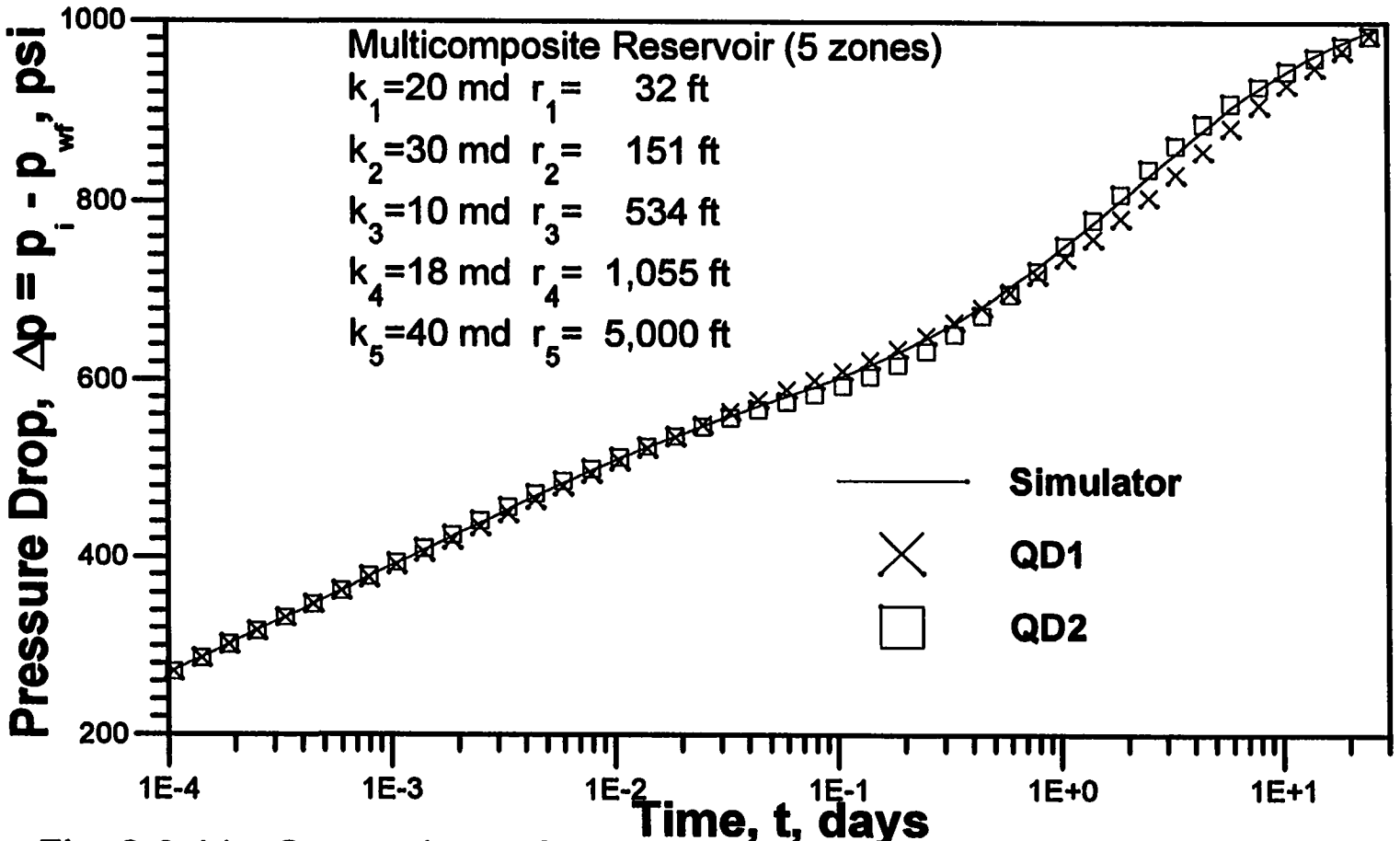

Fig. 2.3.11 - Comparison of pressure drop; simulated versus those computed with the rate-assumed solutions; forward problem.

Reproduced with permission of the copyright owner. Further reproduction prohibited without permission.

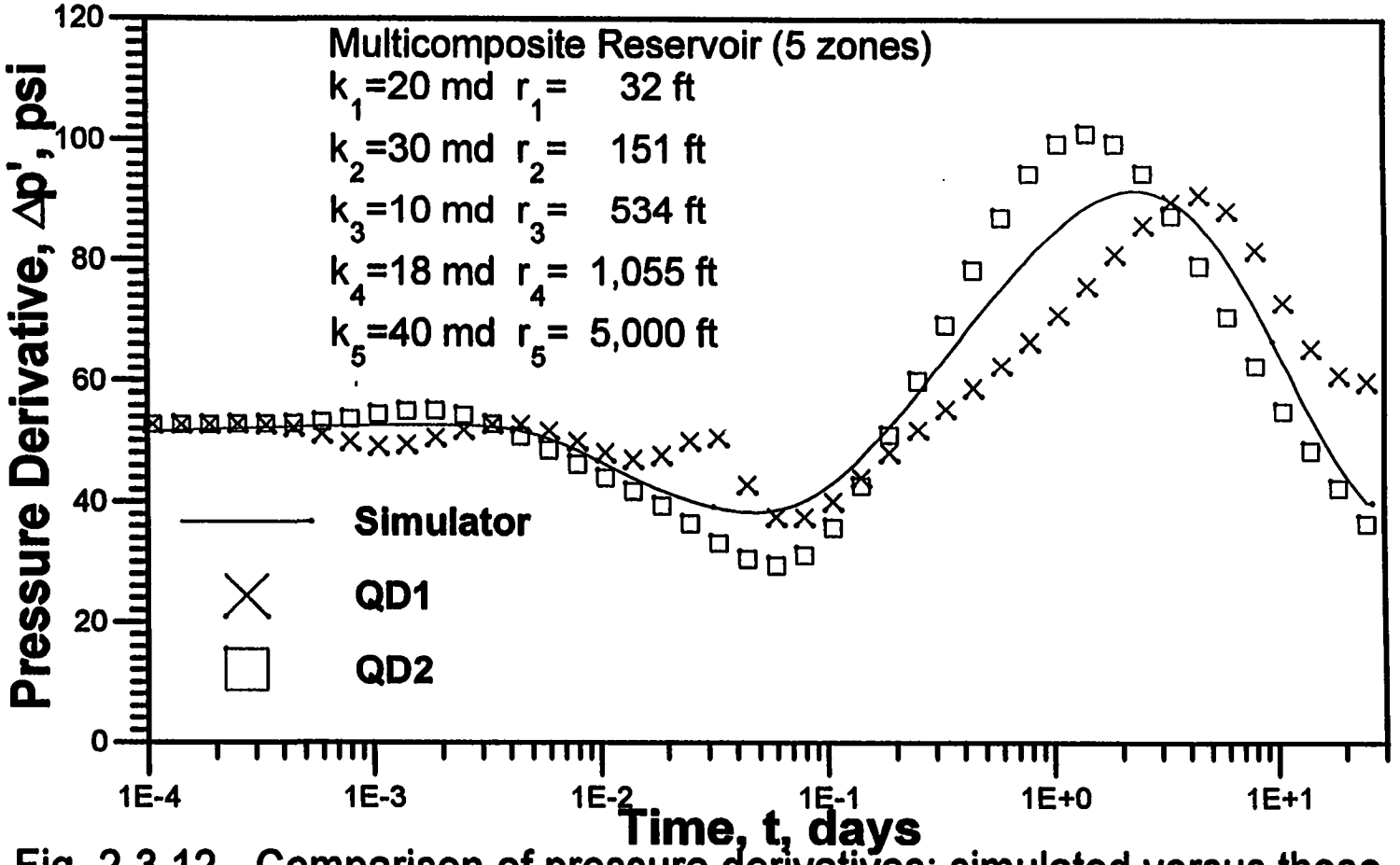

Fig. 2.3.12 - Comparison of pressure derivatives; simulated versus those computed with the rate-assumed solutions; forward problem.

Reproduced with permission of the copyright owner. Further reproduction prohibited without permission.

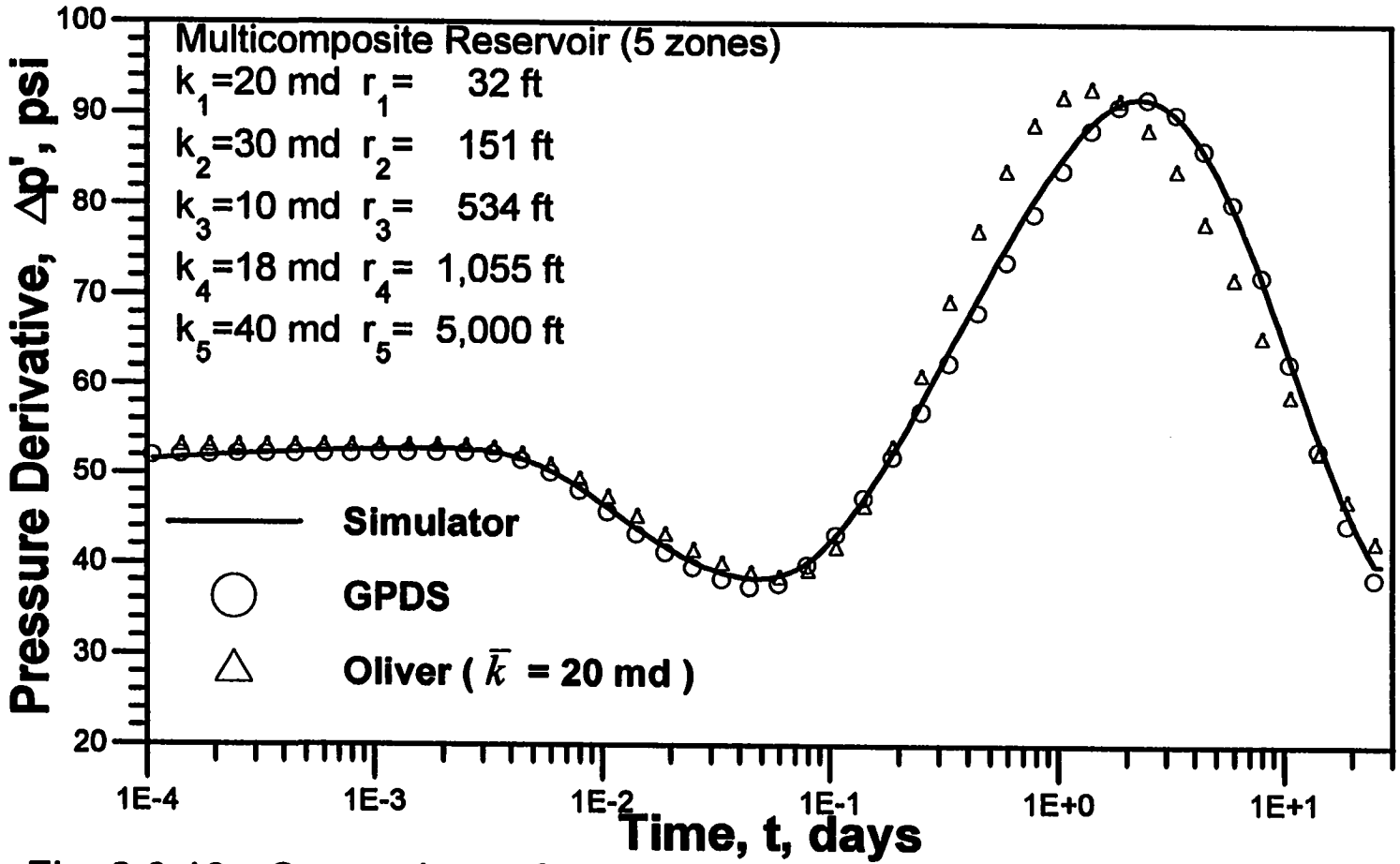

Fig. 2.3.13 - Comparison of pressure derivatives; simulated versus those from the approximate solution by Oliver and this work.

2.3.6 Long-Time Solutions

We consider a radially heterogeneous reservoir producing at a constant rate through a well under outer-boundary dominated flow, either a steady state or pseudosteady regime. We refer to solutions to these problems as long-time drawdown solutions.

The basic mathematical IBVP can expressed as follows :

- Governing PDE:

$$\frac{C_1}{r}\frac{\partial}{\partial r}\left[r\frac{k(r)}{\mu}\frac{\partial p}{\partial r}\right]=\phi c_t\frac{\partial p}{\partial t} \tag{2.3.68}$$

where $C_1 = 0.006328$ for t in days.

- Initial condition:

$$p(r,t)=p_i \text{ for } t=0 \tag{2.3.69}$$

- Inner boundary condition (at r_w):

$$[q]_{r_w}=\left[\frac{hr}{141.2}\frac{k(r)}{\mu}\frac{\partial p(r,t)}{\partial r}\right]_{r_w} \tag{2.3.70}$$

- Outer boundary condition:

(i) closed outer boundary $$\left[\frac{\partial p}{\partial r}\right]_{r_e}=0 \tag{2.3.71}$$

(ii) constant pressure outer boundary $$p(r_e,t)=p_e \tag{2.3.72}$$

2.3.6.1 Steady State Solution

During steady state flow there is no pressure change with time anywhere in the reservoir, i.e.,

Reproduced with permission of the copyright owner. Further reproduction prohibited without permission.

$$\frac{\partial p}{\partial t}=\frac{\partial \bar{p}}{\partial t}=0. \tag{2.3.73}$$

Therefore, in this case, the governing PDE, Eq. 2.3.68, reduces to

$$\frac{C_1}{r}\frac{\partial}{\partial r}\left(rk(r)\frac{\partial p}{\partial r}\right)=0. \tag{2.3.74}$$

Multiplying by $\frac{r}{C_1}$ and integrating this equation with respect to r over the interval $[r_w, r]$ we have:

$$0=\left[r'k(r')\frac{\partial p}{\partial r'}\right]_{r_w}^{r}=rk(r)\frac{\partial p}{\partial r}-\left[rk(r)\frac{\partial p}{\partial r}\right]_{r_w}. \tag{2.3.75}$$

Using the inner boundary condition, Eq. 2.3.70, into Eq. 2.3.75 and rearranging we obtain

$$rk(r)\frac{\partial p}{\partial r}=\frac{141.2q\mu}{h}. \tag{2.3.76}$$

Dividing by $rk(r)$ and integrating once more over the interval $[r_w, r]$, we finally obtain

$$p(r)-p(r_w)=\frac{141.2q\mu}{h}\int_{r_w}^{r}\frac{1}{r'k(r')}dr'. \tag{2.3.77}$$

This is the ***general steady state equation*** for a radially heterogeneous reservoir, with permeability $k=k(r)$. This equation was first presented by Muskat[4] in 1937. Eq. 2.3.77 evaluated at the external radius, r_e, and using standard nomenclature, yields

$$p_e-p_{wf}=\frac{141.2q\mu}{h}\int_{r_w}^{r_e}\frac{1}{r'k(r')}dr'. \tag{2.3.78}$$

For constant permeability Eq. 2.3.78 reduces to the well-known homogeneous steady state equation

Reproduced with permission of the copyright owner. Further reproduction prohibited without permission.

$$p_e - p_{wf} = \frac{141.2 q \mu}{k h} \ln \frac{r_e}{r_w}. \tag{2.3.79}$$

2.3.6.2 Pseudosteady State Solution

The pseudosteady state flow period is characterized by a constant pressure drop with time which is obtained from material balance as

$$\frac{\partial p}{\partial t} = \frac{\partial \bar{p}}{\partial t} = -\frac{q(5.615)}{c_t V_p} = -\frac{q(5.615)}{c_t \pi \left(r_e^2 - r_w^2\right) h \phi}. \tag{2.3.80}$$

Assuming that the wellbore radius, r_w, is negligible with respect to the reservoir external radius, r_e, using Eq. 2.3.80 in Eq. 2.3.68 and performing the obvious simplifications, we obtain the following governing PDE for pseudosteady state flow:

$$C_1 \frac{\partial}{\partial r}\left[\frac{rk(r)}{\mu}\frac{\partial p}{\partial r}\right] = -\frac{5.615 q r}{\pi r_e^2 h}. \tag{2.3.81}$$

Integrating this equation with respect to r over the interval $[r_w, r]$ yields

$$C_1\left[\frac{rk(r)}{\mu}\frac{\partial p}{\partial r}\right] - C_1\left[\frac{rk(r)}{\mu}\frac{\partial p}{\partial r}\right]_{r_w} = -\frac{5.615 q}{\pi r_e^2 h}\frac{1}{2}\left(r^2 - r_w^2\right). \tag{2.3.82}$$

Recalling that

$$C_1 = \left(1.127 \times 10^{-3}\right)(5.615), \tag{2.3.83}$$

using the inner boundary condition, Eq. 2.3.70, in Eq. 2.3.82 and simplifying the resulting equation we obtain

$$C_1\left[rk(r)\frac{\partial p}{\partial r}\right] = \frac{5.615 q \mu}{2\pi h}\left[1 - \left(\frac{r^2}{r_e^2} - \frac{r_w^2}{r_e^2}\right)\right] \cong \frac{5.615 q \mu}{2\pi h}\left(1 - \frac{r^2}{r_e^2}\right). \tag{2.3.84}$$

Reproduced with permission of the copyright owner. Further reproduction prohibited without permission.

Dividing this equation by $C_1 rk(r)$ and integrating over r from r_w to r we obtain after simplifications the ***general pseudosteady state equation for a radially heterogeneous reservoir***, $k = k(r)$, which is:

$$p(r) - p_{wf} = \frac{141.2q\mu}{h} \int_{r_w}^{r} \frac{1}{k(r')} \left(\frac{1}{r'} - \frac{r'}{r_e^2} \right) dr. \tag{2.3.85}$$

The equation 2.3.85 reduces to the homogeneous form (see Dake[34]) for constant permeability, $k(r) = k_{\text{hom}} = const$. Thus, it becomes approximately

$$p(r) - p_{wf} = \frac{141.2q\mu}{k_{\text{hom}} h} \left[\ln\left(\frac{r}{r_w} \right) - \frac{r^2}{2r_e^2} \right], \tag{2.3.86}$$

which evaluated at r_e takes the form of

$$p_e - p_{wf} = \frac{141.2q\mu}{k_{\text{hom}} h} \left[\ln\left(\frac{r_e}{r_w} \right) - \frac{1}{2} \right]. \tag{2.3.87}$$

(i) <u>Average Reservoir Pressure</u>

Of great importance is the determination of average reservoir pressure, $\overline{p}$, at a fixed time, during the pseudosteady state regime. The average reservoir pressure is defined as the volumetric weighted arithmetic average of the pressure distribution over the entire reservoir which can be expressed as :

Reproduced with permission of the copyright owner. Further reproduction prohibited without permission.

$$\overline{p}=\frac{1}{V}\int_V p dV=\frac{\int_{r_w}^{r_e} p(r)2\pi rhdr}{\int_{r_w}^{r_e} 2\pi rhdr}=\frac{2}{r_e^2-r_w^2}\int_{r_w}^{r_e} p(r)rdr, \tag{2.3.88}$$

where we have assumed a constant reservoir thickness, h. Solving Eq. 2.3.85 for $p(r)$ and substituting the resulting equation into Eq. 2.3.88 we can write :

$$\overline{p}=\frac{2}{r_e^2-r_w^2}\int_{r_w}^{r_e} r\left[p_{wf}+\frac{141.2q\mu}{h}\int_{r_w}^{r}\frac{1}{k(r')}\left(\frac{1}{r'}-\frac{r'}{r_e^2}\right)dr'\right]dr. \tag{2.3.89}$$

Developing the right-hand side and simplifying the resulting equation, we obtain the final ***general average reservoir pressure equation for a radially heterogeneous reservoir***, at a time $t \geq t_{pss}$,

$$\overline{p}=p_{wf}+\left(\frac{2}{r_e^2-r_w^2}\right)\frac{141.2q\mu}{h}\int_{r_w}^{r_e} r\left[\int_{r_w}^{r}\frac{1}{k(r')}\left(\frac{1}{r'}-\frac{r'}{r_e^2}\right)dr'\right]dr. \tag{2.3.90}$$

This equation is general. If the reservoir is homogeneous, i.e., $k(r)=k_{\text{hom}}=const$, then it can easily be shown that it reduces to the well-known homogeneous pseudosteady state equation in terms of average pressure

$$\overline{p}=p_{wf}+\frac{141.2q\mu}{k_{\text{hom}}h}\left(\ln\frac{r_e}{r_w}-\frac{3}{4}\right). \tag{2.3.91}$$

Reproduced with permission of the copyright owner. Further reproduction prohibited without permission.

(ii) Equivalent Homogeneous Pseudosteady State Permeability

One parameter of interest that can be obtained from the last two equations is the equivalent pseudosteady state permeability, k_{eq}, which we define as the permeability of the "equivalent" homogeneous reservoir that for a given flow rate yields same pressure drop, $\bar{p}-p_{wf}$, as the corresponding radially heterogeneous reservoir. Substituting k_{eq} for k_{hom} in Eq. 2.3.91, equating the pressure drops and solving for k_{eq}, we derive the following expression

$$k_{eq}=\left(\ln\frac{r_e}{r_w}-\frac{3}{4}\right)\left\{\left(\frac{2}{r_e^2-r_w^2}\right)\int_{r_w}^{r_e} r\left[\int_{r_w}^{r}\frac{1}{k(r')}\left(\frac{1}{r'}-\frac{r'}{r_e^2}\right)dr'\right]dr\right\}^{-1}. \qquad (2.3.92)$$

(iii) Pseudosteady State Dimensionless Pressure Solution

Now we develop the dimensionless form of the pseudosteady state equation for radially heterogeneous reservoirs. We define:

$$\bar{p}_D=\frac{k_{ref}h}{141.2q\mu}(p_i-\bar{p}), \qquad (2.3.93)$$

$$p_{wD}=\frac{k_{ref}h}{141.2q\mu}(p_i-p_{wf}), \qquad (2.3.94)$$

$$t_D=\frac{C_1k_{ref}t}{\phi\mu c_t r_w^2}, \qquad (2.3.95)$$

Reproduced with permission of the copyright owner. Further reproduction prohibited without permission.

$$t_{AD} = \frac{C_1 k_{ref} t}{\phi \mu c_t A} = t_D \frac{r_w^2}{A}, \tag{2.3.96}$$

where k_{ref} is an arbitrary reference value of permeability and $A = \pi r_e^2$ is the reservoir drainage area.

Multiplying Eq. 2.3.90 by (-1) and adding p_i to both sides we have,

$$p_i - \bar{p} = p_i - p_{wf} - \left(\frac{2}{r_e^2 - r_w^2}\right)\frac{141.2 q\mu}{h}\int_{r_w}^{r_e} r\left[\int_{r_w}^{r} \frac{1}{k(r')}\left(\frac{1}{r'} - \frac{r'}{r_e^2}\right)dr'\right]dr. \tag{2.3.97}$$

Multiplying Eq. 2.3.97 by $\left[\frac{k_{ref} h}{141.2 q\mu}\right]$, using the definitions given by Eqs. 2.3.93 through 2.3. 96, and rearranging, we obtain

$$p_{wD} = 2\pi t_{AD} + k_{ref}\left(\frac{2}{r_e^2 - r_w^2}\right)\int_{r_w}^{r_e} r\left[\int_{r_w}^{r} \frac{1}{k(r')}\left(\frac{1}{r'} - \frac{r'}{r_e^2}\right)dr'\right]dr. \tag{2.3.98}$$

This is the ***general dimensionless pressure drawdown equation for a radially heterogeneous reservoir producing under pseudosteady state condition.***

2.3.6.3 <u>Stabilized Inflow Performance Equation</u>

Reproduced with permission of the copyright owner. Further reproduction prohibited without permission.

The inflow performance relationship is basically the flow rate per unit pressure drop that can be delivered from a well producing a reservoir under pseudosteady state condition. It is characterized by the so-called productivity index, PI, which is defined by

$$PI = \frac{q_{sc}}{\bar{p} - p_{wf}}, \tag{2.3.99}$$

where q_{sc} is the surface flow rate in STB/D, i.e., $q_{sc} = q / B$, where B is the formation volume factor, and PI is in STB/D/psi.

The *PI for a radially heterogeneous reservoir* can be obtained directly from Eqs. 2.3.99 and 2.3.90 which yields

$$PI = \frac{q_{sc}}{\bar{p} - p_{wf}} = \frac{h}{141.2\, B\, \mu} \left\{ \left(\frac{2}{r_e^2 - r_w^2} \right) \int_{r_w}^{r_e} r \left[\int_{r_w}^{r} \frac{1}{k(r')} \left(\frac{1}{r'} - \frac{r'}{r_e^2} \right) dr' \right] dr \right\}^{-1} . \tag{2.3.100}$$

2.3.6.4 Rate-Decline Equation for Constant Pressure Production

We present the development of the exponential flow rate decline curve for a constant wellbore flowing pressure production for a long producing time. Since the milestone work of van Everdingen and Hurst[5] in 1949, it is well known the relation between the dimensionless flow rate, q_D, in the constant-pressure problem, and the dimensionless wellbore pressure solution in the constant-rate problem, p_{wcD}; in Laplace space this relation is expressed as

$$\bar{q}_D = \frac{1}{u^2 \bar{p}_{wcD}}, \tag{2.3.101}$$

Reproduced with permission of the copyright owner. Further reproduction prohibited without permission.

where u is the Laplace space variable and $\bar{q}_D$ and $\bar{p}_{wcD}$ are the Laplace transformations of q_D and p_{wcD}, respectively, i.e.,

$$\bar{q}_D(u) = \mathcal{L}[q_D(t_D)] \tag{2.3.102}$$

and

$$\bar{p}_{wcD}(u) = \mathcal{L}[p_{wcD}(t_D)]. \tag{2.3.103}$$

The dimensionless flow rate, q_D, is defined as

$$q_D(t_D) = \left[\frac{141.2\mu}{k_{ref}h(p_i - p_{wf})}\right]q(t). \tag{2.3.104}$$

At late times the constant-rate pressure solution is given by the pseudosteady state flow equation, Eq. 2.3.98. Thus, we can write

$$p_{wcD} = 2\pi t_{AD} + C_{kD} = 2\pi t_D \frac{r_w^2}{A} + C_{kD}, \tag{2.3.105}$$

where C_{kD} is the constant given by

$$C_{kD} = k_{ref}C_k. \tag{2.3106}$$

In Eq. 2.3.106 the constant C_k is in units of md^{-1} and is given by

$$C_k = \left(\frac{2}{r_e^2 - r_w^2}\right)\int_{r_w}^{r_e} r\left[\int_{r_w}^{r} \frac{1}{k(r')}\left(\frac{1}{r'} - \frac{r'}{r_e^2}\right)dr'\right]dr. \tag{2.3.107}$$

Taking the Laplace transform of Eq. 2.3.105 with respect to t_D we obtain

$$\bar{p}_{wcD} = \mathcal{L}\left[2\pi t_D \frac{r_w^2}{A} + C_{kD}\right] = \frac{2\pi r_w^2}{A}\frac{1}{u^2} + \frac{C_{kD}}{u}. \tag{2.3.108}$$

Substituting Eq. 2.3.108 into the Eq. 2.3.101 gives

Reproduced with permission of the copyright owner. Further reproduction prohibited without permission.

$$\bar{q}_D = \frac{1}{u^2}\left[\frac{1}{\frac{2\pi r_w^2}{A}\frac{1}{u^2}+\frac{C_{kD}}{u}}\right] = \frac{1}{\frac{2\pi r_w^2}{A}+u\,C_{kD}}. \tag{2.3.109a}$$

To find q_D from the inverse of Laplace transform of Eq. 2.3.109a, we first reduce the right-hand side to a simpler tabulated form as follows:

$$\bar{q}_D = \frac{1}{\frac{2\pi r_w^2}{A}+u\,C_{kD}} = \frac{1}{C_{kD}}\left(\frac{1}{\frac{2\pi r_w^2}{AC_{kD}}+u}\right). \tag{2.3.109b}$$

Taking the inverse of Laplace transform of Eq. 2.3.109b

$$q_D(t_D) = \frac{1}{C_{kD}}\mathcal{L}^{-1}\left\{\frac{1}{\frac{2\pi r_w^2}{AC_{kD}}+u}\right\}, \tag{2.3.110}$$

and recalling $\mathcal{L}^{-1}\left\{\frac{1}{a+u}\right\} = e^{-at}$ (Churchill[35], page 459, entry 8), we obtain

$$q_D(t_D) = \frac{1}{C_{kD}}\exp\left(-\frac{2\pi r_w^2 t_D}{AC_{kD}}\right), \tag{2.3.111}$$

where C_{kD} is given by Eq. 2.3.106, t_D is given by Eq. 2.3.95 and q_D is defined by Eq. 2.3.104.

We can then express the flow rate in a dimensional form, by using the definitions of t_D and q_D in Eq. 2.3.111, which yields:

$$q(t) = \frac{k_{ref}h(p_i - p_{wf})}{141.2\mu}\frac{1}{C_{kD}}\exp\left(-\frac{2\pi r_w^2}{AC_{kD}}\frac{C_1 k_{ref} t}{\phi\mu c_t r_w^2}\right). \tag{2.3.112}$$

This equation can be further simplified by noticing, from Eqs. 2.3.100 and 2.3.106 that

Reproduced with permission of the copyright owner. Further reproduction prohibited without permission.

$$\frac{1}{C_{kD}} = \frac{141.2B\mu}{k_{ref}h} PI. \tag{2.3.113}$$

Using Eq. 2.3.113 in Eq. 2.3.112 and simplifying, we then obtain

$$q_{sc}B = q(t) = (PI)\left(p_i - p_{wf}\right)B\exp\left(-\frac{5.615B(PI)t}{V_p c_t}\right). \tag{2.3.114}$$

In this equation V_p is the porous volume, in ft^3, time t is in days, p_{wf} is a specified bottomhole flowing pressure, in psi, q is the sandface flow rate in reservoir barrels per day, and q_{sc} is the surface flow rate, in stock tank barrels per day.

Reproduced with permission of the copyright owner. Further reproduction prohibited without permission.

CHAPTER III

INVERSE PROBLEM

3.1 Introduction

We present in this chapter the solution to the inverse problem as stated in the section 2.1. We develop a recursive algorithm to calculate the radial permeability distribution based on our generalized pressure derivative solution (GPDS), presented in subsection 2.3.3, for drawdown and buildup well test data. Also, we develop a technique to obtain the radial permeability distribution based on the ideas of Yeh and Agarwal[25]. We describe a procedure to analyze well test data using both techniques and give examples of application to several types of permeability distributions. Moreover, we show that, if the pseudosteady state flow exists at the instant of shut-in then we can determine the reservoir pressure profile at the shut-in time, from the wellbore up to a certain radial distance, based on either drawdown data or directly from buildup data. We also show that, under certain conditions, we can calculate the reservoir pressure profile up to the external radius, at a given instant of a pseudosteady state drawdown, and, consequently, the reservoir average pressure, the homogeneous-equivalent pseudosteady state permeability and the productivity index. The inverse problem is founded in a radially heterogeneous reservoir with constant porosity. In the last section, we show how the porosity variation can influence our calculated permeability distribution.

Reproduced with permission of the copyright owner. Further reproduction prohibited without permission.

3.2 Inverse Solution Algorithm (ISA)

We present a method to compute a solution to the inverse problem of determination of permeability distribution from well test data. This procedure is based on a recursive algorithm that we refer to as the inverse solution algorithm (ISA), which we describe in this section. We show that ISA is general and can be applied to both drawdown and buildup data. In the case of buildup we show that correcting the pressure derivative data for the producing-time effects yields results identical to those obtained from drawdown data. The corrections for the producing-time effects are presented. A complete step-by-step analysis procedure is presented.

3.2.1 Drawdown

The derivation of ISA for drawdown data is based on our generalized pressure derivative solution (GPDS), Eq. 2.3.44a,

$$p'_{wD}(t_D) = \int_1^{\infty} K\left(r'_D, \hat{t}_D\right)\left[\frac{1}{k_D\left(r'_D\right)}\right] dr'_D. \tag{3.2.1}$$

This equation is known in Mathematics as an integral equation of first kind[27] characterized by the unknown function $1/k_D(r_D)$ within the integrand. We want to estimate the radial permeability distribution function, $k(r)$. The left-hand side of Eq. 3.2.1 is the derivative of dimensionless pressure with respect to the natural logarithm of

Reproduced with permission of the copyright owner. Further reproduction prohibited without permission.

dimensionless time, evaluated at a dimensionless time t_D. We can write Eq. 3.2.1 as follows

$$\frac{k_{ref}h}{141.2q\mu}\Delta p_w' = \int_1^\infty K\left(r_D', \hat{t}_D\right)\left[\frac{k_{ref}}{k\left(r_D'\right)}\right]dr_D', \tag{3.2.2a}$$

or, eliminating k_{ref}

$$\frac{h}{141.2q\mu}\Delta p_w' = \int_1^\infty K\left(r_D', \hat{t}_D\right)\left[\frac{1}{k\left(r_D'\right)}\right]dr_D', \tag{3.2.2b}$$

where $\hat{t}_D$ is given by Eq. 2.3.43, and the kernel or weighting function $K\left(r_D, \hat{t}_D\right)$ is defined by Eq. 2.2.29.

Replacing the definition of $\hat{k}$, Eq. 2.3.41, into Eq. 3.2.2b and multiplying by 2, we end up with the equation which is the basis for our ISA,

$$\frac{1}{\hat{k}} = \int_1^\infty 2K\left(r_D', \hat{t}_D\right)\left[\frac{1}{k\left(r_D'\right)}\right]dr_D'. \tag{3.2.3}$$

To derive an algorithm to estimate $k(r)$ from $\hat{k}$, we assume $k(r)$ can be approximated by k_i in the interval $r_{i-1} < r \le r_i$, with $i = 1, 2, \cdots, n$. Therefore, our problem becomes to find the k_i and the r_i, such that the piecewise constant permeability function closely reproduces the actual permeability function $k(r)$.

We calculate r_n as the radius of investigation at the current time t_n, given by the following equation[36]

Reproduced with permission of the copyright owner. Further reproduction prohibited without permission.

$$r_n = 2.0\sqrt{\frac{C_1 \hat{k}_n t_n}{\phi \mu c_t}}, \tag{3.2.4}$$

where $C_1 = 0.006328$ and $\hat{k}_n$ is the "instantaneous permeability" at time t_n in days, i.e.,

$$\hat{k}_n = \frac{70.6 q\mu}{h\left[\partial \Delta p_w(t_n)/\partial \ln t\right]} \tag{3.2.5}$$

<u>Remark</u>: It is worthwhile to note that r_n *is a monotonically increasing function of time*, although $\hat{k}_n$ may decrease with time, i.e., $\hat{k}_n < \hat{k}_{n-1}$. This is easily shown by using Eq. 3.2.5 in Eq. 3.2.4, recalling that $\partial \Delta p_w(t_n)/\partial \ln t = t_n\, \partial \Delta p_w(t_n)/\partial t$, and observing that, after simplification, r_n is a function of only $1/\left[\partial \Delta p_w(t_n)/\partial t\right]$. Since, during the infinite-acting period, $\partial \Delta p_w(t_n)/\partial t$ is a monotonically decreasing function of time, then r_n is a monotonically increasing function of time.

We calculate k_n using the basic equation 3.2.3 as follows.

We define:

$$r_0 = r_w \;\Rightarrow\; r_{0D} = 1, \tag{3.2.6}$$

$$\Delta\left(\frac{1}{k_i}\right) = \frac{1}{k_i} - \frac{1}{k_{i-1}}, \tag{3.2.7a}$$

$$\Delta\left(\frac{1}{k_1}\right) = \frac{1}{k_1}, \tag{3.2.7b}$$

$$u(r_D - a) = \begin{cases} 0, r_D < a \\ 1, r_D \geq a. \end{cases} \tag{3.2.8}$$

Using Eqs. 3.2.6 through 3.2.8 we can write Eq. 3.2.3 at $t = t_n$ as

$$\begin{aligned} \frac{1}{\hat{k}_n} = \int_1^\infty 2K\left(r_D', \hat{t}_D\right)\Bigg[&\frac{1}{k_1} + \Delta\left(\frac{1}{k_2}\right)u\left(r_D' - r_{1D}\right) + \Delta\left(\frac{1}{k_3}\right)u\left(r_D' - r_{2D}\right) \\ &+ \cdots + \Delta\left(\frac{1}{k_i}\right)u\left(r_D' - r_{i-1D}\right) + \cdots + \Delta\left(\frac{1}{k_n}\right)u\left(r_D' - r_{n-1D}\right)\Bigg]dr_D'. \end{aligned} \tag{3.2.9}$$

Reproduced with permission of the copyright owner. Further reproduction prohibited without permission.

Developing the right-hand side of this equation we obtain

$$\frac{1}{\hat{k}_n}=\frac{1}{k_1}\int_1^{\infty}2K\left(r_D^{'},\hat{t}_D\right)dr_D^{'}+\Delta\left(\frac{1}{k_2}\right)\int_{r_{1D}}^{\infty}2K\left(r_D^{'},\hat{t}_D\right)dr_D^{'}+\Delta\left(\frac{1}{k_3}\right)\int_{r_{2D}}^{\infty}2K\left(r_D^{'},\hat{t}_D\right)dr_D^{'}$$
$$+\cdots+\Delta\left(\frac{1}{k_i}\right)\int_{r_{i-1D}}^{\infty}2K\left(r_D^{'},\hat{t}_D\right)dr_D^{'}+\cdots+\Delta\left(\frac{1}{k_n}\right)\int_{r_{n-1D}}^{\infty}2K\left(r_D^{'},\hat{t}_D\right)dr_D^{'}. \tag{3.2.10}$$

By observing that,

$$\int_1^{\infty}2K\left(r_D^{'},\hat{t}_D\right)dr_D^{'}=1, \tag{3.2.11}$$

according to Eq. 2.3.39, that we demonstrated in Chapter II, subsection 2.3.3.1, and that

$$\int_{r_{jD}}^{\infty}2K\left(r_D^{'},\hat{t}_D\right)dr_D^{'}=\int_1^{\infty}2K\left(r_D^{'},\hat{t}_D\right)dr_D^{'}-\int_1^{r_{jD}}2K\left(r_D^{'},\hat{t}_D\right)dr_D^{'}$$
$$=1-\int_1^{r_{jD}}2K\left(r_D^{'},\hat{t}_D\right)dr_D^{'}, \tag{3.2.12}$$

we can express Eq. 3.2.10 as

$$\frac{1}{\hat{k}_n}=\frac{1}{k_1}+\Delta\left(\frac{1}{k_2}\right)\left[1-\int_1^{r_{1D}}2K\left(r_D^{'},\hat{t}_D\right)dr_D^{'}\right]+\Delta\left(\frac{1}{k_3}\right)\left[1-\int_1^{r_{2D}}2K\left(r_D^{'},\hat{t}_D\right)dr_D^{'}\right]$$
$$+\cdots+\Delta\left(\frac{1}{k_i}\right)\left[1-\int_1^{r_{i-1D}}2K\left(r_D^{'},\hat{t}_D\right)dr_D^{'}\right]+\cdots+\Delta\left(\frac{1}{k_n}\right)\left[1-\int_1^{r_{n-1D}}2K\left(r_D^{'},\hat{t}_D\right)dr_D^{'}\right], \tag{3.2.13}$$

which can be further simplified to

Reproduced with permission of the copyright owner. Further reproduction prohibited without permission.

$$\frac{1}{\hat{k}_n}=\sum_{i=1}^{n-1}\Delta\left(\frac{1}{k_i}\right)-\sum_{i=2}^{n-1}\Delta\left(\frac{1}{k_i}\right)\int_1^{r_{i-1D}}2K\left(r_D',\hat{t}_D\right)dr_D'+\Delta\left(\frac{1}{k_n}\right)\left[1-\int_1^{r_{n-1D}}2K\left(r_D',\hat{t}_D\right)dr_D'\right]. \quad (3.2.14)$$

Our definition of $\Delta\left(\frac{1}{k_i}\right)$ given in Eq. 3.2.7a implies that

$$\sum_{i=1}^{n-1}\Delta\left(\frac{1}{k_i}\right)=\frac{1}{k_{n-1}}, \quad (3.2.15)$$

which when used in Eq. 3.2.14 yields

$$\frac{1}{\hat{k}_n}=\frac{1}{k_{n-1}}-\sum_{i=2}^{n-1}\Delta\left(\frac{1}{k_i}\right)\int_1^{r_{i-1D}}2K\left(r_D',\hat{t}_D\right)dr_D'+\Delta\left(\frac{1}{k_n}\right)\left[1-\int_1^{r_{n-1D}}2K\left(r_D',\hat{t}_D\right)dr_D'\right]. \quad (3.2.16)$$

Eq. 3.2.16 indicates that the sequence $\left\{1/k_n\right\}$ can be computed recursively[37]. To start the process we compute

$$\frac{1}{k_1}=\frac{1}{\hat{k}(t_1)}, \quad (3.2.17)$$

where t_1 is the first point in time at which we have a reliable pressure derivative value, $\Delta p_w'$. Solving Eq. 3.2.16 for $\Delta\left(1/k_n\right)$ we obtain

$$\Delta\left(\frac{1}{k_n}\right)=\frac{\frac{1}{\hat{k}_n}-\frac{1}{k_{n-1}}+\sum_{i=2}^{n-1}\left[\Delta\left(\frac{1}{k_i}\right)\int_1^{r_{i-1D}}2K\left(r_D',\hat{t}_D\right)dr_D'\right]}{1-\int_1^{r_{n-1D}}2K\left(r_D',\hat{t}_D\right)dr_D'}. \quad (3.2.18)$$

Reproduced with permission of the copyright owner. Further reproduction prohibited without permission.

Eq. 3.2.18 can be applied to compute $\Delta\left(1/k_n\right)$ once $\left\{\Delta\left(1/k_n\right)\right\}_{i=1}^{n-1}$ are known, and then k_n can be estimated from Eq. 3.2.7a. A procedure for determining the $r_i^{'}s$ is given later.

The integral in Eq. 3.2.18 can be calculated in a simpler way. Considering the definition of the kernel function $K(r_D,\hat{t}_D)$, given by Eq. 2.2.29, we can write

$$\int_1^{r_{jD}} 2K\left(r_D^{'},\hat{t}_D\right)dr_D^{'} = \int_1^{r_{jD}} \sqrt{\pi}\frac{r_D^{'}}{\hat{t}_D}\exp\left(-\frac{r_D^{'2}}{2\hat{t}_D}\right)W_{\frac{1}{2},\frac{1}{2}}\left(\frac{r_D^{'2}}{\hat{t}_D}\right)dr_D^{'}. \tag{3.2.19}$$

Consider the following change in variable and the resulting relations:

$$\hat{z}_D = \frac{r_D}{\sqrt{\hat{t}_D}} \Rightarrow dr_D = \sqrt{\hat{t}_D}\, d\hat{z}_D, \tag{3.2.20}$$

$$\frac{r_D}{\hat{t}_D}\sqrt{\hat{t}_D}\, d\hat{z}_D = \frac{r_D}{\sqrt{\hat{t}_D}}\, d\hat{z}_D = \hat{z}_D\, d\hat{z}_D, \tag{3.2.21}$$

$$r_D \to 1 \Rightarrow \hat{z}_D \to \frac{1}{\sqrt{\hat{t}_D}} \equiv \hat{z}_{0D}, \tag{3.2.22}$$

$$r_D \to r_{jD} \Rightarrow \hat{z}_D \to \frac{r_{jD}}{\sqrt{\hat{t}_D}} \equiv \hat{z}_{jD}. \tag{3.2.23}$$

By substituting Eqs. 3.2.20 through 3.2.23 into Eq. 3.2.19, we obtain

$$\int_1^{r_{jD}} 2K\left(r_D^{'},\hat{t}_D\right)dr_D^{'} = \int_{\hat{z}_{0D}}^{\hat{z}_{jD}} \sqrt{\pi}\,\hat{z}_D \exp\left(-\frac{\hat{z}_D^2}{2}\right)W_{\frac{1}{2},\frac{1}{2}}\left(\hat{z}_D^2\right)d\hat{z}_D, \tag{3.2.24a}$$

or

Reproduced with permission of the copyright owner. Further reproduction prohibited without permission.

$$\int_{1}^{r_{jD}} 2K\left(r_D^{'},\hat{t}_D\right)dr_D^{'} = \int_{\hat{z}_{0D}}^{\hat{z}_{jD}} \Omega(\hat{z}_D)\, d\hat{z}_D, \tag{3.2.24b}$$

where

$$\hat{z}_{0D} = \frac{1}{\sqrt{\hat{t}_D}}, \tag{3.2.25}$$

$$\hat{z}_{jD} = \frac{r_{jD}}{\sqrt{\hat{t}_D}}, \tag{3.2.26}$$

and

$$\Omega(\hat{z}_D) = \sqrt{\pi}\,\hat{z}_D \exp\left(-\frac{\hat{z}_D^2}{2}\right) W_{\frac{1}{2},\frac{1}{2}}\left(\hat{z}_D^2\right). \tag{3.2.27}$$

Oliver[16] has shown that $K(r_D,t_D) \approx 0$ outside the interval $\left[0.12\sqrt{t_D}, 2.34\sqrt{t_D}\right]$ (see Fig. 2.2.4) which lead us to consider the lower limit of integration $\hat{z}_{0D}$ in the Eq. 3.2.24 as

$$\hat{z}_{0D} = \min\left\{\frac{1}{\sqrt{\hat{t}_D}}, 0.12\right\}. \tag{3.2.28}$$

Replacing Eq. 3.2.24b into Eq. 3.2.18 we obtain

$$\Delta\left(\frac{1}{k_n}\right) = \frac{\dfrac{1}{\hat{k}_n} - \dfrac{1}{k_{n-1}} + \sum_{i=2}^{n-1}\left[\Delta\left(\dfrac{1}{k_i}\right)\int_{\hat{z}_{0D}}^{\hat{z}_{i-1D}} \Omega(\hat{z}_D)\, d\hat{z}_D\right]}{1 - \int_{\hat{z}_{0D}}^{\hat{z}_{n-1D}} \Omega(\hat{z}_D)\, d\hat{z}_D}. \tag{3.2.29}$$

which is the <u>*Inverse Solution Algorithm (ISA)*</u>.

As noted previously, after computing $\Delta\left(1/k_n\right)$, we determine the unknown permeability value, k_n, using the definition given by Eq. 3.2.7a, i.e., by

Reproduced with permission of the copyright owner. Further reproduction prohibited without permission.

$$k_n = \frac{1}{\frac{1}{k_{n-1}} + \Delta\left(\frac{1}{k_n}\right)}. \tag{3.2.30}$$

3.2.2 Buildup

We present here the ISA for buildup well-test data. We consider an infinite-acting buildup period after a drawdown under a steady state, transient or pseudosteady state condition. We use the general pressure derivative solutions for buildup derived in subsection 2.3.3.2. The derivation of ISA for buildup data follows essentially the same steps as for drawdown data. The main differences lie in the GPDS, in the replacement of t, t_D, and $\hat{t}_D$, respectively, by Δt, Δt_D, and $\Delta\hat{t}_D$, and in the equation for calculating the "instantaneous permeability", $\hat{k}$, which is computed based on the pressure buildup derivative corrected for the producing-time effects. The correction for producing-time effects and the equation to compute $\hat{k}$ are discussed in the following.

The right-hand side of the general superposition pressure buildup equation, Eq. 2.3.45, is composed only of drawdown solutions. From this equation, it is clear and well known that, the transient pressure buildup solution, $p_{wD}(\Delta t_D)$, is equivalent to the corresponding transient drawdown solution, $p_{wD}(t_D)$, i.e., $p_{wD}(\Delta t_D) = p_{wD}(t_D)$ when $\Delta t_D = t_D$, provided we correct the pressure buildup data, $\bar{p}_{sD}(\Delta t_D)$, for the producing time effects, which are taken into account by the remaining two terms, $p_{wD}(t_{pD}) - p_{wD}\left[(t_p + \Delta t)_D\right]$. Obviously, this also applies to the buildup solution in terms of the pressure derivative, which can be written as

$$p'_{wD}(\Delta t_D) = \bar{p}'_{sD}(\Delta t_D) + \left\{p_{wD}\left[(t_p + \Delta t)_D\right] - p_{wD}(t_{pD})\right\}', \tag{3.2.31}$$

Reproduced with permission of the copyright owner. Further reproduction prohibited without permission.

where $\left\{p_{wD}\left[\left(t_p+\Delta t\right)_D\right]-p_{wD}\left(t_{pD}\right)\right\}'$ corrects the pressure buildup derivative, $\tilde{p}'_{sD}(\Delta t_D)$, for the producing-time effects, and depends on the flow regime of the drawdown that precedes the buildup period. Appropriate expressions for this correction term, which we will refer to as $C_{pte}(\Delta t)$, are presented in the following subsections.

Hence, the appropriate equation to compute the "instantaneous permeability", $\hat{k}$, from transient buildup data, is given by

$$\hat{k}=\frac{1}{\dfrac{h}{70.6q\mu}\tilde{p}'_s(\Delta t)+C_{pte}(\Delta t)}, \tag{3.2.32}$$

where

$$\tilde{p}'_s(\Delta t)=\frac{d\left(p_{ws}(\Delta t)-p_{wf,s}\right)}{d\ln\Delta t}. \tag{3.2.33}$$

and $C_{pte}(\Delta t)$ is the correction term for the producing-time effects, as noted above.

3.2.2.1 Buildup after Steady-State Flow

The GPDS equation for this case is Eq. 2.3.49, which is repeated here as

$$\tilde{p}'_{sD}(\Delta t_D)=\int_1^{\infty}K\left(r'_D,\Delta\hat{t}_D\right)\left[\frac{1}{k_D\left(r'_D\right)}\right]dr'_D. \tag{3.2.34}$$

As shown in Chapter II, subsection 2.3.3.2, in this case $C_{pte}(\Delta t)=0$, which implies that $p'_{wD}(\Delta t_D)=\tilde{p}'_{sD}(\Delta t_D)=p'_{wD}(t_D)$, when $\Delta t_D=t_D$. Thus, ISA, can be applied to buildup data by simply replacing t by Δt and $\hat{t}_D$ by $\Delta\hat{t}_D$.

Reproduced with permission of the copyright owner. Further reproduction prohibited without permission.

Here, as in the subsequent buildup cases, dimensionless time $\Delta\hat{t}_D$ is defined by Eq. 2.3.43 with t replaced by Δt and $\hat{k}$ given by Eq. 3.2.32.

3.2.2.2 Buildup after Transient Flow

For this case, the GPDS equation is Eq. 2.3.62 which we rewrite as

$$\bar{p}'_{sD}(\Delta t_D)+\frac{\Delta t_D}{(t_p+\Delta t)_D}\int_1^\infty K\left(r'_D,(\hat{t}_p+\Delta\hat{t})_D\right)\frac{1}{k_D(r'_D)}dr'_D=\int_1^\infty K\left(r'_D,\Delta\hat{t}_D\right)\frac{1}{k_D(r'_D)}dr'_D, \quad (3.2.35)$$

where we have replaced the dimensionless time in the argument of the kernel function, originally defined in terms of $\bar{k}$, by dimensionless time defined in terms of the "instantaneous permeability" $\hat{k}$. Notice that the second term in the left side corrects the pressure buildup derivative data, $\bar{p}'_{sD}(\Delta t_D)$, for the producing-time effects.

We observe that Eq. 3.2.35 involves the calculation of the kernel function, K, at two different times, $\Delta\hat{t}_D$ and $(\hat{t}_p+\Delta\hat{t})_D$, which correspond to two distinct values of $\hat{k}$. To properly correct the buildup data for producing-time effects and then apply ISA we need to be able to evaluate the integral on the left-side of Eq. 3.2.35. Since this integral corresponds to drawdown data, we cannot evaluate it directly from buildup data. To circumvent this problem, we might assume that at each time $(\hat{t}_p+\Delta\hat{t})_D$, the kernel in the integral of the left-side of Eq. 3.2.35 is approximately zero except in a zone of constant permeability where $k_D(r_D)=k_{NpD}$. This implies that at the end of drawdown, we have obtained a semilog straight line which reflects k_{NpD} and that, if we had continued the drawdown for a total time of $t_p+\Delta t_{\max}$, the semilog slope would have remained constant. Under this assumption, we can write Eq. 3.2.35 as

Reproduced with permission of the copyright owner. Further reproduction prohibited without permission.

$$\bar{p}'_{sD}(\Delta t_D)+\frac{\Delta t_D}{(t_p+\Delta t)_D}\frac{1}{k_{NpD}}\frac{1}{2}=\int_1^\infty K(r'_D,\Delta\hat{t}_D)\frac{1}{k_D(r'_D)}dr'_D, \qquad (3.2.36)$$

where $k_{NpD}={k_{Np}}/{k_{ref}}$. Using Eq. 2.3.46 in Eq. 3.2.36, multiplying the resulting equation by $\left({2}/{k_{ref}}\right)$, and noticing that the left-side becomes $\frac{1}{\hat{k}}$, we can write

$$\frac{1}{\hat{k}}=\frac{h}{70.6q\mu}\frac{d\left[p_{ws}(\Delta t)-p_{wf,s}\right]}{d\ln\Delta t}+\frac{\Delta t}{(t_p+\Delta t)}\frac{1}{k_{Np}}=\int_1^\infty 2K(r'_D,\Delta\hat{t}_D)\frac{1}{k(r'_D)}dr'_D. \qquad (3.2.37)$$

Thus, the correction term for the producing time effects is

$$C_{pte}(\Delta t)=\frac{\Delta t}{(t_p+\Delta t)}\frac{1}{k_{Np}}. \qquad (3.2.38)$$

where k_{Np} is given by the "instantaneous permeability" $\hat{k}$ computed at the end of the flow period, i.e., $k_{Np}=\hat{k}\big|_{t=t_p}$.

By observing that the right side of Eq. 3.2.37 is identical to the drawdown equation, Eq. 3.2.3, with $\hat{t}_D$ replaced by $\Delta\hat{t}_D$, it becomes clear that, computing $\hat{k}$ using Eq. 3.2.32, with $C_{pte}(\Delta t)$ given by Eq. 3.2.38, we can apply ISA directly as was done for drawdown, replacing $\hat{t}_D$ by $\Delta\hat{t}_D$.

3.2.2.3 Buildup after Pseudosteady State Flow

The GPDS equation for this case is Eq. 2.3.66, derived in subsection 2.3.3.2, which we rewrite as

Reproduced with permission of the copyright owner. Further reproduction prohibited without permission.

$$\tilde{p}'_{sD}(\Delta t_D)+\frac{2r_w^2}{r_e^2}\Delta t_D=\int_1^\infty K\left(r'_D,\Delta t_D\right)\left[\frac{1}{k_D\left(r'_D\right)}\right]dr'_D. \tag{3.2.39}$$

Proceeding in a similar manner as was done for buildup after transient flow, we can write directly

$$\frac{1}{\hat{k}}=\frac{h}{70.6q\mu}\frac{d\left[p_{ws}(\Delta t)-p_{wf,s}\right]}{d\ln\Delta t}+\left(\frac{4r_w^2}{r_e^2}\right)\frac{\Delta t_D}{k_{ref}}=\int_1^\infty 2K\left(r'_D,\Delta\hat{t}_D\right)\frac{1}{k\left(r'_D\right)}dr'_D, \tag{3.2.40}$$

and then, using the definition of dimensionless time given by Eq. 2.2.8, with t replaced by Δt, we obtain

$$\frac{1}{\hat{k}}=\frac{h}{70.6qu}\frac{d\left[p_{ws}(\Delta t)-p_{wf,s}\right]}{d\ln\Delta t}+\left(\frac{4C_1}{r_e^2\phi\mu c_t}\right)\Delta t=\int_1^\infty 2K\left(r'_D,\Delta\hat{t}_D\right)\frac{1}{k\left(r'_D\right)}dr'_D, \tag{3.2.41}$$

where the correction term for the producing time effects is

$$C_{pte}(\Delta t)=\left(\frac{4C_1}{r_e^2\phi\mu c_t}\right)\Delta t, \tag{3.2.42}$$

and $C_1=0.006328$ for Δt in days.

Hence, as indicated by Eq. 3.2.41 compared to the drawdown equation, Eq. 3.2.3, once we compute $\hat{k}$ using Eq. 3.2.32, with $C_{pte}(\Delta t)$ given by Eq. 3.2.42, we can apply ISA directly as was done for drawdown, replacing $\hat{t}_D$ by $\Delta\hat{t}_D$. Notice that in this case the correction for producing-time effects is <u>exact</u>.

Reproduced with permission of the copyright owner. Further reproduction prohibited without permission.

3.2.3 Analysis Procedure

The inverse problem and the inverse solution algorithm (ISA) can be summarized as follows. We have a set of time and pressure derivative values, $\left\{t_j, \Delta p'_j\right\}$, obtained from either a transient drawdown or buildup well test, where $j = 1,2,\ldots,N_p$; t_1 is the first point in time at which we have a reliable pressure derivative value; and N_p is the number of data points. We want to estimate the permeability distribution function $k(r)$, which we approximate by $k(r) = k_j$ for $r_{j-1} < r \le r_j$. Assuming that we have calculated the approximate piecewise constant permeability distribution function up to the radius of investigation r_{n-1} we want to calculate r_n and k_n. The analysis of drawdown or buildup data to determine permeability distribution is summarized in the following steps:

Step 1 Compute the "instantaneous permeability", $\hat{k}_n$, based on well test data, using the appropriate equation: (a) Eq. 2.3.41 for drawdown, or (b) Eq. 3.2.32 for buildup, with the applicable correction term for producing-time effects, C_{pte}, given by either zero, Eq. 3.2.38, or Eq. 3.2.42, depending on whether the buildup follows a flow period under, respectively, steady-state, transient or pseudosteady state condition;

Step 2 Calculate the associated radius of investigation, r_n, applying Eq. 3.2.4 with t_n for drawdown, or Δt_n for buildup;

Step 3 Compute the dimensionless pseudotime, $\hat{t}_D$, for drawdown, ($\Delta\hat{t}_D$ for buildup), with Eq. 2.3.43, using t_n (or Δt_n for buildup);

Step 4 Compute $\Delta\left(1/k_n\right)$ with the *general inverse solution algorithm of* Eq. 3.2.29 *for either, drawdown or buildup* (for buildup, with $\hat{t}_D$ replaced by $\Delta\hat{t}_D$);

Step 5 Finally, compute k_n using Eq. 3.2.30; then $k(r) \cong k_n$ for $r_{n-1} \le r < r_n$.

Reproduced with permission of the copyright owner. Further reproduction prohibited without permission.

3.2.4 Region of Investigation

Oliver[16] has shown that the kernel function $K(r_D,t_D)$ is approximately zero outside the region $0.12\sqrt{t_D} < r_D < 2.34\sqrt{t_D}$ (see Figs 2.2.4). After the introduction of $\hat{t}_D$ in Oliver's kernel function, we define a region of investigation as an annular region $(\hat{r}_{Dinner},\hat{r}_{Douter})$ outside of which $K(r_D,\hat{t}_D)$ vanishes for all practical purposes, where

$$\hat{r}_{Dinner} = 0.12\sqrt{\hat{t}_D}, \tag{3.2.43}$$

and

$$\hat{r}_{Douter} = 2.34\sqrt{\hat{t}_D}. \tag{3.2.44}$$

Therefore, Eq. 3.2.3 can be approximated as

$$\frac{1}{\hat{k}} = \int_1^{\infty} 2K(r_D',\hat{t}_D)\left[\frac{1}{k(r_D')}\right]dr_D' \cong \int_{\hat{r}_{Dinner}}^{\hat{r}_{Douter}} 2K(r_D',\hat{t}_D)\left[\frac{1}{k(r_D')}\right]dr_D'. \tag{3.2.45}$$

Thus, the instantaneous permeability $\hat{k}$ is a weighted-harmonic average of all permeability values within a region of investigation, $(\hat{r}_{Dinner},\hat{r}_{Douter})$, or in dimensional form, $(\hat{r}_{inner},\hat{r}_{outer})$, where

$$\hat{r}_{inner} = 0.12\sqrt{\hat{t}_D}\, r_w, \tag{3.2.46}$$

and

$$\hat{r}_{outer} = 2.34\sqrt{\hat{t}_D}\, r_w. \tag{3.2.47}$$

So, Eq. 3.2.45 and Eq. 3.2.11 indicate that $\hat{k}$, computed from Eq. 3.2.5, will be equal to the permeability of a zone j, $r_{j-1} < r < r_j$, with constant permeability k_j, only if the investigation region $(\hat{r}_{inner},\hat{r}_{outer})$ is within the zone limits, i.e., at a given time, $r_{j-1} < \hat{r}_{inner} = 0.12\sqrt{\hat{t}_D}\, r_w$ and $\hat{r}_{outer} = 2.34\sqrt{\hat{t}_D}\, r_w < r_j$. Since the "width" of the investigation region increases with time, as indicated by Eqs. 3.2.46 and 3.2.47, as the time increases it is more unlikely that we will find a time interval on which the permeability $\hat{k}$ will become constant and equal to some zone permeability value.

Reproduced with permission of the copyright owner. Further reproduction prohibited without permission.

3.3 Inverse Solutions Based on Volumetric Average

We use the ideas of Yeh and Agarwal[25] to calculate permeability distribution from transient drawdown or buildup well-test data. We present two approaches; (i) in the first approach we consider the direct application of their ideas, i.e., we consider the instantaneous derivative (KID) as a volumetrically-weighted *arithmetic* average permeability; (ii) in the second approach, we improved the analysis technique by considering the KID as a volumetrically-weighted *harmonic* average permeability.

3.3.1 KID as Arithmetic Average Permeability

Yeh and Agarwal[25], in their work on the analysis of injection/falloff well test data, consider the instantaneous total mobility, calculated at given time from falloff data, as a volumetrically-weighted arithmetic average of the total mobility profile up to the radius of investigation reached at that particular time. We translated directly this concept to single-phase flow in a radially heterogeneous reservoir problem as a relationship between the "instantaneous permeability" and the permeability profile. The result is

$$\hat{k} = \frac{1}{V}\int_V k(r)\,dV = \frac{1}{\pi r^2 h}\int_{r_w}^{r} k(r')\,2\pi r' h\,dr', \tag{3.3.1a}$$

or

$$\hat{k} = \frac{2}{r^2}\int_{r_w}^{r} k(r')\,r'\,dr', \tag{3.3.1b}$$

where $\hat{k}$, given by Eq. 2.3.41, is the instantaneous permeability at a particular time associated with the radius of investigation r_i, which is calculated here using Eq. 3.3.2

Reproduced with permission of the copyright owner. Further reproduction prohibited without permission.

$$r_i = 1.5\sqrt{\frac{C_1 \hat{k} t}{\phi \mu c_t}}, \tag{3.3.2}$$

where $C_1 = 0.006328$ for t in days. Note the numerical constant (1.5) used in this definition of r_i is different from the one we used to derive ISA; see Eq. 3.2.4.

Similar to the Yeh-Agarwal procedure, we calculate the permeability profile, $k(r_i)$, by taking the derivative of Eq. 3.3.1b with respect to r and solving the resulting equation for $k(r)$, which yields at $r = r_i$

$$k(r_i) = \hat{k}(r_i) + \frac{r_i}{2}\left[\frac{d\hat{k}(r)}{dr}\right]_{r_i}. \tag{3.3.3}$$

3.3.2 <u>KID as Harmonic Average Permeability</u>

Oliver's work[16], as well as our GPDS, shows that the instantaneous derivative, $\hat{k}$, calculated from instantaneous wellbore pressure derivative, is a result of a weighted-harmonic averaging process, in the radial direction, rather than a weighted-arithmetic averaging one. Therefore, we improved the Yeh-Agarwal approach by considering $\hat{k}$ as a volumetric-weighted *harmonic* average expressed as

$$\frac{1}{\hat{k}} = \frac{2}{r^2}\int_{r_w}^{r} \frac{1}{k(r')} r' \, dr'. \tag{3.3.4}$$

We solve Eq. 3.3.4 for $k(r)$ in the same way we did before, i.e., by taking the derivative with respect to r, multiplying the resulting equation by $r^2/2$, and rearranging to obtain

Reproduced with permission of the copyright owner. Further reproduction prohibited without permission.

$$\frac{1}{2}\frac{d}{dr}\left(\frac{r^2}{\hat{k}(r)}\right)=\frac{r}{k(r)}. \tag{3.3.5}$$

Developing the derivative in the left-side and then solving for $k(r)$ gives at $r=r_i$

$$\frac{1}{k(r_i)}=\frac{1}{\hat{k}(r_i)}-\frac{r_i}{2}\frac{1}{\hat{k}^2(r_i)}\left[\frac{d\hat{k}(r)}{dr}\right]_{r_i}. \tag{3.3.6}$$

We refer to the method based on Eq. 3.3.3 as the Yeh-Agarwal procedure (YA) and refer to the method based on Eq. 3.3.6 as the Modified Yeh-Agarwal procedure (MYA). Both methods are applicable to transient drawdown as well as to transient buildup well-test data, provided we correct the buildup data for the producing-time effects in a similar manner as was done previously. In both methods the radius of investigation, r_i, is calculated using Eq. 3.3.2, with t for drawdown or Δt for buildup. Proceeding in a similar manner as was done for ISA, we compute the instantaneous derivative, $\hat{k}$, using the appropriate equation, depending on whether the data come from a drawdown or buildup test. For drawdown data we determine $\hat{k}$ using Eq. 2.3.41. For buildup data we calculate $\hat{k}$ using Eq. 3.2.32, with the correction term for producing-time effects, $C_{pte}(\Delta t)$, equal to zero for buildup after steady-state flow, or given by Eq. 3.2.38 or Eq 3.2.42, for buildup after a transient or a pseudosteady state flow, respectively.

Reproduced with permission of the copyright owner. Further reproduction prohibited without permission.

3.3.3 Analysis Procedure

Based on what was presented in the two previous sections we summarize the necessary steps to analyze transient drawdown or buildup well test data to determine permeability distribution as follows:

Step 1 Compute the instantaneous derivative, $\hat{k}$:

(i) for drawdown data using Eq. 2.3.41;

(ii) for buildup data using Eq. 3.3.32 with the correction term for the producing-time effects, $C_{pte}(\Delta t)$, given by

(a) zero, for buildup after steady-state flow,

(b) Eq. 3.2.38, for a buildup that succeeds a transient flow, or

(c) Eq 3.2.42, for a buildup that follows a pseudosteady state flow.

Step 2 Calculate the associated radius of investigation r_i with Eq. 3.3.2 for drawdown (replace t by Δt for buildup) and relate it to $\hat{k}(r_i)$;

Step 3 Compute the permeability value $k(r_i)$, at r_i, with either Eq. 3.3.3 (YA) or Eq. 3.3.6 (MYA).

Reproduced with permission of the copyright owner. Further reproduction prohibited without permission.

3.4 Applications to Drawdown Data

We present here permeability distribution results obtained from the application of our procedures to transient drawdown data. We compare the results obtained with ISA with those obtained with the Yeh-Agarwal (YA) and the modified Yeh-Agarwal (MYA) procedures. We consider several permeability distributions. It is important to note that drawdown or buildup data are analyzable only when they correspond to the infinite-acting period.

In the examples that follow we use synthetic well-test data generated with our finite-difference numerical simulator. The analysis procedure follows the steps described in the subsections 3.2.3. and 3.3.3.

3.4.1 Drawdown, Case 1

This case pertains to a 5-zone, multicomposite, single-well reservoir producing at a constant sandface flow rate. The main reservoir/well system parameters are presented in Table 2.3.3. We simulated a drawdown of 30 days, with 40 points per time log-cycle equally spaced in the logarithm of time. The transient period ends at about 26.6 days. The simulated pressures and numerically computed pressure derivatives versus time are presented in Figs. 2.3.6 and 2.3.7, respectively.

Fig. 3.4.1 shows a semilog plot of the actual permeability (solid line), and the computed permeabilities using ISA (circles), and instantaneous permeability, KID (squares) versus radial distance, r. We observe the ISA-computed permeability profile approximates reasonably well the actual permeability profile. Since the KID is a result of a weighted harmonic average of all permeability values within the region of investigation, where the kernel function K is nonzero (see Fig. 2.2.4), it should not closely follow the actual permeability profile, as it is clear in Fig. 3.4.1. It is also important to notice that, as

Reproduced with permission of the copyright owner. Further reproduction prohibited without permission.

Reproduced with permission of the copyright owner. Further reproduction prohibited without permission.

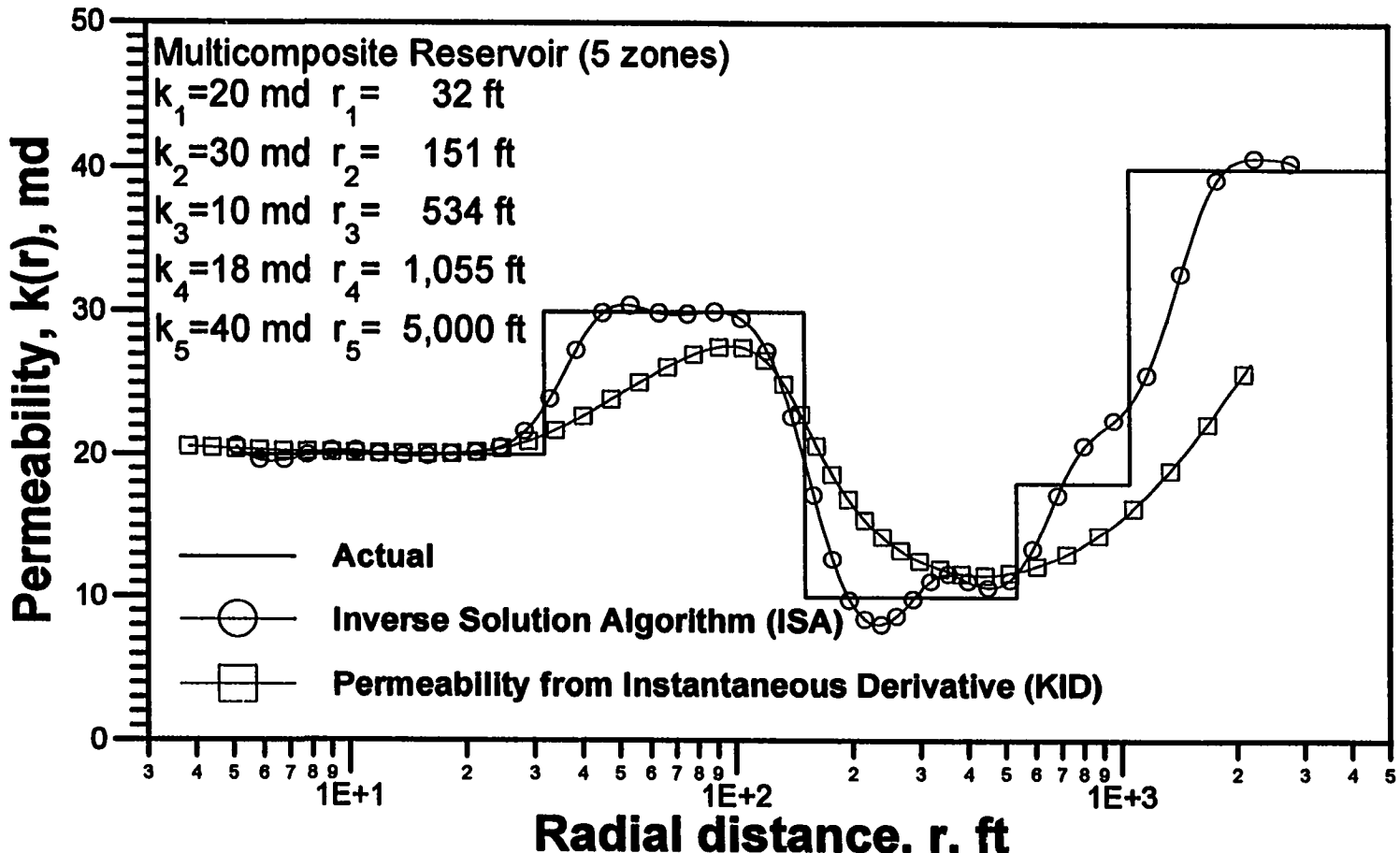

Fig. 3.4.1 - Permeability profile, actual versus KID and calculated via ISA; Drawdown Case 1.

discussed in subsection 3.2.4, the KID gives the actual permeability value of a zone only if the region of investigation is within the zone; this happens only for the first zone.

Fig. 3.4.2 compares the permeability profiles, actual versus those computed with Yeh-Agarwal (YA) and modified Yeh-Agarwal (MYA) procedures. Both computed permeability profiles are reasonable approximations to the actual profile, but the MYA gives a slightly better approximation. This result confirms that an improvement to the YA procedure is obtained by using a volumetric-weighted *harmonic* average instead of a volumetric-weighted *arithmetic* average of the permeability values within the radius of investigation (Eq. 3.3.2). Similar behavior was also found in many other cases. Because of this, we will present only the MYA results throughout this work.

In Fig. 3.4.3, we compare the permeability profiles obtained from ISA and MYA with the actual permeability profile. We observe that ISA tends to reproduce the constant permeability zones more closely, although it occasionally exhibits oscillations. While we will concentrate on the ISA procedure throughout most of this work, all the results we have generated to date indicate that our MYA procedure also yields a reasonable estimate of the permeability distribution.

Using our computed permeability distributions as input to our simulator we generated pressures and then calculated numerically the pressure derivatives, and compared the results in Fig. 3.4.4, with the ones obtained with actual permeability distribution. The pressure derivatives obtained from the ISA-calculated permeability distribution (circles) match very well the original simulated derivatives (solid curve); the pressure derivatives from the MYA-calculated permeability distribution (plus data points) also show a reasonable agreement with the original derivative data; MYA however does not reproduce the correct derivative data as well as the ISA permeability distribution.

Reproduced with permission of the copyright owner. Further reproduction prohibited without permission.

Reproduced with permission of the copyright owner. Further reproduction prohibited without permission.

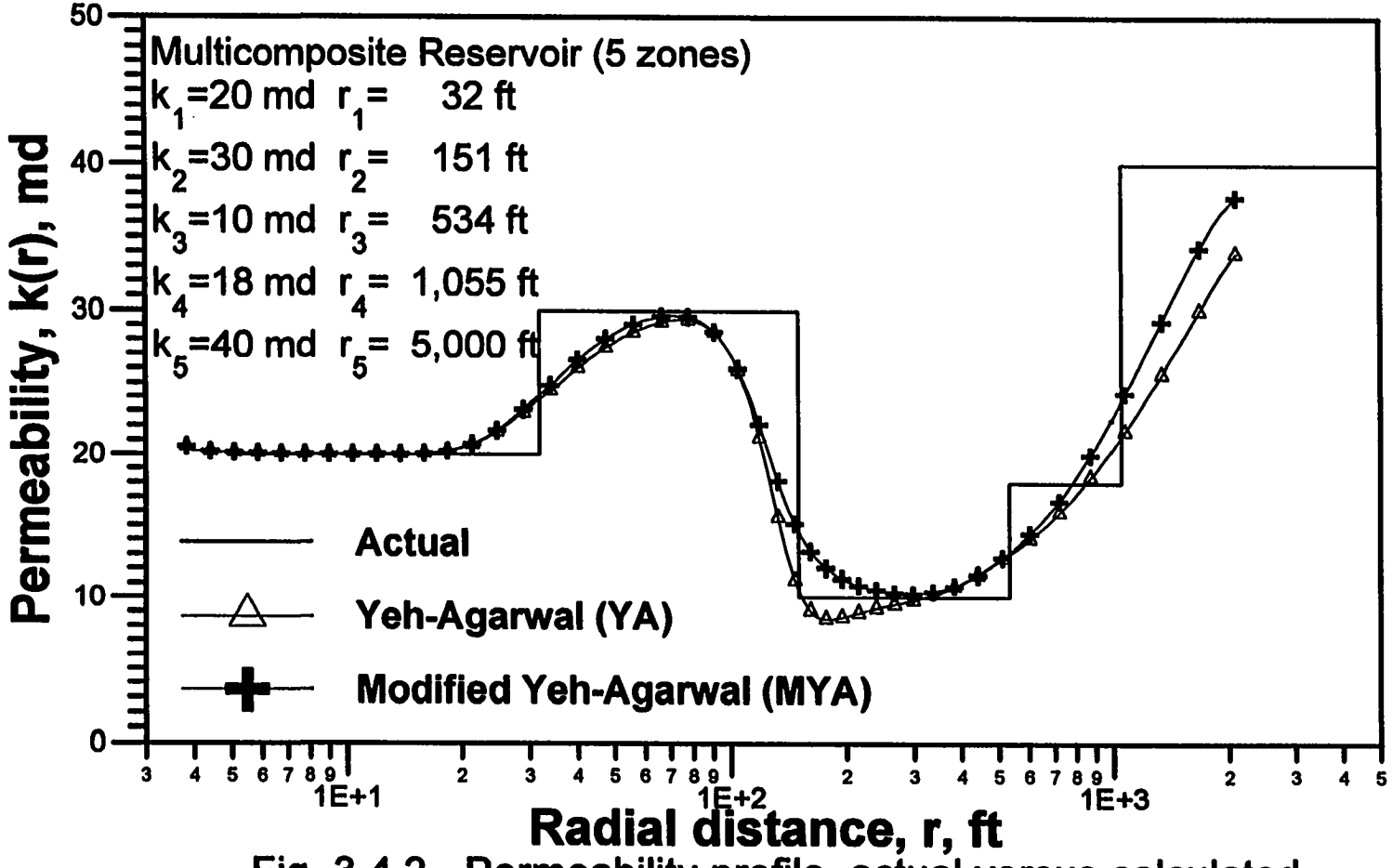

Fig. 3.4.2 - Permeability profile, actual versus calculated via YA and MYA; Drawdown Case 1.

Reproduced with permission of the copyright owner. Further reproduction prohibited without permission.

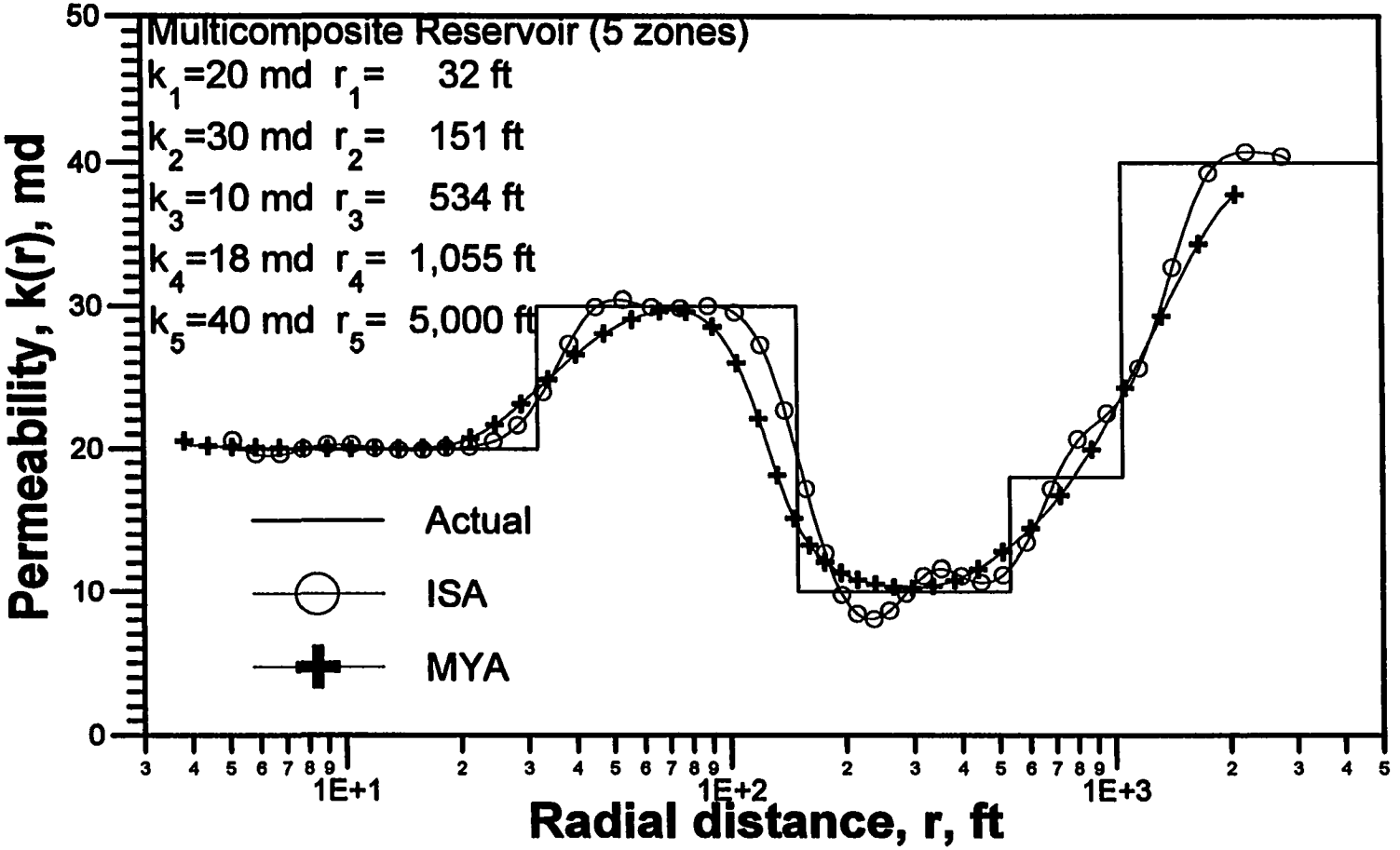

Fig. 3.4.3 - Permeability profile, actual versus calculated via ISA and MYA; Drawdown Case 1.

Reproduced with permission of the copyright owner. Further reproduction prohibited without permission.

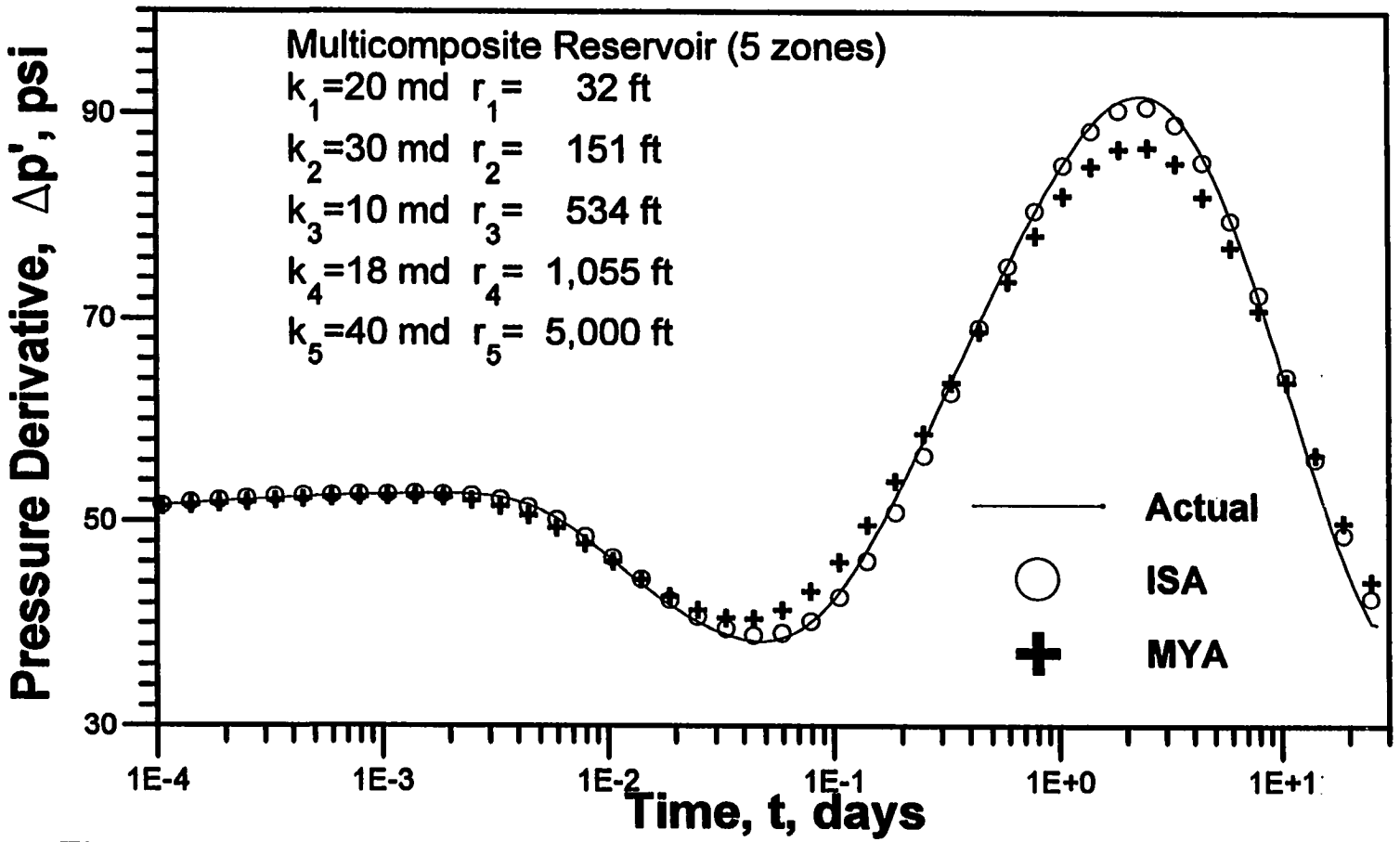

Fig. 3.4.4 - Comparison of pressure derivatives; actual versus computed from estimated permeability distributions; Drawdown Case 1.

Fig. 3.4.5 shows that the pressures essentially overlay one over another, i.e., are graphically indistinguishable. These results illustrate that different permeability distributions might yield practically identical pressure responses, whereas differences could be observed with the pressure derivatives. This illustrates the inherent nonuniqueness of solutions to the inverse problem of finding permeability distribution from well test data. In spite of this, our inverse-problem solutions, which are based on the pressure derivative, often yield a good approximation to the actual permeability distribution.

3.4.2 Drawdown, Case 2

This case refers to a 5-composite reservoir with the permeability of the last zone equal to 10 md, $k_5 = 10$ md, instead of 40 md as in Case 1. Except for this change all the other data are the same as in Case 1.

Fig. 3.4.6 shows the actual piecewise constant permeability distribution (solid line) and the permeability distributions computed with ISA (circular data points) and MYA (plus data point) procedure. As in Case 1, the results from both methods are reasonable approximations to the true permeability profile, however, ISA reproduces more closely the zones of constant permeability and the sharp variation between them. More importantly, as shown in Fig. 3.4.7, when the ISA-computed permeability distribution is used in our simulator, we obtain pressure derivative results (circular data points) which match the actual pressure derivative (solid line), whereas, the simulated pressure derivative generated with the MYA-computed permeability distribution (plus data points) does not match the original simulated pressure derivative nearly as well.

In practically all results we have generated to date with ISA and MYA procedures, we have basically observed similar behavior with respect to the computed permeability distribution and pressure derivative, respectively, as described in Case 1 and Case 2.

Reproduced with permission of the copyright owner. Further reproduction prohibited without permission.

Reproduced with permission of the copyright owner. Further reproduction prohibited without permission.

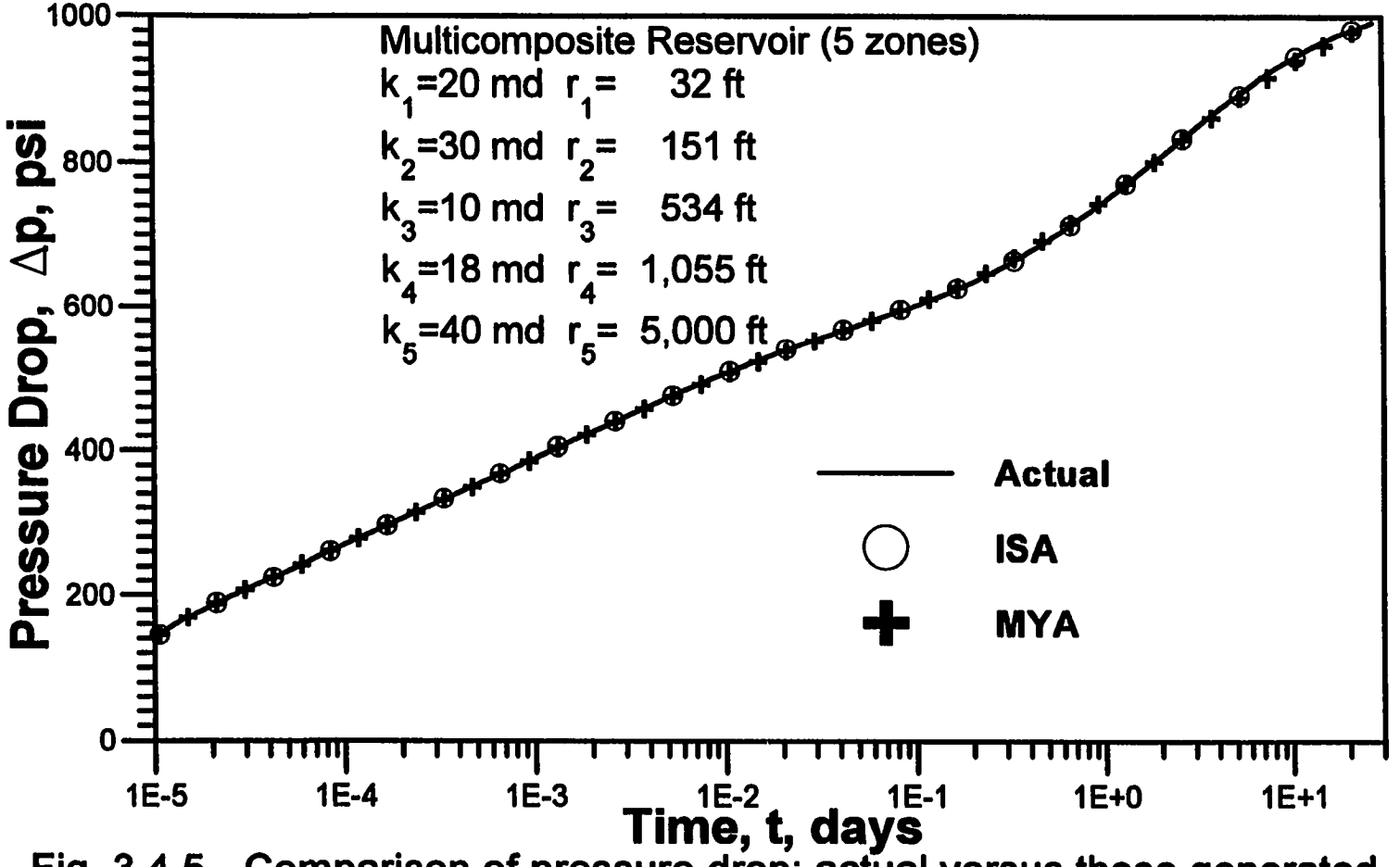

Fig. 3.4.5 - Comparison of pressure drop; actual versus those generated with estimated permeability distributions; Drawdown Case 1.

Reproduced with permission of the copyright owner. Further reproduction prohibited without permission.

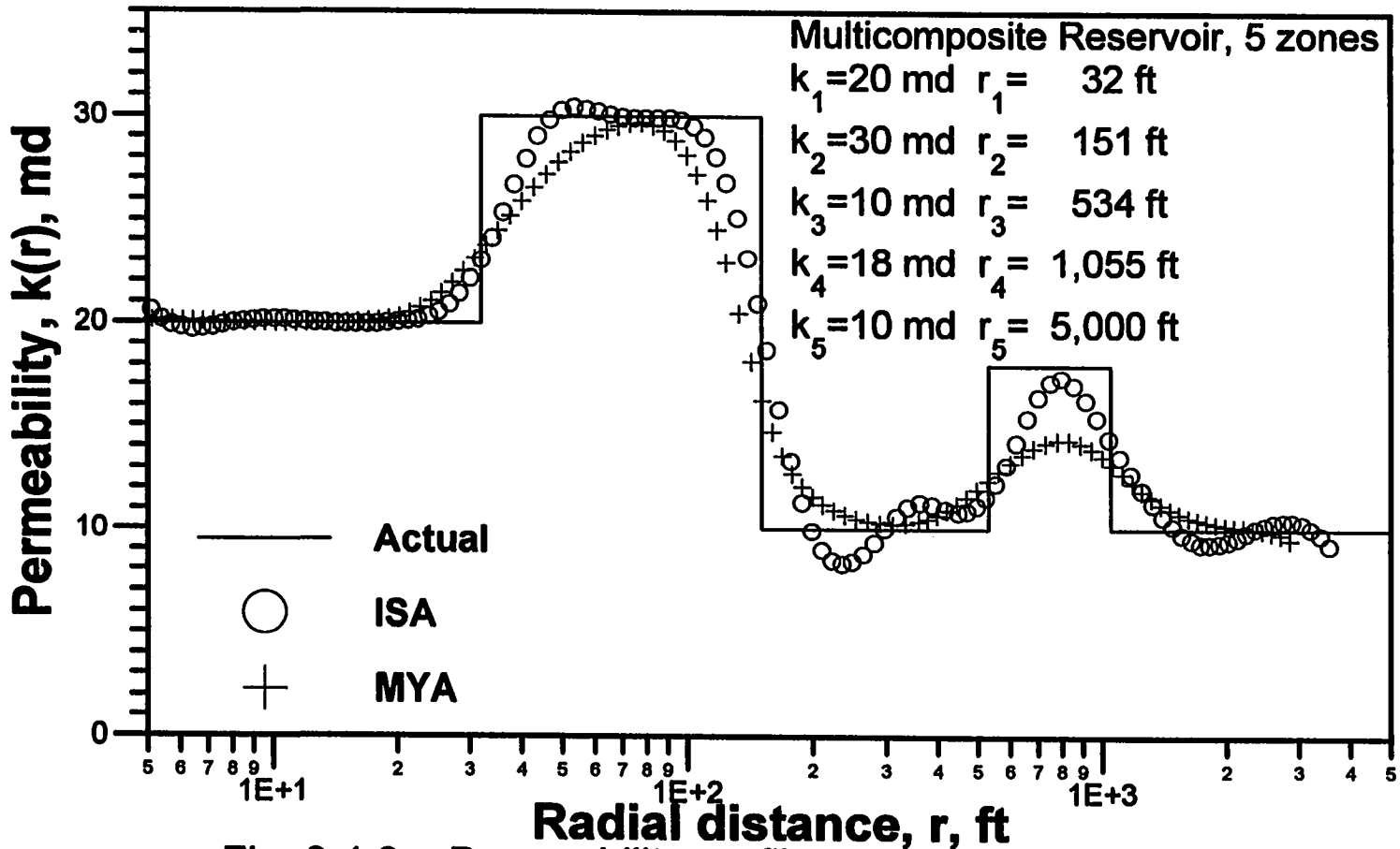

Fig. 3.4.6 - Permeability profile, actual versus calculated; Drawdown Case 2.

Reproduced with permission of the copyright owner. Further reproduction prohibited without permission.

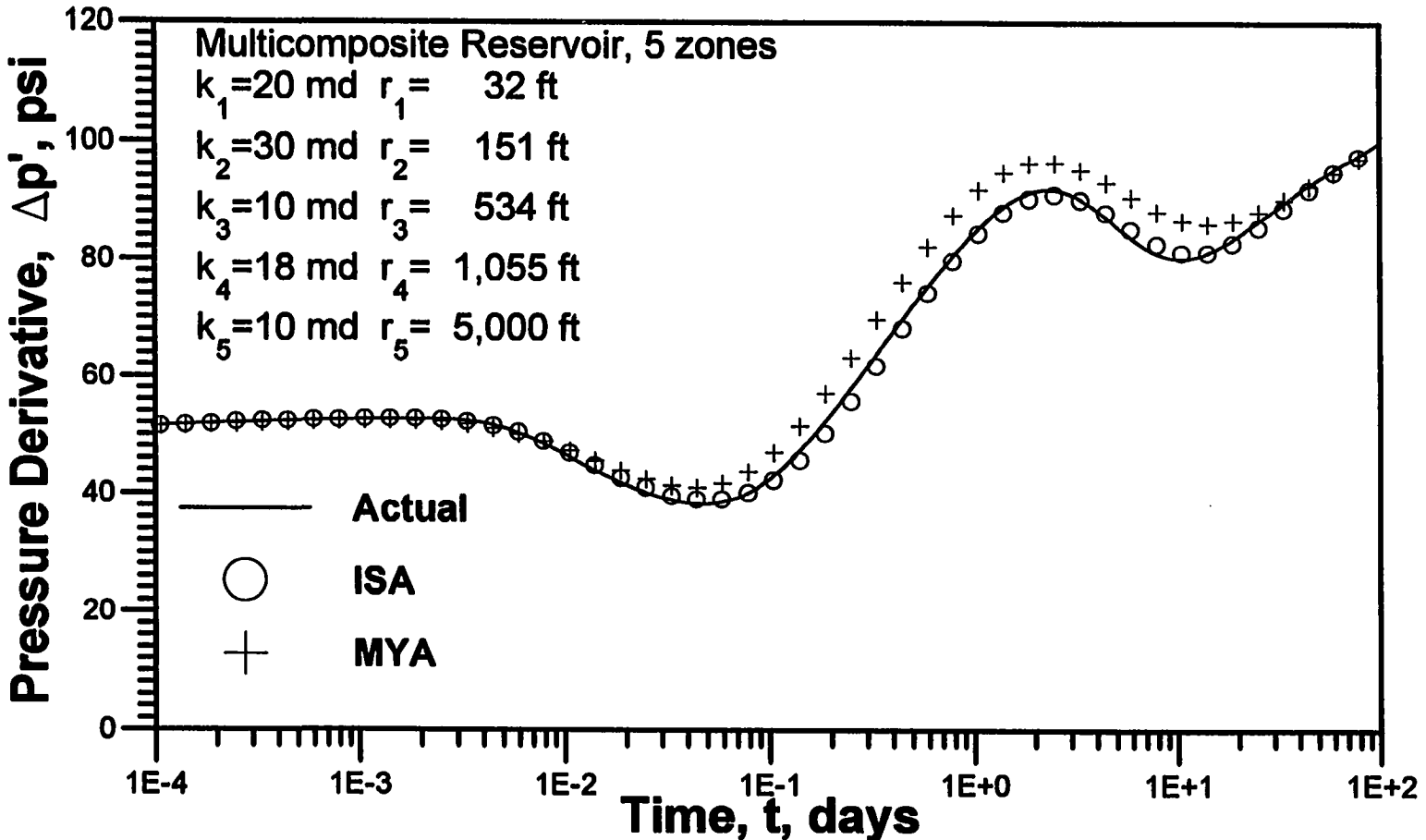

Fig. 3.4.7 - Comparison of pressure derivatives; actual versus computed from estimated permeability distributions; Drawdown Case 2.

3.4.3 Drawdown, Case 3

These case refers to a reservoir with a continuous monotonically increasing permeability function, given by Eq. 3.4.1

$$k(r) = k_0 + a\ln(r), \tag{3.4.1}$$

where $k_0 = 10$ md and $a = 3.543$. All other reservoir/well system parameters and producing conditions as in Case 1 (see Table 2.3.3). According to Eq. 3.4.1 the values of permeability at the wellbore, $r_w = 0.3$ ft, and at the reservoir external radius, $r_e = 5{,}000$ ft, are, respectively, $k(r_w) = 6$ md and $k(r_e) = 40$ md . We consider the drawdown data up to 20 days which is approximately the end of transient flow.

Fig. 3.4.8 compares the actual permeability distribution, Eq. 3.4.1, with the permeability distribution computed using the ISA and MYA procedures. Both methods give an excellent approximation to the true permeability distribution. Also, as shown in Fig. 3.4.9, pressure derivatives obtained from the simulated pressure using both ISA and MYA-calculated permeability distribution are in excellent agreement with the actual original pressure derivative data.

3.4.4 Drawdown, Case 4

This case pertains to a reservoir with the "smoothly" varying radial permeability distribution listed in Table 3.4.1a. Other pertinent reservoir/well system data are presented in Table 3.4.1b. We simulated a drawdown test for 1000 days. The infinite-acting period ends by about 100 days. We applied both methods, ISA and MYA, to the transient data.

Reproduced with permission of the copyright owner. Further reproduction prohibited without permission.

Reproduced with permission of the copyright owner. Further reproduction prohibited without permission.

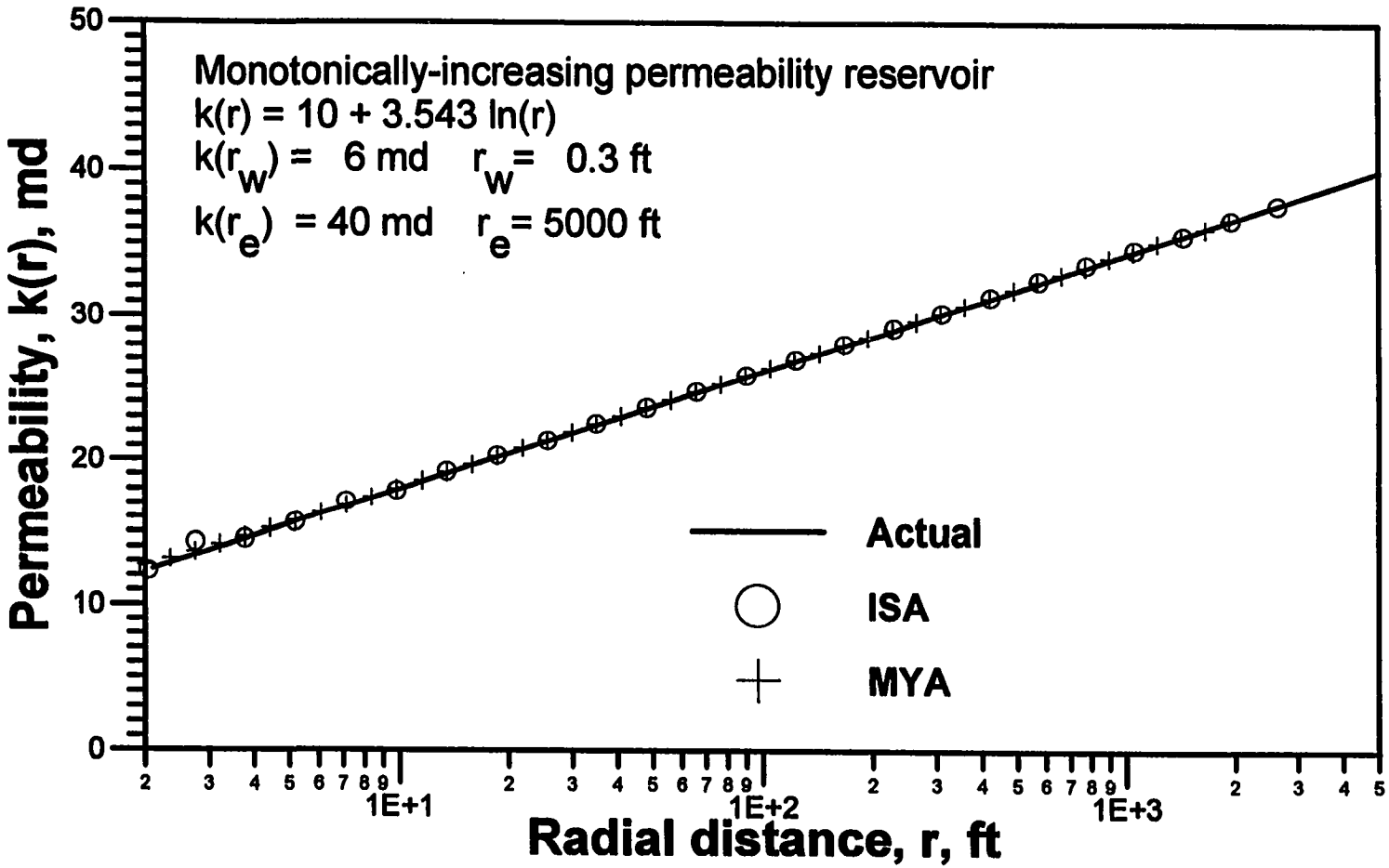

Fig. 3.4.8 - Permeability profile, actual versus calculated; Drawdown Case 3.

Reproduced with permission of the copyright owner. Further reproduction prohibited without permission.

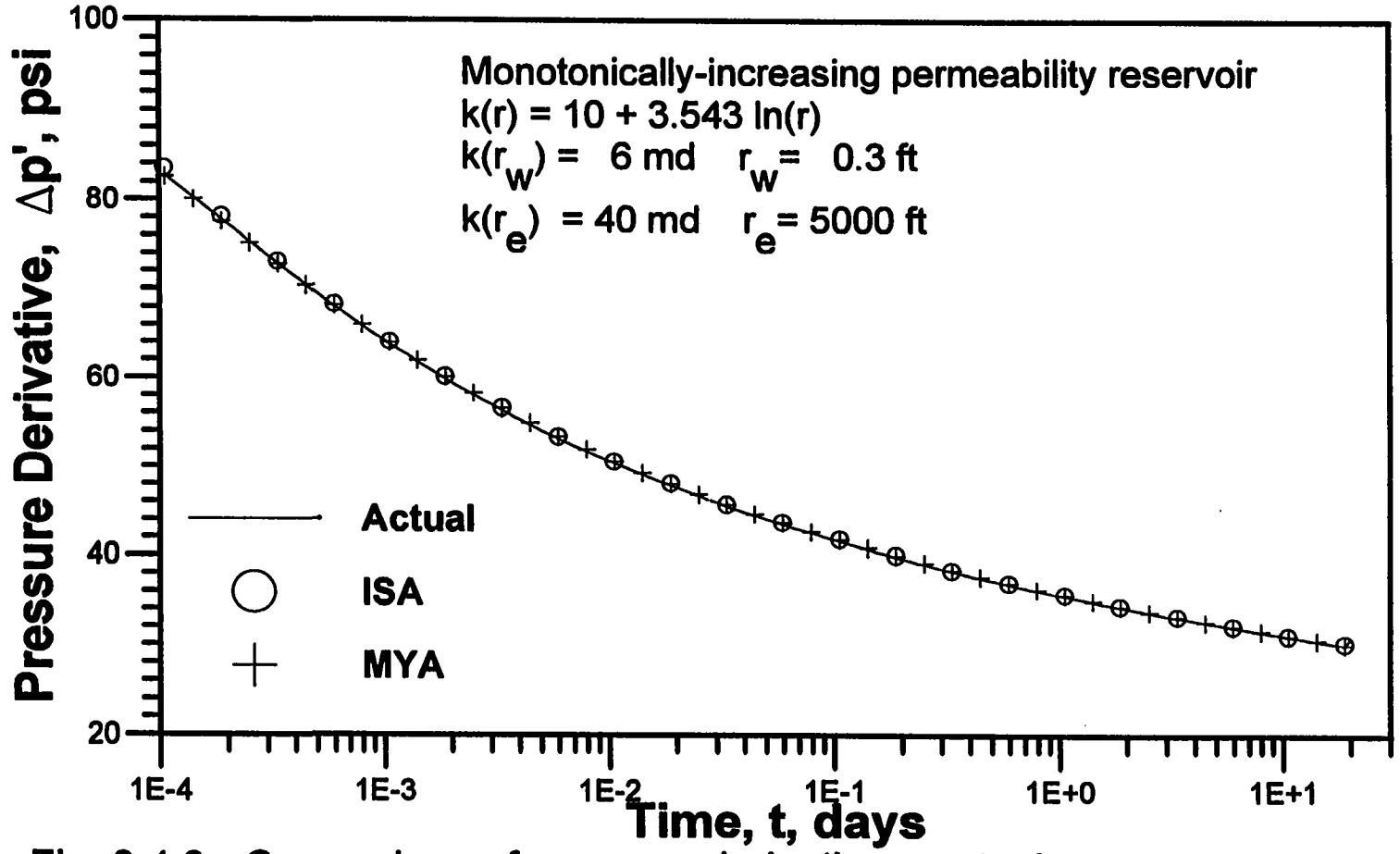

Fig. 3.4.9 - Comparison of pressure derivatives; actual versus computed from estimated permeability distributions; Drawdown Case 3.

Fig. 3.4.10 compares the actual versus calculated permeability profiles. The profile obtained with ISA (circles) is in close agreement with the actual one (solid curve). The profile computed with the MYA procedure (plus data points) gives a reasonable approximation to the actual profile with some small departures in the extreme parts (highest and lowest values) of the permeability profile. Fig. 3.4.10 also presents the KID values (squares). We observe that at a radius of investigation (Eq. 3.2.4) of about 5600 ft (corresponding to 100 days), the KID value is approximately 25 md, which is the value of permeability which extends from approximately 1300 ft up to the external radius, 10,000 ft. At this time (100 days) the region of investigation extends from 339 ft up to 6607 ft (inner and outer limits computed from Eqs. 3.2.46 and 3.2.47, respectively). So, we observe that at this time, although the KID value results from a weighted-harmonic average of all permeability values within the region of investigation, according to Eq. 3.2.45, it is not significantly influenced by the values of permeability between 339 ft and 1300 ft. Most of the contribution to the value of KID comes from the region between 1300 and 6607 ft; this can be explained by the shape of the kernel weighting function (see Fig. 2.2.4). At 100 days the outer boundary starts affecting the wellbore pressures and, consequently the wellbore pressure derivatives. This means the transient period is over and the data beyond that point in time are not suitable for analysis with our methods.

Fig. 3.4.11 shows the simulated pressure derivatives using as input in our simulator the true permeability values of Table 3.4.1a and the permeability values computed with our inversion procedures ISA and MYA. The derivatives that resulted from the ISA permeability distribution are indistinguishable from the derivatives obtained from our simulator using the actual permeability distribution of Table 3.4.1a. The derivative values obtained from the simulator with the MYA permeability distribution differ slightly from the true derivative values over most of the radial range, but differs more noticeably in the

Reproduced with permission of the copyright owner. Further reproduction prohibited without permission.

Table 3.4.1a
Reservoir with Smooth Permeability Distribution; Drawdown Case 4
Reservoir/Well System Parameters (a) Permeability Distribution

i	r_i	k_i	i	r_i	k_i
1	3.329278E-01	30.000	51	6.078402E+01	20.194
2	3.694697E-01	30.000	52	6.745563E+01	20.090
3	4.100224E-01	30.000	53	7.485951E+01	20.050
4	4.550262E-01	30.000	54	8.307604E+01	20.116
5	5.049696E-01	30.000	55	9.219440E+01	20.373
6	5.603946E-01	30.000	56	1.023136E+02	20.918
7	6.219032E-01	30.000	57	1.135435E+02	21.813
8	6.901628E-01	30.000	58	1.260059E+02	23.073
9	7.659146E-01	30.000	59	1.398362E+02	24.677
10	8.499808E-01	30.000	60	1.551846E+02	26.540
11	9.432741E-01	30.000	61	1.722175E+02	28.589
12	1.046807E+00	30.000	62	1.911200E+02	30.740
13	1.161704E+00	30.000	63	2.120972E+02	32.869
14	1.289212E+00	30.000	64	2.353768E+02	34.903
15	1.430715E+00	30.000	65	2.612116E+02	36.646
16	1.587749E+00	30.000	66	2.898820E+02	37.987
17	1.762019E+00	30.000	67	3.216992E+02	38.780
18	1.955417E+00	30.000	68	3.570087E+02	38.776
19	2.170042E+00	30.000	69	3.961937E+02	37.998
20	2.408225E+00	30.000	70	4.396797E+02	36.343
21	2.672550E+00	30.000	71	4.879386E+02	34.086
22	2.965887E+00	30.000	72	5.414944E+02	31.589
23	3.291420E+00	30.000	73	6.009284E+02	29.317
24	3.652684E+00	30.000	74	6.668859E+02	27.596
25	4.053600E+00	30.000	75	7.400828E+02	26.477
26	4.498521E+00	30.000	76	8.213138E+02	25.823
27	4.992275E+00	30.645	77	9.114606E+02	25.463
28	5.540224E+00	30.114	78	1.011502E+03	25.270
29	6.148315E+00	30.091	79	1.122524E+03	25.165
30	6.823149E+00	30.073	80	1.245731E+03	25.108
31	7.572053E+00	30.058	81	1.382461E+03	25.073
32	8.403157E+00	30.046	82	1.534199E+03	25.053
33	9.325481E+00	30.036	83	1.702592E+03	25.037
34	1.034904E+01	30.027	84	1.889467E+03	25.003
35	1.148494E+01	30.022	85	2.096854E+03	25.000
36	1.274552E+01	30.023	86	2.327003E+03	25.000
37	1.414446E+01	30.026	87	2.582413E+03	25.000
38	1.569695E+01	30.011	88	2.865857E+03	25.000
39	1.741983E+01	29.930	89	3.180412E+03	25.000
40	1.933182E+01	29.696	90	3.529491E+03	25.000
41	2.145367E+01	29.204	91	3.916886E+03	25.000
42	2.380841E+01	28.380	92	4.346800E+03	25.000
43	2.642160E+01	27.214	93	4.823902E+03	25.000
44	2.932162E+01	25.795	94	5.353370E+03	25.000
45	3.253994E+01	24.303	95	5.940952E+03	25.000
46	3.611150E+01	22.955	96	6.593027E+03	25.000
47	4.007507E+01	21.906	97	7.316673E+03	25.000
48	4.447368E+01	21.153	98	8.119746E+03	25.000
49	4.935508E+01	20.658	99	9.010963E+03	25.000
50	5.477226E+01	20.367	100	1.000000E+04	25.000

Reproduced with permission of the copyright owner. Further reproduction prohibited without permission.

Table 3.4.1b Reservoir with Smooth Permeability Distribution; Drawdown Case 4 Reservoir/Well System Parameters; (b) Other Parameters		
$h = 20$ ft	$\mu = 1.0$ cp	$r_w = 0.3$ ft
$\phi = 0.20$	$c_t = 10\times10^{-6}$ psi^{-1}	$q = 300$ rb/d
$p_i = 6000$ psi		$r_e = 10{,}000$ ft

region containing the highest values of permeability, i.e., between 200 and 600 ft. Thus, like in most of the cases we have presented , as well as in many other cases we have tested so far, the ISA and MYA methods applied to transient drawdown data yield good estimates of the actual permeability distribution, with the ISA method being somewhat superior to the MYA method.

Fig. 3.4.12 compares simulated pressures using the actual and the computed permeability profiles. Graphically indistinguishable pressure results are obtained for all three permeability distributions.

Reproduced with permission of the copyright owner. Further reproduction prohibited without permission.

Reproduced with permission of the copyright owner. Further reproduction prohibited without permission.

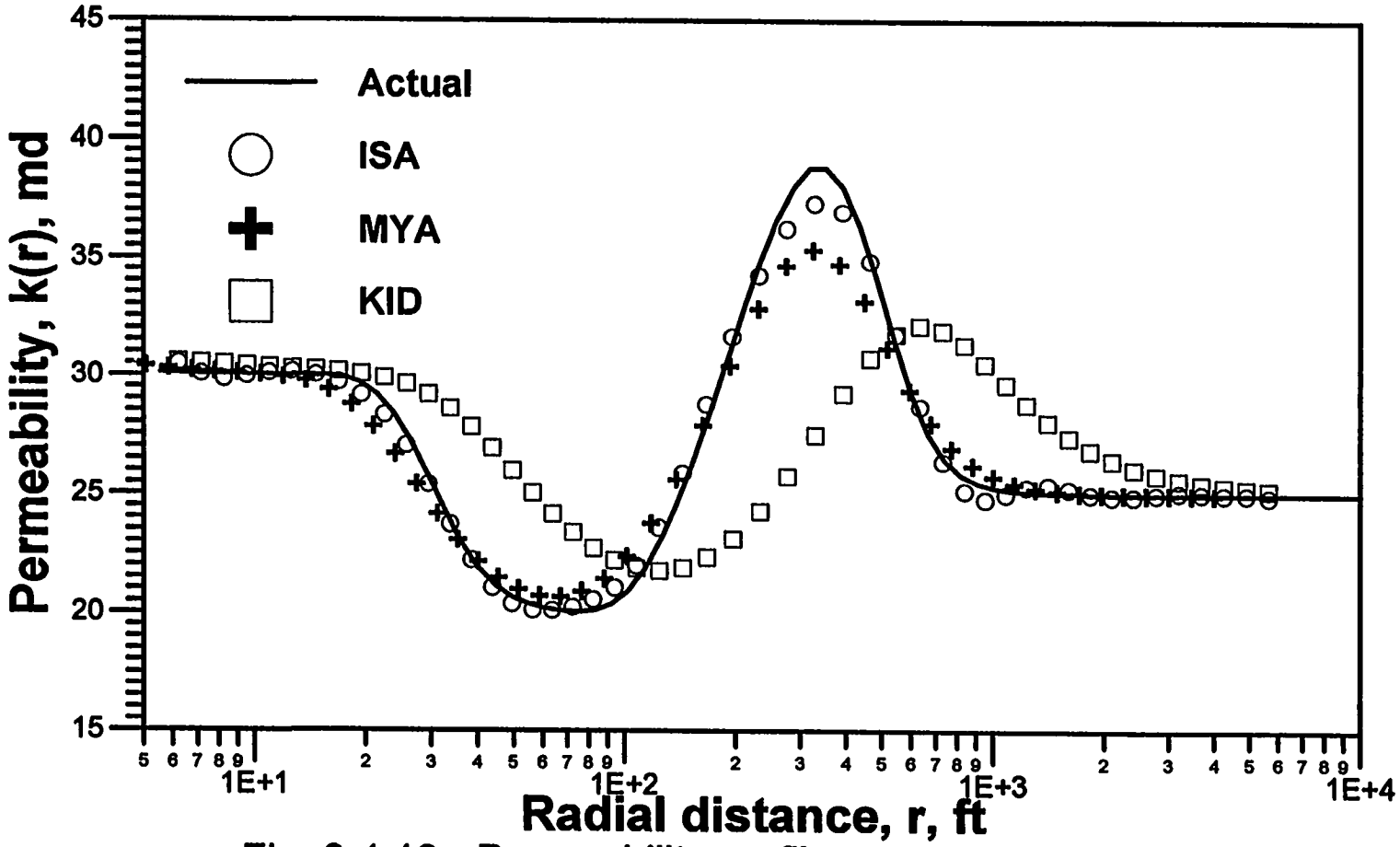

Fig. 3.4.10 - Permeability profile, actual versus calculated; Drawdown Case 4.

Reproduced with permission of the copyright owner. Further reproduction prohibited without permission.

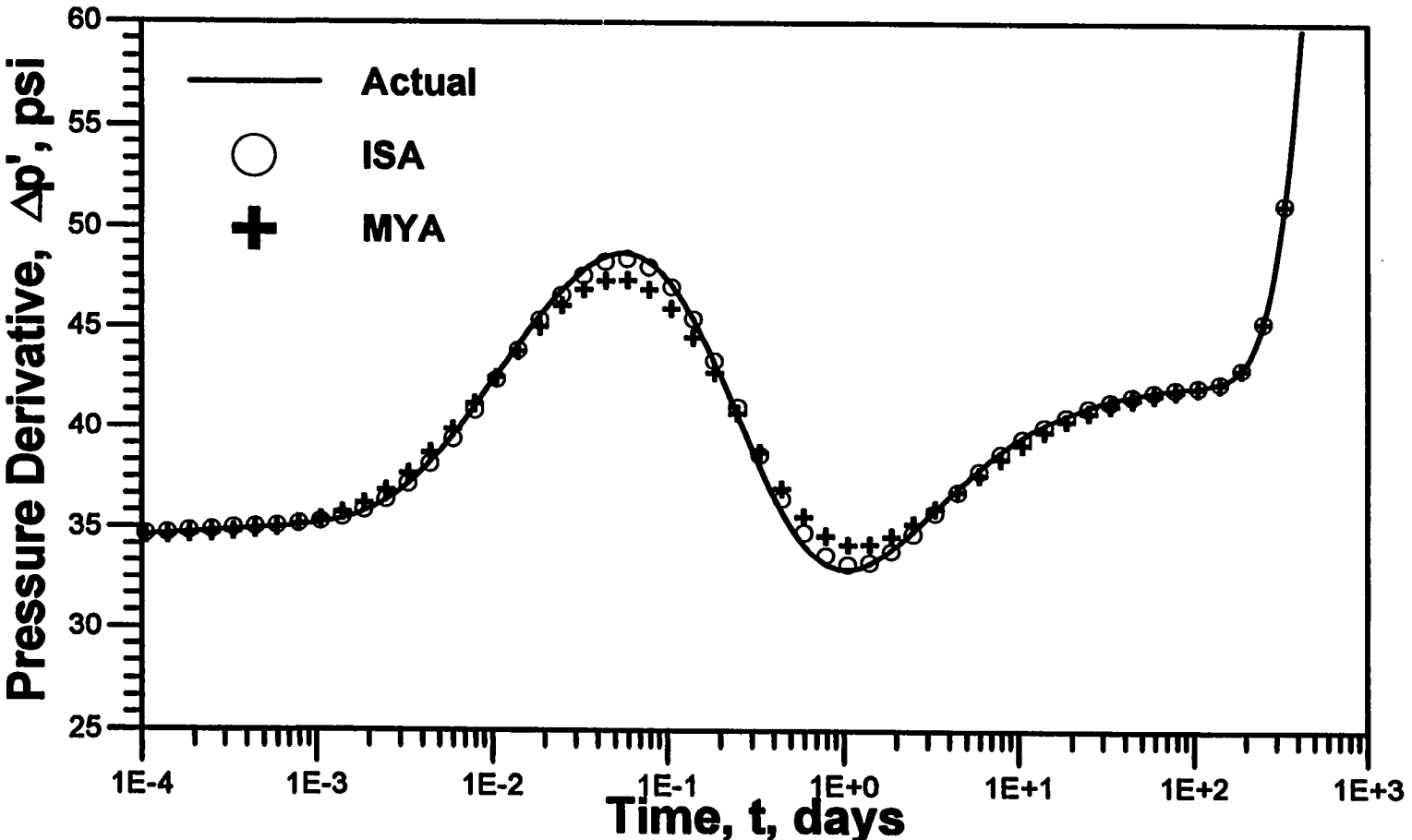

Fig. 3.4.11 - Comparison of pressure derivatives; actual versus computed from estimated permeability distributions; Drawdown Case 4.

Reproduced with permission of the copyright owner. Further reproduction prohibited without permission.

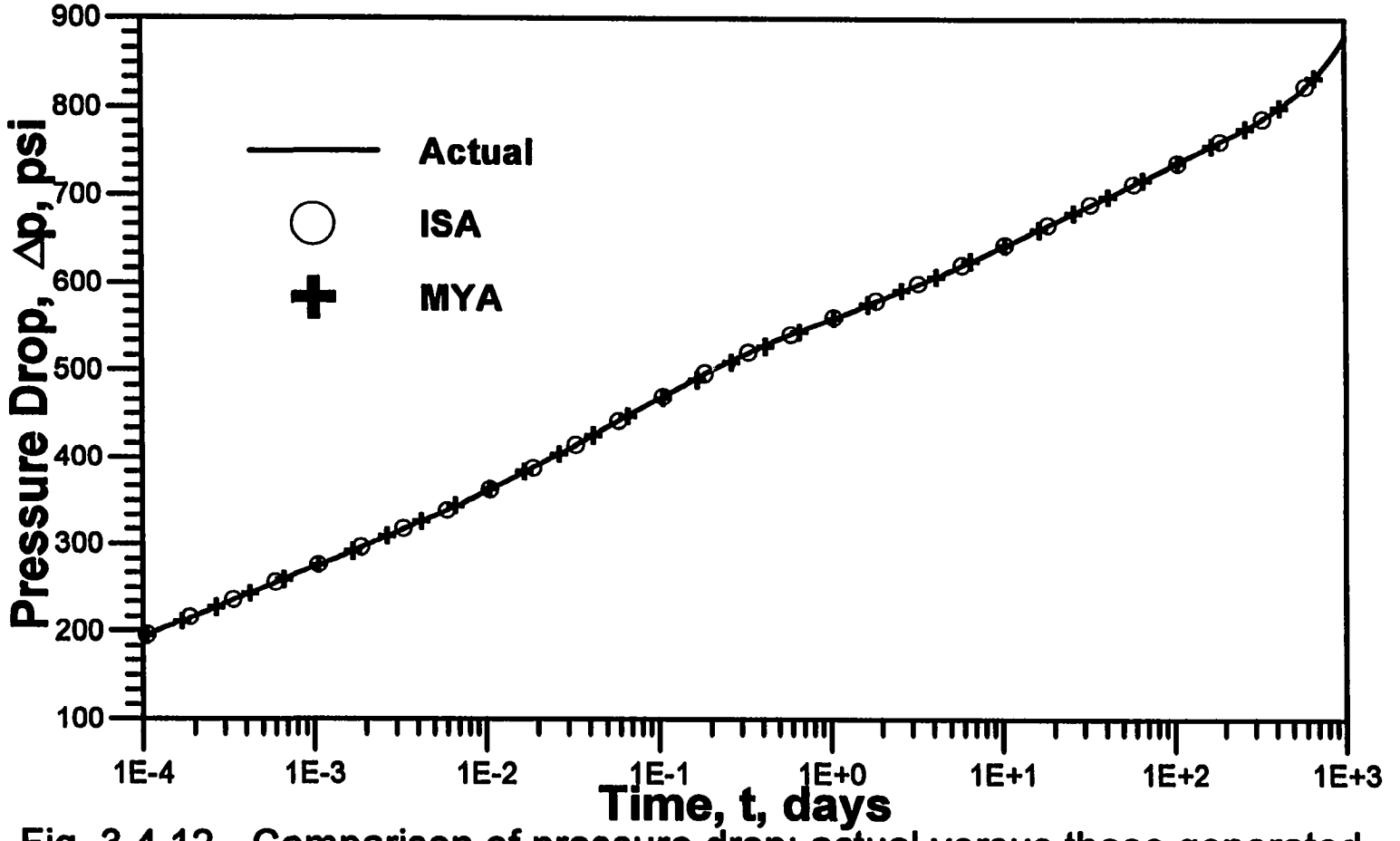

Fig. 3.4.12 - Comparison of pressure drop; actual versus those generated with estimated permeability distributions; Drawdown Case 4.

3.5 Applications to Buildup Data

We present here the results of our inverse solution algorithm (ISA) applied to buildup data. We consider cases where the buildup follows a steady-state flow, a transient flow and a pseudosteady-state flow period. In all cases, we used our simulator to generate the synthetic well-test data. Our methods of analysis are based on transient solutions. Thus, we consider in our analysis only the buildup data during the infinite-acting period, except in one case, where we also present the results of the analysis of data beyond the end of the infinite-acting period, to illustrate the boundary effects in our results. We performed the analysis of the well-test data based on our procedure described in the subsection 3.2.3.

3.5.1 Buildup after Steady-State Flow, Case 1

We consider the 5-zone, multicomposite reservoir with reservoir/well system parameters given in Table 2.3.3, as in Drawdown Case 1. Here, first we considered a constant pressure outer boundary, and simulated the well producing at a constant sandface flow rate of 300 rb/d for a period of 1000 days, long enough to reach the steady-state flow, and then shut the well in for a period of 100 days. We then applied the ISA to the buildup data corresponding to the infinite-acting period which ends at about 26 days.

In Fig 3.5.1 we compare the actual permeability distribution (solid line) with the permeability profiles computed with ISA applied to buildup data (star data points), and ISA applied to drawdown data (circular data points). The buildup and drawdown data derived permeability profiles overlay one over the other, confirming computationally what had been shown in theory, in subsection 3.2.2.1, Eq. 3.2.34. Also, both profiles are in

Reproduced with permission of the copyright owner. Further reproduction prohibited without permission.

Reproduced with permission of the copyright owner. Further reproduction prohibited without permission.

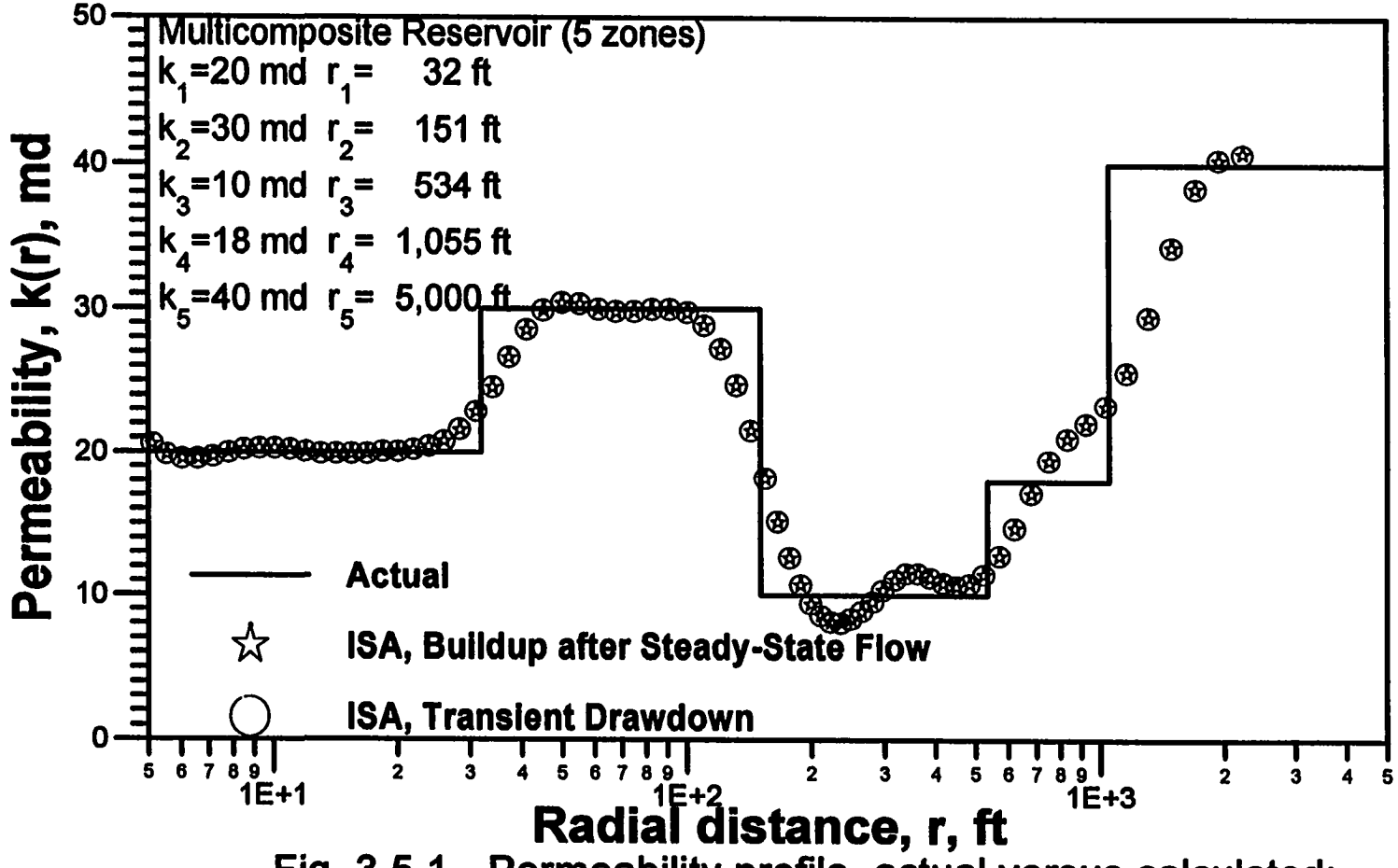

Fig. 3.5.1 - Permeability profile, actual versus calculated; Buildup Case 1.

good agreement with the actual one. This result is general, in the sense that, if we produce until a steady-state flow occurs at the time of shut-in, then the permeability distribution computed with ISA applied to the transient buildup data will reproduce the permeability profile calculated with ISA applied to the transient drawdown data.

3.5.2 Buildup after Transient Flow, Case 2

This case deals with the reservoir with the "smoothly" varying radial permeability distribution presented in Table 3.4.1a and reservoir/well system data shown in Table 3.4.1b. We considered a no-flow outer boundary and simulated the well producing at a constant sandface flow rate of 300 rb/d for a period of 100 days. The length of production time was chosen to be of 100 days to assure that at the time of shutting the well in: (i) the well is producing under transient conditions and, (ii) inner and outer radius of the region of investigation at a time $\hat{t}_{pD} + \Delta\hat{t}_D$ is within the last constant-permeability zone.

We then computed the permeability profile by applying ISA with the simulated buildup data corrected for the producing time effects (see subsection 3.2.2 and sub-subsection 3.2.2.2), and compared this profile with the drawdown derived permeability distribution as shown in Fig. 3.5.2. Note both profiles are identical, until the no-flow outer boundary effects begin to influence the wellbore pressures. Moreover, both permeability profiles show a good agreement with the actual one (solid curve). Fig. 3.5.2 also shows the influence of the boundary in our computed permeability profiles. At very late times, when either buildup or drawdown data are completely influenced by the no-flow outer boundary, the drawdown derived permeability decreases rapidly toward zero, whereas, the buildup derived permeability increases sharply. The presence of a no-flow external boundary is equivalent, during the late time drawdown, to a zero-permeability zone at the reservoir outer radius, thus, justifying the drawdown-derived permeability behavior. In the

Reproduced with permission of the copyright owner. Further reproduction prohibited without permission.

Reproduced with permission of the copyright owner. Further reproduction prohibited without permission.

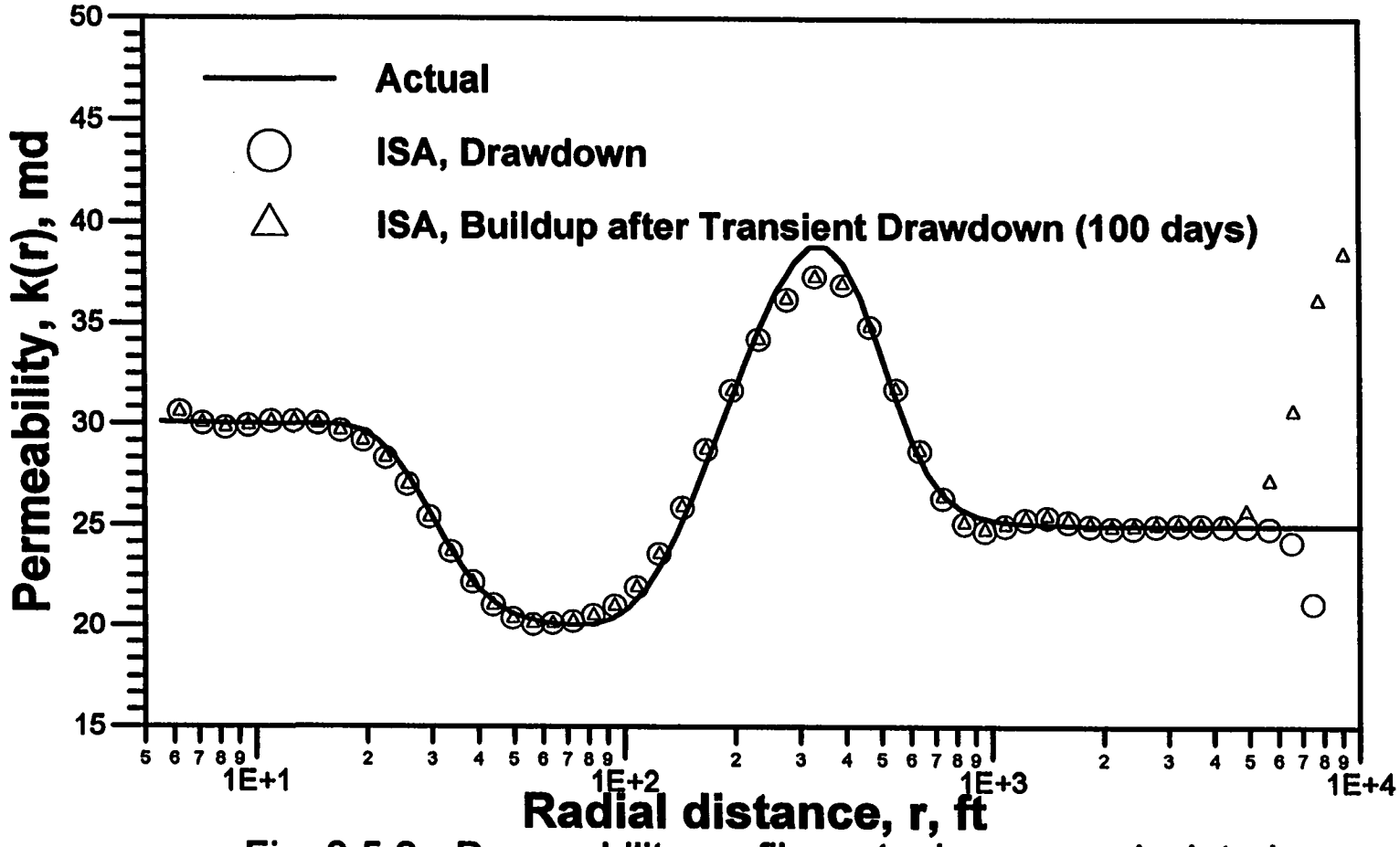

Fig. 3.5.2 - Permeability profile, actual versus calculated; Buildup Case 2.

other hand, during the late time buildup the pressure slowly approaches to the average reservoir pressure; this causes the pressure derivative with respect to natural logarithm of time to decrease, resulting in a sharp increase in the computed-buildup permeability.

3.5.3 Buildup after Pseudosteady Flow, Case 3a and Case 3b

Case 3a

We consider in this case the reservoir with monotonically-increasing permeability distribution and reservoir/well system data as in Drawdown Case 3. We simulated a flow period of 1000 days, allowing the pseudosteady state flow to be established, and then shut the well in for a buildup of 1000 days. We considered only the buildup data points within the transient period which ends about 20 days (same as for drawdown); this is observed from the buildup pressure derivatives after correction for the producing-time effects, as described in subsection 3.2.2.3.

Fig. 3.5.3 compares the permeability distributions calculated by application of ISA to the transient buildup data, with and without considering the correction term due to the pseudosteady state flow effect, to the actual permeability distribution. The permeability profile calculated with our correction (triangular data points) is in excellent agreement with the actual profile (solid line); whereas, the permeability profile calculated without correction (open square data points) departs from the true one at $r \approx 300$ ft. These results provide computational verification of the correctness of our Eqs. 2.3.66 and 3.2.41, for, respectively, the forward problem and for the inverse problem related to a buildup after a pseudosteady-state flow period. Fig. 3.5.3 also shows, for comparison, the permeability distribution computed with ISA using transient drawdown data (circles) which practically

Reproduced with permission of the copyright owner. Further reproduction prohibited without permission.

Reproduced with permission of the copyright owner. Further reproduction prohibited without permission.

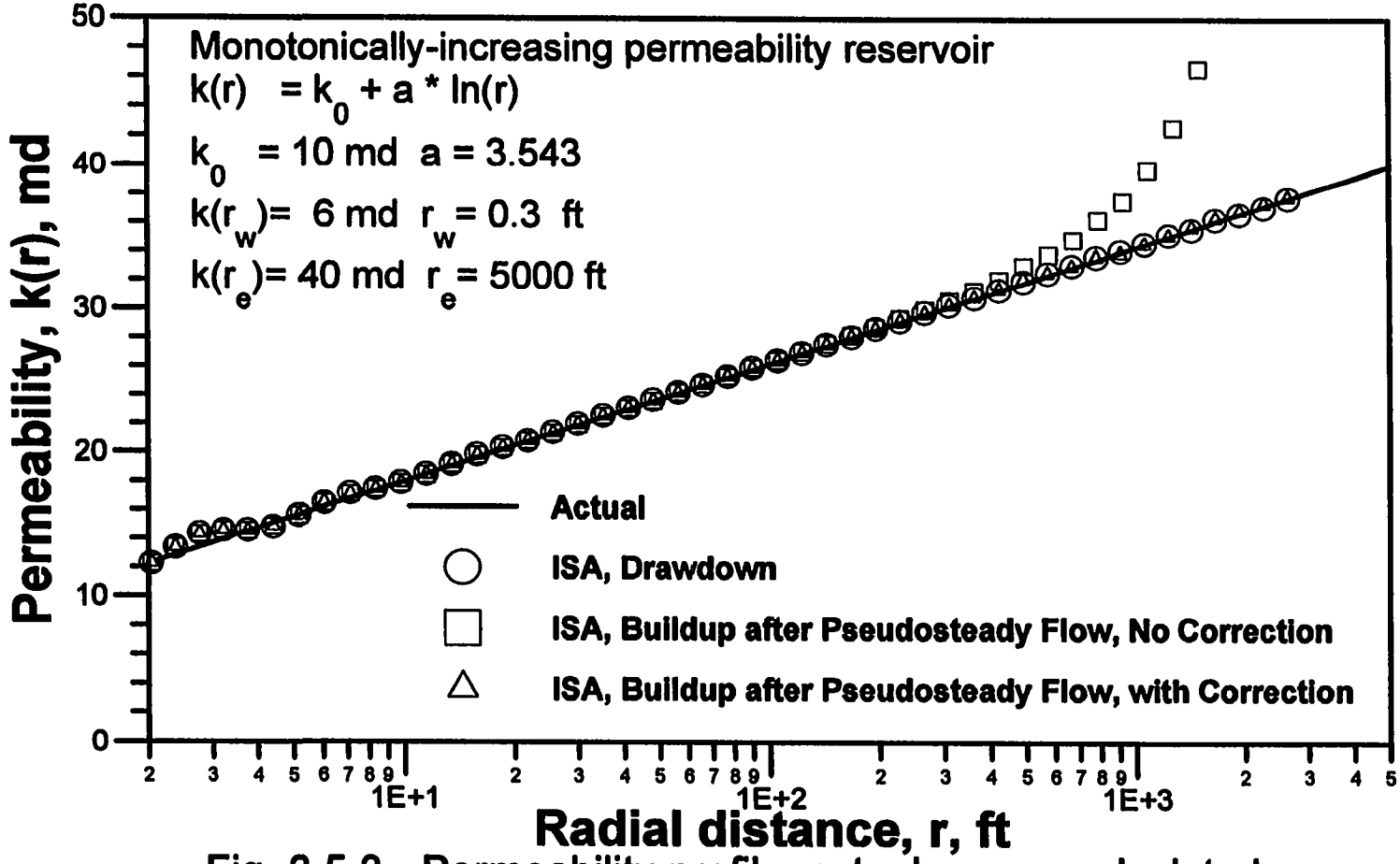

Fig. 3.5.3 - Permeability profile, actual versus calculated; Buildup Case 3a.

reproduces the actual permeability profile and the permeability profile computed with corrected transient buildup data.

Case 3b

In this case, we used the reservoir with the "smoothly" varying radial permeability distribution presented in Table 3.4.1a and reservoir/well system data shown in Table 3.4.1b. We considered a no-flow outer boundary and simulated a buildup of 1000 days, after producing the well for 1000 days until it reached the pseudosteady state flow condition. As in Case 3a, we considered only the buildup data points within the transient period, which ends about 100 days (same as for drawdown); this is observed from the buildup pressure derivatives after correction for the producing-time effects, as described in subsection 3.2.2.3.

As in all other buildup cases, we corrected the well-test pressure derivative buildup data for the producing-time effects (as detailed in subsection 3.2.2) and applied the analysis procedure of subsection 3.2.3.

Fig. 3.5.4 shows that the permeability distribution calculated with the application of ISA to the corrected transient buildup data (star data points) basically reproduces the permeability profile computed by the ISA applied to the transient drawdown data (circles), and both are in very good agreement with the actual permeability profile (solid curve).

Although not shown, we also observed that the permeability distribution computed via MYA applied to the buildup data after correcting for producing-time effects is identical to the permeability distribution obtained from drawdown data.

Reproduced with permission of the copyright owner. Further reproduction prohibited without permission.

Reproduced with permission of the copyright owner. Further reproduction prohibited without permission.

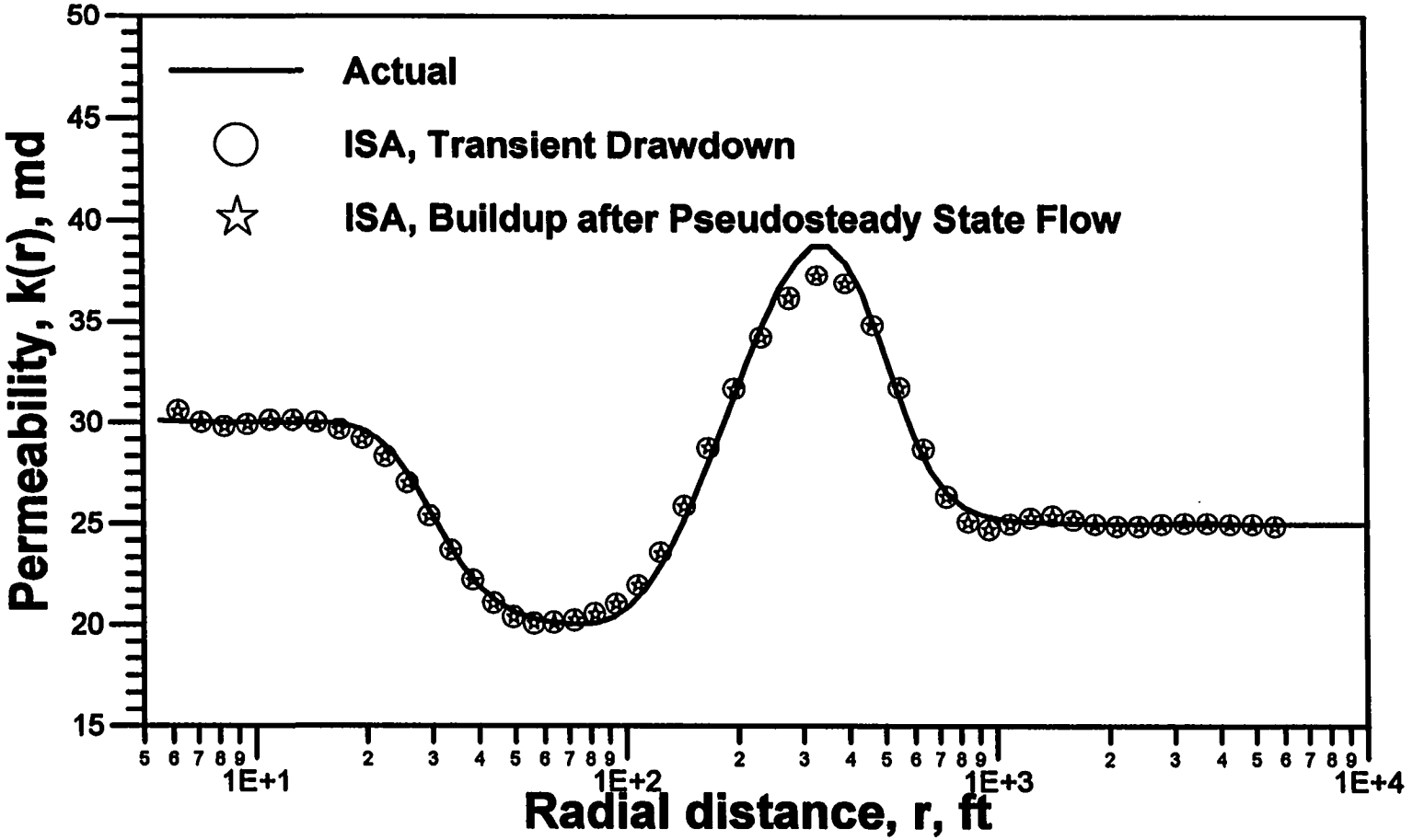

Fig. 3.5.4 - Permeability profile, actual versus calculated; Buildup Case 3b.

3.6 Reservoir Pressure Profile (RPP)

Determination of the average reservoir pressure is of high importance for many reservoir applications including the following: reserve estimation; monitoring of secondary and tertiary recovery projects and assessment of communication between zones or reservoirs. However, rather than determining a single value of average pressure it might be as useful to determine the reservoir pressure profile, as pointed out by Yeh and Agarwal[25]. We show that, once the reservoir pressure profile is calculated we can, under some conditions: (a) compute the average reservoir pressure, with good accuracy; and, if the reservoir pressure profile is established under a steady-state or pseudosteady-state condition, (b) estimate the permeability distribution, $k(r)$; (c) the productivity index; and (d) the equivalent homogeneous permeability. It is also shown the computation of the flow rate during the boundary-dominated flow, in the case of a constant pressure production.

The reservoir pressure profile at the instant of shut-in can be computed by one of the two methods: (i) using the pressure buildup data and a properly defined radius of investigation; (ii) using the drawdown data and the appropriate equation for the reservoir pressure at a fixed time, $p(r,t)$, with the permeability distribution obtained from ISA or MYA, when the profile is established under steady state or pseudosteady state condition. We show that under certain conditions both methods yield good results.

3.6.1 RPP from Buildup Data

The method for computation of the reservoir pressure profile at the time of shut-in, $p(r,\Delta t=0)$, from buildup pressure data, comes from the observation of pressure buildup profiles at different times. Here, we used the 5-zone, multicomposite reservoir whose

Reproduced with permission of the copyright owner. Further reproduction prohibited without permission.

reservoir/well system data are shown in Table 2.3.3 and our simulator, to generate pressure buildup profiles at several shut-in times, shown in Fig. 3.6.1. The simulated pressure buildup data, at the wellbore and throughout the reservoir, was obtained after the well was produced for 26.6 days, at a constant flow rate of 300 reservoir barrels per day, and then shut in for equal period of time of 26.6 days. We recall from the Drawdown Case 1, where this reservoir was used, that the transient flow ends at about 26.6 days. We observe, on each pressure profile, a flat zone that extends from the wellbore up to a certain distance, r, where the $\frac{\partial p(r,\Delta t)}{\partial(r)} \approx 0$, i.e., where there is no flow in the reservoir. This flat zone is a pseudosteady state zone that advances with time into the reservoir due to the zero flow rate. This zone has been recognized, in homogeneous reservoirs, (Streltsova[38]) as having a radial extent given by the following radius of investigation

$$r_i = 1.5\sqrt{C_1 \eta \Delta t}, \tag{3.6.1}$$

where $C_1 = 0.006328$ for Δt in days, and the hydraulic diffusivity, η, is defined for a homogeneous reservoir as

$$\eta = \frac{k_{\text{hom}}}{\phi \mu c_t}. \tag{3.6.2}$$

In Fig. 3.6.1 it is noticed that, during the buildup, the wellbore pressure increases with time in a manner that reflects the reservoir pressure profile at the instant of shut-in. If we can determine the specific relationship between the wellbore pressure buildup behavior with time, $(\Delta t, p_{ws}(\Delta t))$, and the reservoir pressure profile at the shut-in time, $(r, p(r, \Delta t = 0))$, then we can compute the reservoir pressure profile at the shut-in time, at least, up to a maximum radial distance where the average reservoir pressure occurs. Yeh and Agarwal in their work about injection wells[25] have presented similar observations for falloff test. They concluded that the pressure profile at the instant of shut in can be obtained using the wellbore pressure and the radius of investigation given by Eq. 3.6.1,

Reproduced with permission of the copyright owner. Further reproduction prohibited without permission.

Reproduced with permission of the copyright owner. Further reproduction prohibited without permission.

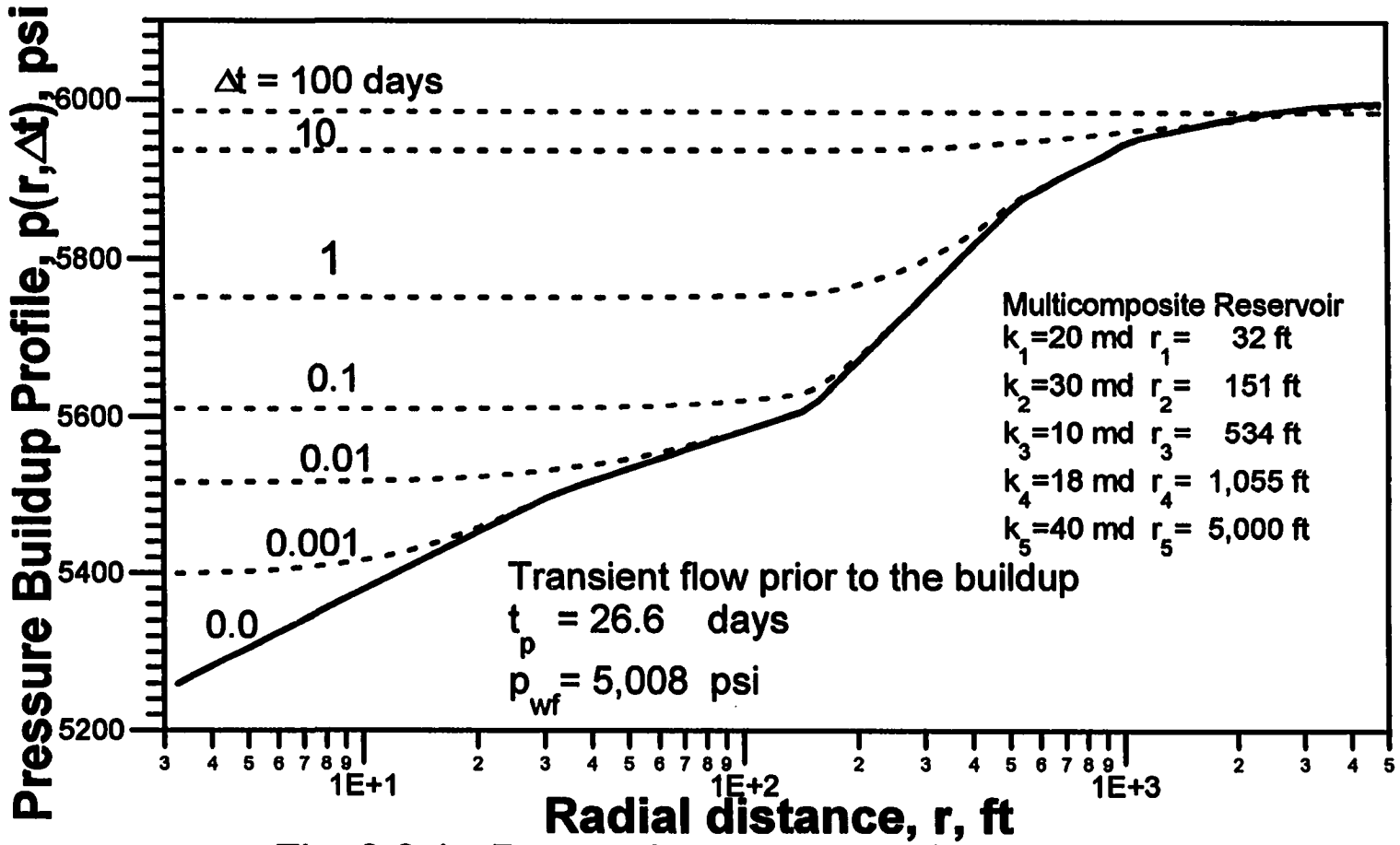

Fig. 3.6.1 - Reservoir pressure profiles during buildup after transient flow.

where they replace the shut-in time Δt by the equivalent time Δt_e, and used the instantaneous total mobility, λ_t, in place of the constant homogeneous mobility, k_{hom}/μ.

Those ideas can be readily translated into our radially heterogeneous reservoir problem. Hence, we compute the reservoir pressure profile at the instant of shut-in using the following equation

$$p(r_i, \Delta t = 0) = p_{ws}(\Delta t), \tag{3.6.3}$$

where the radial distance r_i is given by

$$r_i = 1.5\sqrt{\frac{C_1 \hat{k}\, \Delta t}{\phi \mu c_t}}, \tag{3.6.4}$$

and $\hat{k}$ is computed from Eq. 3.2.32 with the appropriate correction term for the producing-time effects, $C_{pte}(\Delta t)$, under the conditions described in subsection 3.2.2. This correction term is zero when the buildup follows a steady-state flow, or can be computed with Eq. 3.2.38 or Eq. 3.2.42, when the buildup follows a transient or pseudosteady state flow period, respectively.

As pointed out in Ref. 25, Eqs. 3.6.3 and 3.6.4 just convert the wellbore pressure buildup at a time Δt, to the corresponding reservoir pressure at a distance r_i, at the instant of shut in.

In the following, we present examples of applications of the technique described in this subsection to determine the reservoir pressure profile, that exists at the instant of shut in, using buildup data. We used the 5-zone, multicomposite reservoir whose pertinent reservoir/well system parameters are shown in Table 2.3.3, which was used in the Drawdown Case 1. We simulated three cases of a buildup after a transient, steady-state and pseudosteady state flow. In all three cases, we ran a buildup of 26.6 days, which is, approximately the end of infinite-acting period during a corresponding drawdown flow, as discussed in Drawdown Case 1. Under this condition, we generated transient wellbore

Reproduced with permission of the copyright owner. Further reproduction prohibited without permission.

pressures and pressure derivatives from which we computed the reservoir pressure profile based on the method outlined above.

3.6.1.1 Reservoir Pressure Profile, Case 1

We consider here the same buildup test data used to generate the results of Fig. 3.6.1. We recall that at the end of the flow period of 26.6 days the well is still producing under infinite-acting condition. In this case, we illustrate the computation of the reservoir pressure profile existing at the instant of shut in, when the well is producing under *infinite-acting condition.* At the end of the simulated buildup period of 26.6 days, i.e., at $\Delta t_{max} = 26.6$ days, the wellbore shut-in pressure reached 5975 psi and the radius of investigation (from Eq. 3.6.4) is about 2400 ft. The average reservoir pressure at the shut-in time is 5986 psi. We computed the "instantaneous permeability", $\hat{k}$, that appears in the equation of radius of investigation, Eq. 3.6.4, using Eq. 3.2.32 with the correction term for the producing time effects, $C_{pte}(\Delta t)$, given by Eq. 3.2.38.

Fig. 3.6.2 compares the simulated pressure profile at the instant of shut in (solid curve) with the pressure profile computed with Eqs. 3.6.3 and 3.6.4 (circular data points). The computed and the simulated pressure profiles are in excellent agreement, thus, illustrating the applicability of the method to a buildup following a transient flow.

3.6.1.2 Reservoir Pressure Profile, Case 2

We present in this case the determination of reservoir pressure profile based on *buildup pressure data after a steady-state flow period.* First, we considered a constant pressure outer boundary condition of 6,001 psi, simulated a drawdown of 1,000 days, such that the steady-state flow regime was achieved, and then shut the well in for 26.6 days. At

Reproduced with permission of the copyright owner. Further reproduction prohibited without permission.

Reproduced with permission of the copyright owner. Further reproduction prohibited without permission.

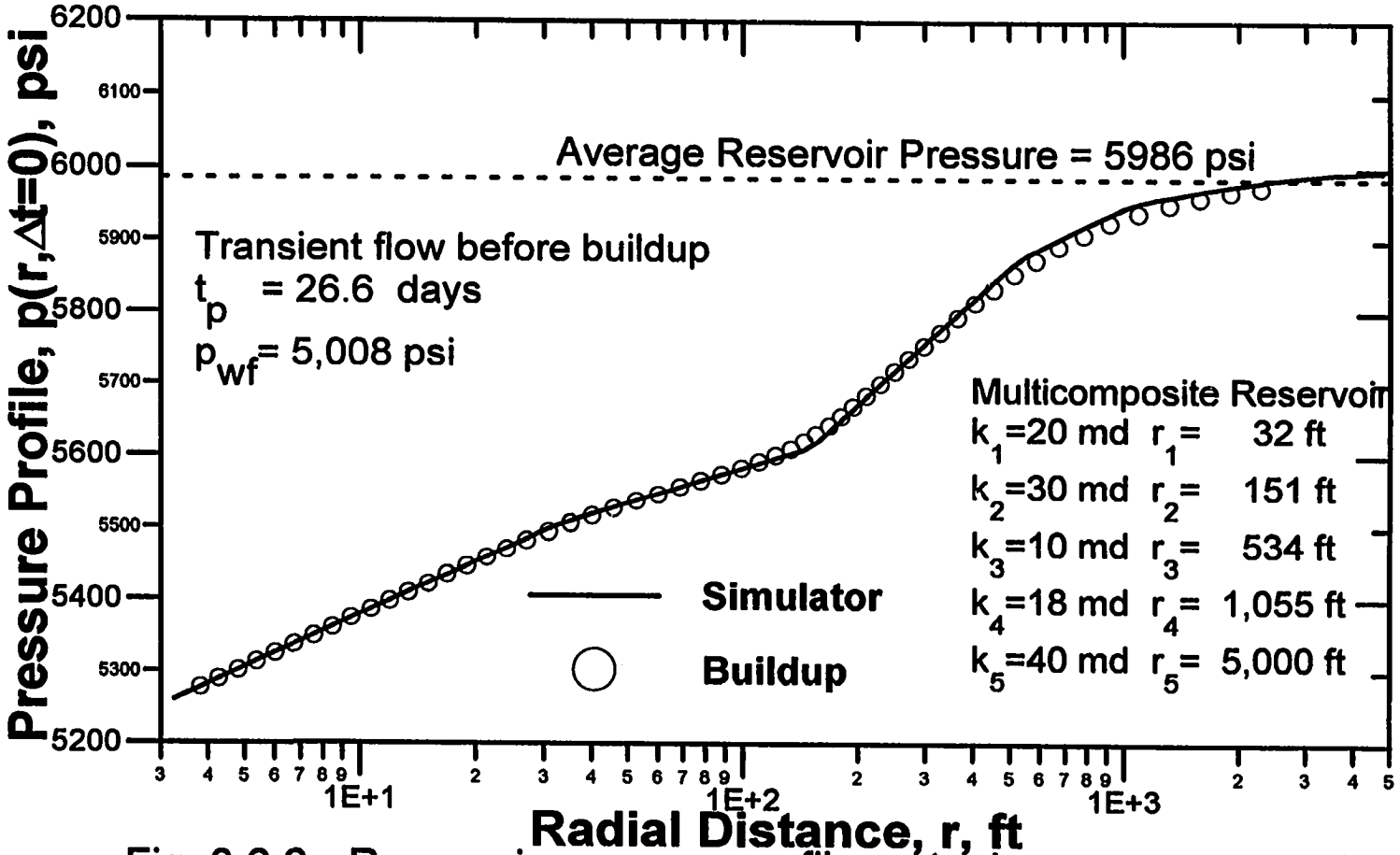

Fig. 3.6.2 - Reservoir pressure profile; actual versus computed with buildup data; Reservoir Pressure Profile, Case 1.

$\Delta t_{max} = 26.6$ days, the wellbore pressure has reached 5959 psi, and the radius of investigation 2250 ft. The average reservoir pressure at the instant of shut in was 5972 psi, and is shown as a dashed line in Fig. 3.6.3, where we compare the actual simulated reservoir pressure profile (solid curve), with the reservoir pressure profile computed from buildup data (circular data points) using Eqs. 3.6.3 and 3.6.4. The two profiles are practically identical. The results illustrate the applicability of the method to calculate a reservoir pressure profile established under steady-state conditions.

3.6.1.3 Reservoir Pressure Profile, Case 3

This example presents the calculation of the *reservoir pressure profile* when *pseudosteady state* flow exists at the end of a drawdown. The reservoir/well system and drawdown and buildup conditions are the same as in Reservoir Pressure Profile, Case 2, except we now impose a no-flow outer boundary. At the end of 1,000 days of flow, we are well beyond the beginning of the pseudosteady state flow and the well is shut in for 26.6 days. At $\Delta t_{max} = 26.6$ days, the wellbore pressure has reached 5451 psi, and the radius of investigation was about 2250 ft. The average reservoir pressure at the instant of shut in was 5464 psi, and is shown as a dashed line in Fig. 3.6.4, where we observe that the reservoir pressure profile computed from the buildup data (circular data points) nearly reproduces the actual reservoir pressure profile (solid curve). The results illustrate the applicability of the method to calculate a reservoir pressure profile established under pseudosteady state conditions.

Reproduced with permission of the copyright owner. Further reproduction prohibited without permission.

Reproduced with permission of the copyright owner. Further reproduction prohibited without permission.

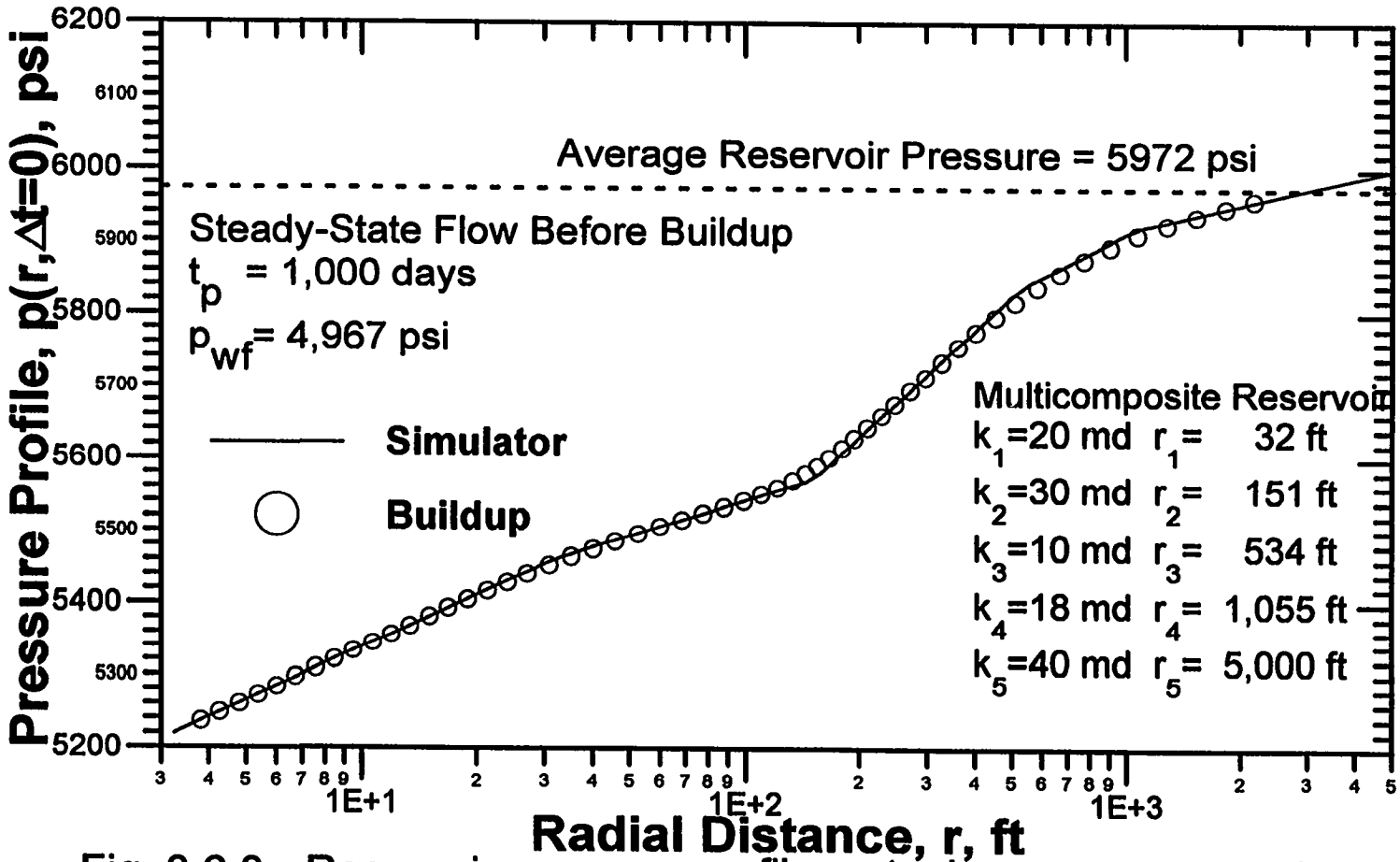

Fig. 3.6.3 - Reservoir pressure profile; actual versus computed with buildup data; Reservoir Pressure Profile, Case 2.

Reproduced with permission of the copyright owner. Further reproduction prohibited without permission.

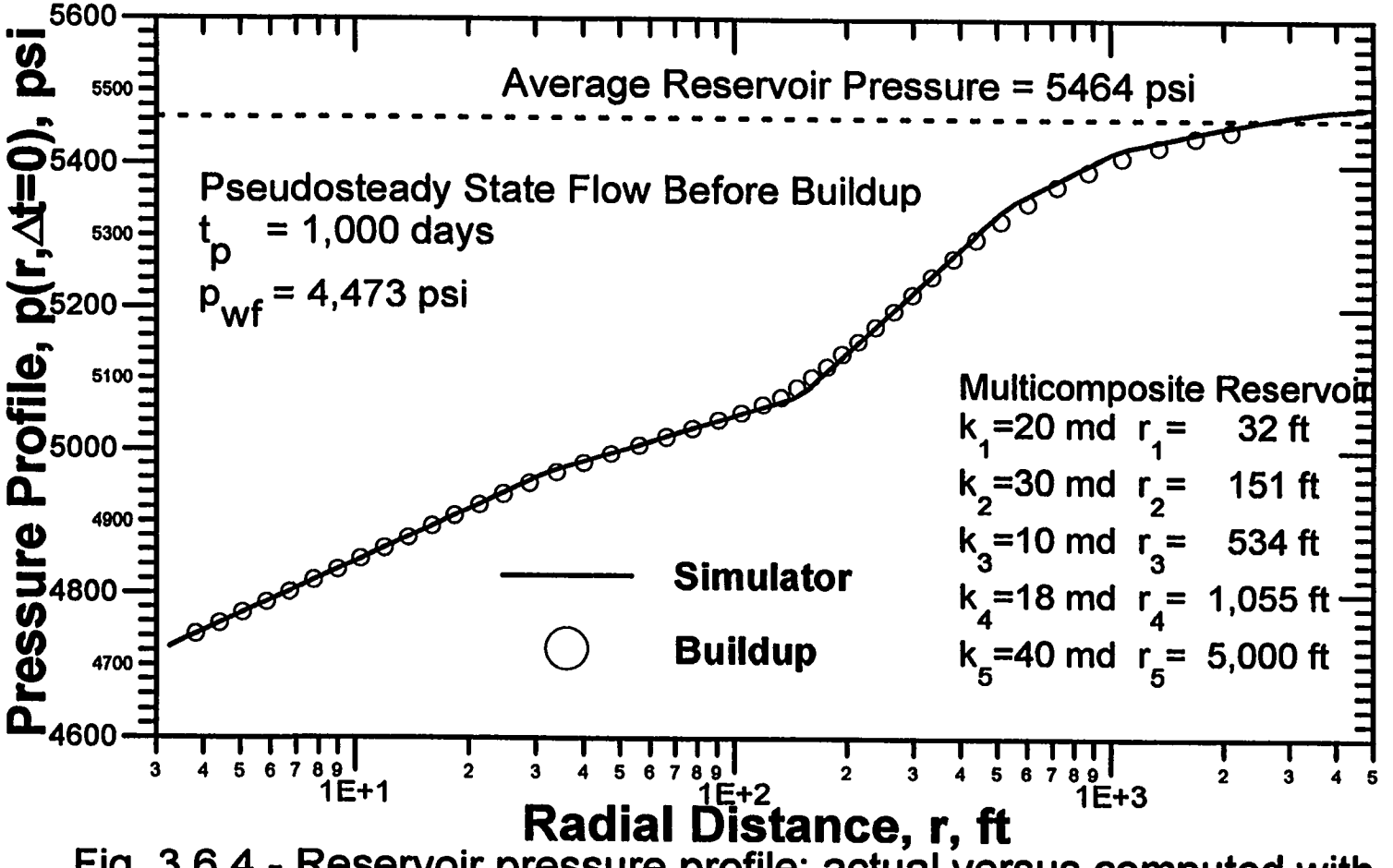

Fig. 3.6.4 - Reservoir pressure profile; actual versus computed with buildup data; Reservoir Pressure Profile, Case 3.

3.6.2 RPP from Computed Permeability Distribution

Once we have computed the permeability distribution, $k(r)$, either using the Inverse Solution Algorithm (ISA) or the Modified Yeh-Agarwal (MYA) method, we can approximate the reservoir pressure profile at any time, during the pseudosteady state or steady-state flow regime. For both flow regimes, we derived in Chapter II the appropriate equations to compute the reservoir pressure at any distance from the well, r, at any fixed time t, $p(r,t)$. In the case of transient flow, it is also possible to compute the reservoir pressure profile once we have the permeability distribution, but there is no simple or practical-to-use equation for this purpose.

In the following, we recall the general equations for steady-state flow and pseudosteady state flow, derived in Chapter II, and present an example application for the pseudosteady state case.

The *general steady-state flow equation* is given by

$$p(r) = p_{wf} + \frac{141.2q\mu}{h}\int_{r_w}^{r} \frac{1}{r'k(r')}dr', \tag{3.6.5}$$

at all times during the steady-state flow.

The *general pseudosteady state flow equation* is

$$p(r,t) = p_{wf}(t) + \frac{141.2q\mu}{h}\int_{r_w}^{r} \frac{1}{k(r')}\left(\frac{1}{r'} - \frac{r'}{r_e^2}\right)dr, \tag{3.6.6}$$

where t is any fixed time during the pseudosteady state flow period.

Reproduced with permission of the copyright owner. Further reproduction prohibited without permission.

We will apply Eq. 3.6.6 to estimate the reservoir pressure profile at the instant of shut in, i.e., at $t = t_p$ or $\Delta t = 0$. The reservoir pressure profile is estimated up to the radius of investigation that corresponds to the end of the infinite-acting period, t_{eia} (Δt_{eia} for buildup). To apply either equation, we need the permeability distribution, $k(r)$, the wellbore flowing pressure at the shut-in time, $p_{wf,s}$ and the external reservoir radius, r_e. The permeability distribution, $k(r)$, is obtained using one of our inversion techniques, either ISA or MYA; $p_{wf,s}$ is read from the last flow point measured; and r_e is obtained from the slope of a Cartesian plot of the pseudosteady state pressure data versus time.

3.6.2.1 Reservoir Pressure Profile, Case 4

This case pertains to a reservoir with the "smoothly" varying radial permeability distribution listed in Table 3.4.1a (see Fig. 3.4.10) and reservoir/well system data given in Table 3.4.1b (as in Drawdown Case 4). We considered a no-flow outer boundary and simulated a flow period of 1000 days until the pseudosteady state is established.

First, we computed the reservoir pressure profile at the end of the flow, i.e., at $t = t_p = 1000$ days, using our generalized pseudosteady state equation, Eq. 3.6.6, with the actual values of the permeability distribution, $k(r)$, the reservoir external radius, r_e, and the wellbore flowing pressure at the end of the flow, $p_{wf}(t = 1000 \text{ days})$. In Fig. 3.6.5, we compare the reservoir pressure profile computed analytically from Eq. 3.6.6 (circular data points) with the reservoir pressure profile obtained from the simulator (solid curve). As we observe they are indistinguishable. This result illustrates the accuracy of our general pseudosteady state equation, Eq. 3.6.6.

Second, we calculated the reservoir pressure profile at the end of the flow, using Eq. 3.6.6 with $k(r)$, r_e and $p_{wf}(t = 1000 \text{ days})$ obtained from the simulated well test data as follows. The permeability distribution, $k(r)$, which is shown as the circular points

Reproduced with permission of the copyright owner. Further reproduction prohibited without permission.

in Fig. 3.4.10, was computed applying the ISA to the transient pressure drawdown data. We recall from the Drawdown Case 4, that the infinite-acting period finishes at about 100 days, reaching a radius of investigation (based on Eq. 3.2.4) of 5600 ft. This is the radial distance up to which we compute the reservoir pressure profile. From the simulated drawdown we "measure" the bottomhole flowing pressure at the end of the flow, $p_{wf}(t = 1000 \text{ days})$ as 5120 psi. A fairly good estimate of the reservoir outer radius, r_e, is obtained from the material-balance derived equation, Eq. 2.3.80, with the known values of sandface flow rate, q, thickness, h and porosity, ϕ, as given in Table 3.4.1b, and the constant pressure decline, $\partial p / \partial t = -0.134$ psi / day computed from the pseudosteady state data. Using these values we obtain $r_e \cong 10{,}000$ ft. Then we computed the reservoir pressure profile, at the end of the simulated drawdown, $p(r, t = 1000 \text{ days})$, using Eq. 3.6.6. The result (triangular data points) is compared in Fig. 3.6.5 with the reservoir pressure profiles obtained analytically (circular data points) and from the simulator (solid curve). All of the three reservoir pressure profiles are in excellent agreement. *These results illustrate the accuracy of our ISA-computed permeability distribution and that the procedure can be applied to estimate the reservoir pressure profile, at a fixed time during the pseudosteady state flow regime based solely on drawdown pressure data.* In the same Fig. 3.6.5, for the sake of comparison, we included the reservoir pressure profile computed from buildup data (star data points); see Reservoir Pressure Profile Case 3. It also matches as nearly as well the simulated reservoir pressure profile.

3.6.3 Average Reservoir Pressure

The average reservoir pressure, $\bar{p}$, is defined as the volumetric-weighted arithmetic average of the reservoir pressure, as defined in Eq. 2.3.88 and reproduced in the following

Reproduced with permission of the copyright owner. Further reproduction prohibited without permission.

Reproduced with permission of the copyright owner. Further reproduction prohibited without permission.

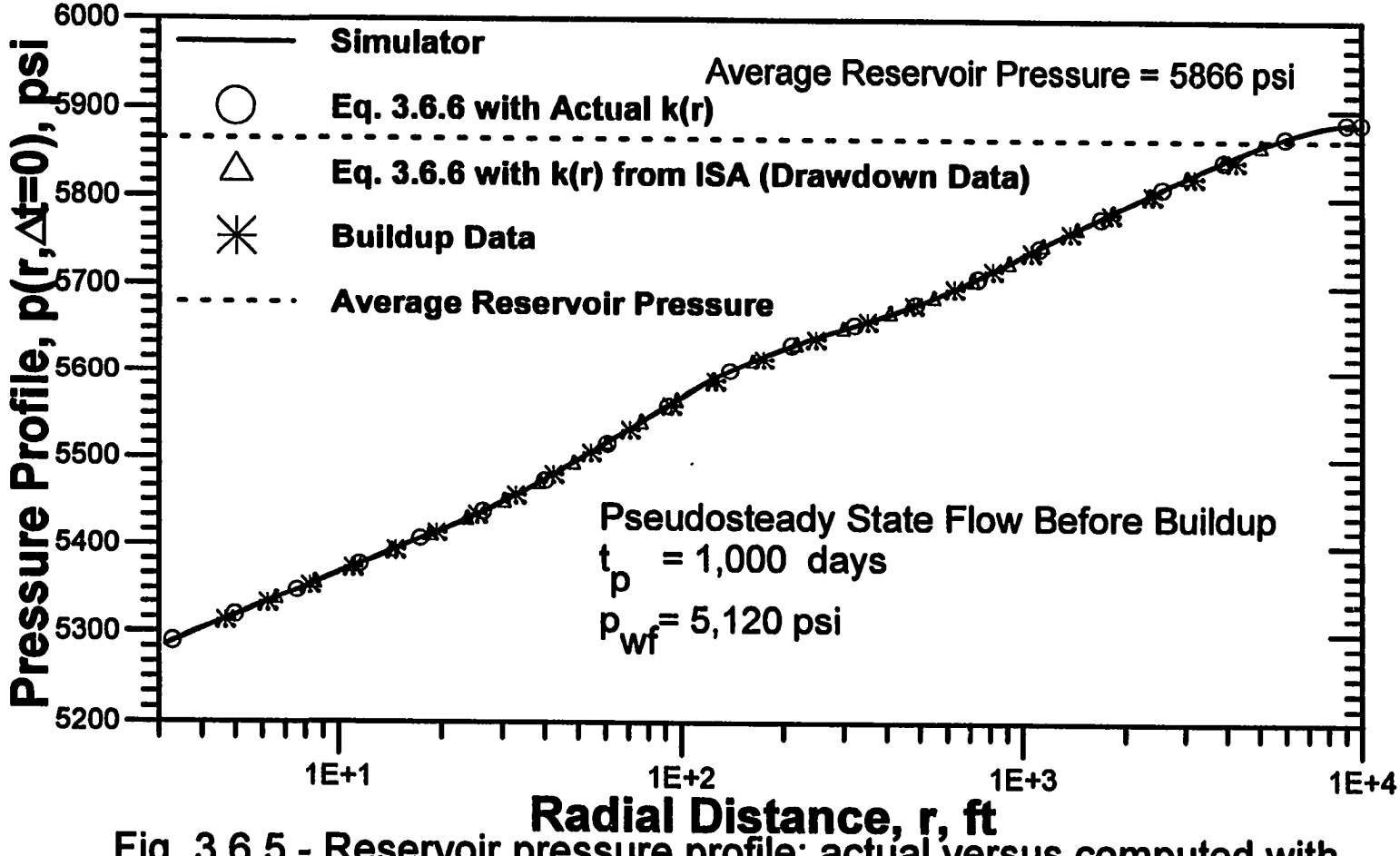

Fig. 3.6.5 - Reservoir pressure profile; actual versus computed with drawdown and buildup data; Reservoir Pressure Profile, Cases 3a and 3b.

$$\bar{p} = \frac{1}{V}\int_V p dV = \frac{1}{\int_{r_w}^{r_e} 2\pi r h dr}\int_{r_w}^{r_e} p(r) 2\pi r h dr = \frac{2}{r_e^2 - r_w^2}\int_{r_w}^{r_e} p(r) r dr. \qquad (3.6.7)$$

Therefore, if we have the reservoir pressure profile, $p(r)$, from $r = r_w$ up to the external reservoir radius, r_e, at a fixed time, then we can compute $\bar{p}$ using Eq. 3.6.7. However, we do not have a priori r_e, and we calculate $p(r)$ only up to the last radius of investigation, r_{Np}, which corresponds to the last point in time, t_{Np}, recorded during the infinite-acting period. So, to estimate $\bar{p}$, we need to obtain r_e and $p(r)$ for $r_{Np} < r \le r_e$. In the cases that follow, we assume that we know the external reservoir radius, r_e, and we can extrapolate $p(r)$ beyond r_{Np} as follows. When the flow regime at the instant of shut in is *transient*, we extrapolate the measured pressures *linearly with the logarithm of the radial distance, r*, assuming the initial pressure at the outer reservoir radius, r_e. When the flow regime at the shut-in time is *either steady state or pseudosteady state*, we extrapolate $p(r)$ beyond r_{Np} using either Eq. 3.6.5 or Eq. 3.6.6, respectively. Since we do not know the permeability distribution beyond the last point measured, we assumed simply a constant value of permeability equal to the last permeability value computed with the ISA or MYA. It is worthwhile to note that this assumption yields good estimates of average reservoir pressure provided we obtain a good estimate of the external reservoir radius, r_e, the transition between the end of the infinite-acting period, t_{eia} and the beginning of the pseudosteady state regime, t_{pss}, is not too large, and that there is no drastic variation of permeability between the last radius of investigation and r_e. Under these conditions, we accurately computed the average reservoir pressure for many cases we have studied, including the following cases.

Reproduced with permission of the copyright owner. Further reproduction prohibited without permission.

3.6.3.1 Average Reservoir Pressure, Case 1

Here, we present the results of average reservoir pressure calculation for the 5-zone, multicomposite reservoir/well system and conditions of Reservoir Pressure Profile Case 1. The well was shut in during *transient flow*, after flowing for 26.6 days. We used Eq. 3.6.7 with the reservoir pressure profile determined with the buildup data, up to the radial distance of 2400 ft, as in Reservoir Pressure Profile Case 1 (see Fig. 3.6.2), and extrapolated up to r_e, as described above, to compute the average reservoir pressure at the shut-in time. The computed value of 5980.2 psi is very close to the actual value of 5985.7 psi, which corresponds to a difference of -0.09 percent. This case illustrates the high accuracy of the method to calculate average reservoir pressure using reservoir pressure profile even under infinite-acting condition.

3.6.3.2 Average Reservoir Pressure, Case 2

In this case, we considered the same 5-zone, multicomposite reservoir with a constant pressure outer boundary and test conditions as in Reservoir Pressure Profile Case 2. We recall that it refers to a buildup test of 26.6 days after a flow period of 1000 days, a time long enough to achieve a *steady-state flow* condition. The reservoir pressure profile, calculated in Reservoir Pressure Profile Case 2 with buildup data, up to a radius of investigation of 2250 ft, shown in Fig. 3.6.3, was extrapolated up to r_e using Eq. 3.6.5, as explained in the beginning of this subsection, and used in Eq. 3.6.7, to accurately compute an average reservoir pressure value of 5972.2 psi, nearly identical to the true value of 5972.4 psi.

Reproduced with permission of the copyright owner. Further reproduction prohibited without permission.

3.6.3.3 Average Reservoir Pressure, Case 3

This case pertains to a single-well, 5-zone, multicomposite reservoir, with a no-flow boundary, whose main reservoir/well properties are given in Table 2.3.3. The well is produced at constant rate of 300 reservoir barrels a day for 1000 days, until pseudosteady state flow is established, and then shut in for 26.6 days. This is the same case considered in Reservoir Pressure Profile Case 3, where the reservoir pressure profile was calculated, from buildup data, up to the radius of investigation of 2250 ft, shown as circular data points in Fig. 3.6.4. The reservoir pressure profile was extrapolated up to r_e using Eq. 3.6.6, as explained in the beginning of this subsection, assuming a constant permeability value of 40 md (which is the last value computed from ISA at $t_{eia} \cong 26.6$ days), and then used in Eq. 3.6.7, to compute $\bar{p} \cong 5457$ psi, corresponding to 99.90 percent of the true value of 5464 psi. In this case, if instead of using the value of 40 md to extrapolate the reservoir pressure profile beyond 2250 ft, we had used a value of either 20 md (-50%) or 60 md (+50%) md, we would have obtained the value of average reservoir pressure of 5469 psi or 5453 psi, corresponding to 100.10 percent or 99.80 percent of the actual value, respectively. These results illustrate: (i) that our assumption to extrapolate the permeability distribution is quite reasonable, and (ii) the correctness of our method to accurately compute the average reservoir pressure based on the reservoir pressure profile established under pseudosteady state condition. These results are confirmed by many other cases we have studied during this work.

3.6.3.4 Average Reservoir Pressure, Case 4a, 4b and 4c

We present the results of the calculation of average reservoir pressure at the end of the pseudosteady state flow period, using drawdown data (Cases 4a and 4b) and using buildup data (Case 4c). Here we used the reservoir with "smoothly" varying permeability

Reproduced with permission of the copyright owner. Further reproduction prohibited without permission.

of Table 3.4.1a and well test conditions as in Reservoir Pressure Profile Case 4. We recall that the well was produced at constant rate for 1000 days until a pseudosteady state flow is established. We then computed the reservoir average pressure at $t_p = 1000$ days.

Cases 4a and 4b refers to the reservoir pressure profiles shown in Fig. 3.6.5 as circular and triangular data points, respectively. We computed $\bar{p}$ directly from Eq. 2.3.89, derived in Chapter II, using the actual permeability distribution, $k(r)$, in Case 4a, whereas in Case 4b we used $k(r)$ computed with ISA applied to drawdown data and extrapolated up to r_e , under the considerations in the beginning of this subsection. We obtained the average reservoir pressure value of 5865 psi, in Case 4a and 5864 psi in Case 4b, corresponding, respectively, to 99.98 and 99.97 percent of the actual value of 5866 psi obtained with our simulator. Case 4a validates our Eq. 2.3.89. Case 4b illustrates that we can accurately compute the reservoir average pressure based only in drawdown data.

Case 4c refers to the reservoir pressure profile determined using buildup data, represented by star data points in Fig. 3.6.5, obtained in Buildup after Pseudosteady State Flow Case 3b. We then extrapolated the calculated profile up to r_e, assuming a constant permeability value of 25 md (the last value computed from ISA) and applied Eq. 3.6.7 to obtain a value of $\bar{p}$ of 5860 psi corresponding to 99.90 percent of the true value of 5866 psi. In this case, if instead of using the value of 25 md to extrapolate the reservoir pressure profile beyond 4200 ft (obtained at $\Delta t = 26.6$ days from Eq. 3.6.4), we had used a value of either 12.5 md (-50%) or 37.5 md (+50%) md, we would have obtained the value of average reservoir pressure of 5884 psi or 5852 psi, corresponding to 100.30 percent or 99.80 percent of the actual value, respectively. Once more, these results indicate that it is reasonable to extrapolate $p(r)$ beyond the last radius of investigation computed at t_{eia}, using the pseudosteady state equation, Eq. 3.6.6, and assuming a constant value of permeability equal to the last value computed from ISA.

Reproduced with permission of the copyright owner. Further reproduction prohibited without permission.

These results illustrate that we can accurately compute average reservoir pressure during the pseudosteady state flow, either using buildup data, as in Case 4c, or, maybe *more importantly, solely using drawdown data*, as in Case 4b.

3.6.4 Permeability Distribution

The permeability distribution, $k(r)$, can be computed rigorously, at least theoretically, from the reservoir pressure profile, $p(r)$, at a fixed time, during any one of the two boundary dominated flow regimes, either pseudosteady state or steady state flow regime. If we can generate the reservoir pressure profile at the instant of shut in from the buildup data, then Eqs. 3.6.5 and 3.6.6 provide a means to estimate $k(r)$ from $p(r)$. We present in the following the appropriate equations for $k(r)$ derived from those equations and applications.

The equation for estimating $k(r)$, during the steady-state flow, is obtained directly from Eq. 3.6.5. Taking the derivative of Eq. 3.6.5 with respect to r, we obtain

$$\frac{\partial p(r)}{\partial r} = \frac{141.2qu}{h}\left[\frac{1}{r\,k(r)}\right], \tag{3.6.8}$$

which yields

$$k(r) = \frac{141.2qu}{h}\left[\frac{1}{r\dfrac{\partial p(r)}{\partial r}}\right], \tag{3.6.9a}$$

or,

$$k(r) = \frac{141.2qu}{h}\left[\frac{1}{\dfrac{\partial p(r)}{\partial \ln r}}\right]. \tag{3.6.9b}$$

Reproduced with permission of the copyright owner. Further reproduction prohibited without permission.

Notice the Eq. 3.6.9a and 3.6.9b are just rearrangements of the Darcy's Law for a radially heterogeneous reservoir.

The equation for estimating $k(r)$, during the pseudosteady state flow, is obtained directly from Eq. 3.6.6. Taking the derivative of Eq. 3.6.6 with respect to r, we obtain

$$\frac{\partial p(r)}{\partial r} = \frac{141.2qu}{h}\frac{1}{k(r)}\left[\frac{1}{r} - \frac{r}{r_e^2}\right], \tag{3.6.10}$$

and solving for $k(r)$ gives

$$k(r) = \frac{141.2qu}{h}\frac{1}{\frac{\partial p(r)}{\partial r}}\left[\frac{1}{r} - \frac{r}{r_e^2}\right], \tag{3.6.11}$$

which can be further simplified by multiplying the right side by $\left(r/r\right)$ to yield

$$k(r) = \frac{141.2qu}{h}\frac{1}{r\frac{\partial p(r)}{\partial r}}\left[1 - \frac{r^2}{r_e^2}\right], \tag{3.6.12a}$$

or,

$$k(r) = \frac{141.2qu}{h}\frac{1}{\frac{\partial p(r)}{\partial \ln r}}\left[1 - \frac{r^2}{r_e^2}\right]. \tag{3.6.12b}$$

Eqs 3.6.9 and 3.6.12 allow us to accurately compute the permeability distribution based on, respectively, the steady-state or pseudosteady state reservoir pressure profile. To accurately compute $k(r)$, using Eq. 3.6.9 or Eq. 3.6.12, it is crucial to accurately determine the reservoir pressure profile, $p(r)$, and to have a good estimate of the reservoir external radius, r_e.

In the first four cases considered, Cases 1a, 1b, 2a and 2b, we used the pressure profile obtained from the simulator to verify the accuracy of Eqs. 3.6.9 and 3.6.12 for estimating $k(r)$.

Reproduced with permission of the copyright owner. Further reproduction prohibited without permission.

3.6.4.1 Permeability Distribution, Case 1a and 1b

Case 1a refers to the 5-composite reservoir/well system and flow conditions considered in Reservoir Pressure Profile Case 2. We used the Eq. 3.6.9 and the simulated steady-state reservoir pressure profile, $p(r)$, generated in that case, shown as a solid line in Fig. 3.6.3, to compute the permeability distribution, $k(r)$, shown as star data points in Fig. 3.6.6. The agreement between the actual (solid line) and the computed permeability profile (square data points) is excellent.

Case 1b deals with the same 5-composite/well system and flow conditions considered in Reservoir Pressure Profile Case 3. In this case, we used the pseudosteady state Eq. 3.6.12 with the simulated pseudosteady state reservoir pressure profile, calculated in that case (solid line in Fig. 3.6.4), to compute $k(r)$ represented in Fig. 3.6.6 as square data points. The computed $k(r)$ (star data points) basically reproduces the actual $k(r)$.

3.6.4.2 Permeability Distribution, Case 2a and 2b

Cases 2a and 2b pertains to the same reservoir/wellbore system as in Reservoir Pressure Profile Case 4. In Case 2a, we considered a constant pressure (6,001 psi) outer boundary condition and simulated a drawdown of 1000 days, such that the steady-state flow regime is reached. Using the simulated steady-state reservoir pressure profile at the end of the flow and Eq. 3.6.9, we computed the permeability distribution, $k(r)$. Plotted in Fig. 3.6.7 as square data points, the computed $k(r)$ shows a very good match with the actual $k(r)$ represented by the solid line.

Case 2b is similar to Case 2a with the difference being that in Case 2b, we considered a no-flow boundary and the reservoir reaches the pseudosteady state flow regime. The resulting simulated pseudosteady state reservoir pressure profile (solid line in

Reproduced with permission of the copyright owner. Further reproduction prohibited without permission.

Reproduced with permission of the copyright owner. Further reproduction prohibited without permission.

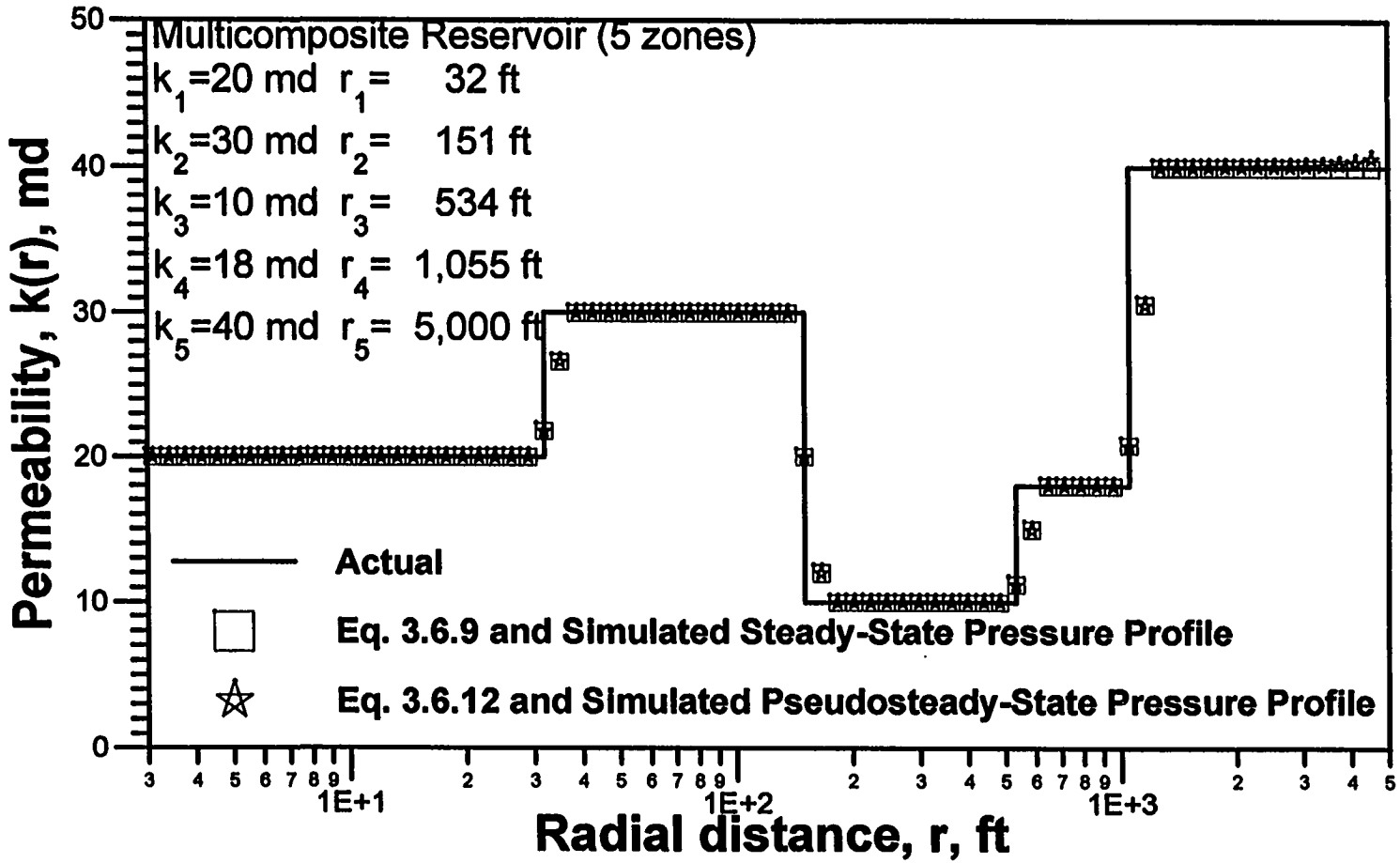

Fig. 3.6.6 - Permeability profile, actual versus calculated; Permeability Distribution, Cases 1a and 1b.

Fig. 3.6.5) is used in Eq. 3.6.12 to calculate $k(r)$, which is plotted in Fig. 3.6.7 as star data points. The agreement with the true $k(r)$ is excellent.

- Remarks

These four examples, Permeability Distribution Cases 1a, 1b, 2a, and 2b, show the correctness of Eqs. 3.6.9 and 3.6.12 and that it is possible, at least in theory, to accurately compute permeability distribution based on a boundary-dominated reservoir pressure profile. Thus, we validated the theoretical equations 3.6.9 and 3.6.12 for determining permeability distribution from the reservoir pressure profile during either a steady-state or pseudosteady state flow regime.

3.6.4.3 Permeability Distribution, Case 3

Here, we considered the same reservoir/well system and simulation conditions as in Reservoir Pressure Profile Case 2. The buildup follows a steady-state flow period. We calculated the permeability distribution, $k(r)$, using the steady-state Eq. 3.6.9 and the reservoir pressure profile computed in that case (circular data points in Fig. 3.6.3). The calculated $k(r)$, shown in Fig. 3.6.8 as square data points, is a fairly good approximation to the actual $k(r)$ (solid curve).

3.6.4.4 Permeability Distribution, Case 4

In this case we deal with the reservoir with the "smoothly" varying radial permeability distribution listed in Table 3.4.1a (see Fig. 3.4.10) and reservoir/well system data given in Table 3.4.1b which was considered in Reservoir Pressure Profile Case 4. At the end of a drawdown of 1000 days, under pseudosteady state flow conditions, the well is shut in for a buildup. The transient buildup data is then used to compute the reservoir

Reproduced with permission of the copyright owner. Further reproduction prohibited without permission.

Reproduced with permission of the copyright owner. Further reproduction prohibited without permission.

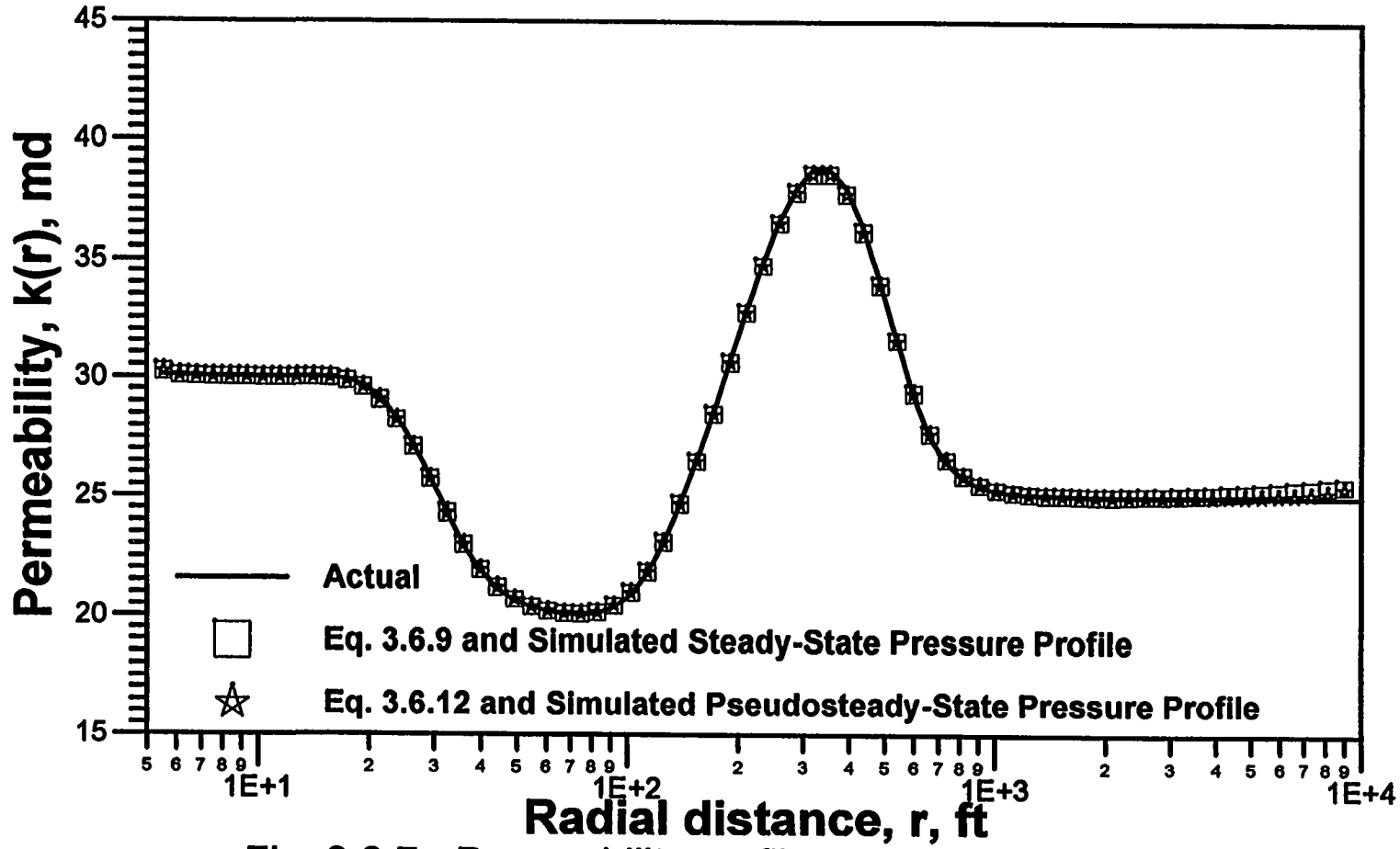

Fig. 3.6.7 - Permeability profile, actual versus calculated; Permeability Distribution, Cases 2a and 2b.

pressure profile, shown as big star data points in Fig. 3.6.5. Using this computed reservoir pressure profile in Eq. 3.6.12, we then calculated $k(r)$. The result (triangular data points) is compared in Fig. 3.6.9 with the true $k(r)$ (solid line) and with $k(r)$ computed with ISA and the buildup data (star data points). We observe that the $k(r)$ values computed by using the estimated reservoir pressure profile and Eq. 3.6.12 is in reasonable agreement with the actual permeability distribution, although the approximation is not as good as the one obtained from ISA.

- Remarks

The results obtained so far, taking into account the assumptions and limitations discussed in the previous sections, warrant the following conclusions:

- we can compute the reservoir pressure profile at the instant of shut in, either from buildup or from drawdown data;
- if either a steady-state or pseudosteady state flow regime is attained, we can calculate the reservoir pressure profile by one of the following two ways : (i) using the buildup data (if a buildup is taken after the drawdown); or (ii) using the appropriate flow equation, Eq. 3.6.5 or 3.6.6, and the permeability distribution computed by ISA or MYA with transient pressure drawdown data; additionally, we can also compute the average reservoir pressure;
- we can compute at a fixed time during a steady-state or pseudosteady state flow, the reservoir pressure profile and the reservoir average pressure using only drawdown data;
- if we can determine the steady-state or the pseudosteady-state reservoir pressure profile at the instant of shut in from buildup data then we can estimate the permeability distribution using Eqs. 3.6.9 or 3.6.12.

Reproduced with permission of the copyright owner. Further reproduction prohibited without permission.

Reproduced with permission of the copyright owner. Further reproduction prohibited without permission.

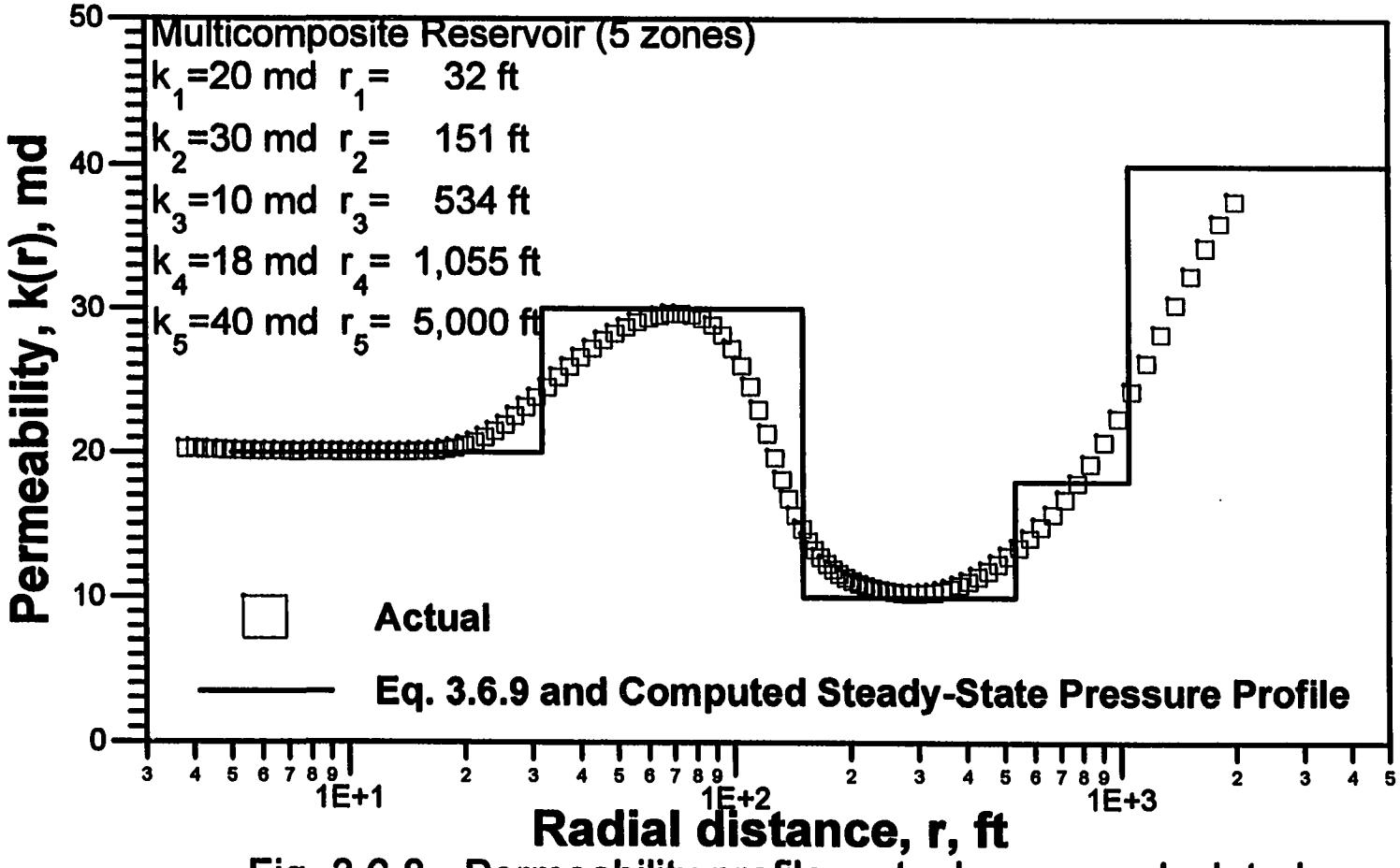

Fig. 3.6.8 - Permeability profile, actual versus calculated; Permeability Distribution, Case 3.

Reproduced with permission of the copyright owner. Further reproduction prohibited without permission.

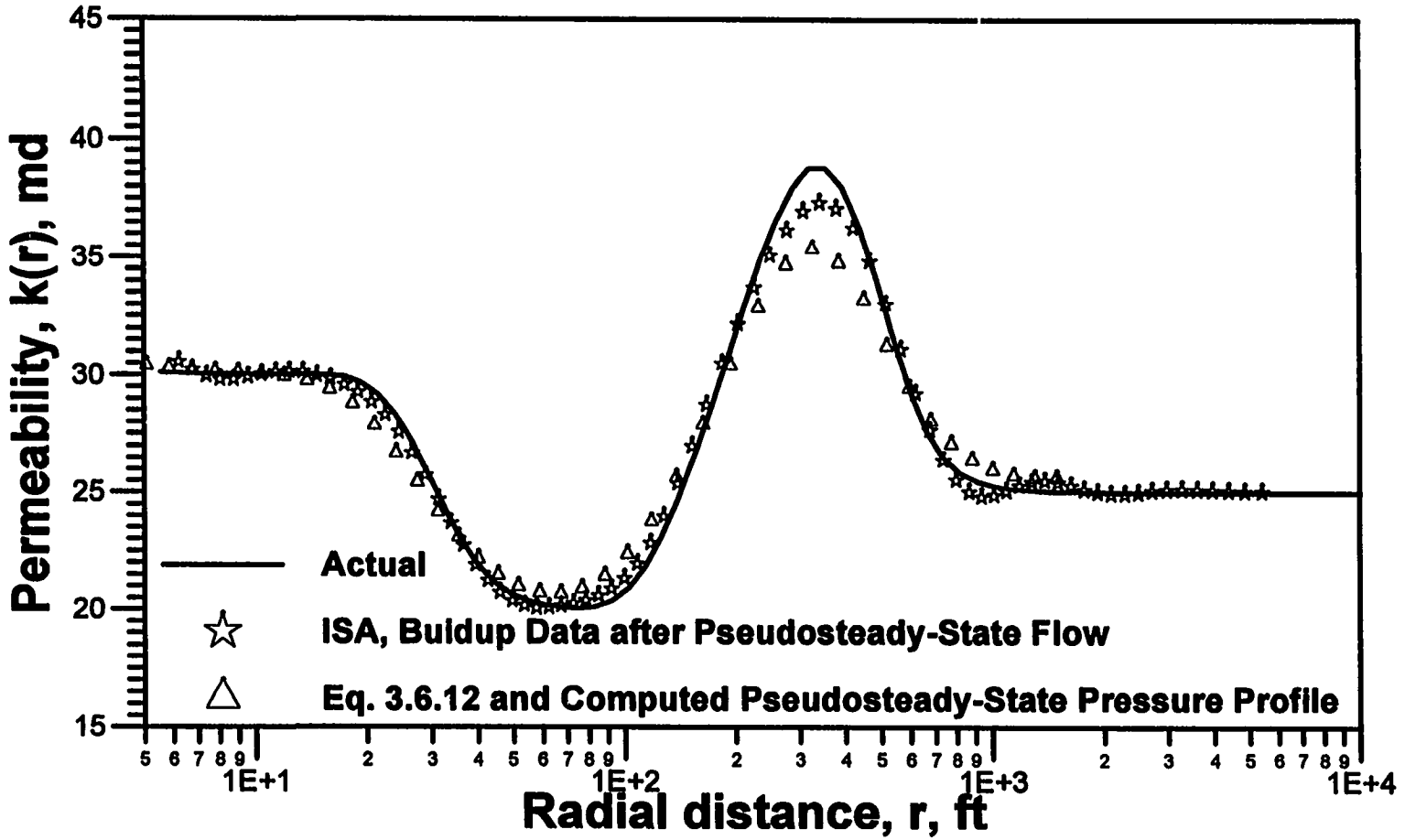

Fig. 3.6.9 - Permeability profile, actual versus calculated; Permeability Distribution, Case 4.

3.7 Boundary-Dominated Flow Parameters

We present here procedures to compute parameters of interest during the outer boundary-dominated flow period and example applications. We will consider the most important ones, namely, the productivity index, *PI*, the homogeneous-equivalent pseudosteady state permeability, k_{eq}, and the flow rate decline for constant pressure production. We show examples illustrating the accuracy of the theoretical equations derived in Chapter II, subsection 2.3.6, to compute the above parameters .

3.7.1 Productivity Index, *PI*

The productivity index, *PI*, is defined by Eq. 2.3.99, that we reproduce as the following equation

$$PI = \frac{q_{sc}}{\overline{p} - p_{wf}}, \tag{3.7.1}$$

where q_{sc} is the surface flow rate, in standard conditions, and p_{wf} is the bottomhole flowing pressure. Since q_{sc} and p_{wf} are measured during the well test, to properly determine *PI*, we just need to calculate $\overline{p}$, which can be computed, under ideal conditions, according to procedure presented in subsection 3.6.3. Another way to compute *PI* is directly from Eq. 2.3.100, derived in Chapter II, where the permeability distribution, $k(r)$, is obtained from the ISA (or MYA) applied to transient buildup or drawdown data and extrapolated up to the reservoir external radius, using the method described in subsection 3.6.3.

Reproduced with permission of the copyright owner. Further reproduction prohibited without permission.

We considered two cases referred to as Case A and Case B, involving two different reservoir/well systems that will be described later. For each case we computed the productivity index, *PI*, considering the actual $k(r)$ and $k(r)$ computed from the ISA, and summarized the results in Table 3.7.1. The results shown in columns 1 and 2 are obtained using the actual $k(r)$ and are intended to verify the accuracy of Eq. 2.3.100. In column 1 we use Eq. 3.7.1 and the correct $\bar{p}$ obtained from the simulation; whereas in column 2 we use directly Eq. 2.3.100. The results shown in columns 3 and 4 are obtained using $k(r)$ computed from ISA and extrapolated up to r_e under the assumptions described in subsection 3.6.3. In column 3 we use directly Eq. 100; whereas in column 4 we use Eq. 3.7.1 with $\bar{p}$ computed as described in subsection 3.6.3.

The reservoir/well system in Case A is a single-well 5-composite reservoir considered in Reservoir Pressure Profile (RPP) Case 3, which permeability distribution is shown as circular data points in Fig. 3.4.3. The well is produced at constant flow rate of 300 reservoir barrels per day, for 1000 days, reaching the pseudosteady-state flow, and then is shut in. We considered only the drawdown data. First, we computed *PI* for the actual $k(r)$ using the simulated data and using Eq. 2.3.100, at $t = 1000$ days, and present the results in columns 1 and 2. The close agreement between the two values in these columns substantiates the accuracy of Eq. 2.3.100. Second, we computed the permeability distribution from the transient part of the drawdown data using ISA. Using the computed $k(r)$ we then calculated the reservoir average pressure, $\bar{p}$, and subsequently *PI*, which is shown in column 4. We also calculated *PI*, using the $k(r)$ computed from ISA and Eq. 2.3.100, whose result is presented in column 3. The results of the columns 3 and 4 are within 99.77 percent of the actual value of column 1; thus, indicating the high accuracy of the method for determination of the productivity index based on our calculated permeability distribution and, either Eq. 2.3.100 or Eq. 3.7.1 with $\bar{p}$ computed from the reservoir pressure profile as shown in subsection 3.6.3.

Reproduced with permission of the copyright owner. Further reproduction prohibited without permission.

	Table 3.7.1 Productivity Index (STB/D/psi)			
	Actual $k(r)$		Computed $k(r)$	
	Eq. 3.7.1 Simulated $\bar{p}$	Eq. 2.3.100	Eq. 2.3.100	Eq. 3.7.1 Computed $\bar{p}$
	(1)	(2)	(3)	(4)
Case A	0.3028	0.3029	0.3035 (+0.23%)	0.3031 (+0.10%)
Case B	0.4024	0.4024	0.4035 (+0.27%)	0.4036 (+0.30%)

Case B refers to the reservoir with "smoothly" varying permeability listed in Table 3.4.1a, with reservoir/well system data shown in Table 3.4.1b, identical to the one considered in Drawdown Case 4. We recall that we produced the well for 1000 days until a pseudosteady state is established. Following the same steps as described above we obtained the results presented in Table 3.7.1. These results are, clearly, as good as in the previous case. Thus, identical conclusions are applicable.

3.7.2 Homogeneous-Equivalent Pseudosteady State Permeability, k_{eq}

The homogeneous-equivalent pseudosteady state permeability of a radially heterogeneous reservoir is defined in Chapter II, as the permeability of the associated homogeneous reservoir which produces at the same flow rate under a given pseudosteady state pressure drop $(\bar{p} - p_{wf})$. Thus, by definition

$$k_{eq} = \frac{141.2 q\mu}{h(\bar{p} - p_{wf})}\left(\ln\frac{r_e}{r_w} - \frac{3}{4}\right). \tag{3.7.2}$$

Reproduced with permission of the copyright owner. Further reproduction prohibited without permission.

We can also compute k_{eq} directly from Eq. 2.3.92, derived in Chapter II, where the permeability distribution, $k(r)$, is obtained from ISA (or MYA) applied to transient buildup or drawdown data and extrapolated up to the reservoir external radius, using the method described in subsection 3.6.3.

Here, we considered the same two Cases A and B considered in the previous subsection. Similarly, for each case we computed k_{eq} considering the actual $k(r)$ and $k(r)$ computed by ISA applied to transient drawdown data, and summarized the results in Table 3.7.2. The results shown in columns 1 and 2 are obtained using the actual $k(r)$ and are intended to verify the accuracy of Eq. 2.3.92. In column 1 we use Eq. 3.7.2 and the correct $\overline{p}$ obtained from the simulation; whereas in column 2 we use directly Eq. 2.3.92. The results shown in columns 3 and 4 are obtained using $k(r)$ computed from ISA and extrapolated up to r_e under the assumptions described in subsection 3.6.3. In column 3 we use directly Eq. 2.3.92, whereas in column 4 we use Eq. 3.7.2 with $\overline{p}$ computed from the reservoir pressure profile as described in subsection 3.6.3.

The close agreement, for both Cases A and B, between the corresponding values of columns 1 and 2 provides a numerical verification of Eq. 2.3.92.

The values of k_{eq} obtained from the well test data, i.e., based on $k(r)$ computed from ISA, using Eq. 2.3.92 (column 3) or using Eq. 3.7.2 (column 4) with an estimated $\overline{p}$, are within 99.77 percent and 99.72 percent of the correct value given in column 1, for both reservoir/well systems considered. These results clearly indicate: (i) we have determined with ISA an excellent approximated permeability distribution, $k(r)$; (ii) the accuracy of the computed average reservoir pressure, $\overline{p}$, and finally (iii) as a consequence, we accurately compute the equivalent pseudosteady state permeability, k_{eq}.

Reproduced with permission of the copyright owner. Further reproduction prohibited without permission.

	Table 3.7.2 Equivalent Pseudosteady State Permeability (md)			
	Actual $k(r)$		Computed $k(r)$	
	Eq. 3.7.2 Simulated $\bar{p}$	Eq. 2.3.92	Eq. 2.3.92	Eq. 3.7.2 Computed $\bar{p}$
	(1)	(2)	(3)	(4)
Case A	19.181	19.183	19.226 (+0.23%)	19.197 (+0.08%)
Case B	27.455	27.459	27.533 (+0.28%)	27.538 (+0.30%)

3.7.3 Exponential-Decline Flow Rate for Constant Pressure Production

We derived in Chapter II, subsection 2.3.6.4, the equation that models the exponential flow rate decline for constant pressure production under boundary dominated flow, Eq. 2.3.114. Here, we present an application of Eq. 2.3.114. We considered the 5-zone,multicomposite reservoir/well system whose main parameters are shown in Table 2.3.3. We simulated a drawdown flow period of 1,000 days with a constant bottomhole flowing pressure of 5,000 psi and a no-flow outer boundary. The flow rate declines with time. Fig. 3.7.1 compares the flow rate obtained from the simulator (solid curve) with the flow rate computed with Eq. 2.3.114 (circular data points). The value of PI used in Eq. Eq. 2.3.114 was calculated as described on subsection 3.7.1, based only on the simulated drawdown test data. For $t > 50$ days note the flow is dominated by the effect of the no-flow external boundary, and from this time on, we observe that both simulated and computed flow rate are, practically, the same. This illustrates the validity of Eq. 2.3.114.

Reproduced with permission of the copyright owner. Further reproduction prohibited without permission.

We recall that the computations presented in subsection 3.7.1, 3.7.2 and 3.7.3 were based solely in drawdown data. Therefore, taking into account the assumptions under which we performed these computations, based on the results presented in these subsections and throughout this Chapter, we have shown tha we can compute, at least theoretically, the most important reservoir parameters, namely (i) permeability distribution, $k(r)$, (ii) reservoir pressure profile, (iii) average reservoir pressure, $\overline{p}$, (iv) productivity index, *PI*, (v) equivalent pseudosteady state permeability, k_{eq}, and (vi) if the *PI* value is available (from pseudosteady state measurements), the exponential flow rate decline for constant pressure production, *using only drawdown data*. These results are highly significant considering the situations, that often happen in the field practice, where shut a well in is not practical, or possible, either due to operational, safety or economical reasons.

Reproduced with permission of the copyright owner. Further reproduction prohibited without permission.

Reproduced with permission of the copyright owner. Further reproduction prohibited without permission.

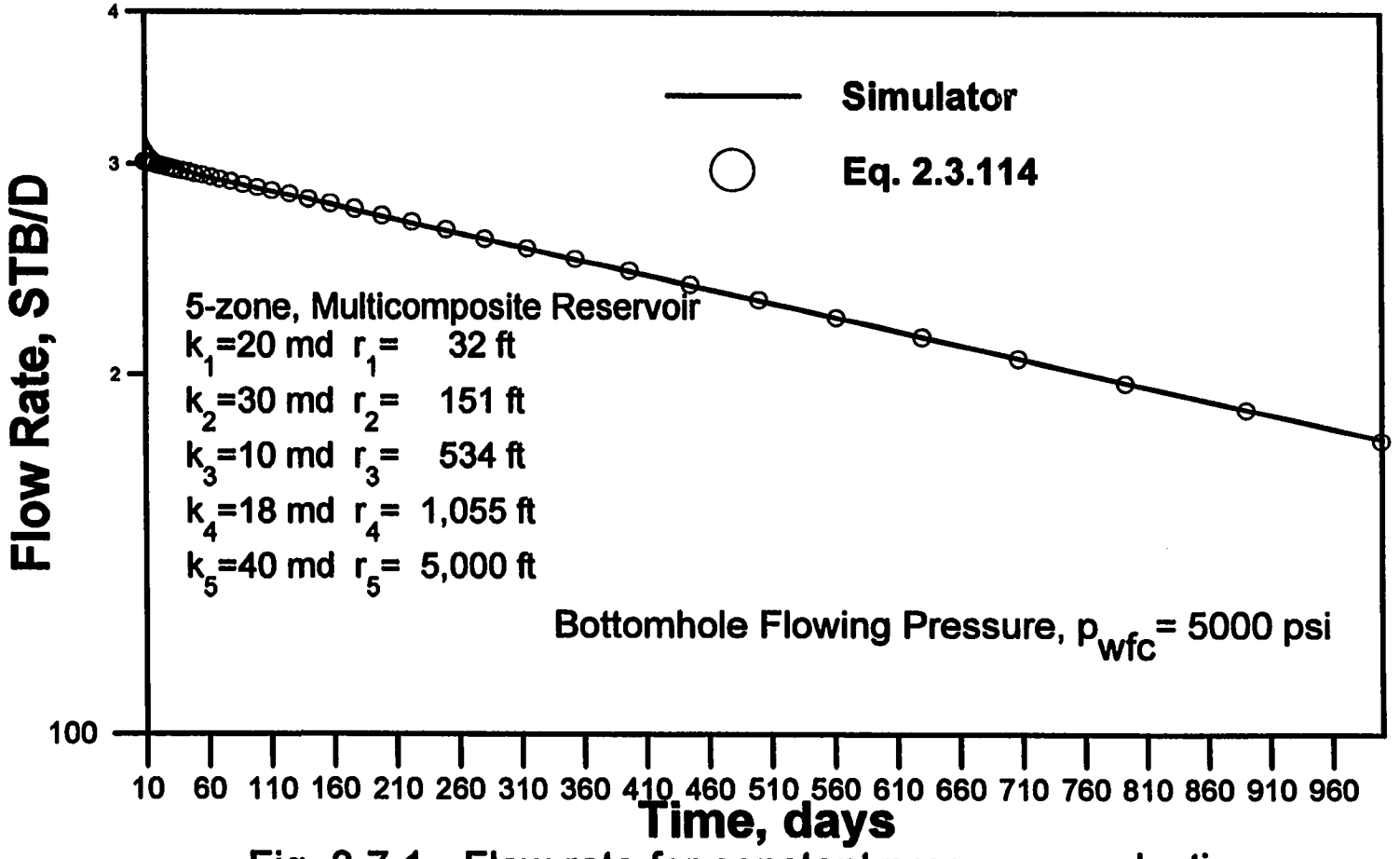

Fig. 3.7.1 - Flow rate for constant pressure production.

3.8 Influence of Porosity Variation

We have presented, so far, cases of radially heterogeneous reservoirs with constant porosity and heterogeneous permeability. To show the effect of variation in porosity in the results of our Inverse Solution Algorithm, we simulated three cases with porosity and/or permeability variation, i.e., with $\phi = \phi(r)$ and/or $k = k(r)$.

We considered the 5-zone, multicomposite reservoir/well system of Drawdown Case 1, except that in the present case, we also considered variation in porosity. We estimated porosity based on the following empirical correlation, given in Ref. 39,

$$\phi = \left[\frac{k^{1/2} S_{wi}}{100} \right]^{1/2.25} \tag{3.8.1}$$

where S_{wi} is the irreducible water saturation and k is the absolute permeability in millidarcies. We assumed $S_{wi} = 30\%$, and computed the values of porosity with Eq. 3.8.1, using the previously assigned values of permeability. Porosity and permeability distribution as well as other main parameters of the reservoir/well under consideration are shown in Table 3.8.1. The reservoir has a no-flow outer boundary.

We simulated a flow period of 1000 days, with the well producing at a constant flow rate of 300 reservoirs barrels a day, for three cases of combinations of permeability and porosity distributions as follows: Case (i) constant permeability with $k = 20$ md and zonal porosity given in column 2 of Table 3.8.1; Case (ii) constant porosity with $\phi = 14.70\%$ and zonal permeabilities given in column 1 of Table 3.8.1; and Case (iii) permeability and porosity both variables with zonal values given in columns 1 and 2 of Table 3.8.1.

The simulated pressures and pressure derivatives are shown, respectively, in Figs. 3.8.1 and 3.8.2, where the results are represented by plus data points in Case (i), star data

Reproduced with permission of the copyright owner. Further reproduction prohibited without permission.

Table 3.8.1

5-Zone Multicomposite Reservoir Variable Permeability and Porosity

Reservoir/Well System Parameters

$k_1 = 20$ md	$\phi_1 = 14.70\%$	$r_1 = 32$ ft	$\mu = 1.0$ cp	$r_w = 0.3$ ft
$k_2 = 30$ md	$\phi_2 = 16.10\%$	$r_2 = 151$ ft	$c_t = 10\times10^{-6}$ psi^{-1}	$q = 300$ rb/d
$k_3 = 10$ md	$\phi_3 = 12.60\%$	$r_3 = 534$ ft	$h = 20$ ft	
$k_4 = 18$ md	$\phi_2 = 14.40\%$	$r_4 = 1{,}055$ ft	$p_i = 6000$ psi	
$k_5 = 40$ md	$\phi_2 = 17.20\%$	$r_5 = 5{,}000$ ft		

points in Case (ii), and solid curve in Case (iii). As expected, we observe that the porosity variation impacts the pressure and pressure derivatives to much less degree than the permeability variation. In Case (i), the pressure behavior appears to be nearly homogeneous; however the pressure derivatives show some small variation. In Case (ii), we notice a considerable variation in pressures and a larger variation in pressure derivatives. When considering the variation of both permeability and porosity of Case (iii), the pressures are almost identical to those in Case (ii), but we notice that the pressure derivatives obtained from Cases (ii) and (iii) differ significantly at points where the derivatives reached a local maximum or minimum. These extreme values reflect the effects of the boundary between zones.

Applying ISA to the pressure derivatives of Fig. 3.8.2, and assuming a constant porosity of 14.70 %, we then computed the permeability distribution for Cases (ii) and (iii). In Fig. 3.8.3, the results obtained are compared with the actual permeability profile (solid line). Note the estimated permeability distributions are close to the actual one, with

Reproduced with permission of the copyright owner. Further reproduction prohibited without permission.

Reproduced with permission of the copyright owner. Further reproduction prohibited without permission.

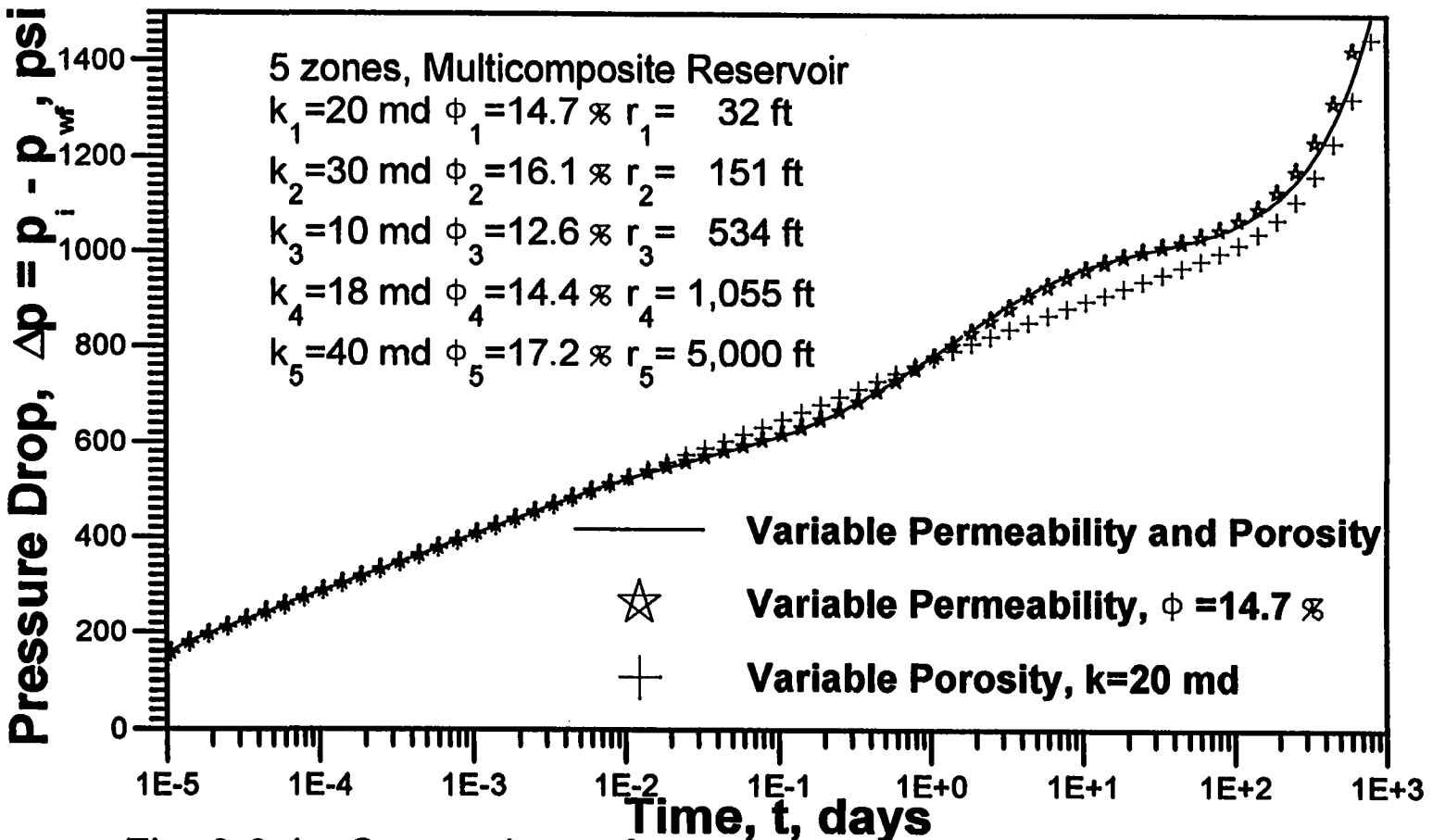

Fig. 3.8.1 - Comparison of pressure drop; variation of permeability and porosity; Cases (i), (ii) and (iii).

Reproduced with permission of the copyright owner. Further reproduction prohibited without permission.

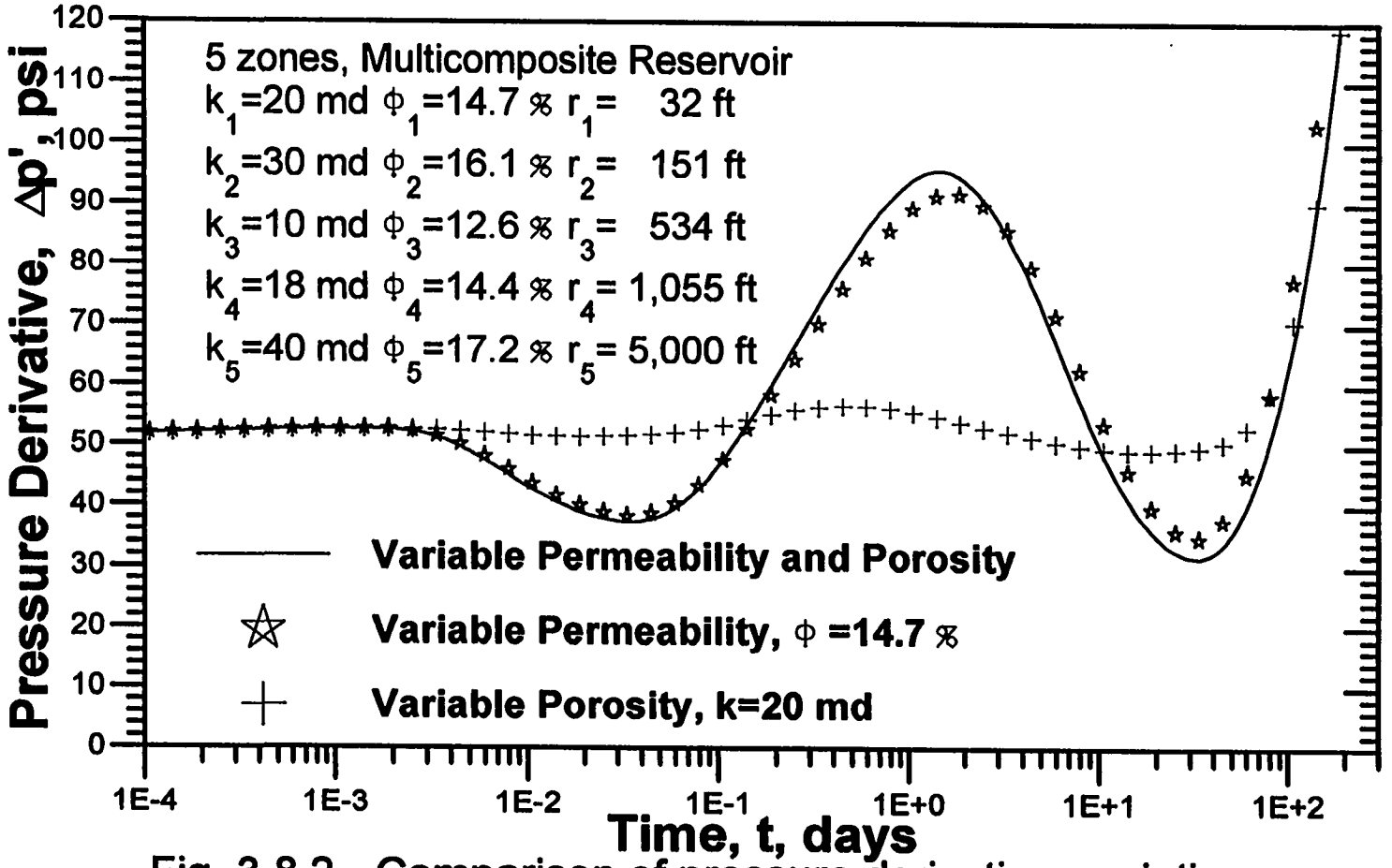

Fig. 3.8.2 - Comparison of pressure derivative; variation of permeability and porosity; Cases (i), (ii) and (iii).

the $k(r)$ calculated with the derivatives of Case (iii) (circular data points) being, in general, higher than $k(r)$ values obtained for Case (ii) (star data points), due to the effect of the porosity variation.

Using $k(r)$ calculated from ISA applied to the pressure derivatives obtained in Case (iii), with a constant porosity of 14.70%, we computed with our simulator pressures and pressure derivatives. The derivatives obtained are compared in Fig. 3.8.4 with the simulated values (solid line) based on the actual porosity and permeability distributions. The agreement between the simulated and computed pressure derivatives is excellent. If, instead of 14.70 %, we had considered another constant value of porosity to apply the ISA we would have obtained a different $k(r)$ that input into the simulator would reproduce the original pressures and pressure derivatives.

So, basically, we observe: (1) porosity variation has a small but noticeable effect on the results of our ISA; (2) when permeability and porosity variation are present, the permeability distribution computed with ISA, $k(r)$, is somewhat different from the case when only permeability changes, and combined with the constant porosity assumed in its computation, yields identical results, in terms of pressure and pressure derivative, as the simulated ones. This is the essence of the nonuniqueness of the inverse problem: more than one permeability/porosity distribution can yield the same pressure, pressure derivative response.

Reproduced with permission of the copyright owner. Further reproduction prohibited without permission.

Reproduced with permission of the copyright owner. Further reproduction prohibited without permission.

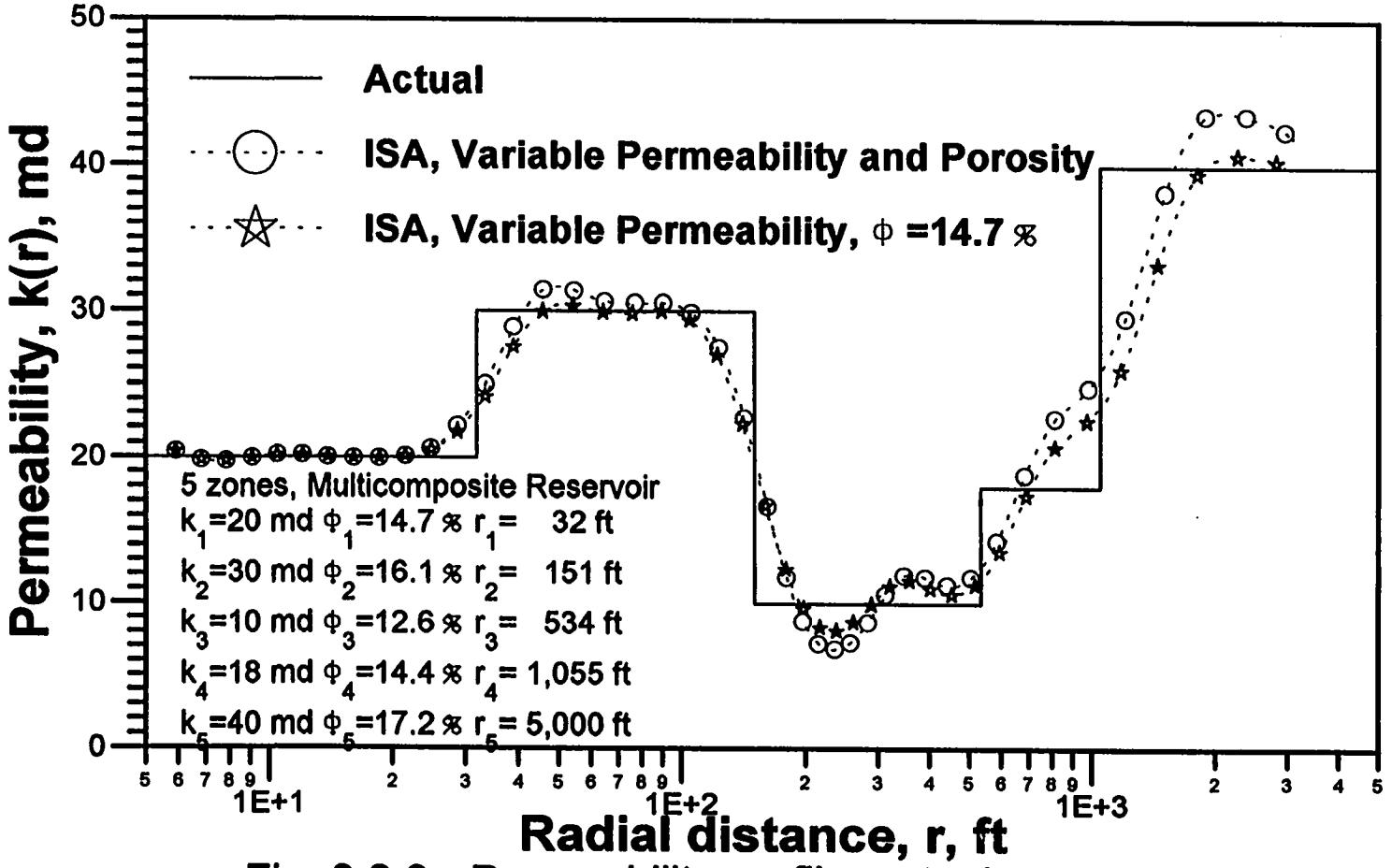

Fig. 3.8.3 - Permeability profile, actual versus calculated; Cases (ii) and (iii).

Reproduced with permission of the copyright owner. Further reproduction prohibited without permission.

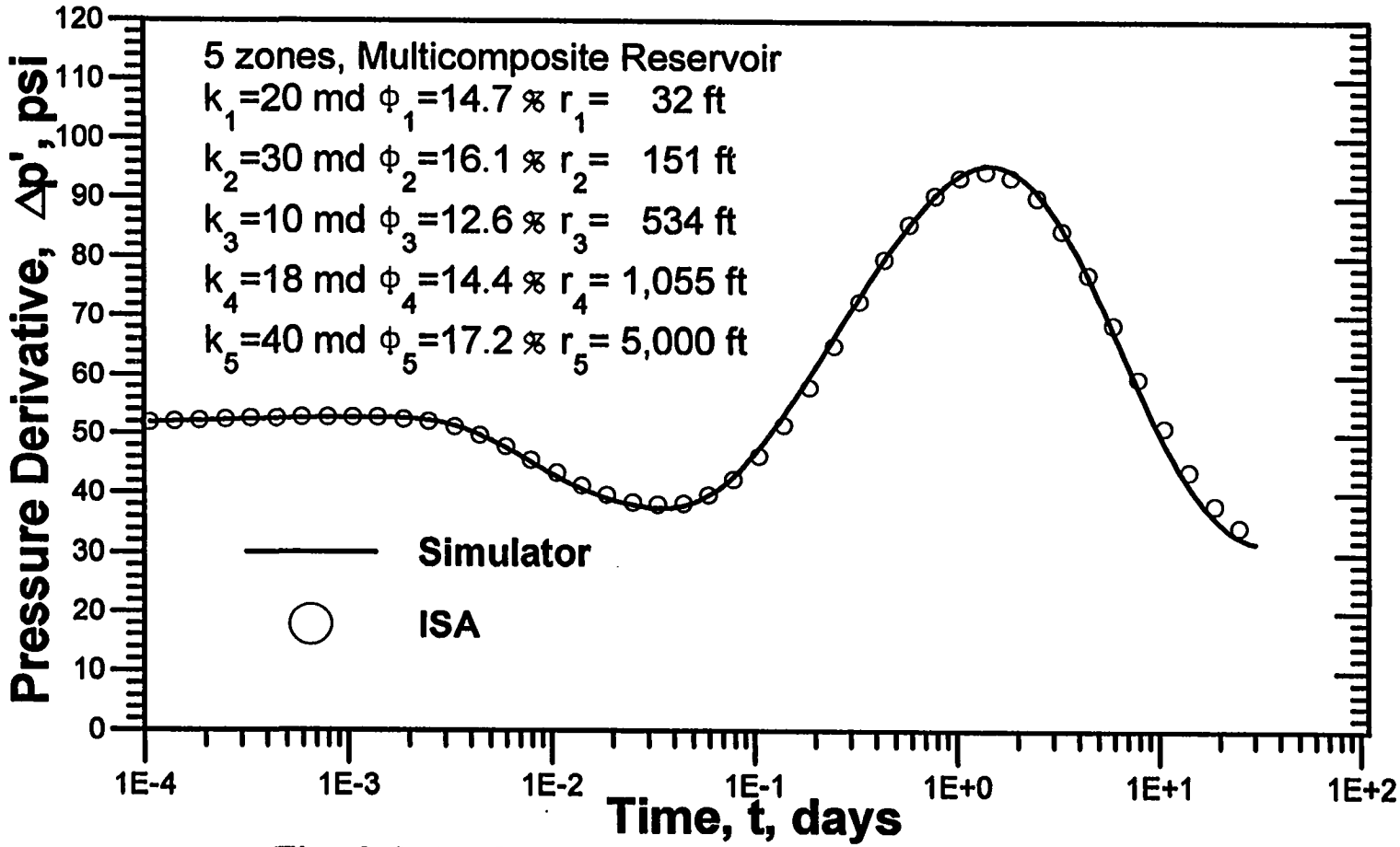

Fig. 3.8.4 - Comparison of pressure derivative; simulator versus ISA, Case (iii).

CHAPTER IV

APPLICATION OF THE INVERSE PROBLEM SOLUTIONS TO AREALLY HETEROGENEOUS RESERVOIRS

4.1 Introduction

We present examples of analysis of well-test pressure data obtained from an areally heterogeneous reservoir in which the permeability is a function of r and θ, or of x and y, i.e., $k(r,\theta)$ or $k(x,y)$. The analysis is based on the techniques presented on Chapter III to determine the main reservoir parameters. In these examples we compute: (i) an equivalent radial permeability distribution, $k = k(r)$, using our novel Inverse Solution Algorithm (ISA) applied to the transient data; (ii) a homogeneous-equivalent reservoir pressure profile; (iii) the average reservoir pressure; and (iii) the boundary-dominated flow parameters, such as, productivity index, equivalent pseudosteady state permeability and, in two cases, the exponential flow rate decline for constant pressure production . We then verify our results by comparison with the actual ones obtained with our numerical (r,θ) simulator. We show that our computed equivalent radial permeability distribution when input in our simulator reproduces the actual wellbore pressures and pressure derivatives. It also yields accurate values of average reservoir pressure and boundary-dominated flow parameters.

According to Oliver's work[16], the approximate pressure and pressure derivative solutions for a two-dimensional permeability distribution, $k = k(r,\theta)$, is identical to the solutions to a radially distributed permeability, $k = k(r)$, where $k(r)$ is the harmonic average of $k(r,\theta)$ over θ, expressed as

Reproduced with permission of the copyright owner. Further reproduction prohibited without permission.

$$\frac{1}{k(r)} = \frac{1}{2\pi}\int_0^{2\pi} \frac{1}{k(r,\theta)} d\theta. \tag{4.1.1}$$

Oliver's solution[16] is based on perturbation theory technique and as such it does not assure whether it yields an accurate solution when variations of the permeability distribution are large. In fact, it is not clear yet whether Eq. 4.1.1 gives the correct averaging over θ . This issue is addressed in the examples ahead. We compare, in the first three examples, the wellbore pressure derivatives numerically calculated from simulated wellbore pressures obtained with the actual specified $k(r,\theta)$, and with the harmonic, arithmetic and geometric average of $k(r,\theta)$ over θ. Interestingly enough, the results indicate the actual wellbore pressure derivatives are in between those computed with the harmonic average and the arithmetic average, and closest to the geometric average of $k(r,\theta)$ over θ, which had been observed by Sagar[40]. In all cases the equivalent radial permeability, $k(r)$, computed with ISA, yielded excellent results in terms of wellbore pressure and pressure derivative.

4.2 Equivalent Radially Heterogeneous Reservoir

4.2.1 Example 1

This case deals with a *small variation of permeability in both the radial and θ–directions.* We considered a no-flow outer boundary reservoir in which the permeability varies with r and θ, constituted of five annular zones. We divided the reservoir into 1000 gridblocks: 100 gridblocks in the radial direction, distributed according to the Coats grid approach[31], and 10 gridblocks uniformly distributed in the θ–direction. The permeability values, $k = k(r,\theta)$ were randomly generated for each annular zone, using

Reproduced with permission of the copyright owner. Further reproduction prohibited without permission.

a different seed number for each zone, and assuming a Gaussian distribution in θ-direction. In each annular zone, the distribution has an mean value assigned to the zone (in this case equal to 20 md for all zones), standard deviation of 25% of the mean, with all the values constrained to within one standard deviation of the mean value. The main reservoir/well system parameters are presented in Table 4.2.1. We simulated the system producing through the well at a constant rate of 300 reservoir barrels per day for 1000 days. The infinite-acting flow period ends at about 25 days and pseudosteady state flow regime prevails from soon after that time onwards.

Table 4.2.1

Areally Heterogeneous Reservoir; Example 1

Reservoir/Well System Parameters

Permeability Distribution							Other parameters
Annular Zone	Outer Radius ft	Mean value md	Seed #	Average of $k(r,\theta)$ over θ (md) st. deviation = 25% of the mean			
				Harm	Geom	Arith	
1	$r_1 = 32$	20	-1	19.18	19.28	19.38	$\mu = 1.0$ cp
2	$r_2 = 151$	20	-33	19.10	19.40	19.70	$c_t = 10\times10^{-6}$ psi^{-1}
3	$r_3 = 534$	20	-27	20.15	20.34	20.52	h = 20 ft
4	$r_4 = 1{,}055$	20	-100	19.73	19.89	20.06	$\phi = 20$ %
5	$r_5 = 5{,}000$	20	-56	19.85	20.03	20.22	$p_i = 6000$ psi $r_w = 0.3$ ft q = 300 rb/d

Fig. 4.2.1 compares the pressure derivatives, $\Delta p_w'$, which were numerically calculated from the simulated pressures computed with the actual permeability distribution, $k = k(r,\theta)$ (solid line), with a homogeneous permeability, $k = 20$ md (dashed line), and with the $k(r)$ generated from, respectively, harmonic (star data points), geometric (plus data points) and arithmetic average (triangular data points) of $k = k(r,\theta)$ over θ. It is clear that the actual derivatives are closest to the ones obtained with the

Reproduced with permission of the copyright owner. Further reproduction prohibited without permission.

geometric average, just between the ones computed with the harmonic and arithmetic averages. Is this interesting observation also valid for other cases with large variation in permeability? In the next two cases we will try to answer this question.

In Fig. 4.2.2 we present the equivalent radial permeability, $k(r)$, computed with ISA (solid line), and the permeability profiles for the cases of harmonic (large-dash line) and arithmetic (small-dash line) averaged permeabilities presented in Table 4.2.1. As expected, the ISA-computed permeability distribution fall between both of them. Because of the scales used in Fig. 4.2.2, it looks like the ISA-computed permeability distribution, $k(r)$, is far from a homogeneous one, but in fact, all values are within 19.1 and 20.5 md, i.e., the permeability is nearly homogeneous. As a consequence, the wellbore pressures and pressure derivatives should present a near-homogeneous behavior (see Fig. 4.2.1).

Fig. 4.2.3 compares the actual pressure derivatives (solid line) with those obtained with the equivalent radial permeability distribution computed with ISA (circular data points). The agreement between both curves is excellent, graphically indistinguishable, even though y-axis scale is quite fine.

We also simulated a buildup period after the 1000-days drawdown period. We recall that at the instant of shut in a pseudosteady state flow has been established. We then computed, at the instant of shut in, the average reservoir pressure, $\overline{p}$, and boundary-dominated flow parameters, namely, productivity index, PI, and the homogeneous-equivalent pseudosteady state permeability, k_{eq}, using the techniques described in the sections 3.6 and 3.7 of Chapter III, applied to both drawdown and buildup data. In particular, when using drawdown data we computed $\overline{p}$, k_{eq} and PI, using the exact analytical equations, respectively, Eqs. 2.3.90, 2.3.92, and 2.3.100, with the equivalent radial permeability $k(r)$ computed from ISA. When using buildup data we first constructed the pressure profile for the equivalent radial permeability distribution (as in subsection 3.6.1). Then, based on this pressure profile, we calculated $\overline{p}$ using Eq. 2.3.88,

Reproduced with permission of the copyright owner. Further reproduction prohibited without permission.

Reproduced with permission of the copyright owner. Further reproduction prohibited without permission.

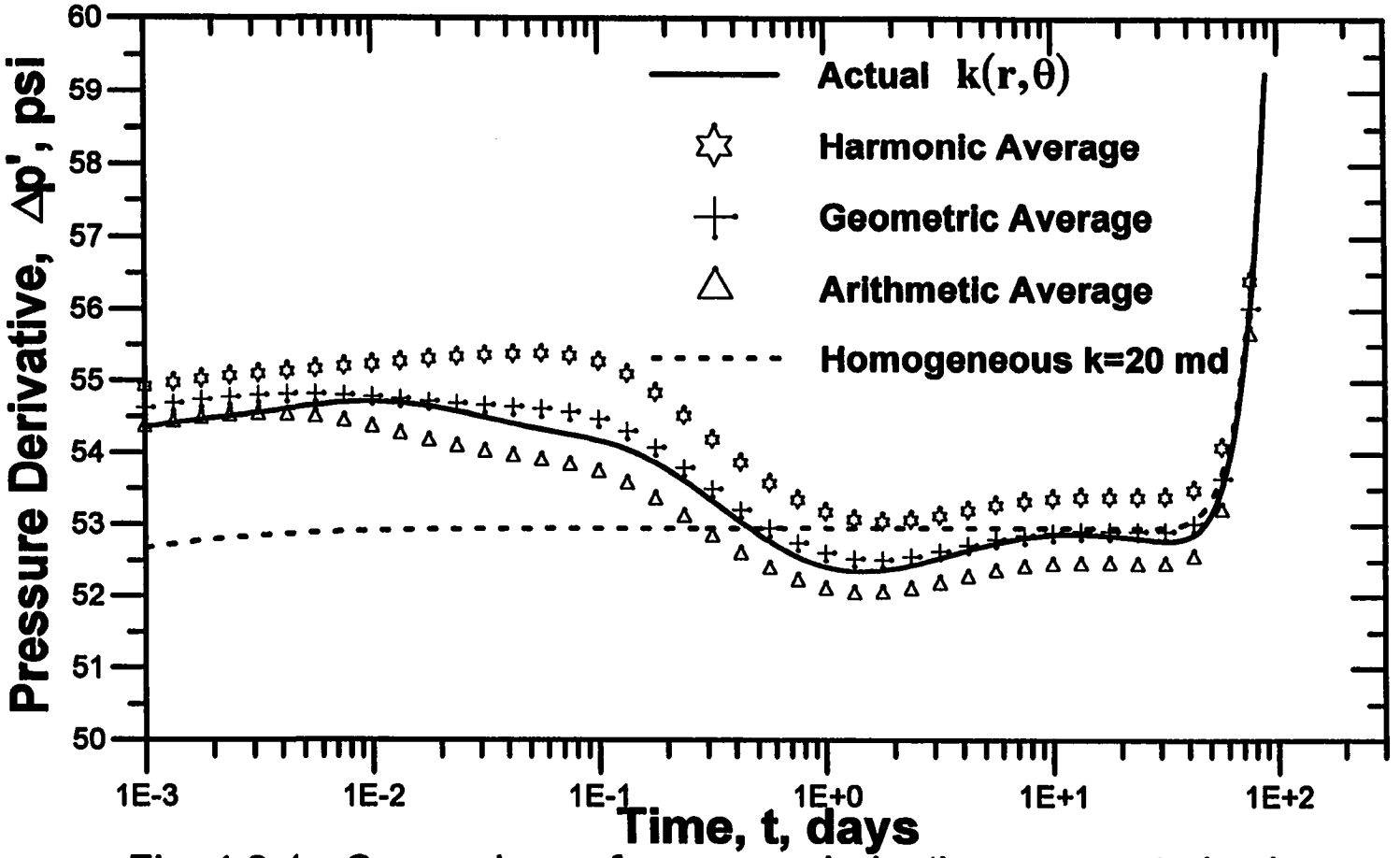

Fig. 4.2.1 - Comparison of pressure derivatives computed using the actual k(r,θ) and the harmonic, geometric, and arithmetic average of k(r,θ) over θ; Example 1.

Reproduced with permission of the copyright owner. Further reproduction prohibited without permission.

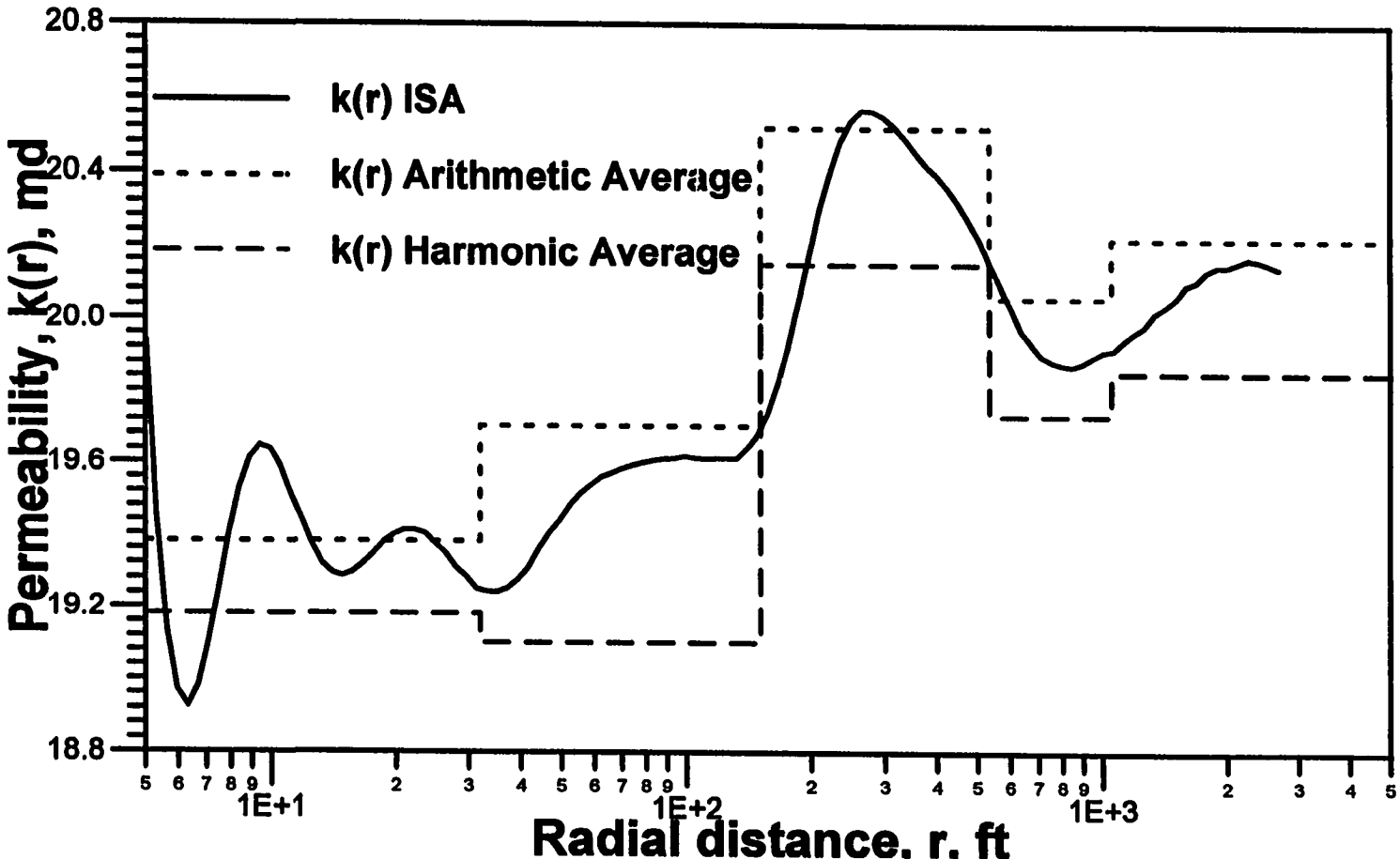

Fig. 4.2.2 - Comparison of permeability profiles computed via ISA and via the harmonic and arithmetic average of $k(r,\theta)$ over θ; Example 1.

Reproduced with permission of the copyright owner. Further reproduction prohibited without permission.

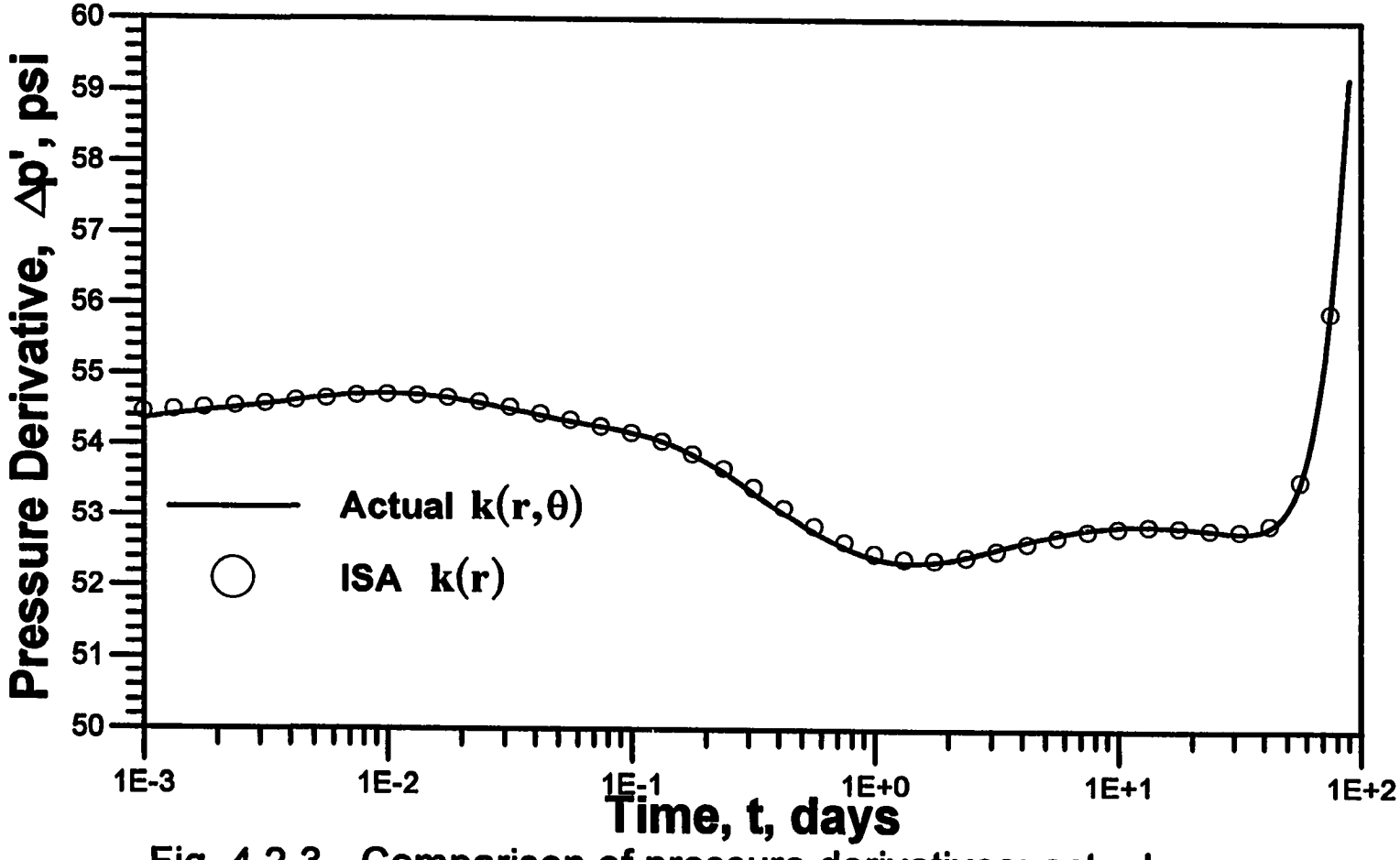

Fig. 4.2.3 - Comparison of pressure derivatives: actual versus computed from ISA's results; Example 1.

as detailed in subsection 3.6.3. The values of PI and k_{eq} were computed using, respectively, Eqs. 3.7.1 and 3.7.2. with the calculated $\bar{p}$. The results are compared in Table 4.2.2 with the values computed from our (r,θ) simulator using the actual permeability distribution $k(r,\theta)$. The close agreement between simulated and computed values substantiates the accuracy and reliability of our computational techniques.

Table 4.2.2

Boundary-Dominated Flow Parameters; Example 1

	Simulator	Computed with Test Data	
		Drawdown	Buildup
$\bar{p}$, psi	5463.8	5468.0 (+0.08%)	5461.8 (-0.04%)
PI, STB/D/psi	0.3098	0.3085 (-0.04%)	0.3105 (+0.02%)
k_{eq}, md	19.6	19.5 (-0.04%)	19.7 (+0.02%)

4.2.2 Example 2

This example presents a case of an areal *permeability distribution*, $k = k(r,\theta)$, *with large variation in the radial direction and a small variation in the* θ*-direction.* The reservoir/well system is as in Example 1, except for the permeability distribution, which is generated in similar manner as explained in that example. In this case the mean value of the permeability distribution $k = k(r,\theta)$ changes significantly from annular zone to annular zone. The pertinent reservoir/well system parameters are presented in Table 4.2.3.

Reproduced with permission of the copyright owner. Further reproduction prohibited without permission.

Table 4.2.3

Areally Heterogeneous Reservoir; Example 2

Reservoir/Well System Parameters

Permeability Distribution							Other parameters
Annular Zone	Outer Radius ft	Mean value md	Seed #	Average of $k(r,\theta)$ over θ (md) st. deviation = 25% of the mean			
				Harm	Geom	Arith	
1	$r_1 = 32$	20	-1	19.18	19.28	19.38	$\mu = 1.0$ cp
2	$r_2 = 151$	30	-33	28.65	29.09	29.55	$c_t = 10\times10^{-6}$ psi^{-1}
3	$r_3 = 534$	10	-27	10.07	10.17	10.26	h = 20 ft
4	$r_4 = 1{,}055$	18	-100	17.75	17.90	18.05	$\phi = 20$ %
5	$r_5 = 5{,}000$	40	-56	39.70	40.07	40.43	$p_i = 6000$ psi $r_w = 0.3$ ft q = 300 rb/d

Similar to the previous example, we simulated a drawdown of 1000 days. The transient period lasts for approximately 26 days and shortly after that the pseudosteady state flow regime prevails. The analysis of this case follows the basic steps of Example 1.

Fig. 4.2.4 compares the pressures derivatives resulting from the simulation using the actual permeability distribution (solid line), $k = k(r,\theta)$, and using the radial permeability distribution, $k(r)$, obtained by the harmonic, geometric and arithmetic average of $k = k(r,\theta)$ over θ, represented, respectively, by star, plus and triangular data points. We observe that the actual values of $\Delta p_w'$ nearly overlay the geometric-average-$k(r)$ computed ones, and consequently, they just fall between the arithmetic and harmonic-average-$k(r)$ computed ones, for the whole period simulated, from the infinite-acting period until the outer boundary completely dominates the wellbore pressure behavior. Actually for this case the results depend only slightly on the averaging used in the θ direction.

Reproduced with permission of the copyright owner. Further reproduction prohibited without permission.

Reproduced with permission of the copyright owner. Further reproduction prohibited without permission.

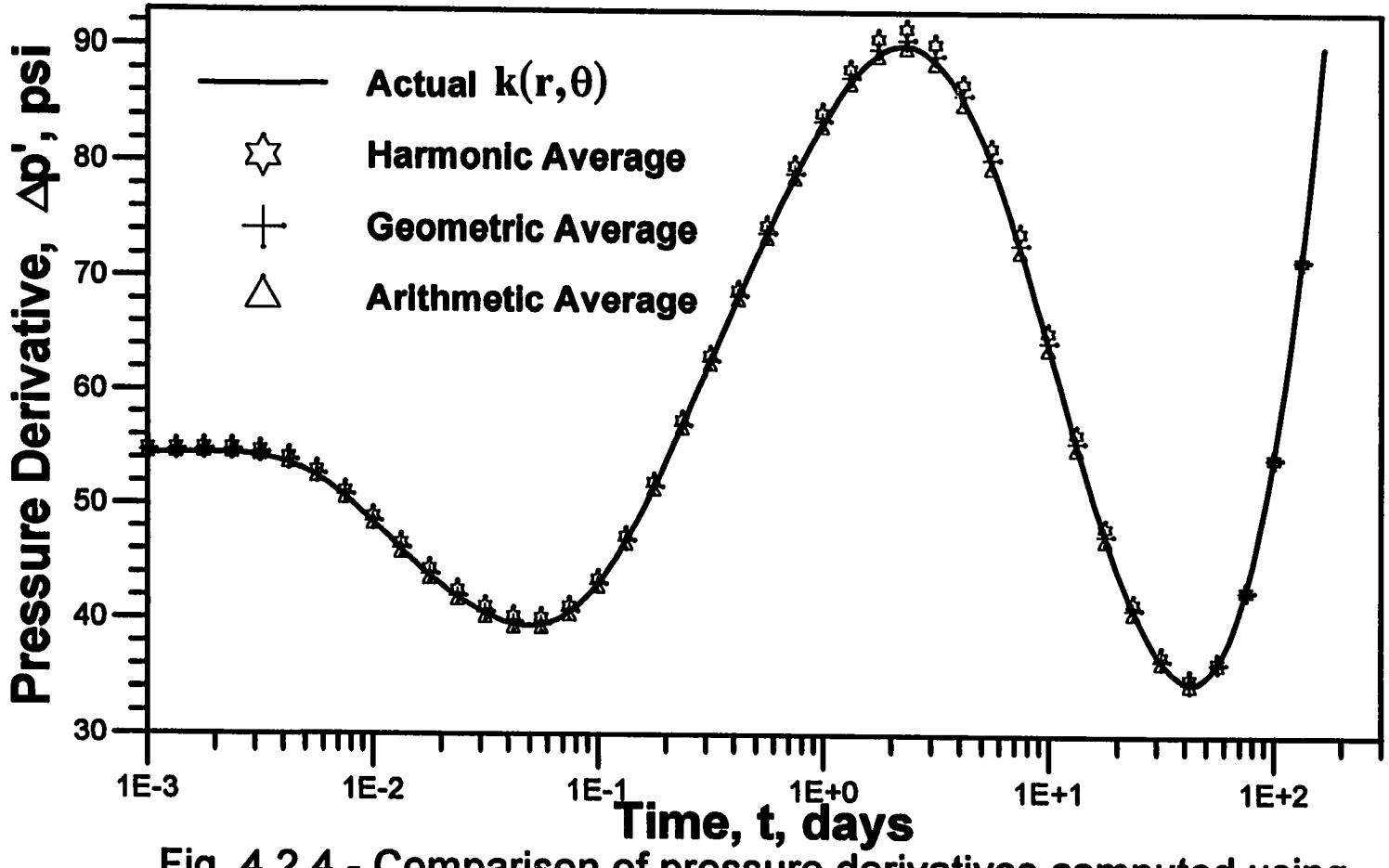

Fig. 4.2.4 - Comparison of pressure derivatives computed using the actual k(r,θ) and the harmonic, geometric, and arithmetic average of k(r,θ) over θ; Example 2.

Fig. 4.2.5 presents the equivalent radial permeability profile calculated with ISA (solid line) applied to the transient part of the simulated drawdown data. Given that the variation between the harmonic, arithmetic and geometric averages is small, it is difficult to say from these results which permeability average is represented best by the ISA computed permeability distribution.

As shown in Fig. 4.2.6, the ISA-computed permeability distribution when input into our simulator, yields pressure derivatives which are in good agreement with the derivatives generated with the original permeability distribution, $k(r,\theta)$. The equivalent radial permeability distribution obtained with ISA is then used to compute the average reservoir pressure, $\bar{p}$, and the boundary-dominated flow parameters PI and k_{eq}. For comparison purposes, these three parameters were also computed based on the buildup data we simulated after the drawdown. Computed and simulated results are compared in Table 4.2.4. The close agreement between simulated and computed values of $\bar{p}$, PI and k_{eq}, indicates the applicability of our techniques for this case, where $k(r,\theta)$ varies significantly in the radial direction but has only a small variation in the $\theta-$direction.

4.2.3 Example 3

In this case, the actual *permeability distribution,* $k(r,\theta)$, *has a large variation in both the radial and* $\theta-$directions. The reservoir/well system and simulation conditions are the same as in Example 2, except for the permeability distribution. In the current example all values of $k(r,\theta)$ within an annular zone are within 50% of the mean value assigned to that zone, instead of 25% as in the two previous examples. This yields permeability values ranging from 5 md up to 57 md. The relevant data are presented in Table 4.2.5.

Reproduced with permission of the copyright owner. Further reproduction prohibited without permission.

Reproduced with permission of the copyright owner. Further reproduction prohibited without permission.

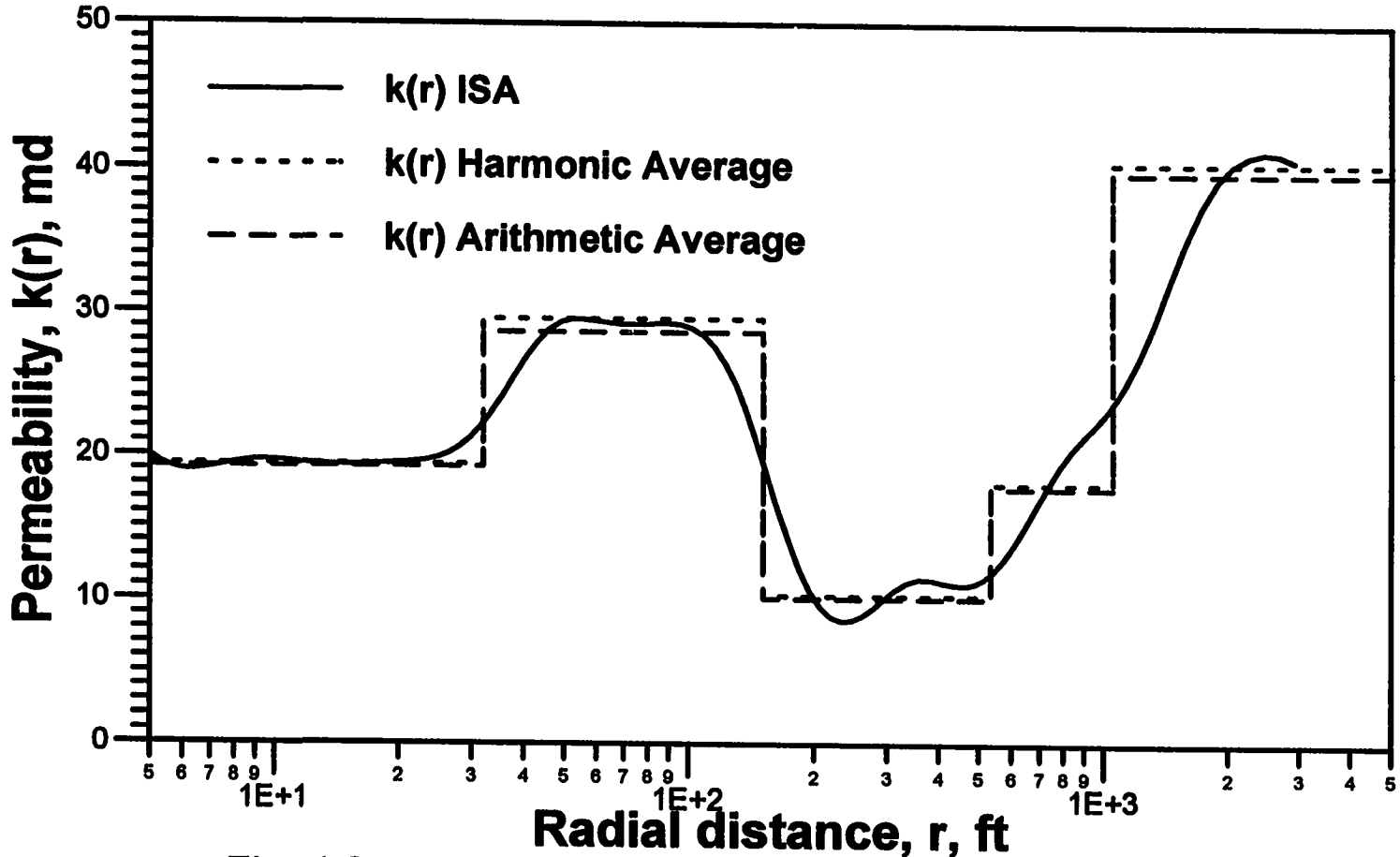

Fig. 4.2.5 - Comparison of permeability profiles computed via ISA and via the harmonic and arithmetic average of $k(r,\theta)$ over θ; Example 2.

Reproduced with permission of the copyright owner. Further reproduction prohibited without permission.

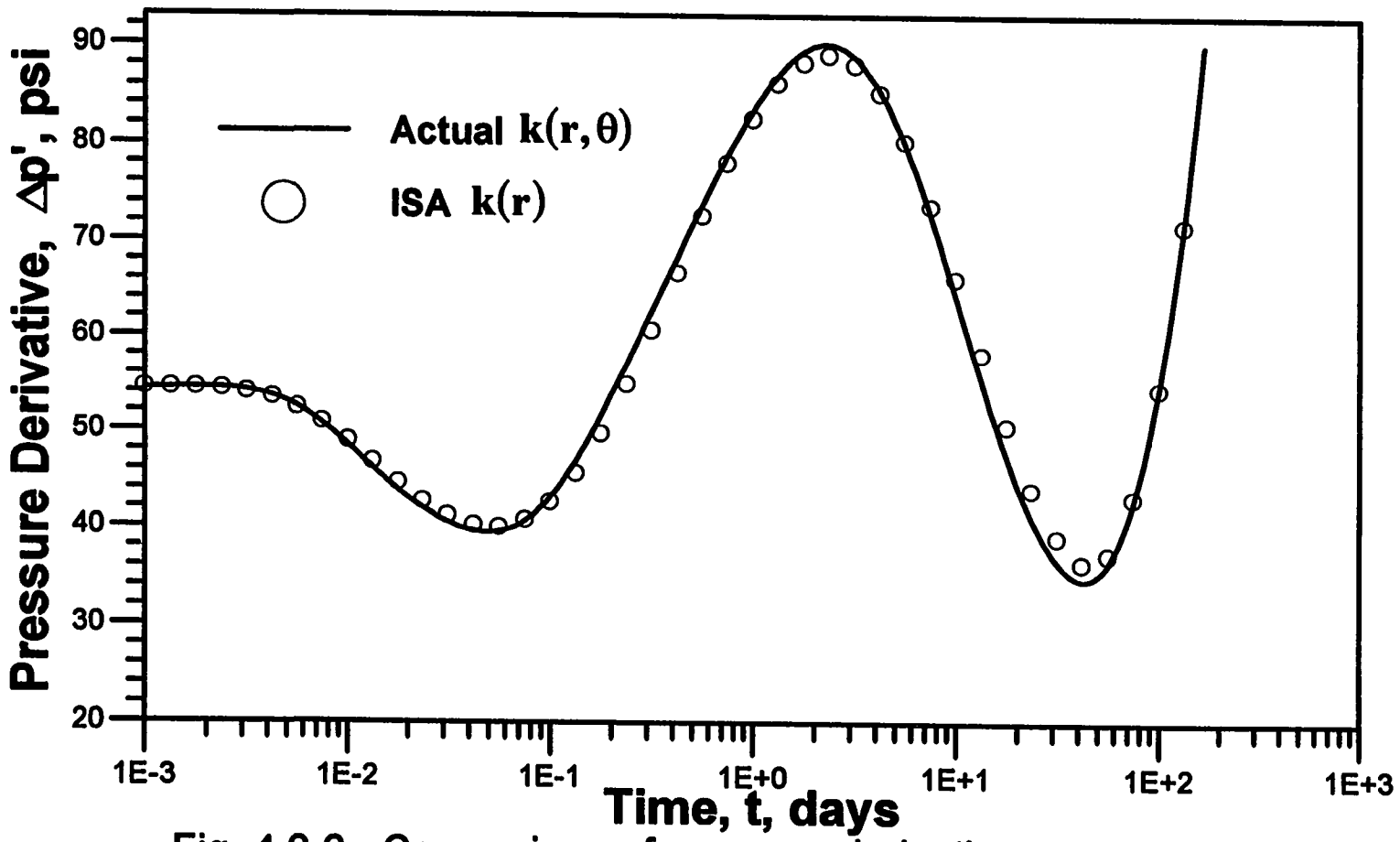

Fig. 4.2.6 - Comparison of pressure derivatives: actual versus computed from ISA's results; Example 2

Table 4.2.4

Boundary-Dominated Flow Parameters; Example 2

	Simulator	Computed with Test Data	
		Drawdown	Buildup
$\bar{p}$, psi	5463.8	5467.3 (+0.06%)	5453.0 (-0.20%)
PI, STB/D/psi	0.2986	0.2981 (-0.17%)	0.3019 (+1.10%)
k_{eq}, md	18.9	18.9 (-0.17%)	19.1 (+1.10%)

Table 4.2.5

Areally Heterogeneous Reservoir; Example 3

Reservoir/Well System Parameters

Permeability Distribution							Other parameters
Annular Zone	Outer Radius ft	Mean Value md	Seed #	Average of $k(r,\theta)$ over θ(md) st. deviation = 50% of the mean			
				Harm	Geom	Arith	
1	$r_1 = 32$	20	-1	17.97	18.35	18.76	$\mu = 1.0$ cp
2	$r_2 = 151$	30	-33	25.37	27.20	29.09	$c_t = 10\times10^{-6}$ psi^{-1}
3	$r_3 = 534$	10	-27	9.68	10.13	10.52	h = 20 ft
4	$r_4 = 1{,}055$	18	-100	16.84	17.49	18.10	$\phi = 20$ %
5	$r_5 = 5{,}000$	40	-56	37.38	39.36	40.87	$p_i = 6000$ psi $r_w = 0.3$ ft q = 300 rb/d

Reproduced with permission of the copyright owner. Further reproduction prohibited without permission.

We simulated a 1000 days drawdown with the actual permeability distribution, $k(r,\theta)$, and with radial permeability distribution, $k(r)$, obtained with the harmonic, geometric and arithmetic average of $k(r,\theta)$ over θ, for each one of the five annular zones. The infinite-acting period lasts for about 26 days and shortly thereafter pseudosteady state flow begins. The corresponding resulting pressure derivatives, $\Delta p_w'$, are represented in Fig. 4.2.7, as in all previous examples, by, respectively, a solid line, stars, plus signs, and triangles. Once more, the actual values of $\Delta p_w'$ fall between the ones from harmonic and arithmetic average, and reasonably close to the ones from geometric average. This observation, in addition to what was also observed in the two previous cases, suggests that, in terms of wellbore pressure derivatives obtained from a well test, an areally permeability distribution, $k(r,\theta)$, is nearly equivalent to an associated radial permeability distribution computed as the geometric average of $k(r,\theta)$ over θ. This had been already observed by Sagar[40]. For the few (r,θ) cases we have considered, the proper average is always between an arithmetic and a harmonic average and can be modeled better by a geometric average than the harmonic average that resulted from the perturbation-theory-derived Oliver solution.

Fig. 4.2.8 shows the equivalent radial permeability distribution, $k(r)$, calculated with ISA (solid line), using the drawdown data obtained during the infinite-acting period, and the harmonic average (long dashes), arithmetic average (short dashes), and geometric average of $k(r,\theta)$ over θ. ISA's $k(r)$ tends to be between the harmonic and the arithmetic permeability distributions, and consequently, approximates reasonably well the geometric average of $k(r,\theta)$ over θ permeability distribution.

Fig. 4.2.9 compares pressure derivatives resulting from the actual $k(r,\theta)$ (solid line) and from the equivalent radial permeability computed with ISA (circular data points). The agreement is excellent for the whole period simulated.

Reproduced with permission of the copyright owner. Further reproduction prohibited without permission.

Reproduced with permission of the copyright owner. Further reproduction prohibited without permission.

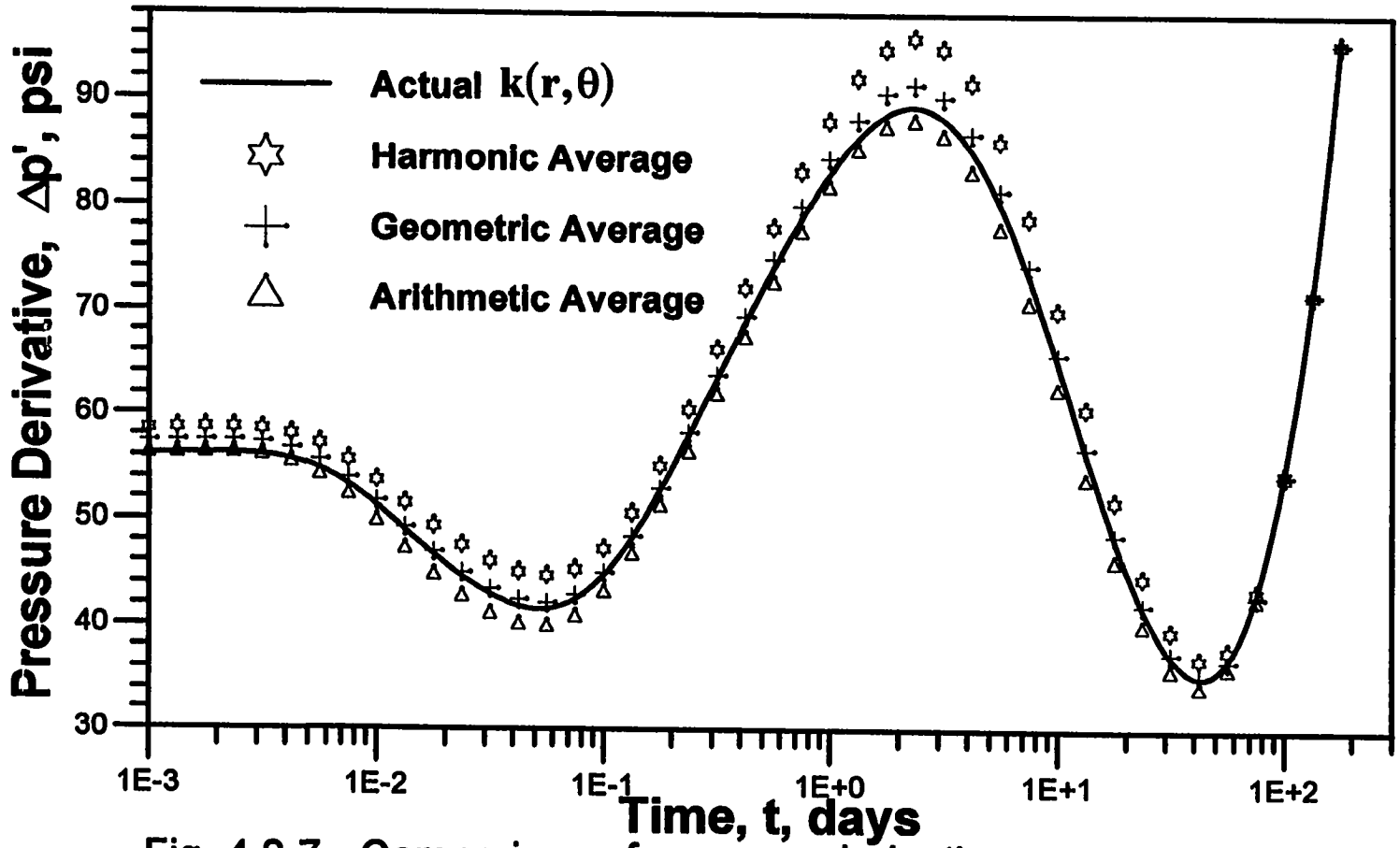

Fig. 4.2.7 - Comparison of pressure derivatives computed using the actual k(r,θ) and the harmonic, geometric, and arithmetic average of k(r,θ) over θ; Example 3.

Reproduced with permission of the copyright owner. Further reproduction prohibited without permission.

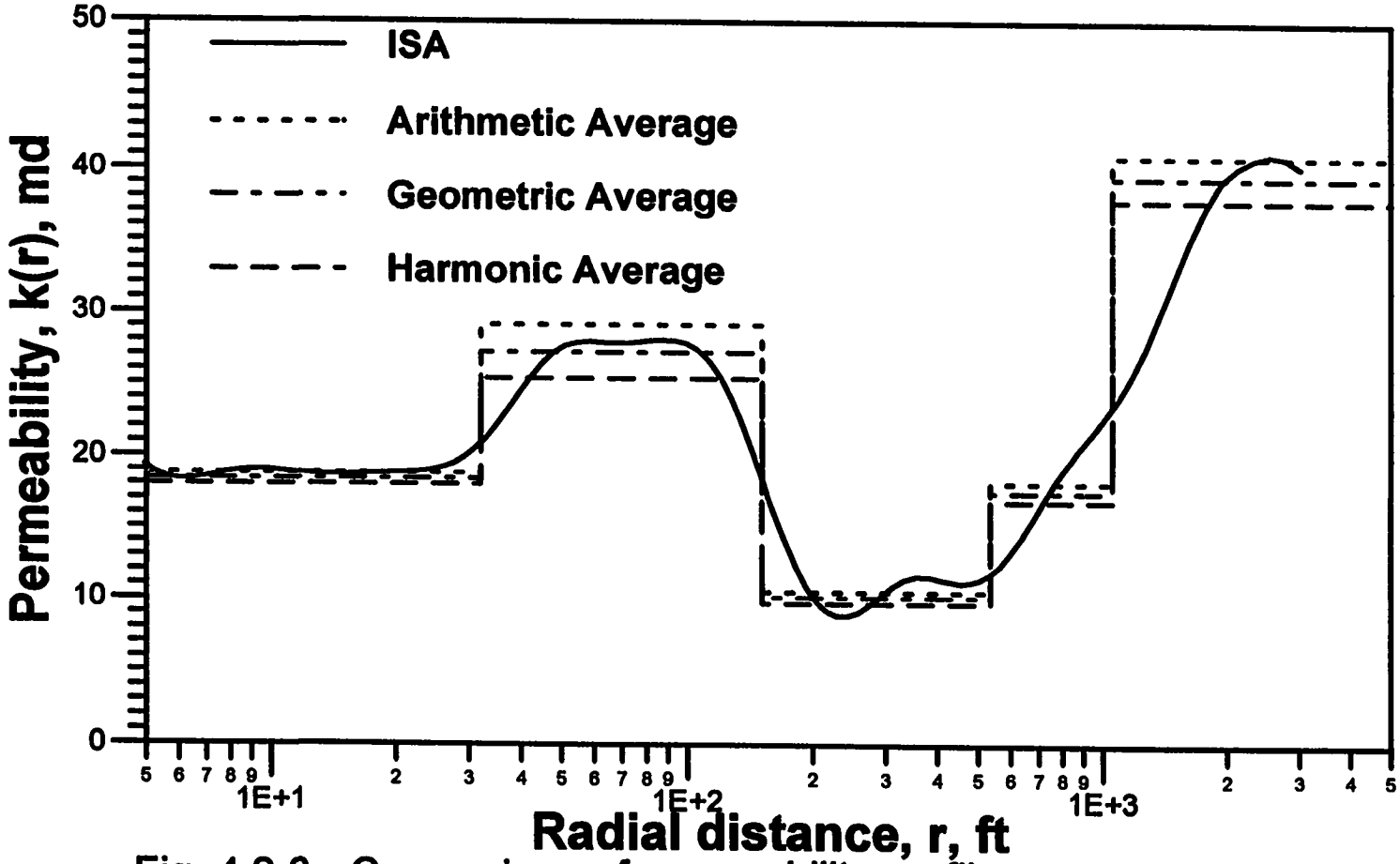

Fig. 4.2.8 - Comparison of permeability profiles computed via ISA and via the harmonic, geometric and arithmetic average of $k(r,\theta)$ over θ; Example 3.

Reproduced with permission of the copyright owner. Further reproduction prohibited without permission.

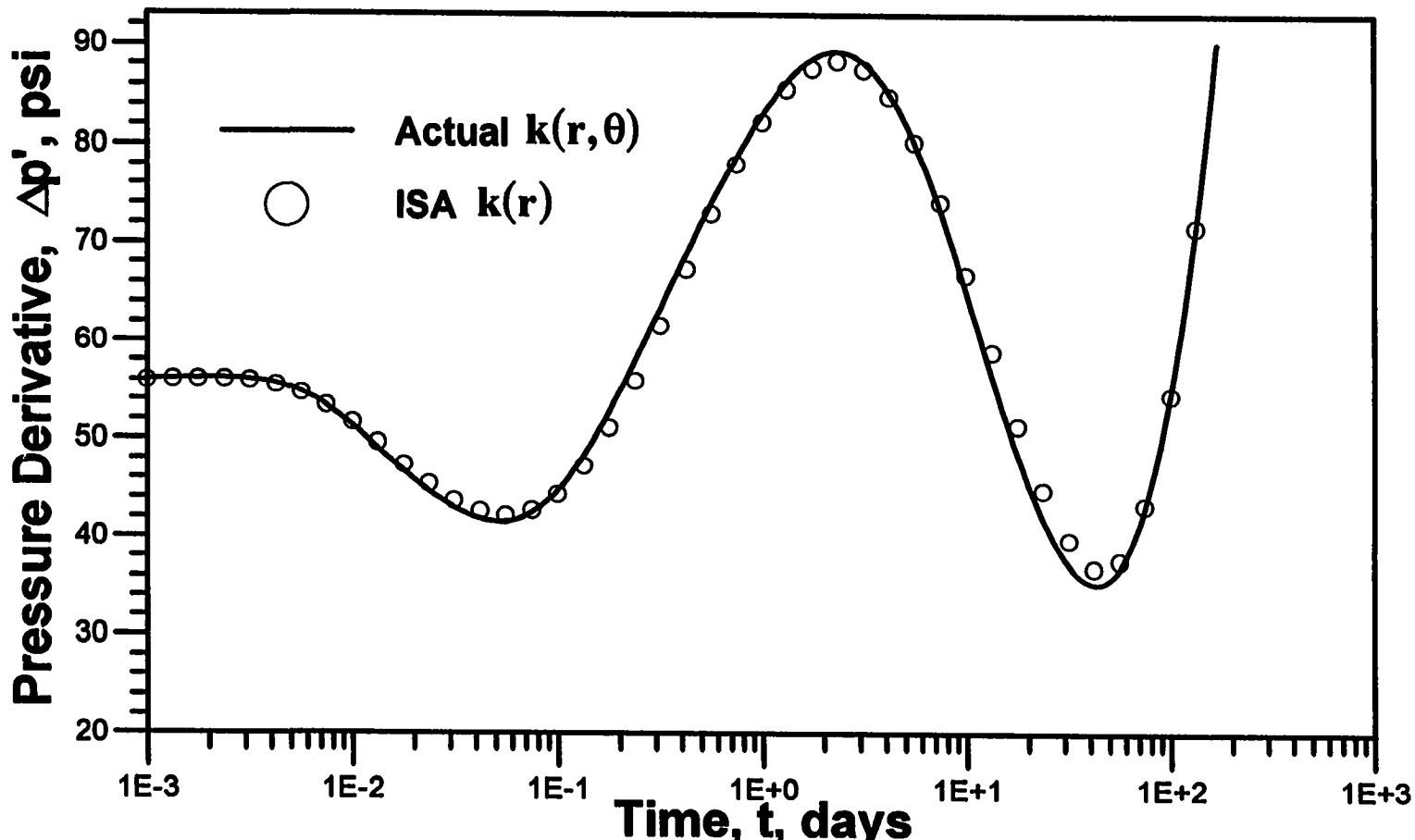

Fig. 4.2.9 - Comparison of pressure derivatives: actual versus computed from ISA's results; Example 3.

Based on the ISA-computed equivalent radial permeability we calculated $\overline{p}$, and PI and k_{eq} at the end of the 1000-days flow period (pseudosteady state flow). We also calculated these parameters based on the buildup data we simulated after the drawdown period. The computed values of $\overline{p}$, PI and k_{eq} based on drawdown and on buildup data are compared in Table 4.2.6 with the actual ones, obtained with our numerical (r,θ) simulator. As shown, the agreement between computed and simulated values of $\overline{p}$, PI and k_{eq} is very good.

Table 4.2.6

Boundary-Dominated Flow Parameters; Example 3

	Simulator	Computed with Test Data	
		Drawdown	Buildup
$\overline{p}$, psi	5463.8	5466.9 (+0.06%)	5453.0 (-0.20%)
PI, STB/D/psi	0.2914	0.2910 (-0.14%)	0.2945 (+1.06%)
k_{eq}, md	18.5	18.4 (-0.54%)	18.6 (+0.54%)

In addition, we simulated a constant-pressure production flow period of 1000 days, with a constant bottomhole flowing pressure of 5000 psi, using both, the actual permeability distribution, $k(r,\theta)$, and the ISA-computed equivalent radial permeability distribution, $k(r)$. The infinite-acting flow period ends by about 25 days and soon after that a boundary-dominated flow occurs. Fig. 4.2.10 compares the resulting flow rates. Fig. 4.2.10 also shows the boundary-dominated flow rate (star data points) computed with Eq. 2.3.114 and the ISA-derived PI. The flow rate (circular data points) obtained by using the ISA derived radial permeability distribution in our simulator is in very good agreement with the actual flow rate (solid line), for the whole period simulated. During the boundary-

Reproduced with permission of the copyright owner. Further reproduction prohibited without permission.

Reproduced with permission of the copyright owner. Further reproduction prohibited without permission.

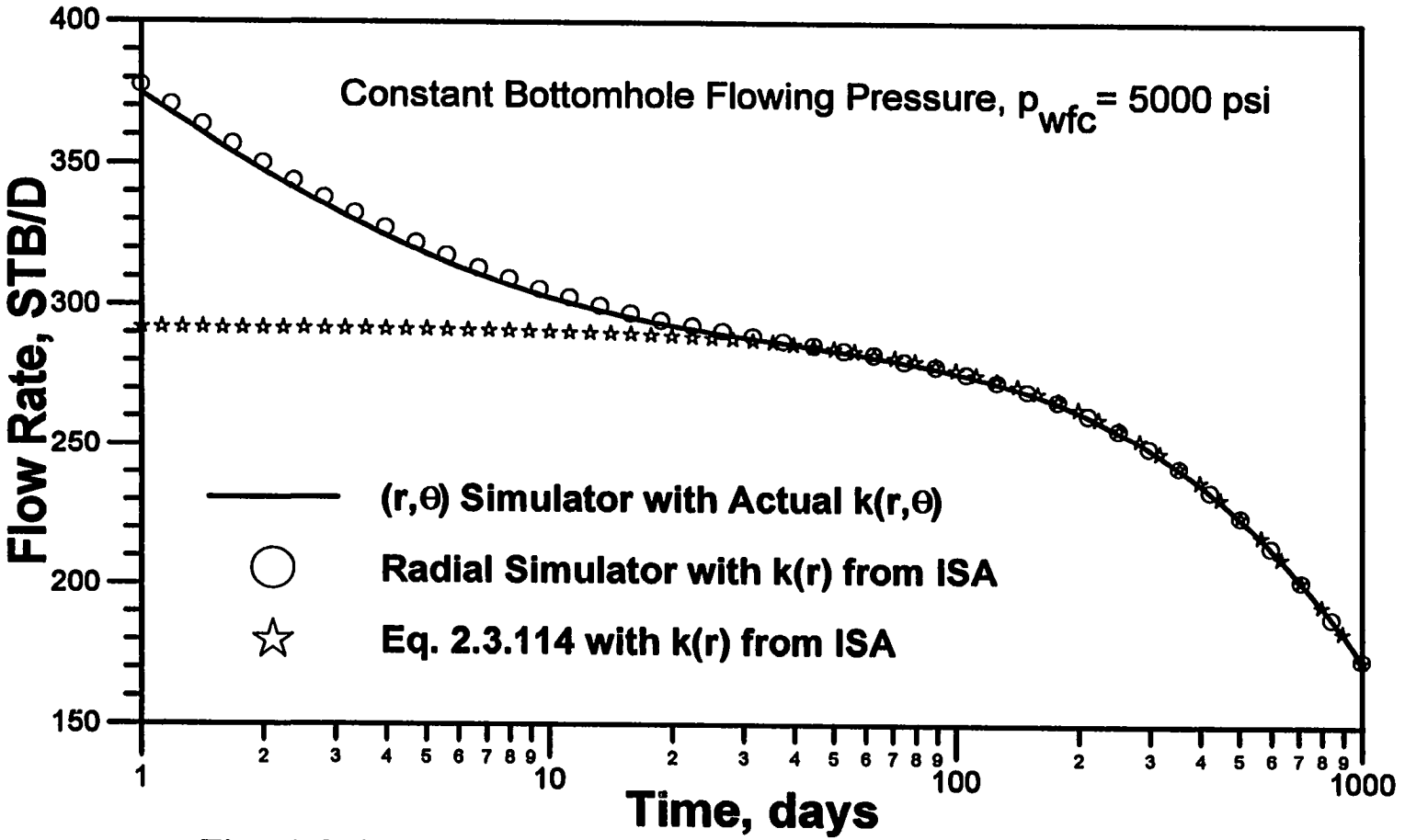

Fig. 4.2.10 - Flow rate for constant pressure production: simulated versus computed; Example 3.

dominated flow period all three computed flow rate curves merge together. This illustrates the applicability of our technique to compute average reservoir pressure, the constant-pressure production flow rate, the productivity index and the homogeneous-equivalent pseudosteady state permeability.

4.2.4 Example 4

This case pertains to a reservoir with an areal *permeability distribution* $k(x,y)$ *generated by geostatistic techniques*, which is depicted in Fig. 4.2.11. The reservoir drainage area is a square shaped with each side of length 4,025 ft and the reservoir has a uniform thickness of 10 ft. It is discretized into 13,225 square gridblocks of dimensions 35 by 35 ft. The permeability distribution is based on a log-normal distribution and complies with a spherical variogram model with a sill of 440, range of 509, seed number 1079602 and the value of the center gridblock is conditioned to be 34.3 md. The technique to generate $k(x,y)$ is described in Ref. 40. The pertinent reservoir/well system parameters are presented in Table 4.2.7.

A well is located at the center of the reservoir and a no-flow outer boundaries are imposed. Using the commercial simulator ECLIPSE[41], a drawdown flow period of 20.8 days were simulated for a constant surface flow rate of 106.3 stock tank barrels per day. The infinite-acting period ends by about 0.31 days (7.5 hours) of flow. Pseudosteady state flow starts at about 1.5 days, when the wellbore pressure drops at a constant rate of 30 psi per day. We calculate the porous volume, from which we compute an equivalent outer reservoir radius, r_e, of approximately, 2271 ft, using the known value of porosity and thickness (see Table 4.2.7) and the pseudosteady state slope, $m^* = 30$ psi / day, assuming $A = \pi r_e^2$, where A is the reservoir drainage area.

Reproduced with permission of the copyright owner. Further reproduction prohibited without permission.

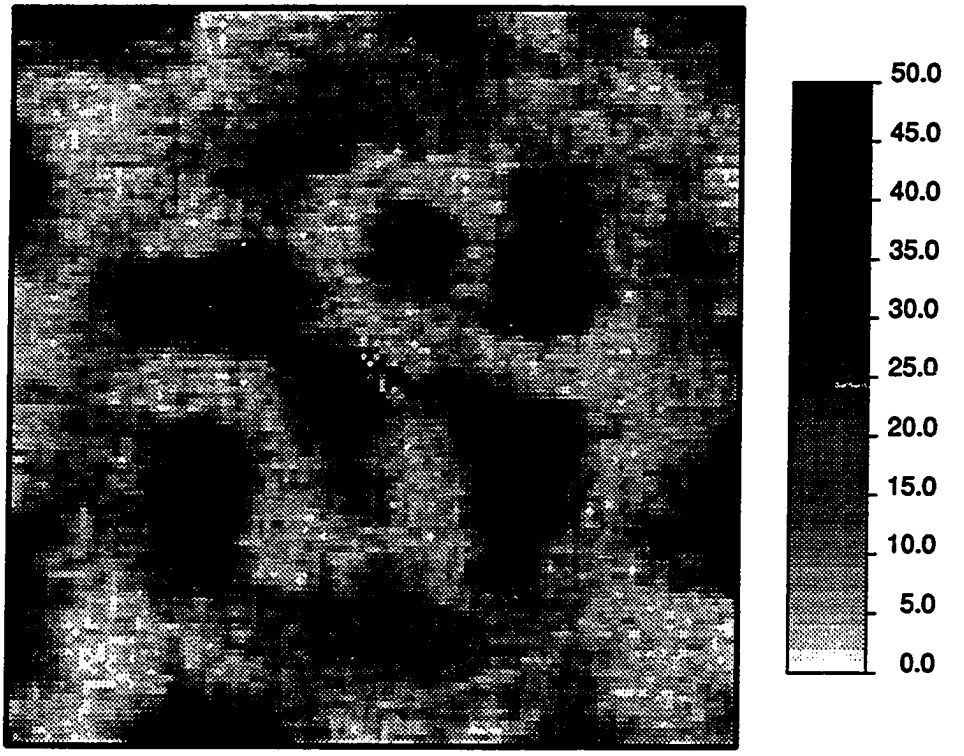

Fig. 4.2.11 - Reservoir permeability distribution, $k(x, y)$, md . Example 4.

Reproduced with permission of the copyright owner. Further reproduction prohibited without permission.

Table 4.2.7 Areally Heterogeneous Reservoir; Example 4 Reservoir/Well System Parameters	
Permeability Distribution	Other Parameters
number of data = 13,225 mean = 20.0571 md standard deviation = 20.9649 coefficient of variance = 1.0453 maximum = 386.8142 md upper quartile = 26.1495 md median = 13.5860 md lower quartile = 7.0381 md minimum = 0.0954 md	no-flow outer boundary $B_o = 1.20$ $\mu = 0.4$ cp $c_t = 0.49\times10^{-6}$ psi^{-1} h = 10 ft $\phi = 30$ % $p_i = 2000$ psi $r_w = 0.5$ ft q = 127.56 rb/d

Applying our inverse solution techniques, ISA and MYA, to the pressure derivatives obtained by numerical calculation from the simulated pressure drop, during the transient flow regime, we computed two equivalent radial permeability distributions, $k(r)$, shown in Fig. 4.2.12, respectively, as circular and plus data points. Using these computed equivalent radial permeability distributions in our simulator we generated, under the same original simulation conditions, wellbore pressure derivatives, $\Delta p_w'$, which are compared in Fig. 4.2.13 with the actual $\Delta p_w'$ values obtained using the simulator ECLIPSE with the actual permeability distribution $k(x,y)$. The ISA resulting $\Delta p_w'$ (circles) is in very good agreement with the actual $\Delta p_w'$(solid line), whereas, the MYA-derived $\Delta p_w'$ (cross), although close to the actual one, is not quite as good.

At the end of the simulated period, a pseudosteady state flow regime prevails. Based on the equivalent radial permeability distribution computed with ISA, we then determined the average reservoir pressure, $\bar{p}$, and the boundary-dominated flow parameters such as productivity index, *PI*, and the homogeneous-equivalent pseudosteady state permeability, k_{eq}. In Table 4.2.8, the computed values are compared with the actual values obtained from simulator ECLIPSE and actual permeability distribution, $k(x,y)$.

Reproduced with permission of the copyright owner. Further reproduction prohibited without permission.

Reproduced with permission of the copyright owner. Further reproduction prohibited without permission.

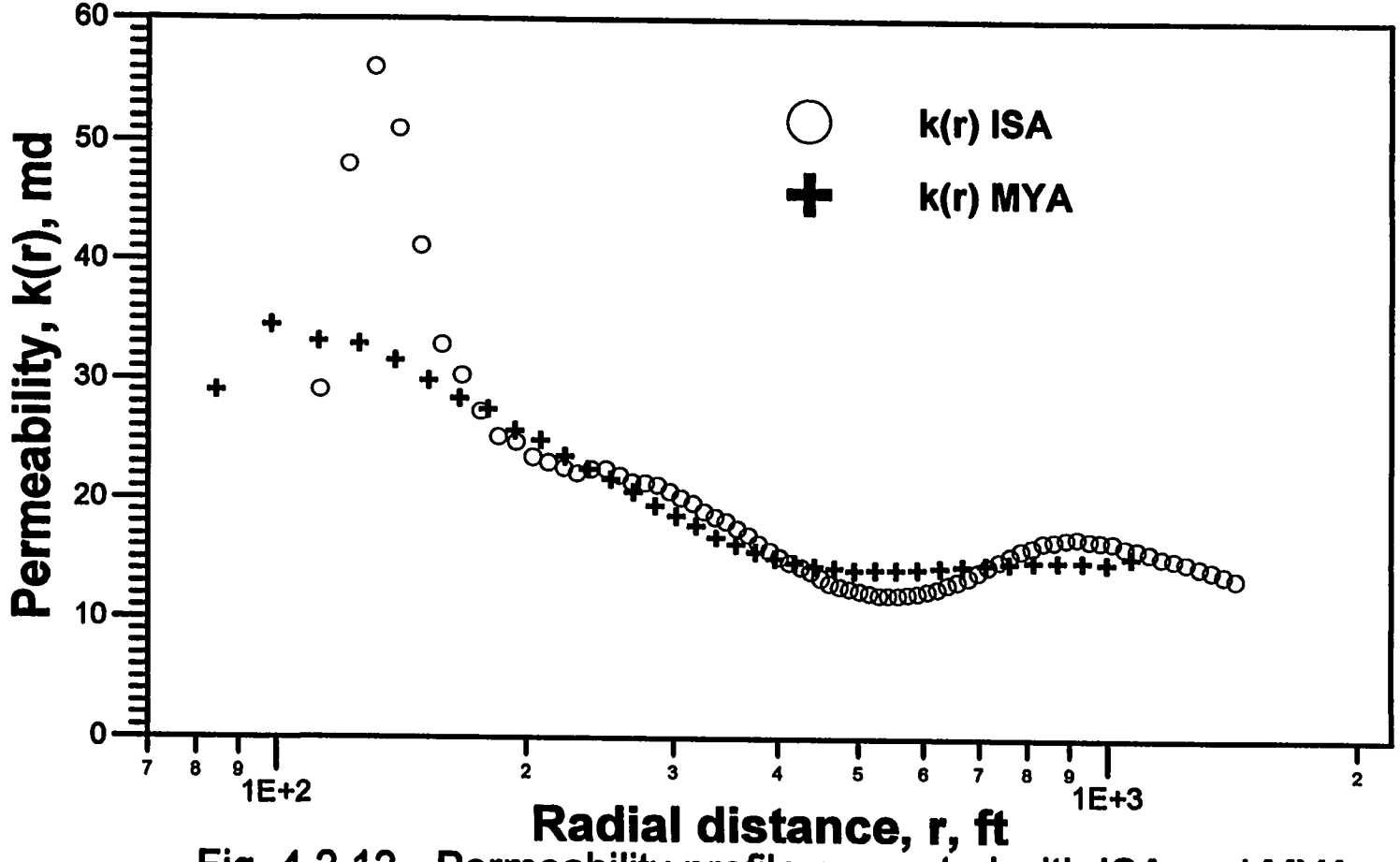

Fig. 4.2.12 - Permeability profile computed with ISA and MYA. Example 4.

Reproduced with permission of the copyright owner. Further reproduction prohibited without permission.

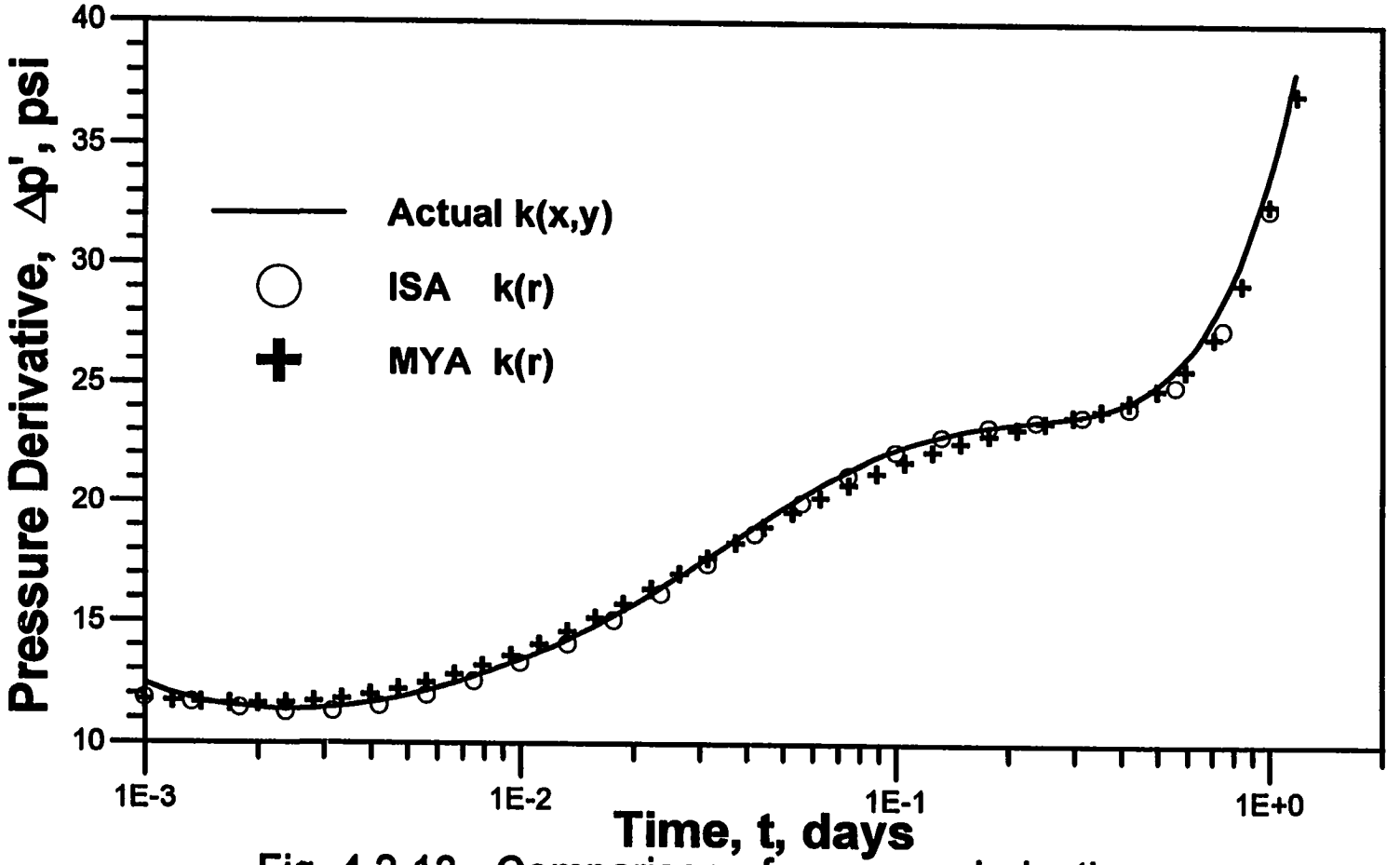

Fig. 4.2.13 - Comparison of pressure derivatives: actual versus computed; Example 4.

The agreement between computed and actual values of $\bar{p}$, PI and k_{eq}, is excellent. This illustrates that, the techniques developed in Chapter III for radial permeability distributions can be approximately applied for random areal permeability distributions to generate an equivalent radial permeability distribution, and to compute the average reservoir pressure and boundary-dominated flow parameters, at least, if the permeability variation is not too large and the well is at the center of a square drainage area.

Table 4.2.8

Boundary-Dominated Flow Parameters; Example 4

	Simulator	Computed with Test Data
$\bar{p}$, psi	1374.2	1382.6 (+0.60%)
PI, STB/D/psi	0.4980	0.4783 (-0.39%
k_{eq}, md	25.9	24.9 (-0.39%)

Similar to the Example 3, we also simulated a constant-pressure production period of 20.8 days, with a constant bottomhole flowing pressure of 1500 psi, using the actual permeability distribution $k(x,y)$ with the simulator ECLIPSE, and then using the equivalent radial permeability distribution, $k(r)$, with our (r,θ) simulator. The resulting flow rates are compared in Fig. 4.2.14, where are also shown the boundary-dominated flow rate computed with the ISA-calculated $k(r)$, the flow rate computed with Eq. 2.3.114 (star data points) with the PI value derived from ISA's results. The ISA-resulting flow rates (circles) agree very well with the actual ones (solid line) during the whole period, which includes both the transient and boundary-dominated flow periods. During the latter period all the three flow rate curves merge together.

Reproduced with permission of the copyright owner. Further reproduction prohibited without permission.

Reproduced with permission of the copyright owner. Further reproduction prohibited without permission.

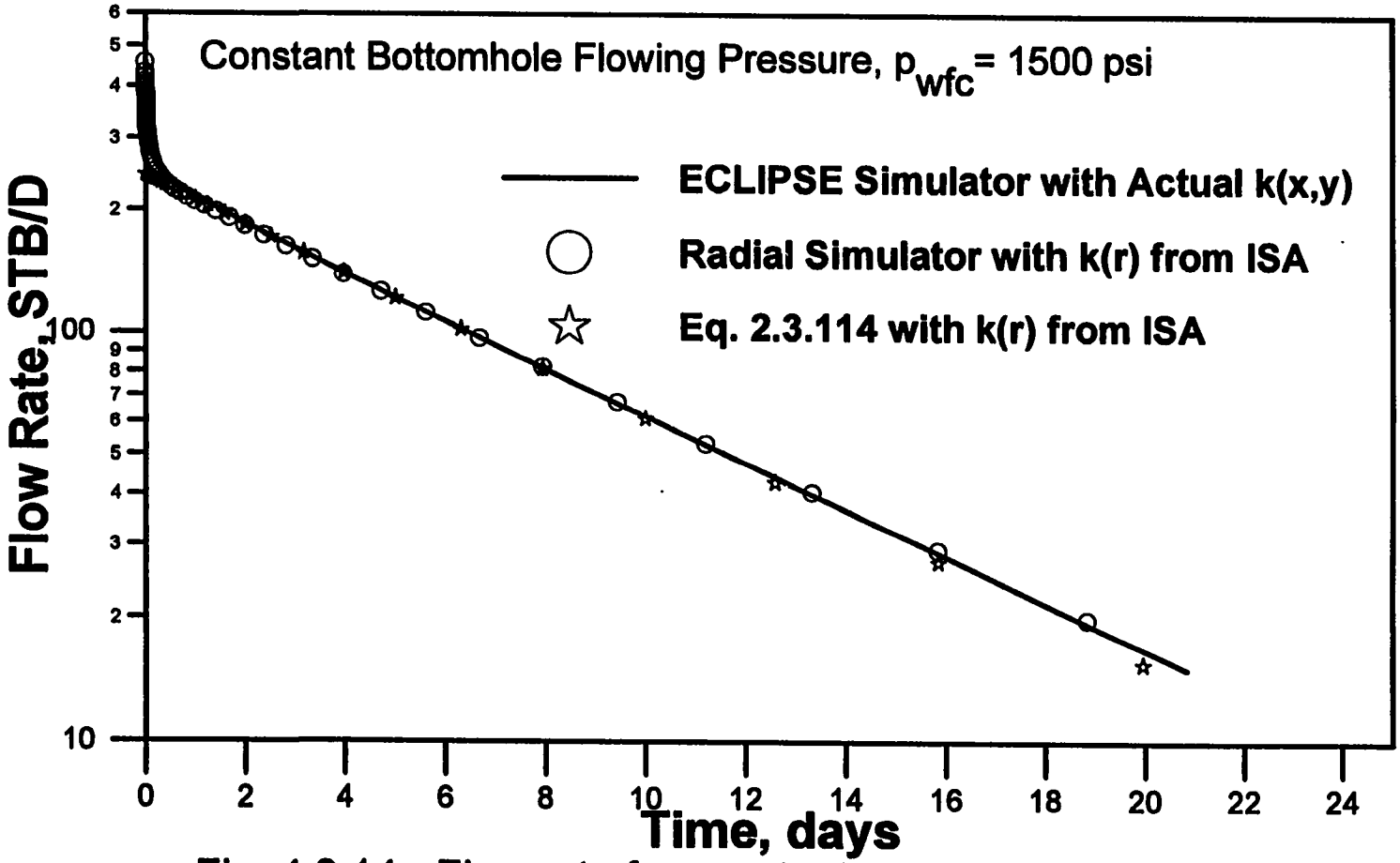

Fig. 4.2.14 - Flow rate for constant pressure production: simulated versus computed; Example 4.

These examples suggest that based on well test data from an areally heterogeneous reservoir we can: (i) obtain an equivalent radial permeability distribution, $k(r)$, using our inverse problem solution techniques, which we have shown to be quite reliable; (ii) compute accurately the average reservoir pressure; (iii) calculate, with accuracy, boundary-dominated flow parameters, namely, productivity index, homogeneous-equivalent pseudosteady state permeability, and constant-pressure production flow rate. We have tested successfully few cases in which the well is located at the center of a closed drainage area of either circular or square shape. The results seem to indicate that considerably accurate results are expected to be obtained in the cases where the well is located at the center of a drainage area approximately symmetric with respect to the center, and in the cases where the transition between the infinite-acting period and the beginning of the pseudosteady state flow is not too long.

Reproduced with permission of the copyright owner. Further reproduction prohibited without permission.

CHAPTER V

CONCLUSIONS

The objective of this work has been to develop procedures for analyzing well-test pressure data obtained from a well located in a heterogeneous reservoir where the permeability varies with the position, or with only the radial distance from a well at the origin of a cylindrical-coordinate system.

We considered single-phase flow of a slightly compressible fluid of constant compressibility and constant viscosity to a fully-penetrating well in the center of a cylindrical reservoir of uniform thickness, constant porosity and rock compressibility, with closed top and bottom boundaries. We neglected gravity, wellbore storage, skin and capillary effects. We assumed an uniform initial pressure. In the majority of the cases we considered constant rate production and a no-flow outer boundary. We also have considered constant pressure production and a constant pressure outer boundary, as well as combinations of these boundary conditions. In many cases, we considered only the infinite-acting period. Although we have focused primarily on pure radial flow problems with permeability as a function of only radial distance of the well and porosity constant, we also briefly investigated the effect of porosity variations and two-dimensional permeability functions.

A numerical approximate solution to the problems posed above has been developed. This solution was formulated as an implicit, finite-difference, areal, (r,θ), single-well, numerical simulator which generates the reservoir responses for either constant rate or constant pressure production. It handles all commonly encountered inner and outer boundary conditions, variable permeability, porosity and/or thickness, as well as

Reproduced with permission of the copyright owner. Further reproduction prohibited without permission.

any initial pressure distribution. This simulator was validated by comparison with exact analytical solutions for multicomposite reservoirs, available in the literature. Utilizing the simulator, we generated the wellbore pressures and the reservoir pressure profile as a function of time used in this work.

Two methods for generating an approximation of the permeability distribution directly from well-test pressure derivative data were presented. An equivalent-radial permeability distribution is computed based on the instantaneous well-test pressure derivatives during the infinite-acting period. In the first method, the permeability function is obtained from a numerical solution of an integral equation of first kind, which we have shown to be a generalization of Oliver's approximate analytical solution. In this integral equation, the left side is the known value of the "instantaneous permeability" (obtained from the well-test pressure data) and the right side is a definite integral, over the radial distance within a region of investigation, of the product of a known weighting function by the inverse of the unknown radial permeability function. A recursive algorithm was developed to solve for the permeability distribution. We have referred to this procedure as the Inverse Solution Algorithm (ISA). The method does not require the variation in permeability to be small. The permeability distribution computed from ISA when input into our simulator reproduces the original wellbore pressure and pressure derivative.

The second method, that we refer to as the Modified Yeh-Agarwal (MYA), was derived based on the idea that the "instantaneous permeability" is a volumetric-weighted harmonic average of all permeability values extending from the wellbore up to a radius of investigation. We have shown that both methods yield good estimates of the actual permeability distribution, with ISA being slightly superior to MYA. Originally, these methods were derived for transient drawdown. We have presented a method to correct buildup data for producing-time effects, such that both ISA and MYA applied to the corrected buildup data gives identical results as obtained with drawdown data.

Reproduced with permission of the copyright owner. Further reproduction prohibited without permission.

A procedure to obtain the reservoir pressure profile at the instant of shut in from pressure buildup data has been presented. In this procedure the wellbore pressure buildup is converted to the reservoir pressure profile using an appropriate equation for the radius of investigation. It has been shown that, under certain conditions, we can construct a fairly good approximation to the reservoir pressure profile up to the external reservoir radius. Using these results, the average reservoir pressure value can be estimated. In the case the reservoir pressure profile is established under either steady-state or pseudosteady state flow, a reasonably good approximation can be obtained for (i) the radial permeability distribution, (ii) the productivity index, and (iii) the homogeneous-equivalent pseudosteady-state permeability. We have shown that, if we are able to compute a good estimate of the reservoir permeability distribution from transient drawdown data, then we can also construct a fairly good approximation to the reservoir pressure profile at a fixed time, during either a steady state or pseudosteady state flow, using the appropriate reservoir flow equations derived in this work.

Based on this work the following conclusions are warranted:

1. Two methods to compute an approximate radial equivalent permeability distribution directly from well-test pressure data have been presented. The first method, ISA, was derived from a generalization to an approximate analytical solution of Oliver, which gives the infinite-acting solution for the dimensionless pressure derivative obtained at a well located at the center of a radially heterogeneous cylindrical reservoir. The Modified Yeh-Agarwal or MYA, represents a modification of a procedure presented in Ref. 25.
2. For many realistic reservoir descriptions, both MYA and ISA gives good estimates of the permeability distribution. ISA gives better estimates of permeability profile in multicomposite reservoirs, but for the same problem, the permeability distribution computed with MYA is in general smoother.

Reproduced with permission of the copyright owner. Further reproduction prohibited without permission.

3. Both methods, ISA and MYA, can be applied to either transient drawdown or transient buildup data. The application to buildup data requires that we correct the well-test buildup pressure derivatives for the producing-time effects. The appropriate correction terms, which are exact for buildup after either a steady-state or a pseudosteady state flow, were presented. It has been shown that when applied to the corrected buildup data, both ISA and MYA yield identical results as obtained with drawdown data.
4. For the case where the buildup follows a transient flow period the correction for producing-time effects was developed based on the assumption that the well-test pressure derivative at the end of the flow period would have remained constant if we had continued the flow up to the maximum shut-in time. This is equivalent to assuming that the investigation region would be within a zone of constant permeability of the same value as the last one computed at the end of the flow. The results of many cases we have studied indicated that this assumption is quite reasonable. We have observed that even when the region of investigation is not completely within a "last constant-permeability zone" the results obtained from the corrected buildup data still compare very well with results obtained from the drawdown data. More importantly, it has been noticed that the assumption yields results comparable to those obtained from drawdown data when no drastic variation of permeability occurs beyond the last radius investigated during the flowing period.
5. The correction for producing-time effects presented is exact in the case the buildup follows a pseudosteady state flow period. It has been shown that the permeability distribution computed from the corrected buildup data reproduce the permeability distribution calculated from drawdown data. In case of a buildup after a steady-state flow there is no correction for producing-time effects and the drawdown and buildup solutions are the same.

Reproduced with permission of the copyright owner. Further reproduction prohibited without permission.

6. We have presented exact theoretical solutions for the reservoir pressure response at any radial distance from the well during boundary dominated flow for constant rate production. Using these solutions, we have developed analytical equations for the average reservoir pressure, for the stabilized inflow performance relation (productivity index), and for the homogeneous-equivalent pseudosteady state permeability. The exact equation for the flow rate during boundary dominated flow for constant pressure production has also been presented.
7. A method to calculate the reservoir pressure profile at the instant of shut in from pressure buildup data has been presented. The pressure profile is initially computed up to the last radius of investigation reached during the infinite-acting buildup period. It has been shown that a fairly good approximation to the reservoir pressure profile up to the external reservoir radius can be constructed, provided we have a reasonable estimate of the reservoir outer radius and of the permeability distribution beyond the last radius of investigation. Based on this pressure profile the average reservoir pressure value can be accurately computed.
8. If the reservoir pressure profile is established under either steady-state or pseudosteady state flow, the extrapolation beyond the last radius of investigation can be performed using the pertinent equations derived in this work with an assumed permeability distribution. It has been observed that, provided there is no drastic variation in permeability beyond the last radius of investigation, approximating the permeability function up to the external radius by a constant value equal to the last computed permeability value, yields a reasonable estimate of the reservoir pressure profile. In the cases we have studied, an accurate value of average pressure computed from the pressure profile approximated under this condition has been obtained.
9. We have shown that we can also construct a fairly good approximation to the reservoir pressure profile at a fixed time, during either a steady state or pseudosteady

Reproduced with permission of the copyright owner. Further reproduction prohibited without permission.

state flow, using the appropriate reservoir flow equations derived in this work, with the permeability distribution obtained from drawdown data during the infinite-acting period.

10. Analytical equations to determine the radial permeability distribution from either a steady-state or a pseudosteady state reservoir pressure profile have been derived and applied. To apply these equations one needs to have a good estimate of the reservoir pressure profile at the shut-in time from the transient buildup data.
11. It has been demonstrated that, at least theoretically, one can compute major reservoir parameters, namely (i) permeability distribution, (ii) reservoir pressure profile, (iii) average reservoir pressure, (iv) productivity index (v) equivalent pseudosteady state permeability, and (vi) exponential flow rate decline for constant pressure production, *using only drawdown data.*
12. The influence of porosity variation on the wellbore pressure response to a constant rate production and on the ISA-computed permeability distribution was considered briefly. When there is variation in both porosity and permeability, the permeability distribution computed with ISA, assuming a constant porosity value, has more error than in the case where the actual reservoir has uniform porosity. When permeability and porosity both vary with position, ISA gives an equivalent radial permeability distribution which, when input into our simulator, reproduces almost exactly the original pressures and pressure derivatives. (These results illustrate the nonuniqueness of the inverse problem.)
13. We have also considered the analysis of well-test data from a two-dimensional (areal) heterogeneous reservoir where the permeability varies with position. The application of ISA to the pressure data yields an equivalent radial permeability distribution which when input into our simulator regenerates the original well-test pressure and pressure derivative.

Reproduced with permission of the copyright owner. Further reproduction prohibited without permission.

Future work may involve the following: (i) sensitivity analysis of the inversion procedures; (ii) wellbore effects; (iii) improvement of the inversion algorithms; (iv) porosity variation; (v) two-dimensional permeability function; (vi) one and two-dimensional variation in thickness; (vii) three-dimensional variation in permeability, porosity and/or thickness (viii) multiple well systems; (ix) variable flow rate; (x) analysis of actual data; (xi) multiphase flow.

Reproduced with permission of the copyright owner. Further reproduction prohibited without permission.

NOMENCLATURE

Symbol	
A	reservoir drainage area, ft^2
B	formation volume factor, RB/STB
c_t	system compressibility, psi^{-1}
C_1	factor for conversion of units; $C_1 = 0.006328$ for time in days
C_k	pseudosteady state constant defined by Eq. 2.3.107, md^{-1}
C_{kD}	dimensionless pseudosteady state constant defined by Eq. 2.3.106
C_{pte}	correction factor for producing-time effects, psi
f	permeability function defined by Eq. 2.2.17
G	kernel or weighting function defined by Eq. 2.2.26
h	reservoir thickness, ft
I_0	modified Bessel function of the first kind of order zero
I_1	modified Bessel function of the first kind of order one
K_0	modified Bessel function of the second kind of order zero
K_1	modified Bessel function of the second kind of order one
K	kernel or weighting function defined by Eq. 2.2.29
$\bar{k}$	average permeability, md
$\hat{k}$	"instantaneous permeability" defined by Eq. 2.3.41 and Eq. 3.2.32, md
k_D	dimensionless permeability, $\frac{k(r,\theta)}{k_{ref}}$ or $\frac{k(r)}{k_{ref}}$
k_{eq}	homogeneous-equivalent pseudosteady state permeability defined by Eq. 2.3.92 or Eq. 3.7.2, md

Reproduced with permission of the copyright owner. Further reproduction prohibited without permission.

k_{hom}	homogeneous permeability, md
k_{ref}	reference permeability value, md
$k(r)$	permeability value at a radial distance r, md
$k(r,\theta)$	permeability value at a position (r,θ), md
$k(x,y)$	permeability value at a position (x,y), md
m^*	pseudosteady state slope; $m^* = \frac{dp}{dt}$ given by Eq. 2.3.80, psi/day
$O(\,)$	order notation
p	pressure, psi
$\bar{p}$	average reservoir pressure, psi
p_e	reservoir pressure at the external radius r_e, psi
p_i	initial reservoir pressure, psi
$\tilde{p}_{sD}$	dimensionless pressure buildup change defined by Eq. 2.3.46
$\tilde{p}'_{sD}$	logarithmic derivative of $\tilde{p}_{sD}$
p_{wD}	dimensionless wellbore flowing pressure
p'_{wD}	logarithmic derivative of p_{wD}
p_{wf}	wellbore flowing presssure, psi
p_{ws}	wellbore shut-in presssure, psi
$p_{wf,s}$	wellbore flowing pressure at the instant of shut in, psi
p_D	dimensionless pressure
$\bar{p}_D$	dimensionless pressure in Laplace space
p_{D0}	dimensionless homogeneous pressure solution given by Eqs. 2.2.24
p_{D1}	dimensionless first-order perturbation pressure solution given by Eq. 2.2.25
$\bar{p}_{D0}$	Laplace transform of p_{D0}
$\bar{p}_{D1}$	Laplace transform of p_{D1}
q	sandface flow rate, RB/D
q_{sc}	surface flow rate, STB/D

Reproduced with permission of the copyright owner. Further reproduction prohibited without permission.

q_D	dimensionless flow rate
$\bar{q}_D$	Laplace transform of q_D
r	radial distance from the well, ft
r_D	dimensionless radial distance, r/r_w
r_e	external reservoir radius, ft
r_w	well radius, ft
r_i	radius of investigation at a time t_i, ft
$\hat{r}_{inner}$	inner radius of region of investigation defined by Eq. 3.2.46, ft
$\hat{r}_{outer}$	outer radius of region of investigation defined by Eq. 3.2.47, ft
t	time, days,
t_D	dimensionless time defined by Eq. 2.2.8
$\hat{t}_D$	dimensionless time based on "instantaneous permeability" defined by Eq. 2.3.43
t_{eia}	end of the infinite-acting period, days
t_p	producing time, days
t_{pss}	beginning of the pseudosteady state flow period, days
t_{AD}	dimensionless time based on reservoir drainage area
u	Laplace variable
γ	Euler's constant (0.57722)
ε	small number, <<1
η	hydraulic diffusivity, $\frac{k}{\phi \mu c_t}$, ft^2/day
θ	angular coordinate in a cylindrical coordinate-system
μ	viscosity, cp
π	constant $\cong 3.1415926$
ϕ	porosity, fraction

Reproduced with permission of the copyright owner. Further reproduction prohibited without permission.

Δp	pressure drop, psi
$\Delta p'$	logarithmic derivative of pressure drop, psi
Δt	shut-in time, days
Δt_{AD}	dimensionless shut-in time based on drainage area
Δt_D	dimensionless shut-in time

Reproduced with permission of the copyright owner. Further reproduction prohibited without permission.

REFERENCES

1 Hurst, W.: "Unsteady Flow of Fluids in Oil Reservoirs", *Physics* (Jan. 1934) **5**.

2 Hurst, W.: "Water Influx into a Reservoir and Its Application to the Equation of Volumetric Balance," *Trans.* AIME (1943), **151**, 57-72.

3 Muskat, M.: "The Flow of Compressible Fluids Through Porous Media and Some Problems in Heat Conduction," *Physics* (March 1934) **5**.

4 Muskat, M.: *The Flow of Homogeneous Fluids in Porous Media,* McGraw-Hill Book Co. Inc., New York City (1937).

5 van Everdingen, A. F., and Hurst, W.: "The Application of Laplace Transformation to Flow Problems in Reservoirs," *Trans.*, AIME (1949) **186**, 305-324.

6 Horner, D. R.: "Pressure Build-Up in Wells," *Proc.*, Third World Pet. Cong., The Hague (1951), Sec. II, 503-523; also in *Reprint Series,* SPE, Dallas (1967) **9**, 25-43.

7 Bixel, H. C., and van Poolen, H. K.: "Effect of Linear Discontinuities on Pressure Build-Up and Drawdown Behavior," *JPT* (Aug. 1963) 885-895; *Trans.*, AIME, **228**.

8 Hurst, W.: "Interference Between Oil Fields", *Trans.*, AIME (1960) **219**, 175-190.

9 Larkin, B. K.: "Solutions to the Diffusion Equation for a Region Bounded By a Circular Discontinuity," *SPEJ* (June 1963) 113-115; *Trans.*, AIME, **228**.

10 Carter, R. D.: "Pressure Behavior of a Limited Circular Composite Reservoir," *SPEJ* (Dec. 1966) 328-334; *Trans.*, AIME, **237**.

Reproduced with permission of the copyright owner. Further reproduction prohibited without permission.

11 Odeh, A. S.: "Flow Test Analysis for a Well with Radial Discontinuity," *JPT* (Feb. 1969) 207-210; *Trans.*, AIME, **246**.

12 Ramey, H. J. Jr.: "Approximate Solutions for Unsteady Liquid Flow in Composite Reservoirs," *J. Cdn. Pet. Tech.* (Jan.-March 1970) 32-37.

13 Gringarten, A. C.: "Interpretation of Tests in Fissured Reservoirs and Multilayered Reservoirs with Double Porosity Behavior: Theory and Practice," paper SPE 10044 presented at the 1982 SPE International Petroleum Exhibition and Technical Symposium, Beijing, China, March 18-26; published in *JPT* (Apr. 1984) 549-564.

14 Ehlig-Economides, C. A. *et al.*: "Evaluation of Single-Layer Transients in a Multilayered System," paper SPE 15860 presented at the 1986 European Offshore Petroleum Conference, London, Oct. 20-22.

15 Britto, P. R., Grader, A. S.: "The Effects of Size, Shape and Orientation of an Impermeable Region on Transient Pressure Testing," *SPE Formation Evaluation* (Sept. 1988) 595-606.

16 Oliver, D. S.: "The Averaging Process in Permeability Estimation From Well-Test Data," *SPE Formation Evaluation* (Sept. 1990) 319-324.

17 Carslaw, H. S., and Jaeger, J. C.: *Conduction of Heat in Solids*, Oxford U. Press, Oxford (1959) 412-415.

18 Loucks, T. L.: "Pressure Distribution in Systems with Continuously Varying Permeability," paper SPE 72.

19 Hantush, M. S.: "Flow of Ground Water in Sands of Nonuniform Thickness, 3. Flow to Wells," *Journal of Geophysical Research*, 67(4), (Apr. 1962), 1527-1534.

20 Kamal, M. M.: "The Use of Pressure Transients To Describe Reservoir Heterogeneity," *JPT* (Aug. 1979) 1060-1070.

Reproduced with permission of the copyright owner. Further reproduction prohibited without permission.

21 Earlougher, R. C. Jr.: *Advances in Well Test Analysis*, Monograph Series, SPE, Dallas (1977), 5.

22 Oliver, D. S.: "Estimation of Radial Permeability Distribution From Well Test Data," *SPE Formation Evaluation* (Dec. 1992) 290-296.

23 Backus, G. E. and Gilbert, F.: "The Resolving Power of Gross Earth Data," *Geophys. J. R. Astron. Soc.* (1968), **16**, 169-205.

24 Rosa, A. J., and Horne, R. N.: "Reservoir Description by Well Test Analysis Using Cyclic Flow Rate Variation," paper SPE 22698 presented at the 1991 SPE Annual Technical Conference and Exhibition, Dallas, Oct. 6-9.

25 Yeh, N-S. and Agarwal, R. G.: "Pressure Transient Analysis of Injection Wells in Reservoirs With Multiple Fluid Banks," paper SPE 19775 presented at the 1989 SPE Annual Technical Conference and Exhibition, San Antonio, Oct. 8-11.

26 Stehfest, H.: "Algorithm 368, Numerical Inversion of Laplace Transforms," *Communications of the ACM* (1970), **13**, No. 1, 47-49.

27 Whittaker, E. T. and Watson, G. N.: *A Course of Modern Analysis*, Cambridge University Press, Cambridge (1952).

28 Gradshteyn, I. S. and Ryzhik, I. M.: *Table of Integrals, Series, and Products*, Academic Press, Orlando (1980) 1059-1062.

29 Abramowitz, M. and Stegun, I. A.: *Handbook of Mathematical Functions*, Dover Publications, Inc., New York (1970).

30 Rosa, A. J.: "Reservoir Description by Well Test Analysis Using Cyclic Flow Rate Variation," PhD dissertation, Stanford U., Stanford, CA (1991).

31 MacDonald, R. C. and Coats, K. H.: "Methods of Numerical Simulation of Water and Gas Coning," *SPEJ* (Dec. 1970) 425-436; *Trans.*, AIME, **249**.

32 Abbaszadeh, M. and Kamal, M.: "Pressure-Transient Testing of Water-Injection Wells," *SPE Reservoir Engineering* (Feb. 1989) 115-124.

Reproduced with permission of the copyright owner. Further reproduction prohibited without permission.

33 Aziz, K. and Settari, A.: *Petroleum Reservoir Simulation*, Applied Science Publishers, Ltd., London (1979).

34 Dake, L. P.: *Fundamentals of Reservoir Engineering*, Elsevier Scientific Publishing Company, New York (1978).

35 Churchill, R. V.: *Operational Mathematics*, third edition, McGraw-Hill Kogakusha, Ltd., London (1972).

36 van Poolen, H. K.: "Radius-of-drainage and stabilization-time equations," *The Oil and Gas Journal* (Sep. 14, 1964) 138-146.

37 Salas, S. L *et. al.*: *Calculus; One and Several Variables*, John Wiley and Sons, New York, fith edition (1986), 599.

38 Streltsova, T. D.: *Well Testing in Heterogeneous Formations*, John Wiley & Sons, New York (1988).

39 *Log Interpretation Charts*, Schlumberger Educational Services, USA (1991) 158-159.

40 Sagar, R., Kelkar, and Thompson, L. G.: "Incorporating Well Test Data in Stochastic Conditional Simulations," Tulsa University, Petroleum Reservoir Exploitation Projects (TUPREP), Research Report 8, Vol. II, presented at the 1992 TUPREP Meeting, Tulsa, OK, Nov. 17.

41 *ECLIPSE 100 - Black Oil Simulator*, ECL-Bergeson Petroleum Technologies, Inc., Oxfordshire, England (1990).

42 Thompson, L. G.: *Reservoir Simulation I Class Notes*, The University of Tulsa, Fall 1991.

Reproduced with permission of the copyright owner. Further reproduction prohibited without permission.

APPENDIX A

FINITE-DIFFERENCE NUMERICAL SOLUTION TO THE AREALLY HETEROGENEOUS RESERVOIR INITIAL-BOUNDARY-VALUE PROBLEM

Here, we present a finite-difference method for the problem of single-phase flow of a slightly compressible fluid with constant viscosity in an areally heterogeneous reservoir. The problem considered is represented by the Initial-Boundary-Value Problem given by Eqs. 2.2.1 through 2.2.6 in (r, θ) coordinates. The solution is based on an implicit, finite-difference formulation. A standard notation is used throughout.

We consider a grid system over the entire domain of r and θ defined as

$$\{r_i\}_{i=1}^{N_R} \text{ with } r_{N_R+1/2} = r_e \text{ and } r_{1/2} = r_w,$$

and

$$\{\theta\}_{j=1}^{N_\theta} \text{ with } \theta_{1/2} = 0 \text{ and } \theta_{N_\theta+1/2} = 2\pi,$$

where N_R and N_θ are the total number of gridblocks in the r and θ direction, respectively; a fractional subscript denotes the gridblock interface, while an integer number subscript denotes the position inside the gridblock where the pressure is computed. The radial gridpoints are either input to the simulator or generated using Coats' Grid formulation[31]. Similarly, the θ_j's can be uniformly distributed or can be assigned arbitrarily.

The discretization of the governing PDE, Eq. 2.2.1 is performed by replacing the space and time derivatives by finite-difference approximations. The "block centered" θ-derivative is generated by integrating the PDE over θ from $\theta_{j-1/2}$ to $\theta_{j+1/2}$ and using Taylor series approximation. The resulting equation is then multiplied by r,

Reproduced with permission of the copyright owner. Further reproduction prohibited without permission.

integrated over r from $r_{i-1/2}$ to $r_{i+1/2}$ and again, using a Taylor series approximation, the discrete form of the r-derivative is then generated. The time derivative is approximated by the first term of Taylor expansion about the current time. See Ref. 42 for details.

The discrete form of the original PDE, Eq. 2.2.1 is then given by the following finite-difference equation:

$$C_1\left[\left(\frac{r_{i+1/2}}{r_{i+1}-r_i}\right)\frac{(kh)_{i+1/2,j}}{\mu}\Delta\theta_j\left(p_{i+1,j}^{n+1}-p_{i,j}^{n+1}\right)-\left(\frac{r_{i-1/2}}{r_i-r_{i-1}}\right)\frac{(kh)_{i-1/2,j}}{\mu}\Delta\theta_j\left(p_{i,j}^{n+1}-p_{i-1,j}^{n+1}\right)\right]$$
$$+C_1\ln\left(\frac{r_{i+1/2}}{r_{i-1/2}}\right)\left[\frac{(kh)_{i,j+1/2}}{\mu}\left(\frac{p_{i,j+1}^{n+1}-p_{i,j}^{n+1}}{\theta_{j+1}-\theta_j}\right)-\frac{(kh)_{i,j-1/2}}{\mu}\left(\frac{p_{i,j}^{n+1}-p_{i,j-1}^{n+1}}{\theta_j-\theta_{j-1}}\right)\right]$$
$$=c_t\,\phi_{i,j}h_{i,j}\frac{1}{2}\left(r_{i+1/2}^2-r_{i-1/2}^2\right)\Delta\theta_j\frac{\left(p_{i,j}^{n+1}-p_{i,j}^{n}\right)}{\Delta t}. \tag{A-1}$$

The coefficients of the terms in Eq. A-1 involving the pressure difference between two adjacent gridblocks, in r and θ direction, are called, in general, the interblock "transmissibilities" in r, T_r, and θ direction, T_θ, respectively. The "transmissibility" in the radial direction, r, at the interface between two adjacent gridblocks (i,j) and $(i+1,j)$, $T_{r_{i+1/2,j}}$, is clearly given by

$$T_{r_{i+1/2,j}}=C_1\left(\frac{r_{i+1/2}}{r_{i+1}-r_i}\right)\Delta\theta_j\frac{(kh)_{i+1/2,j}}{\mu}, \tag{A-2}$$

where the flow capacity at the interface, $(kh)_{i+1/2,j}$, is obtained from the weighted-harmonic average of the flow capacities of the two adjacent gridblocks given by

Reproduced with permission of the copyright owner. Further reproduction prohibited without permission.

$$(kh)_{i+1/2,j} = \frac{(kh)_{i,j}(kh)_{i+1,j}\ln\left(\frac{r_{i+1}}{r_i}\right)}{(kh)_{i,j}\ln\left(\frac{r_{i+1}}{r_{i+1/2}}\right)+(kh)_{i+1,j}\ln\left(\frac{r_{i+1/2}}{r_i}\right)}. \tag{A-3}$$

The "transmissibility" in θ direction at the interface between two adjacent gridblocks (i,j) and $(i,j+1)$, $T_{\theta_{i,j+1/2}}$, is written as

$$T_{\theta_{i,j+1/2}} = C_1 \ln\left(\frac{r_{i+1/2}}{r_{i-1/2}}\right)\left(\frac{2}{\Delta\theta_j + \Delta\theta_{j+1}}\right)\frac{(kh)_{i,j+1/2}}{\mu}, \tag{A-4}$$

where the flow capacity in the θ direction at the interface, $(kh)_{i,j+1/2}$, is obtained from the weighted-harmonic average of the flow capacities of the two gridblocks given by

$$(kh)_{i,j+1/2} = \frac{(kh)_{i,j}(kh)_{i,j+1}\left(\Delta\theta_j + \Delta\theta_{j+1}\right)}{\Delta\theta_{j+1}(kh)_{i,j} + \Delta\theta_j(kh)_{i,j+1}}. \tag{A-5}$$

Using Eqs. A-2 through A-5 into Eq. A-1 and after rearranging terms, we can write Eq. A-1 in the following standard compact form

$$\begin{aligned}&\left[-T_{r_{i-1/2,j}}\right]p_{i-1,j}^{n+1} + \left[-T_{\theta_{i,j-1/2}}\right]p_{i,j-1}^{n+1} + \left[\beta_{i,j}\right]p_{i,j}^{n+1}\\ &+\left[-T_{\theta_{i,j+1/2}}\right]p_{i,j+1}^{n+1} + \left[-T_{r_{i+1/2,j}}\right]p_{i+1,j}^{n+1} = \left[\gamma_{i,j}\right]p_{i,j}^{n},\end{aligned} \tag{A-6}$$

where

$$\beta_{i,j} = -T_{r_{i-1/2,j}} - T_{\theta_{i,j-1/2}} - T_{r_{i+1/2,j}} + \gamma_{i,j}, \tag{A-7}$$

$$\gamma_{i,j} = c_t\,\phi_{i,j}\,h_{i,j}\left(\frac{r_{i+1/2}^2 - r_{i-1/2}^2}{2}\right)\Delta\theta_j\frac{1}{\Delta t}, \tag{A-8}$$

with $\Delta\theta_j$ defined as

$$\Delta\theta_j = \theta_{j+1/2} - \theta_{j-1/2}. \tag{A-9}$$

Reproduced with permission of the copyright owner. Further reproduction prohibited without permission.

The general finite-difference equation in compact form, Eq. A-6, is directly applicable to all interior gridblocks, i.e., for $i=2,\cdots,N_R-1$ and $j=2,\cdots,N_\theta-1$. For the gridblocks near to the inner and outer boundaries in the r-direction the equation is adjusted by using the appropriate boundary condition in the terms involving the radial "transmissibilities" T_r. Constant rate or constant pressure inner boundary is treated according to standard procedures. Similar treatment is given to the outer boundary condition, which can be a no-flow or a constant pressure boundary. At the end values of the θ domain, i.e., at $\theta=0$ and $\theta=2\pi$, there is no physical discontinuity. So, at $\theta=0$ and $\theta=2\pi$ the continuity of pressure and flux are taking into account by using the following relations in the equation for the gridblock denoted by $(i,j=1)$ and $(i,j=N_\theta)$

$$T_{\theta_{i,1/2}} \equiv T_{\theta_{i,N_\theta+1/2}}, \tag{A-10}$$

$$p_{i,j-1}^{n+1} \equiv p_{i,N_\theta}^{n+1} \quad \text{for } j=1, \tag{A-11}$$

and

$$p_{i,j+1}^{n+1} \equiv p_{i,1}^{n+1} \quad \text{for } j=N_\theta. \tag{A-12}$$

In our grid system we use the standard ordering in which the j index (indicative of angular position) varies faster than index i (indicative of radial position). As it is well known, this yields a smaller band-width for the matrix of the system of linear equations, since the number of gridblocks in $\theta-$direction is, in general, much smaller than the number of gridblocks in r-direction.

The system of equations is characterized by a matrix that is symmetric, diagonally dominant and banded. It is solved using the subroutine GEBAND (available at the Petroleum Engineering Department of Tulsa University), especially designed to solve banded systems by Gaussian elimination.

Reproduced with permission of the copyright owner. Further reproduction prohibited without permission.

The development of the (r, θ) simulator presented here was largely based on the material presented in Ref. 42, where a detailed and comprehensive treatment to the subject is given.

Reproduced with permission of the copyright owner. Further reproduction prohibited without permission.

APPENDIX B

APPROXIMATE SOLUTION TO THE RADIALLY HETEROGENEOUS RESERVOIR INITIAL-BOUNDARY-VALUE PROBLEM BASED ON FLOW RATE ASSUMPTION (i)

The pertinent Initial-Boundary-Value Problem (IBVP) is written in dimensionless variables as follows :

$$\frac{1}{r_D}\frac{\partial}{\partial r_D}\left[r_D k_D(r_D)\frac{\partial p_D}{\partial r_D}\right]=\frac{\partial p_D}{\partial t_D} \tag{B-1}$$

$$p_D(r_D,t_D=0)=0 \tag{B-2}$$

$$p_D(r_D\to\infty,t_D)=0 \tag{B-3}$$

$$\lim_{r_D\to 0}\left[r_D k_D(r_D)\frac{\partial p_D}{\partial r_D}\right]=-1 \tag{B-4}$$

Here, we derive a solution based on the assumption labeled (i), see Eq. 2.3.23, in the section 2.3.2.2, given by Eq. B-5 :

$$r_D k_D(r_D)\frac{\partial p_D}{\partial r_D}=-\exp\left(-\frac{\alpha(t_D)r_D^2}{k_D}\right). \tag{B-5}$$

We first obtain a solution for p_D as a function of $\alpha(t_D)$ and r_D. Then we calculate $\alpha(t_D)$ using the diffusivity equation as will be shown next.

Divide equation B-5 by $r_D k_D$ to obtain :

Reproduced with permission of the copyright owner. Further reproduction prohibited without permission.

$$\frac{\partial p_D}{\partial r_D} = -\frac{\exp\left(-\frac{\alpha(t_D) r_D^2}{k_D}\right)}{r_D k_D(r_D)}. \tag{B-6}$$

Then integrate between r_D and ∞ to obtain:

$$[p_D]_{r_D}^{\infty} = \int_{r_D}^{\infty} -\frac{\exp\left(-\frac{\alpha(t_D) r_D'^2}{k_D}\right)}{r_D' k_D(r_D')} dr_D'. \tag{B-7}$$

From the last equation and the outer boundary condition we have

$$p_D(r_D, t_D) = \int_{r_D}^{\infty} \exp\left(-\frac{\alpha(t_D) r_D'^2}{k_D(r_D')}\right) \frac{1}{r_D' k_D(r_D')} dr_D' \tag{B-8}$$

A semianalytical solution to Eq. B-8 is developed in the following. We assume that the permeability distribution is approximated by a piecewise constant function of the form $k_D(r_D) = k_{Di}$ for $r_{Di-1/2} < r_D \le r_{Di+1/2}$, for $i = 1, 2, \cdots, \infty$. Here $r_{Di+1/2}$ is the outer boundary radius of region i, and $r_{D1/2} = 1$. Thus, we can approximate Eq. B-8 as follows:

$$p_D(r_D, t_D) = \int_{r_D}^{r_{Dj+1/2}} \frac{\exp\left(-\frac{\alpha(t_D) r_D'^2}{k_{D_j}}\right)}{r_D' k_{D_j}} dr_D' + \sum_{i=j+1}^{\infty} \int_{r_{Di-1/2}}^{r_{Di+1/2}} \frac{\exp\left(-\frac{\alpha(t_D) r_D'^2}{k_{D_i}}\right)}{r_D' k_{D_i}} dr_D' \tag{B-9}$$

Reproduced with permission of the copyright owner. Further reproduction prohibited without permission.

Here we have assumed that the dimensionless radial distance, r_D, at which dimensionless pressure is computed, is located within a region j, i.e, $r_{Dj-1/2} < r_D < r_{Dj+1/2}$. In the summation term in the right-hand side of Eq. B-9, we perform the calculation using n terms such that, the integral involving the term $n+1$ does not contribute to the results; 10^{-6} can be used as the cut-off number.

The following change of variable and the resulting equations

$$u = \frac{\alpha(t_D) r_D'^{\,2}}{k_{Dj}} \Rightarrow du = \frac{\alpha(t_D) 2 r_D'}{k_{Dj}} dr_D' \tag{B-10}$$

$$r_D' = \sqrt{\frac{u k_{D_j}}{\alpha(t_D)}} \Rightarrow dr_D' = \frac{1}{2}\sqrt{\frac{k_{D_j}}{\alpha(t_D) u}} du \tag{B-11}$$

$$r_D' \rightarrow r_D \Rightarrow u \rightarrow \frac{\alpha(t_D) r_D^2}{k_{D_j}} \tag{B-12}$$

$$\frac{dr_D'}{r_D'} = \frac{1}{2u} du, \tag{B-13}$$

when used in the first integral of equation B-9 will result in the following equation:

$$\int_{r_D}^{r_{Dj+1/2}} \frac{\exp\left(-\frac{\alpha(t_D) r_D'^2}{k_{D_j}}\right)}{r_D' k_{D_j}} dr_D' = \frac{1}{2k_{D_j}} \int_{\frac{\alpha(t_D) r_D^2}{k_{D_j}}}^{\frac{\alpha(t_D) r_{Dj+1/2}^2}{k_{D_j}}} \frac{\exp(-u)}{u} du$$

$$= \frac{1}{2k_{D_j}} \left[\mathrm{E}_1\left(\frac{\alpha(t_D) r_D^2}{k_{D_j}}\right) - \mathrm{E}_1\left(\frac{\alpha(t_D) r_{Dj+1/2}^2}{k_{D_j}}\right) \right] \tag{B-14}$$

Reproduced with permission of the copyright owner. Further reproduction prohibited without permission.

Similarly for the sum of integrals in equation B-9 we obtain:

$$\sum_{i=j+1}^{\infty}\int_{r_{D_{i-1/2}}}^{r_{D_{i+1/2}}}\frac{\exp\left(-\frac{\alpha(t_D)r_D'^2}{k_{D_i}}\right)}{r_D' k_{D_i}}dr_D' = \sum_{i=j+1}^{\infty}\frac{1}{2k_{D_i}}\int_{\frac{\alpha(t_D)r_{D_{i-1/2}}^2}{k_{D_i}}}^{\frac{\alpha(t_D)r_{D_{i+1/2}}^2}{k_{D_i}}}\frac{\exp(-u)}{u}du$$

$$= \sum_{i=j+1}^{\infty}\frac{1}{2k_{D_i}}\left[\mathrm{E}_1\left(\frac{\alpha(t_D)r_{D_{i-1/2}}^2}{k_{D_i}}\right)-\mathrm{E}_1\left(\frac{\alpha(t_D)r_{D_{i+1/2}}^2}{k_{D_i}}\right)\right]. \qquad \text{(B-15)}$$

Substituting Eqs. B-15 and B-14 into equation B-9 we finally obtain:

$$p_D(r_D,t_D)=\frac{1}{2k_{D_j}}\left[\mathrm{E}_1\left(\frac{\alpha(t_D)r_D^2}{k_{D_j}}\right)-\mathrm{E}_1\left(\frac{\alpha(t_D)r_{D_{j+1/2}}^2}{k_{D_j}}\right)\right]$$

$$+\sum_{i=j+1}^{\infty}\frac{1}{2k_{D_i}}\left[\mathrm{E}_1\left(\frac{\alpha(t_D)r_{D_{i-1/2}}^2}{k_{D_i}}\right)-\mathrm{E}_1\left(\frac{\alpha(t_D)r_{D_{i+1/2}}^2}{k_{D_i}}\right)\right] \qquad \text{(B-16)}$$

where

$$\mathrm{E}_1(x)=-\mathrm{E}_i(-x)=\int_x^{\infty}\frac{\exp(-u)}{u}du\,. \qquad \text{(B-17)}$$

The dimensionless pressure at the wellbore is obtained by calculating Eq. B-16 at $r_D=1$ and is given by:

$$p_D(r_D=1,t_D)=\sum_{i=1}^{\infty}\frac{1}{2k_{D_i}}\left[\mathrm{E}_1\left(\frac{\alpha(t_D)r_{D_{i-1/2}}^2}{k_{D_i}}\right)-\mathrm{E}_1\left(\frac{\alpha(t_D)r_{D_{i+1/2}}^2}{k_{D_i}}\right)\right], \qquad \text{(B-18)}$$

Reproduced with permission of the copyright owner. Further reproduction prohibited without permission.

where $r_{D1/2} \equiv 1$.

Now we will calculate the value of $\alpha(t_D)$. In order to do this, we substitute Eq. B-5 into the diffusivity equation, Eq. B-1, to obtain

$$\frac{1}{r_D}\frac{\partial}{\partial r_D}\left[-\exp\left(-\frac{\alpha(t_D)r_D^2}{k_D}\right)\right]=\frac{\partial p_D}{\partial t_D}. \tag{B-19}$$

Using Eq. B-8 in the above equation and multiplying by r_D we obtain

$$-\frac{\partial}{\partial r_D}\left[\exp\left(-\frac{\alpha(t_D)r_D^2}{k_D(r_D)}\right)\right]=r_D\frac{\partial}{\partial r_D}\left[\int_{r_D}^{\infty}\exp\left(-\frac{\alpha(t_D)r_D'^2}{k_D(r_D')}\right)\frac{1}{r_D'k_D(r_D')}dr_D'\right], \tag{B-20}$$

or,

$$-\frac{\partial}{\partial r_D}\left[\exp\left(-\frac{\alpha(t_D)r_D^2}{k_D(r_D)}\right)\right]=r_D\int_{r_D}^{\infty}\frac{1}{r_D'k_D(r_D')}\frac{\partial}{\partial t_D}\left[\exp\left(-\frac{\alpha(t_D)r_D'^2}{k_D(r_D')}\right)\right]dr_D' \tag{B-21}$$

Expanding the time derivative in the right-hand side of Eq. B-21 yields after simplifications

$$\begin{aligned}-\frac{\partial}{\partial r_D}\left[\exp\left(-\frac{\alpha(t_D)r_D^2}{k_D(r_D)}\right)\right]&=r_D\int_{r_D}^{\infty}\frac{1}{r_D'k_D(r_D')}\exp\left(-\frac{\alpha(t_D)r_D'^2}{k_D(r_D')}\right)\left(-\frac{r_D'^2}{k_D(r_D')}\right)\frac{d\alpha(t_D)}{dt_D}dr_D'\\&=r_D\int_{r_D}^{\infty}\frac{1}{k_D(r_D')}\exp\left(-\frac{\alpha(t_D)r_D'^2}{k_D(r_D')}\right)\left(-\frac{r_D'}{k_D(r_D')}\right)\frac{d\alpha(t_D)}{dt_D}dr_D'\end{aligned} \tag{B-22}$$

Reproduced with permission of the copyright owner. Further reproduction prohibited without permission.

Integrating Eq. B-22 over r_D' from 1 to ∞, we have

$$\int_1^\infty \frac{\partial}{\partial r_D'}\left[\exp\left(-\frac{\alpha(t_D)r_D'^2}{k_D(r_D')}\right)\right]dr_D' = \frac{d\alpha(t_D)}{dt_D}\int_1^\infty r_D'\left[\int_{r_D'}^\infty \frac{r_D''}{k_D^2(r_D'')}\exp\left(-\frac{\alpha(t_D)r_D''^2}{k_D(r_D'')}\right)dr_D''\right]dr_D'. \quad \text{(B-23)}$$

The left-hand side of equation B-23 can be rewritten as follows:

$$\int_1^\infty \frac{\partial}{\partial r_D'}\left[\exp\left(-\frac{\alpha(t_D)r_D'^2}{k_D(r_D')}\right)\right]dr_D' = \exp\left(-\frac{\alpha(t_D)r_D'^2}{k_D(r_D')}\right)\Bigg|_1^\infty$$

$$= -\exp\left(-\frac{\alpha(t_D)}{k_D(r_D'=1)}\right). \quad \text{(B-24)}$$

We temporarily denote the right-hand side of Eq. B-23 by RHS. Considering our grid system, the right-hand side of Eq. B-23 can be approximated by the following equation:

$$RHS = \frac{d\alpha(t_D)}{dt_D}\int_{r_{Dj-1/2}}^{r_{Dj+1/2}} r_D'\left[\int_{r_D'}^{r_{Dj+1/2}} \frac{r_D''}{k_{Dj}^2}\exp\left(-\frac{\alpha(t_D)r_D''^2}{k_{Dj}}\right)dr_D'' + \sum_{i=j+1}^{\infty}\int_{r_{Di-1/2}}^{r_{Di+1/2}} \frac{r_D''}{k_{Di}^2}\exp\left(-\frac{\alpha(t_D)r_D''^2}{k_{Di}}\right)dr_D''\right]dr_D'$$

(B-25)

By making the change of variable of Eq. B-10, we can analytically perform the inner integrations in Eq. B-25 to obtain the following equation:

Reproduced with permission of the copyright owner. Further reproduction prohibited without permission.

$$RHS = \frac{d\alpha(t_D)}{dt_D}\sum_{j=1}^{\infty}\left\{\int_{r_{Dj-1/2}}^{r_{Dj+1/2}} \frac{r_D'}{2\alpha k_{Dj}}\exp\left(-\frac{\alpha(t_D)r_D'^2}{k_{Dj}}\right)dr_D'\right.$$

$$-\int_{r_{Dj-1/2}}^{r_{Dj+1/2}} \frac{r_D'}{2\alpha k_{Dj}}\exp\left(-\frac{\alpha(t_D)r_{D_{j+1/2}}'^2}{k_{Dj}}\right)dr_D'$$

$$+\sum_{i=j+1}^{\infty}\left[\int_{r_{Dj-1/2}}^{r_{Dj+1/2}} \frac{r_D'}{2\alpha k_{Di}}\exp\left(-\frac{\alpha(t_D)r_{D_{i+1/2}}'^2}{k_{Di}}\right)dr_D'\right.$$

$$\left.\left.-\int_{r_{Dj-1/2}}^{r_{Dj+1/2}} \frac{r_D'}{2\alpha k_{Di}}\exp\left(-\frac{\alpha(t_D)r_{D_{i+1/2}}'^2}{k_{Di}}\right)dr_D'\right]\right\} \quad \text{(B-26)}$$

We can rewrite the first integral of Eq. B-26 by making the change of variable of Eq. B-10. Specifically,

$$\int_{r_{Dj-1/2}}^{r_{Dj+1/2}} r_D'\exp\left(-\frac{\alpha(t_D)r_D'^2}{k_{Dj}}\right)dr_D' = \int_{\frac{\alpha(t_D)r_{Dj-1/2}^2}{k_{D_j}}}^{\frac{\alpha(t_D)r_{Dj+1/2}^2}{k_{D_j}}} \frac{k_{Dj}}{2\alpha}\exp(-u)du$$

$$= \frac{k_{D_j}}{2\alpha}(-\exp(-u))\Big|_{\frac{\alpha(t_D)r_{Dj-1/2}^2}{k_{D_j}}}^{\frac{\alpha(t_D)r_{Dj+1/2}^2}{k_{D_j}}} . \quad \text{(B-27)}$$

The integrand of the other integrals in Eq. B-26 involves r_D' times a term independent of r_D' and can be integrated directly. By performing this integration and using Eq. B-27, Eq. B-26 can be written as

Reproduced with permission of the copyright owner. Further reproduction prohibited without permission.

$$RHS = \frac{d\alpha(t_D)}{dt_D}\left\{\sum_{j=1}^{\infty}\left[\frac{1}{4\alpha^2}\left(\exp\left(-\frac{\alpha(t_D)r_{D_{j+1/2}}^2}{k_{Dj}}\right)-\exp\left(-\frac{\alpha(t_D)r_{D_{j-1/2}}^2}{k_{Dj}}\right)\right)\right.\right.$$

$$-\frac{1}{4\alpha k_{Dj}}\left(r_{D_{j+1/2}}^2-r_{D_{j-1/2}}^2\right)\exp\left(-\frac{\alpha(t_D)r_{D_{j+1/2}}^2}{k_{Dj}}\right)$$

$$\left.\left.+\sum_{i=j+1}^{\infty}\frac{1}{4\alpha k_{Di}}\left(r_{D_{j+1/2}}^2-r_{D_{j-1/2}}^2\right)\left(\exp\left(-\frac{\alpha r_{D_{i+1/2}}^2}{k_{Di}}\right)-\exp\left(-\frac{\alpha r_{D_{i-1/2}}^2}{k_{Di}}\right)\right)\right]\right\}. \qquad \text{(B-28)}$$

Substituting Eqs. B-24 and B-28 into Eq. B-23, multiplying by (-1) and rearranging, we have

$$\frac{d\alpha(t_D)}{dt_D} = \exp\left(-\frac{\alpha(t_D)}{k_D(r_D=1)}\right)\left\{\sum_{j=1}^{\infty}\left[\frac{1}{4\alpha^2}\left(\exp\left(-\frac{\alpha(t_D)r_{D_{j+1/2}}^2}{k_{Dj}}\right)-\exp\left(-\frac{\alpha(t_D)r_{D_{j-1/2}}^2}{k_{Dj}}\right)\right)\right.\right.$$

$$-\frac{1}{4\alpha k_{Dj}}\left(r_{D_{j+1/2}}^2-r_{D_{j-1/2}}^2\right)\exp\left(-\frac{\alpha(t_D)r_{D_{j+1/2}}^2}{k_{Dj}}\right)$$

$$\left.\left.+\sum_{i=j+1}^{\infty}\frac{1}{4\alpha k_{Di}}\left(r_{D_{j+1/2}}^2-r_{D_{j-1/2}}^2\right)\left(\exp\left(-\frac{\alpha r_{D_{i+1/2}}^2}{k_{Di}}\right)-\exp\left(-\frac{\alpha r_{D_{i-1/2}}^2}{k_{Di}}\right)\right)\right]\right\}^{-1}. \qquad \text{(B-29)}$$

This is a first order ordinary differential equation in α with t_D as the independent variable, which coupled with an initial condition constitutes an Initial-Value Problem (IVP). We will assume that at early times

$$\alpha(t_D) = \frac{1}{4t_D}. \qquad \text{(B-30)}$$

Then our initial condition can be written as

$$\alpha(t_D) = 0.025 \quad \text{for} \quad t_D = 10. \qquad \text{(B-31)}$$

To solve the above IVP to obtain $\alpha(t_D)$, we used a Runge-Kutta-Fehlberg procedure which is implemented in a FORTRAN program.

Reproduced with permission of the copyright owner. Further reproduction prohibited without permission.

The logarithmic derivative of the dimensionless wellbore pressure represented by Eq. B-18 can be obtained using the following two equations,

$$\frac{\partial p_D}{\partial \ln t_D} = t_D \frac{\partial p_D}{\partial t_D}, \tag{B-32}$$

$$\begin{aligned}
\frac{\partial}{\partial t_D} \mathrm{E}_1\left(\frac{\alpha(t_D) r_D^2}{k_{D_j}}\right) &= \frac{\partial}{\partial t_D} \int_{\frac{\alpha(t_D) r_D^2}{k_{D_j}}}^{\infty} \frac{\exp(-u)}{u} du \\
&= -\frac{\exp\left(-\frac{\alpha(t_D) r_D^2}{k_{D_j}}\right)}{\frac{\alpha(t_D) r_D^2}{k_{D_j}}} \frac{r_D^2}{k_{D_j}} \frac{d\alpha(t_D)}{dt_D} \\
&= -\exp\left(-\frac{\alpha(t_D) r_D^2}{k_{D_j}}\right) \frac{1}{\alpha(t_D)} \frac{d\alpha(t_D)}{dt_D}.
\end{aligned} \tag{B-33}$$

Then using Eqs. B-32 and B-33 in Eq. B-18, we obtain the dimensionless wellbore pressure derivatives as

$$\begin{aligned}
t_D \frac{\partial p_{wD}}{\partial t_D} = t_D \Bigg\{ \frac{1}{2} \sum_{j=1}^{\infty} \frac{1}{k_{D_j}} \Bigg[&-\exp\left(-\frac{\alpha(t_D) r_{D_{j-1/2}}^2}{k_{D_j}}\right) \frac{1}{\alpha(t_D)} \frac{d\alpha(t_D)}{dt_D} \\
&+\exp\left(-\frac{\alpha(t_D) r_{D_{j+1/2}}^2}{k_{D_j}}\right) \frac{1}{\alpha(t_D)} \frac{d\alpha(t_D)}{dt_D} \Bigg] \Bigg\}.
\end{aligned} \tag{B-34}$$

Reproduced with permission of the copyright owner. Further reproduction prohibited without permission.

APPENDIX C

APPROXIMATE SOLUTION TO THE RADIALLY HETEROGENEOUS RESERVOIR INITIAL-BOUNDARY-VALUE PROBLEM BASED ON FLOW RATE ASSUMPTION (ii)

We develop here an approximate solution to the radially heterogeneous reservoir IBVP, given by Eqs. 2.3.9 through 2.3.12, based on the assumption labeled (ii), in section 2.3.2.2, i.e., we assume the flow rate profile is well approximated by the following equation:

$$q_D(r_D,t_D)=r_D k_D(r_D)\frac{\partial p_D}{\partial r_D}=-exp\left[-\frac{r_D^2}{4t_D k_D}\right]. \tag{C-1}$$

The rate assumption of Eq. C-1 can be obtained by setting $\alpha(t_D)=1/4t_D$ in Eq. B-5. Thus, the dimensionless pressure solution, $p_D(r_D,t_D)$, resulting from Eq. C-1 can be obtained directly from the general solution of Eq. B-16, by setting $\alpha(t_D)=1/4t_D$, which yields

$$\begin{aligned} p_D(r_D,t_D)=&\frac{1}{2k_{D_j}}\left[\mathrm{E}_1\left(\frac{r_D^2}{4t_D k_{D_j}}\right)-\mathrm{E}_1\left(\frac{r_{D_{j+1/2}}^2}{4t_D k_{D_j}}\right)\right] \\ &+\frac{1}{2}\sum_{i=j+1}^{\infty}\frac{1}{k_{D_i}}\left[\mathrm{E}_1\left(\frac{r_{D_{i-1/2}}^2}{4t_D k_{D_i}}\right)-\mathrm{E}_1\left(\frac{r_{D_{i+1/2}}^2}{4t_D k_{D_i}}\right)\right]. \end{aligned} \tag{C-2}$$

Reproduced with permission of the copyright owner. Further reproduction prohibited without permission.

Similarly, the dimensionless wellbore pressure and pressure derivative are obtained by setting $\alpha(t_D) = 1/4t_D$, respectively, in Eqs. B-18 and B-34, to obtain

$$p_D(r_D = 1, t_D) = \frac{1}{2}\sum_{j=1}^{n}\frac{1}{k_{D_j}}\left[\mathrm{E}_1\left(\frac{r_{D_{j-1/2}}^2}{4t_D k_{D_j}}\right) - \mathrm{E}_1\left(\frac{r_{D_{j+1/2}}^2}{4t_D k_{D_j}}\right)\right], \tag{C-3}$$

and

$$\frac{\partial p_D(r_D = 1, t_D)}{\partial \ln t_D} = \frac{1}{2}\sum_{j=1}^{\infty}\frac{1}{k_{Dj}}\left[\exp\left(-\frac{r_{Dj-\frac{1}{2}}^2}{k_{Dj}4t_D}\right) - \exp\left(-\frac{r_{Dj+\frac{1}{2}}^2}{k_{Dj}4t_D}\right)\right], \tag{C-4}$$

where

$$\mathrm{E}_1(x) = -\mathrm{E}_i(-x) = \int_x^{\infty}\frac{\exp(-u)}{u}du. \tag{C-5}$$

An approximate dimensionless wellbore pressure solution identical to Eq. C-3 was also derived by Abbaszadeh and Kamal[32], based on a different approach. They developed a single-phase drawdown solution of a N-zone multicomposite reservoir, based on the classical ideas, developed by Ramey[12], of continuity of pressure and volumetric flux at the N-1 interfaces. The solution is developed in Laplace space, for either a no-flow or a constant pressure outer boundary. A long-time approximate solution is then derived for the constant pressure outer boundary case, which is inverted into real time to yield an equation (see Ref. 32, Eq. C-16) identical to Eq. C-3.

Reproduced with permission of the copyright owner. Further reproduction prohibited without permission.